Crash helmet testing and design specifications

Document Version:
Publisher's PDF, also known as Version of Record (includes final page, issue and volume numbers)

Please check the document version of this publication:

• A submitted manuscript is the version of the article upon submission and before peer-review. There can be important differences between the submitted version and the official published version of record. People interested in the research are advised to contact the author for the final version of the publication, or visit the DOI to the publisher's website.
• The final author version and the galley proof are versions of the publication after peer review.
• The final published version features the final layout of the paper including the volume, issue and page numbers.

Link to publication

Download date: 27. Nov. 2024

Crash Helmet Testing and Design Specifications

Dit proefschrift is goedgekeurd door de promotoren:

prof.dr.ir. J.S.H.M. Wismans
en
prof.dr. H. Nijmeijer

Copromotor:
dr.ir. A.A.H.J. Sauren

Een vriend zal vrolijk met je mee zingen
op de toppen van de bergen,
en zwijgzaam naast je lopen
als je door een dal gaat.

Uit: *Een boekje over vriendschap.*

voor mijn ouders

Contents

Summary

In motorcycle traffic accidents, the human head is exposed to loads exceeding several times the loading capacities of its natural protection. Annually, approximately five thousand motorcyclists get killed in Europe as a result of traffic accidents. They account for 9% of all road fatalities. Wearing a helmet reduces the risk of fatality with about 50%. Over the years, helmet standards have evolved to be an effective means to assure helmet quality in terms of minimal performance. In general, helmet testing standards are the result of often rather pragmatic compromises in meetings of technical experts, more than scientific research. As helmet quality improves, the criteria of shock absorption tests are raised and impact severities are increased.

The shock absorption test of the ECE Regulation 22 (ECE-R.22) is the focal point of this thesis. In this test, the helmet quality is assessed by measuring the acceleration time history of a headform during a helmeted headform impact. Helmet quality is expressed in terms of the injury parameters: *maximum resultant translational headform acceleration* ($a_{\max}$) of the headform's centre of gravity and *Head Injury Criterion* (HIC). The HIC is currently the leading head injury criterion in automotive research, however the ECE standard is still the only helmet standard that has implemented it in its shock absorption test. The head model used in this test is an aluminium alloy, "rigid" headform.

The shock absorption test of the ECE-R.22 has two main limitations with respect to injury assessment. Firstly, the currently used headform may not properly mimic the response of the human head correctly in helmeted head impact. The rigid headform does not model the flexibility of the human brain and skull, which may be inadequate to model the helmet-head interaction correctly. Secondly, advances in injury biomechanics have resulted in other, possibly better, injury criteria that are not or can not be measured in the current shock absorption test.

To date, little has been done to explore how helmet designs may change as a result of applying these different criteria. This thesis deals specifically with the question:
How could motorcycle helmet designs change as a result of applying new and different head injury criteria in the shock absorption test of ECE-R.22?

To implement these criteria in these tests, more quantitative data must be available from the drop test, like rotational accelerations and strains inside the brain. This requires an anatomically more detailed headform or at least a numerical model of such a headform. This holds especially for the strain-based injury criteria, since strains cannot be assessed using a conventional, rigid headform. Furthermore, the interaction between headform and helmet is likely to influence the outcome of the test. To better model the head-helmet interaction, the headform must at least have a deformable skull and brain.

In this study, an anatomically more detailed, deformable headform is developed that allows more realistic helmet-head interaction. Furthermore, it allows for the assessment of helmet performance using different types of head injury criteria, compared to the standard ECE-R.22 rigid magnesium alloy headform. With this headform, the effects of the anatomically more detailed headform on helmet-

head interactions are studied as well as the assessment of head injury risk in the shock absorption test of ECE-R.22. Besides the currently applied translational acceleration based head injury criteria, the injury risk is also assessed in terms of rotational velocity/acceleration and strain based head injury criteria. Furthermore, it is studied whether and how the use of the latter injury criteria in the shock absorption test has additional effects on helmet design compared to the use of the former. From the results, guidelines are developed for improved helmet quality and the assessment thereof.

Results

From the experimental drop test results, it has become clear that the rotational response can reach injurious magnitudes, without exceeding the thresholds for head injury with respect to translational response. Especially for eccentric loading conditions, the application of rotational response based injury criteria can affect the way helmets are designed. Determining only the injury criteria, HIC and $a_{\max}$, in helmet certification tests is therefore not sufficient to evaluate helmet performance. Therefore, the test protocol should be extended with measurement of the rotational headform motion. To implement this, headform rotations must be allowed for in shock absorption tests.

Numerical simulations of helmeted headform drop tests are used to investigate the effects of strain-based injury parameters on helmet design. The simulations show that strain-based injury parameters correlate well with the rotational response, but poorly with translational response. Therefore, helmet design changes result in similar changes in strain-based injury parameters as in rotational response based injury parameters. However, due to the strong relation between these two types of injury parameters, it is not needed to measure them both in helmet drop tests. Measuring the rotational response is preferred over measuring the strains inside the brain, since it is much easier to implement.

The protective padding liner optimisation shows that the protective padding liner that minimises the various injury criteria (called the optimal protective padding liner density) at a given impact velocity differs for the various injury criteria. Therefore, the application of different kinds of injury criteria results in different optimal protective padding liner densities. Furthermore, it is shown that the optimal protective padding liner density depends on the impact site. This means that the protective padding liner density should be lower when the impact is more eccentric (i.e. Front and Rear impact) and should be higher when the impact is more centric (i.e. Top impact), like helmet investigated in this study.

The optimal protecting helmet can be defined in various ways, under the condition of a fixed geometry. One possibility, that is often found in literature, is to minimise certain injury parameters during a helmeted head drop test. This optimal helmet has a strongly increased injury risk at only slightly higher impact severities, due to bottoming out of the protective padding liner. Another possibility for finding the optimal helmet, which is not found in literature, is to maximise the load at predefined injury criteria. In this study, the impact velocity is maximised without exceeding the thresholds for $a_{\max}$ en HIC. To offer protection in both high-impact and in low-impact situations, helmets should be tested in both these situations. This means that not only the injury criteria should be reduced at the current level of impact velocity, but also that the impact velocity should be increased at the current levels of the injury criteria. This study shows that at the current level of impact velocity a reduction of the values for the injury parameters of over 40 % is achievable, whereas an increase in impact velocity of 16 % is also possible without exceeding the injury criteria as set in ECE-R.22.

List of Symbols and Abbreviations

%	percent
$\int f(t)dt$	integral of function $f(t)$ over time
Ø	circumference
2D	two dimensional
3D	three dimensional
α	rotational acceleration
$\dot{\alpha}$	rotational velocity
$\ddot{\alpha}$	rotational acceleration
$\ddot{\alpha}_c$	maximum allowable (critical) rotational acceleration (in GAMBIT function)
$\ddot{\alpha}_m$	mean rotational acceleration (in GAMBIT function)
α_r	resultant rotational acceleration
$\alpha_x, \alpha_y, \alpha_z$	rotational acceleration in x-, y- and z-direction, respectively (in HIP function)
Δ	increment
$\dot{\varepsilon}$	strain rate
ε	strain
λ	eigenvalue
λ	optimisation parameter
λ	scaling factor
η_1, η_2, η_3	damper coefficient in lumped mass model
ρ	density
σ	stress
$\sum$	sum
τ	time constant
ω	rotational velocity
ω_r	resultant rotational velocity
A, B, C, η, β and χ	injury sensitivity coefficients in HIP function
A, B, C, D	constants in strain energy function
a	translational acceleration
a_c	maximum allowable (critical) translational acceleration (in GAMBIT function)
a_m	mean translational acceleration (in GAMBIT function)
a_r	resultant translational acceleration
a_x, a_y, a_z	translational acceleration in x-, y- and z-direction, respectively (in HIP function)
a-p	anterior-posterior
ABS	Acrylenitrile-Butadiene-Styrole
AIS	Abbreviated Injury Scale
ASA	American Standards Association
$\boldsymbol{B}$	right Cauchy-Green strain tensor
B.C.	Before Christ
BSI	British Standard Institution
$\boldsymbol{C}$	covariance matrix
C_{10}, C_{11}	constants in strain energy function
CFC	Cambridge Filter Corporation

cm	centimeter
COG	Centre of Gravity
CSDM	Cumulative Strain Damage Measure
CSF	cerebrospinal fluid
DAI	diffuse axonal injury
DDM	Dilatation Damage Measure
DLT	Direct Linear Transformation
DOT	Department of Transport
E	Young's modulus
ECE	Economic Commission for Europe
ECE-R.22	ECE Regulation 22
EPS	Expanded Polystyrene
Exp	experiment
f	frequency
F, T, R, C	frontal, top, rear and chin impact site
FE	Finite Element
FMVSS	Federal Motor Vehicle Safety Standard
FOAM	crushable foam material model
FRF	frequency response function
FRP	Fibre Reinforced Plastic
g	gravitational acceleration, 9.81 m/s
G'	storage modulus
G''	loss modulus
G_∞	elastic shear modulus
Gd	dynamic shear modulus
G	GAMBIT
GAMBIT	Generalized Acceleration Model for Brain Injury Threshold
GPa	giga Pascal
h	hour
|H|	amplitude of frequency response function
HIC	Head Injury Criterion
HIP	Head Injury Power
Hz	Herz
HUMOS	HUman MOdel for Safety
Hybrid III	type of crash test dummy
I_1, I_2, I_3	first, second and third invariant of the right Cauchy-Green strain tensor
I_{xx}, I_{yy}, I_{zz}	principal moments of inertia in x-, y- and z-direction respectively
ICH	intracerebral haemorrhage/haematoma
ISOLIN	isotropic, linear elastic material model
ISOPLA	isotropic, elastoplastic material model
J	Joule
k$_1$, k$_2$, k$_3$	spring stiffness in lumped mass model
K	bulk modulus
kg	kilogram
kHz	kilo Hertz
km	kilometer
kN	kilo Newton
kPa	kilo Pascal
krad	kilo radian
kW	kilo Watt
L	distance
lbs.	pounds
m	meter
m	mass

m	number of markers
M_1, M_2, M_3, M_4	masses in lumped mass model
MAV	Multi-factor Analysis of Variance
max	maximum
MHz	mega Hertz
min	minimum
MIPS	Multi-direction Impact Protection System
ml	milliliter
mm	millimeter
MRI	Magnetic Resonance Imaging
n, n	number of measurements/computations
N	Newton
NHTSA	National Highway Traffic Safety Administration
NOCSAE	National Operation Committee on Standards for Athletic Equipment
opt	optimum
Pa	Pascal
PC	Polycarbonate
PCA	Principal Component Analysis
PMA	polymethyl acrylate
POM	Poly-Oxy-Methylene
psi	pounds per square inch
PU	Polyurethane
PVC	Poly-Vinyl-Chloride
r	characteristic length
r_0	reference characteristic length
R^2	correlation factor in regression analysis
rad	radian
RMDM	Relative Motion Damage Measure
s	second
$\boldsymbol{S}$	matrix of shape vectors
(A)SDH	(acute) subdural haematoma
SI, (G)SI, (V)SI	(Gadd/Versace) Severity Index
sim	simulation
SMF	Snell Memorial Foundation
$t, t_1, t_2, t_3, t_4, t_j, t_n$	point in time
T	impact duration
TBI	Traumatic Brain Injury
tot	total
US	United States
USA	United States of America
V, v, v	velocity
V	volume
$\bar{V}$	mean head volume
W	strain energy
WSTC	Wayne State Tolerance Curve
x	x-coordinate
y	y-coordinate
z	z-coordinate

Chapter 1

Introduction: Crash Helmet Design as Driven by Standards

1.1 Crash Helmet Design Then and Now

Humans began protecting their heads using helmets long before injury mechanisms were studied. The way helmets were designed was, and still is, heavily dependent on the application of the helmet. Already in the 15th century B.C., helmets were effective means of protecting the head. Figure 1.1 shows a Corinthian helmet that dates back to the 4th century B.C., weighing about 1.5 kg [Gurdjian, 1975] and obviously designed to protect against penetration in combat.

Not until the end of the 19th century, it was discovered that serious head injuries could occur without penetration. It took another 50 years to understand that non-penetrating head injuries are caused by short-duration accelerations acting on the head and its contents [Holbourn, 1945]. These acceleration injuries are the most common and dangerous form of injuries for motorcyclists and are often caused by blunt impact rather than penetration. The early motorcycle helmets were designed accordingly: a

Figure 1.1: Corinthian helmet that dates back to the 4th century B.C. [Gurdjian, 1975].
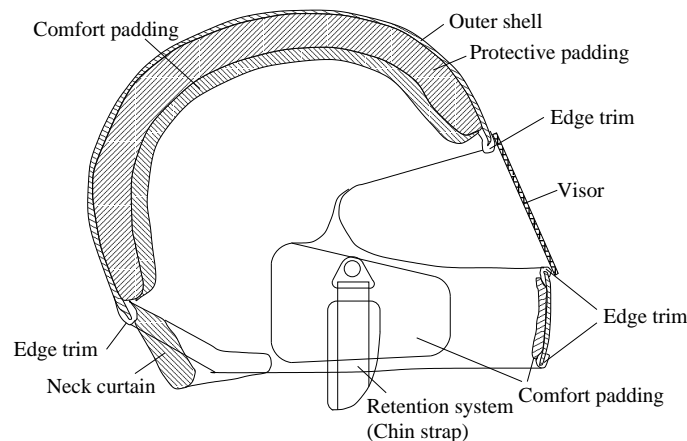
Figure 1.2: Cross section of a full-face motorcycle helmet [UN, 2000].

leather covered, shock absorbing liner. In later designs, the leather cover was replaced by a stiffer, plastic outer shell. The function of this shell is not only to prevent penetration, but also to distribute the load over a larger area. Figure 1.2 illustrates the components of a modern full-face motorcycle helmet. The modern motorcycle helmet generally consists of four main parts: the comfort padding liner, the protective padding liner, the outer shell and the retention system. The retention system is used to keep the helmet in position prior to or during an impact.

The purpose of the comfort padding liner is to increase the wearing comfort of the helmet and to provide a good fit on the head. It consists of low-density, flexible, open-celled, polyurethane or PVC foams and is often faced with a cloth layer [Gilchrist & Mills, 1993].

The protective padding liner, or impact liner, is the main shock absorbing component of a helmet. It is usually made of Expanded Polystyrene (EPS) foam. The liner thickness applied in helmets is limited by aerodynamic and styling requirements and varies from about 25 mm to 40 mm. The mass density of the EPS foam applied in motorcycle helmets varies from approximately 30 to 90 kg/m^3.

The outer shell of a motorcycle helmet has three main functions: to distribute the shock load, to prevent penetration and to prevent injury as a result of abrasion along a rough object. Three types of material are commonly used in outer shells of motorcycle helmets: a Polycarbonate (PC), Acrylenitrile-Butadiene-Styrole (ABS) or a stiffer thermosetting Fibre Reinforced Plastic (FRP). The shock absorbing capacities of a helmet are mainly a function of the outer shell and protective padding liner stiffnesses. The stiffer FRP outer shell is often used in combination with a low-density EPS foam, whereas the softer PC and ABS outer shells compensate their compliance with a stiffer, high-density EPS foam.

1.1.1 Effectiveness of Current Day Motorcycle Helmets

Motorcyclists are among the most vulnerable road users. Together with moped riders, they have the highest risk of getting killed in a traffic accident [EEVC, 1993]. In car crashes, car occupants are protected by safety belt systems, airbags, retracting steering systems, the padding of the car interior and the car body itself. Motorcyclists involved in traffic accidents are much more vulnerable than car occupants. Almost the only protection offered to a motorcyclist is the crash helmet.

Otte *et al.* [1982] provide a detailed categorisation by body part of injuries sustained by motorcyclists involved in traffic accidents. The injury severity is indicated using the *Abbreviated Injury Scale* (AIS)

Table 1.1: Motorcyclist fatalities in various countries.

Country	Number of Fatalities					As a percentage of all road fatalities				
	1980	1990	1997	% change 1980-1990	% change 1990-1997	1980	1990	1997	% change 1980-1990	% change 1990-1997
Austria	106	107	111	+1	+4	7.3	7.2	10.0	−1	−39
Belgium	170	106	125	−38	+18	7.5	5.4	9.2	−24	+70
Denmark	59	39	23	−34	−41	8.3	6.2	4.7	−28	−24
Finland	21	28	8	−38	−71	3.1	4.3	1.8	+13	−58
France	1136	1031	831	−9	−19	8.6	9.2	10.4	+8	+13
Germany	1232	769	974	−38	+27	10.5	9.6	11.4	−8	+19
GB	1113	621	492	−44	−21	17.8	11.7	11.9	−34	+2
Italy	822	706	482	−14	−32	9.0	10.0	7.7	+11	−23
Netherlands	130	72	92	−45	+28	6.5	5.2	7.9	−20	+33
Norway	29	25	27	−14	+8	8.0	7.5	8.9	−6	+19
Spain	316	792	460	+151	−42	4.8	8.8	8.2	+81	−7
Sweden	43	46	36	+7	−22	5.1	6.0	6.7	+18	+12
Switzerland	139	160	83	+15	−48	11.2	16.8	14.1	+50	−16
Europe[#]	5316	4502	3744	−15	−17	8.3	8.3	8.7	0	+5
USA	5079	3173	2084	−38	−34	9.8	7.0	5.0	−29	−29
Total	10395	7675	5828	−26	−24	8.4	8.2	8.4	−2	+2

[#] 13 countries above.

Data from UNECE Statistics of Road Traffic Accidents in Europe, with fatalities adjusted to standard 30 day definition by the Institut für Zweirad-sicherheit, and from the OECD IRTAD database.

which is a threat to life scale. The AIS ranges from slight injury at AIS 1 to almost certainly fatal injury at AIS 6. The findings of Otte *et al.* [1982] are similar to those of other accident investigators [for a summary, see: Harms, 1993]. The most frequently injured parts of the body are the legs (39% of all injuries), the head (23%) and the arms (19%). However, head injuries are generally more serious (at an average AIS score of 2.4) than leg injuries (AIS 1.9) or arm injuries (AIS 1.5). They account for 80 percent of the fatalities. Furthermore, injuries to the central nervous system are often of an irreversible nature.

Table 1.1 shows the trends in motorcyclist fatalities in absolute numbers and as a percentage of all road deaths[1], in a number of countries for which statistics were available, over the period 1980 - 1997. The table shows that the number of fatalities varies substantially over a large period of time and between countries. The general trend in Europe and the USA shows a decrease in motorcycle fatalities (columns 5 and 6). However, fatalities among other types of road users are decreasing more quickly, so motorcycle fatalities form a (slightly) increasing proportion of all road deaths (columns 10 and 11). On average, the motorcycle fatalities account for 8% of all road deaths. Also, in 1990, the motorcycle death rate per vehicle in Europe was four times larger than that for cars [EEVC, 1993]. This figure is an underestimate of the higher risk of motorcycles, since it takes no account of the smaller average distance travelled per year by motorcycles than by cars. Per mile traveled, the death rate on motorcycles is 18 times higher than in passenger vehicles [IIHS, 2001].

The table also shows faster decrease in number of fatalities in the USA compared to Europe. This may be due to the fact that nowadays in the USA almost every state has a helmet law, whereas in

---

[1] The table concentrates on fatalities, because this is the most serious category of injury, and is least affected by problems of definition. In general, there are ten to fifteen times as many serious injuries than fatalities, and thirty to fifty times as many minor injuries than fatalities.

1980 there was no helmet law at all. Still, in Europe, where helmet laws have become effective since 1975, the number of fatalities is higher than in the USA. Furthermore, the number of fatalities as a percentage of all road fatalities has increased over the period 1990-1997. This is probably because the different traffic situation in Europe compared to the US traffic situation. Especially in southern European countries traffic is more chaotic.

To determine the effectiveness of helmets to prevent head injury or reduce injury severity in a statistically reliable way, it is necessary to investigate the sustained injuries of a sample of road accident victims in which there is a significant number of both wearers and non-wearers. In most Western European countries the helmet wearing rate has been above 80% since the middle sixties. Therefore data suitable for determining helmet effectiveness are available from Europe only before that period, but more recent data are available from the US.

Goldstein [1988] extensively reviewed helmet and helmet law effectiveness studies. Most of these studies show an increase in motorcyclist fatality rate after the repeal of a helmet law, however differences between studies are quite large (fatality rates ranging from 10% to 63%). Some studies do not show a significant difference and none of the studies show a decrease of the fatality rate. Typical conclusions are that the non-use of a helmet is responsible for these differences. However, time trends such as lower median age and experience of motorcycle owners, higher average miles travelled annually, and faster motorcycles may also contribute to these results. The study of Evans & Frick [1986] is the only study that compensated for these time trends. They used the *Double Pair Comparison Method* [Evans, 1986] where one of the occupants of a motorcycle, either the driver or the passenger, is used as a control for the other occupant in motorcycle accidents involving a male driver and a male or female passenger in which there is at least one fatality. This study concludes that helmeted riders are 27% less likely to die in an accident compared to non-helmeted riders.

The study of Hurt Jr. *et al.* [1981] is the most widely referenced study on motorcycle accidents and motorcycle safety issues. It is based on data from the on-scene, in-depth investigation of 900 motorcycle accidents in the Los Angeles area. They found a fatality rate of 3.5% for helmeted and 8.2% for non-helmeted motorcyclists involved in traffic accidents. So according to this study, wearing a helmet decreases the chance of motorcyclists getting killed in a traffic accident by 57%, which is more than twice the result found by Evans & Frick [1986]. The large differences between fatality rates of the various studies may be caused by the method of investigation. For example, Hurt Jr. *et al.* [1981] performed an on-scene, in-depth investigation, which may be biased, because of underreported minor and no-injury accidents. Even though each method of accident investigation has its disadvantages, it can be concluded that the helmet is an effective means of head protection.

1.2   Origin and Outline of the Crash Helmet Standards

To make sure that all motorcycle helmets reach a certain level of effectiveness, current helmets are required to pass a certain standard test before they are allowed to be put on the market. Therefore, helmets are designed to pass these tests, even though some helmet manufacturers do more than that, and thus the quality of the helmet depends largely on the quality of these tests. The first standard tests for motorcycle helmets was the British Standard 1869:1952 [BSI, 1952], issued by the British Standard Institution (BSI). This test applied shock loadings to a helmeted headform. In the test, technicians would drop a hardwood block weighing ten lbs. (4.5 kg) from a height of nine feet (2.7 m) onto a helmeted headform. The output consisted of dynamic force measurements recorded from a gauge mounted between the base of the headform and a massive, stationary reaction block. The test criterion

DROP TEST   REALITY
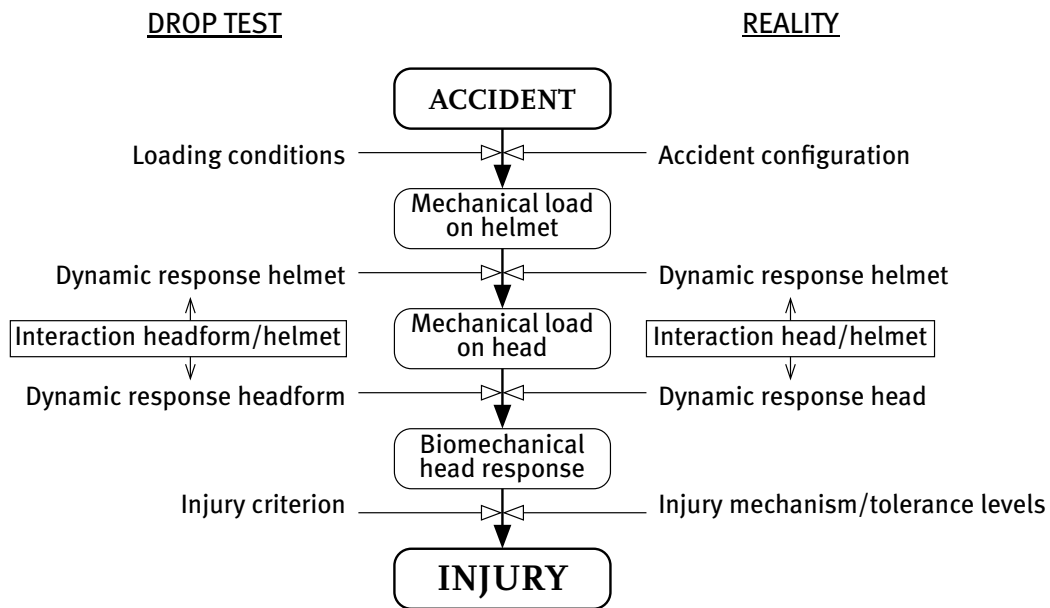
Figure 1.3: Load-injury scheme for helmeted head impact [modified after: Wismans *et al.*, 1994].

required that the output force did not exceed 5000 lbs. (22.2 kN). Only qualified helmets were to be sold in Great Britain.

The standard served two immediate purposes: it was a tool for the evaluation of available headgear and it also served as a guide for the design of new headgear. It set performance levels that every crash helmet should satisfy. Currently, ECE Regulation 22 [UN, 2000] is the leading standard in Europe. Like many other helmet standards, it is heavily influenced by the standard of the BSI [1985]. Impact protection is the primary consideration of almost every helmet standard. The general term for a test to assess impact protection is *shock absorption test*, which is the focus of this thesis. In concept, the leading helmet standards are the same: A helmeted headform is dropped onto an anvil and the headform acceleration is measured. However, there are differences in headform shape and mass, in impact site, in anvil type, in impact velocity and in headform support during impact. The developments of some of the leading standards (ECE, Snell and DOT) are discussed and compared in detail in Appendix A.

To effectively assess the quality of a helmet, the shock absorption test must be a good representation of reality. Figure 1.3 shows a load-injury scheme for helmeted head impact [based on: Wismans *et al.*, 1994]. This scheme shows how a load on the head(form) during an accident (drop test) leads to injury. To understand how protective measures, such as the use of a helmet, can be effective, one has to understand how an accident leads to injury. During a motorcycle accident, a mechanical load is applied to the helmeted head. The direction and magnitude of this load are determined by the accident configuration. The dynamic response of the helmet together with the helmet-head interaction determines how the load is transferred to the head. The load on the head, in turn, determines the biomechanical response of the head which can be expressed in terms of physical parameters such as stresses and strains. An *injury criterion* or *injury parameter* is used to assess the risk of sustaining an injury. It is defined as a physical parameter or a function of several physical parameters which correlates well with the injury severity of the body under consideration [Ommaya *et al.*, 1994]. When the injury criterion exceeds a specific value, injury is likely to occur. The value at which a specific type

of injury occurs is called a *tolerance level* (or *injury criterion level*). Tolerance levels for specific types of injury are obtained from *injury risk functions* which predict the chance of sustaining an injury at a specific load. The way in which the biomechanical response leads to injury is called *injury mechanism.* Injury mechanisms are not the same for the different parts of the head and are not always easy to understand [Wismans *et al.*, 1994]. For example skull fracture is often caused by direct contact to the head, whereas Traumatic Brain Injury (TBI) does not necessarily involve direct contact.

So three main factors are of importance in shock absorption tests:

The load: In real accidents, a wide variety of accident configurations occurs, resulting in many different loads onto the helmeted head. The shock absorption test should simulate the most common accident configurations correctly.

The assessment: Criteria must be set to assess the risk of injury. What parameters should be measured, depends on the choice of the injury criteria.

The head model: The headform used in the test must model the human head in such a way that a realistic or at least a relevant response is to be expected in order to give realistic or relevant measurements. "Realistic or relevant" here means that the head response should bear relevance to the injury mechanisms of the injury under consideration and that the assessment of the injury can be derived from the response.

Section 1.2.1, 1.2.2 and 1.2.3 will elaborate on the issues of load, injury assessment and headforms in helmet testing procedures, respectively.

1.2.1   Aetiology of Motorcycle Accidents

The first factor in the quality of helmet testing standards is the ability to simulate the load on the head during an accident. In real motorcycle accidents, this load is very complex. Many researchers have investigated motorcycle accidents in terms of (head) injuries and accident configurations to understand more of the real accident situation [e.g.: Harms, 1981; Hurt Jr. *et al.*, 1981; Otte *et al.*, 1981]. These studies show that average impact speeds are around 30 km/h and that in most accidents a hard surface was hit. Furthermore, 80% of all injuries are sustained at speeds of 40 km/h or less [Thomas & Bradford, 1992]. Currently, more and more data is becoming available from in-depth studies [e.g.: Otte *et al.*, 1999; ACEM, 1997; Mooi & Galliano, 2001]. These studies have the potential to reconstruct accidents and retrieve data on the actual loading of the helmeted head during an accident more accurately. This data is needed to keep the standards up-to-date with respect to simulating the load onto the helmeted head.

Head injuries occur in a variety of accident configurations [Hurt Jr. & Thom, 1992]. Serious and fatal head and neck injuries are much more likely to occur in a head-on direct impact, than in either a side swipe collision or in one where the rider is ejected [Ramet *et al.*, 1981; Sporner *et al.*, 1990]. This is because a head-on impact into a relatively unyielding surface can cause the motorcycle to pivot upward about the front axle, causing the rider to be thrown over the top of the handlebars, striking the head and torso on the vehicle or a roadside obstacle (contact). Sporner *et al.* [1990] also draw a distinction between frontal impacts in which the rider's trajectory causes him to fly head first into the side of the impacted vehicle and those in which the rider flies over the top of the impacted vehicle: head injuries are markedly less prevalent in the latter case (inertial). In helmeted head impact, the

distinction between contact injuries and inertial injuries is less clear, since the helmet attenuates and spreads the load on the head. This way, inertial injuries can occur in contact situations.

In the early eighties, Otte *et al.* [1984] investigated motorcycle accidents in the district of Hannover, Germany. They found that injuries were predominantly located at the front of the head. Although there were a large number of different kinetic patterns in crash and post-crash phases, the face region, especially the chin and forehead, was nearly always exposed to impact risks. Approximately one third of all injuries to the helmet-protected heads of motorcyclists are minor soft part injuries, like contusions and abrasions (32.9% and 32.8% respectively). More serious soft tissue injuries, such as lacerations/contusions, cut or scalping injuries represent another 21.9% of helmet-protected heads.

1.2.2 Head Injury Criteria

Head injuries can be divided into *contact injuries* and *inertial injuries* [Gennarelli, 1985]. Contact injuries occur in case of a direct impact to the head, but head motion is not necessary. Examples of contact injuries are: skull fractures, epidural haemorrhages/haematoma, coup/contrecoup contusions and lacerations. Inertial injuries do not necessarily involve a direct impact to the head, but they are caused by acceleration of the head. Examples of inertial injuries are: concussion, (acute) subdural haematoma [(A)SDH], contrecoup contusions, diffuse axonal injury [DAI] and intracerebral haemorrhage/haematoma [ICH].

For over 30 years, research has been undertaken to assess the injury mechanisms causing inertial head injury during impact and to establish associated tolerance levels of the human head. The development of injury criteria has been a major goal, in order to be able to assess the risk of sustaining a head injury, and to assess the effectiveness of potential protection measures such as a motorcycle helmet. Injury criteria for inertially induced head injuries can roughly be divided into three categories: Injury criteria based on translational accelerations of the head's centre of gravity; injury criteria based on translational and rotational accelerations of the head's centre of gravity; and injury criteria based on stresses and strains inside the brain. Each category is discussed in the following. All these injury criteria are mainly developed to consider closed head brain injury. Thus, they generally do not consider skull fracture, facial injury, etc. A more detailed description of head injury criteria is given in Appendix B.

1.2.2.1 Translational Acceleration Based Injury Criteria

Wayne State Tolerance Curve, WSTC   The *Wayne State Tolerance Curve* (WSTC) is considered to be the foundation of research on human head injury criteria. This curve evolved from the work of Lissner *et al.* [1960]; Gurdjian [1953]; Gurdjian *et al.* [1961] and Patrick *et al.* [1965], and gives tolerable average acceleration magnitude in A-P direction (Anterior-Posterior) as a function of the acceleration duration. It still is the basis for most currently accepted injury criteria. The curve is given in Figure 1.4. Slight cerebral concussion without any permanent effects was considered to be within human tolerance. Only translational accelerations were used in the development of the curve which was obtained from different experiments with post mortem human subjects (area I in Figure 1.4); from experiments with animals (area II in Figure 1.4); and from experiments with human volunteers (area III in Figure 1.4). Shock absorption tests of helmets are concentrated mainly in area II of Figure 1.4.

Head Injury Criterion, HIC   The WSTC served as the basis for the most commonly used injury criterion for head injury in automotive research and regulations, the *Head Injury Criterion* (HIC). The
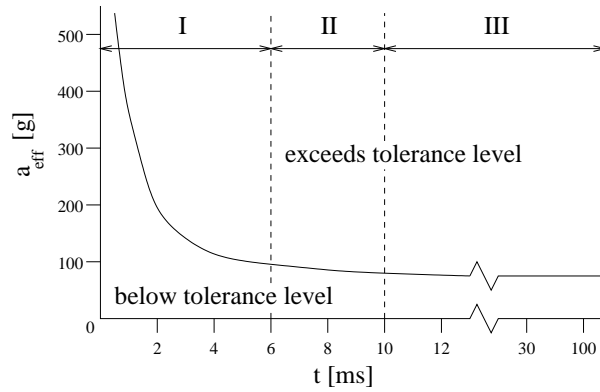
Figure 1.4: Wayne State Tolerance Curve [Lissner *et al.*, 1960].

HIC is defined as:

$$\text{HIC} = \left\{ \left[\frac{\int_{t_1}^{t_2} a(t)dt}{t_2 - t_1} \right]^{2.5} (t_2 - t_1) \right\}_{\max} \tag{1.1}$$

with $a(t)$ the resultant head acceleration in g's (measured at the head's centre of gravity[2]) and t_1 and $t_2[s]$ any two points in time, during any interval in the impact, that maximise HIC.

HIC has been shown to be a reasonable discriminator between severe and less severe injury [Tarriere, 1981], however it does not correlate well with injury severity for impact in various impact directions [Newman, 1980]. An important limitation of the HIC is that head rotational acceleration is not taken into account although rotation is debated to be the primary cause for various types of traumatic brain injury, in particular acute subdural haematoma and diffuse brain injury [Adams *et al.*, 1983; Gennarelli *et al.*, 1987; Holbourn, 1945]. Despite its limitations, HIC is currently the most commonly used criterion for head injury in automotive research.

Maximum resultant head acceleration   A head injury criterion which is often used because of its simplicity is the *maximum resultant head acceleration* ($a_{\max}$). The thresholds for $a_{\max}$ depends on its application, because of the time dependent nature of the resultant acceleration with respect to head injury. To account for this time dependency, this criterion can be replaced/supplemented by a value for the resultant acceleration that should not be exceeded longer than a certain time interval.

1.2.2.2 Combined Rotational and Translational Acceleration Based Injury Criteria

Generalized Acceleration Model for Brain Injury Threshold, GAMBIT   Newman [1986] attempted to combine translational and rotational head acceleration response into one injury criterion. Considering both these accelerations as the cause for stresses generated in the brain and resulting in brain injury, he proposed the *Generalized Acceleration Model for Brain Injury Threshold* (GAMBIT). On the assumption that translational and rotational acceleration equally and independently contribute to head injury, the GAMBIT equation is:

$$G = \frac{|a_m|}{a_c} + \frac{|\ddot{\alpha}_m|}{\ddot{\alpha}_c} \leq 1 \tag{1.2}$$

---

[2]g = 9.81 m/s^2

where a_m and $\ddot{\alpha}_m$ are the mean values for the translational and rotational acceleration, respectively; and $a_c = 250$ g and $\ddot{\alpha}_c = 10,000$ rad/s^2 are the maximum allowable values for the translational and rotational acceleration, respectively. The GAMBIT has never been extensively validated as an injury criterion.

Head Injury Power, HIP   Newman *et al.* [2000b] reasoned that the rate of change of translational and rotational kinetic energy, i.e. power, could be a viable biomechanical function for the assessment of head injury. An empirical expression for this *Head Impact Power* (HIP), relating a measure of power to head injury, would be of the form:

$$\text{HIP} = Aa_x \int a_x dt + Ba_y \int a_y dt + Ca_z \int a_z dt + \eta\alpha_x \int \alpha_x dt + \beta\alpha_y \int \alpha_y dt + \chi\alpha_z \int \alpha_z dt \quad (1.3)$$

Each term in this expression represents the change in kinetic energy for one degree of freedom. The coefficients A, B, C, η, β and χ denote the injury sensitivity for each of the six degrees of freedom of the head and a_x, a_y, a_z, α_x, α_y and , α_z are the time dependent accelerations in each of the six degrees of freedom. The development of the HIP function is described in Newman *et al.* [2000a]. The directional sensitivity of the human head is not known. Therefore, the coefficients of equation (1.3) are currently set to reflect mass and mass moments of inertia of the human head. The HIP$_{\text{max}}$ is only validated for mild traumatic brain injury. When used for higher severity head injuries as can occur in helmeted head impact, the tolerance level needs to be adjusted compared to the tolerance established for mild traumatic brain injury.

1.2.2.3 Stress and Strain Based Injury Criteria

Advancements in computational techniques have led to more accurate and more detailed numerical models of the human head. These models bring a detailed injury assessment closer to reality, since they enable stresses and strains to be examined. Bandak [1995, 1997] developed three measures representing the general types of brain injuries experienced in traffic accidents:

Cumulative Strain Damage Measure (CSDM) is based on the hypothesis that diffuse axonal injury (DAI) is associated with the cumulative volume fraction of the brain matter experiencing tensile strains over a critical level. Bandak *et al.* [2001] found that a CSDM level 5 corresponds to mild DAI and a CSDM level of 22 corresponds to moderate DAI severity. Thus, 5 percent, respectively 22 percent, of the brain volume experienced strain in excess of 15%, the proposed critical level [Thibault *et al.*, 1990].

Dilatation Damage Measure (DDM) monitors the cumulative volume fraction of the brain experiencing specified negative pressure levels. Bandak *et al.* [2001] suggested a DDM value of 5 at a threshold level of -14.7 psi (-101 kPa) as an injury threshold, but also reported that further research was necessary.

Relative Motion Damage Measure (RMDM) monitors the tangential motion of the brain surface resulting from combined rotational and translational accelerations of the head. Such motions are a suspected cause of subdural haematomas associated with large-stretch ruptures of the parasagittal bridging veins.

Stresses and strains used to compute the above injury parameters are calculated from Finite Element simulations, using a Finite Element model of the skull and intracranial contents.

1.2.2.4 Discussion on Head Injury Criteria

Over the past years, several head injury assessment functions have evolved. Most of them are based on the Wayne State Tolerance curve (Figure 1.4). The most commonly acknowledged and widely applied head injury criterion is the HIC which is based on the assumption that the translational resultant acceleration of the head is a valid indicator of head injury thresholds. This criterion has enabled vehicle safety to be improved. Nevertheless, it has shortcomings and does not take into account rotational acceleration and direction of impact. Furthermore, it is not clear how this injury criterion relates to the (unknown) injury mechanisms.

The only injury assessment function found that takes into account translational acceleration as well as rotational acceleration and directional sensitivity is the HIP_{max}. However, it has only been validated for mild traumatic brain injury. Whether this function is also applicable for more severe brain injuries, as occur in traffic accidents, remains to be investigated.

The DDM is a pressure-based injury criterion. However, as the authors themselves report, there is no direct observational evidence on the relationship between intracranial pressure and head injury. Therefore, this injury criterion may not be adequate. The RMDM heavily relies on a correct model of the interface between brain and skull. However, the mechanical behaviour of the skull-brain interface is not yet known, but research on this is ongoing [Hardy *et al.*, 1998; Al-Bsharat *et al.*, 1999; Hardy *et al.*, 2001]. If the interface is modelled correctly, the RMDM is potentially a good injury criterion to predict (A)SDH. The CSDM is the most promising stress and strain based injury criterion, since it is based on probably one of the most important parameters in brain injury (strain) and it is least hampered by model uncertainties. However, all the stress and strain based injury criteria discussed above are based on a Finite Element model of the head which is not validated for actual stresses and strains inside the head.

A final remark concerns the tolerance levels for the injury criteria. The choice of tolerance level depends on the headform, on the application, and on the level of injury risk allowed. For example: the tolerance level for HIC in the helmet standard ECE-R.22 is 2400 using a rigid headform, whereas the tolerance level for HIC in the car crash standard FMVSS 208 [NHTSA, 1972] using a Hybrid III headform (see next section) is 1000.

1.2.3   Headforms and Biomechanics in Helmet Testing Procedures

Even though the currently used rigid headform is still the only headform applied in motorcycle helmet certification tests, several, more advanced headforms exist today. The most commonly accepted surrogate headform is the Hybrid III headform (Figure 1.5) which is used on the Hybrid III crash test dummy. This headform is introduced in 1976 and is designed for application in car crash tests. It is a rigid headform, surrounded by a vinyl rubber skin surrogate, and is designed in such a way that the headform accelerations respond human-like in hard contact impacts that occur in car crashes.

From this headform, Willinger *et al.* [2001] developed the Bi-mass 150 headform (see Figure 1.5). They inserted a mass (representing the brain) which is elastically coupled to the skull of the headform in such a way, that the natural frequency of the Bi-mass 150 headform corresponds to the 150 Hz measured in-vivo [Willinger & Cesari, 1990]. Using eight triaxial accelerometers, Willinger *et al.* were able to measure the 3D kinematics of both the skull and the brain. With this headform, using all the measured accelerations, they claim that it is possible to discriminate between several types of head injury mechanisms:
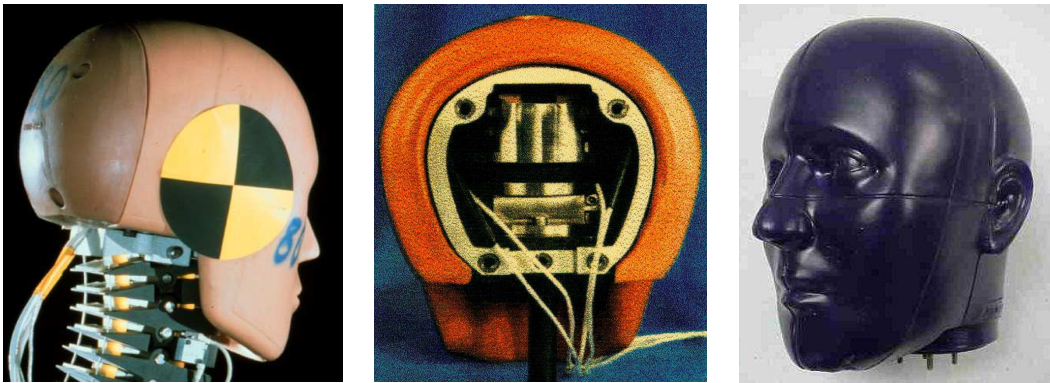
Figure 1.5: Picture of the Hybrid III headform (*left*), the Bi-mass 150 headform (*middle*) and the NOC-SAE headform (*right*).

Skull acceleration may be related to extra-dural haematoma and skull fracture.

Brain-skull differential acceleration or relative motion is an injury parameter to indicate subdural haematoma or focal cerebral contusion.

Brain acceleration is an injury parameter to indicate diffuse axonal injury and intra-cerebral contusion or haematoma.

Around the same time as the Hybrid III headform was introduced, Hodgson [1976] developed a surrogate headform for assessing the performance of protective headgear in sports [NOCSAE, 2002]. This headform, called the NOCSAE headform (Figure 1.5), has three major design differences with respect to the conventional headform used in helmet testing standards: It has a more human-like anthropometry, a gel-filled cavity to model the brain, and a more human-like, compliant skull. This headform can only be used in a pass/fail drop test at SI = 1200, because of the way it is calibrated. SI is the Severity Index (see Appendix B).

The above discussed headforms have been proven to be more biofidelic than the conventional, rigid headform. However, none of them are implemented in motorcycle helmet certification tests, since the benefit of doing so was not sufficiently shown.

1.3 Review of Helmet Shock Absorption Studies

Many researchers have investigated helmet design and helmet testing standards with respect to helmet performance in shock absorption tests. These studies can be divided into three categories:

Experimental studies based on standard drop tests, which evaluate and compare the performance of different existing helmet designs (Section 1.3.1).

Numerical modelling of standard drop tests, which investigate the effect of the material parameters on helmet performance, using a parametric study (Section 1.3.2).

Experimental studies of modified drop tests, which investigate the effect of changes in helmet testing procedures on the evaluation of helmet performance (Section 1.3.3).
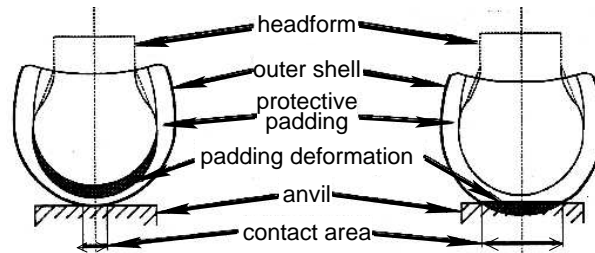
Figure 1.6: Helmet deformation modes with FRP (left) and PC (right) shelled helmets [Beusenberg & Happee, 1993].

Studies in the first two categories investigate and search for means to improve helmet effectiveness, using the current standards (such as ECE-R.22), whereas the studies in the final category search for ways to also improve these standards in terms of the *load*, the *assessment* and the *head model*. Since helmet design is still driven by these standards, improving the standards would eventually also lead to an improved helmet design. Furthermore, it is not hampered by the limitations of the current standards.

1.3.1   Experimental Studies Based on Standard Drop Tests

Beusenberg & Happee [1993] used the ECE-R.22 standard drop test on a set of (approved) crash helmets to investigate the relationships between design parameters and helmet performance according to several criteria. Main attention was given to outer shell and protective padding material properties. They assessed testhead resultant accelerations, HIC values and anvil reaction forces in frontal (forehead) impact. Furthermore, they inspected the residual deformation of the protective padding liner 24 hours after the tests. Existing helmets can roughly be classified into two categories: helmets with a stiff outer shell in combination with a low-density protective padding liner (e.g. polycarbonate (PC) shelled helmets) and helmets with a low-stiffness outer shell in combination with a high-density protective padding liner (e.g. Fiber Reinforced Plastic (FRP) shelled helmets). They found typical differences in deformation modes between the two (see Figure 1.6).

Energy absorption of FRP shelled helmets is predominantly caused by deformation of the protective padding 'from the inside' and the load distribution is determined by the compatibility of the protective padding dimensions and headform shape, whereas PC shelled helmets predominantly show deformation 'from the outside' and load distribution is determined by the geometry of the object hit as well as the load distribution capacity of the protective padding material. FRP shelled helmets show a higher maximum load and rate of onset while force distribution and time duration of the impact are more favourable compared to PC shelled helmets. The total energy absorbed by helmet deformation is quite similar for all helmets tested. The authors make no statement on which helmet protects the head better, but if the total energy absorbed by the helmet is the same, one tends to conclude that the PC shelled helmet gives better protection, since the time duration of the impact is longer. Thus, the rate of change in absorbed energy is lower (see also Section 1.2.2). However, it is not proven that the rate of change in absorbed energy is a good head injury criterion for impact severities occurring in traffic accidents. Furthermore, a longer impact duration means a larger deformation of the protective padding liner (considering the same impact velocity and headform mass), which means a higher risk of *bottoming-out*. Bottoming-out is the phenomenon that the protective padding liner has used all of its energy absorbing capacities.

Schuller & Beier [1981] investigated a sample of 131 helmeted motorcyclists who had been involved in traffic accidents, with respect to head injury incidence and outer shell material. They found that users of PC shelled helmets seemed to suffer less cerebral concussions, skull fractures and severe cerebral injuries than those wearing ABS (Acrylenitrile-Butadiene-Styrole) and FRP shelled helmets. The incidence of cerebral concussion connected with skull fractures is significantly different between PC and FRP shelled helmets. From less severe impacts, wearers of FRP helmets often suffered minor head contusions, moderate cerebral concussions and non-minor lacerations. For those wearing PC or ABS helmets, these injuries are less common. The authors did not perform a classification of injury severity within these groups of injury. This study indicates that PC shelled helmets also better protect the head than FRP shelled helmets in real traffic accidents.

Hopes & Chinn [1989] tested a variety of combinations of outer shell stiffness and protective padding liner density. They investigated results from drop tests according to the British Standard 6658 [BSI, 1985]. Each helmet was tested at five impact sites: the crown, the front, the left side, the right side and the rear. They found decreasing HIC values with decreasing shell stiffness and decreasing protective padding liner density. They also tested helmets without the outer shell, which resulted in even lower HIC values. These tests also resulted in the lowest rebound velocity. They concluded that the outer shell is the main cause for higher rebound velocities and thus for higher HIC values, since HIC is a function of both the magnitude and duration of the resultant acceleration. Hopes & Chinn [1989] also found that if the crush depth of the helmet is fully utilised, a significantly lower HIC value can be obtained. Current helmets only use a small part of their crush depth. A conclusion which was also drawn from the study of Beusenberg & Happee [1993].

The general conclusion of helmet testing studies is, that both protective padding liner and outer shell of current motorcycle helmets are too stiff. Reducing the outer shell stiffness reduces the duration of the acceleration pulse and reducing the protective padding liner density reduces the magnitude of the acceleration pulse. There are however limitations to these conclusions. No outer shell (stiffness zero) yields the lowest rebound, however it has also the weakest load distribution capacities. Especially in traffic, these load distribution capacities may be indispensable, since localised loadings are not uncommon (> 10% [Vallée *et al.*, 1981; Hurt Jr. *et al.*, 1981]). Localised loadings to the head increase the chances of skull fractures. On the other hand, when the protective padding liner density is too low, bottoming-out occurs, resulting in rapidly rising load onto the head.

1.3.2 Numerical Modelling of Standard Drop Tests

Another way of gaining more insight in the way helmets protect the head is by means of numerical simulation. Two types of numerical models for describing the impact behaviour of the helmeted head are found in literature: Lumped Mass models and Finite Element models (FE-models).

Lumped mass models

Lumped mass models are computationally inexpensive and can easily be used for trend studies. In lumped mass models, the (components of the) helmet and the head are modelled as rigid masses connected by massless springs and dampers.

Not many lumped mass models were found in literature. Mills & Gilchrist [1988] used a lumped mass model to simulate the helmet deformation as a result of impacts by flat and hemispherical strikers. They concluded that careful design of the softer foams inside the helmet may be of major importance in improving shock absorbing capacities of crash helmets. Gilchrist & Mills [1993] improved
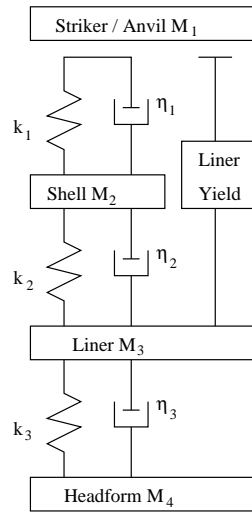
Figure 1.7: Lumped mass model of a helmet [Gilchrist & Mills, 1993].

this model by including the outer shell (Figure 1.7). They investigated striker/anvil forces in second impacts and the influence of impact velocity on striker/anvil force. Just like the previously discussed experimental studies, they also concluded that the anvil force could be reduced by using a more compliant outer shell in combination with a lower density (less stiff) protective padding. Test standards for crash helmets require a double impact and a penetration test (Appendix A), which leads to the use of a stiff outer shell and protective padding. If these requirements would be dropped, helmet design could be improved according to the authors. In fact, the penetration test of the ECE helmet testing standard [UN, 2000] was deleted in 1995.
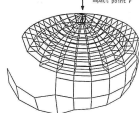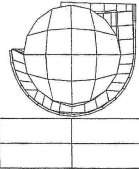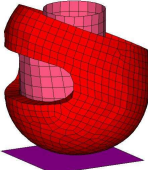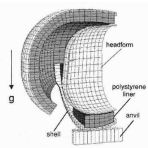
Köstner & Stöcker [1987] developed a lumped parameter model using the transfer matrix method [Fahlbusch, 1984]. They found that an increase of the protective padding liner density and the thickness of the shell leads to an increase of headform acceleration. An increase in the thickness of the protective padding liner had only a minor reducing effect on the headform acceleration.

The major disadvantage of lumped mass models is that they often involve far-reaching geometrical model assumptions and are therefore not suitable for quantitative studies. Furthermore, they are only capable of describing deformation for one specified loading direction, requiring a recalibration of the model parameters for each impact configuration.

Finite Element models

Finite Element models are far more computational expensive than lumped mass models and are therefore less appropriate for extensive parameter studies. Furthermore, the construction of the models is often time consuming. However, once a 3D Finite Element model is constructed, it can be used in any impact configuration, without changing the model parameters and still yield quantitative results. Also the geometrical and material model parameters are often more accurate and easier to assess. During impact, the shape of the helmet, in particular the protective padding liner, changes, which influences the mechanical behaviour of the helmet. This effect cannot be modelled with lumped mass models. Furthermore, rotational accelerations can be computed as well. This is important because rotational accelerations may be of great influence to head injury.

Table 1.2: Comparison between Finite Element helmet models.

References	Helmet type	Materials				Impact site
		shell	protective padding	comfort padding	head	
Köstner & Stöcker [1987]	full-face	ISOLIN	ISOPLA	-		F
Yettram *et al.* [1994]	full-face	ISOLIN	ISOPLA	-	solid	T
Brands *et al.* [1997]	full-face	ISOLIN	ISOPLA	gap	rigid	T, F, R
Chang *et al.* [2000]	full-face	ISOPLA	FOAM	-	rigid	C

ISOLIN = isotropic, linear elastic; ISOPLA = isotropic, elastoplastic; FOAM = crushable foam
T = top impact; F = frontal impact; R = rear impact; C = chin impact

Several Finite Element models of a motorcycle helmet were found in literature [e.g.: Köstner & Stöcker, 1987; Yettram *et al.*, 1994; Brands *et al.*, 1997; Chang *et al.*, 2000]. All studies modelled the outer shell and the protective padding liner, but none of them took into account the effect of the soft comfort liner, that provides the fit of the helmet on the head. Only the models of Brands *et al.* and Chang *et al.* were validated with experimental data. Table 1.2 gives an overview of the Finite Element helmet models and what impact sites were investigated.

Köstner & Stöcker [1987] varied shell thickness, padding thickness, padding density and impact energy in simulations of top impact. From their simulations resulted the following:

- maximum head acceleration increases with increasing shell thickness,

- maximum head acceleration increases with increasing padding density,

- maximum head acceleration decreases slightly with increasing padding thickness,

- maximum head acceleration increases with increasing impact energy.

To reduce the effect of impact energy on head acceleration, they found that paddings with an ideally

plastic material behaviour should be used, which, combined with a rigid shell, should ensure constancy of acceleration over a wide range of impact energy levels.

Yettram *et al.* [1994] only varied shell stiffness (thickness 4 mm) and protective padding liner density (thickness 25 mm) in their simulations. They used measured stress-strain-curves of EPS foam to characterize the material properties of the protective padding liner. They also performed calculations using a 'theoretical material', a hypothetical material with a very low density and stiffness. From their calculations, they computed peak accelerations and HIC values. Although the authors recognise that this model does not represent an existing crash helmet because of its simplified geometry — and thus the numerical values of peak acceleration and HIC should not be considered in relation to any values specified in relation to injury — the trends that emerge do correspond to those found in experimental investigations [e.g.: Beusenberg & Happee, 1993; Hopes & Chinn, 1989]. These trends confirm that for optimal head protection (i.e. low peak acceleration and HIC), the shell should be more compliant and the liner less dense than is currently the case.

Brands *et al.* [1997] conducted a parametric study as well as a model validation using experimental data from drop tests. The material parameters of the protective padding were used to tune the model to match the drop test experiments. The results from their parametric study (top impact) showed that the impact load is applied on the headform via two mechanisms: crushing the protective padding liner and vibrations of the outer shell. These findings are confirmed by previously discussed studies of Gilchrist & Mills [1993] and Beusenberg & Happee [1993]. Brands *et al.* [1997] also found that the material behaviour of the protective padding liner has a significant influence on the energy absorption of the helmet, however they noted that they were not able to use a correct material model for this component. They used an isotropic, elastoplastic material model which is incompressible during yielding, whereas EPS foam has Poisson ratio zero.

Brands *et al.* [1997] also validated their model for side and frontal impact, with reasonable results. However, the material properties of the protective padding liner in the real helmet on which their model was based, are not constant over the helmet and the authors think that modelling the helmet accordingly could improve the results. Furthermore, they concluded that modelling the comfort liner could also further improve the helmet model.

Most numerical studies, both lumped mass and Finite element studies, as well as most experimental studies found that protective padding liner density as well as outer shell stiffness should be reduced in order to reduce the magnitude and duration of the resultant acceleration of the head. Obviously, there is a limit in reducing the helmet's stiffness, with respect to the protective capacities of the helmet considering unchanged geometrical properties, however none of the studies report on this.

1.3.3   Experimental Studies with Modified Drop Tests

Many researchers question whether the standard headform used in standard drop tests represents the human head/body correctly. Vincze-Pap & Áfra [2001] performed a comparative laboratory drop test series on helmets, which were carried out with a sitting type Hybrid III whole body, a Hybrid III head-neck unit and the standard Mg-alloy headform. They only considered translational accelerations of the headform's centre of gravity. The lowest resultant accelerations were measured with the whole body drop tests. The standard headform yielded the highest resultant accelerations. The authors conclude from this that during a real accident the impact force acting onto the head is transmitted by the neck to the body resulting in a lower resultant acceleration of the headform's centre of gravity. Furthermore, the head's rebound was significantly less and the head's rotational motion was significantly higher in
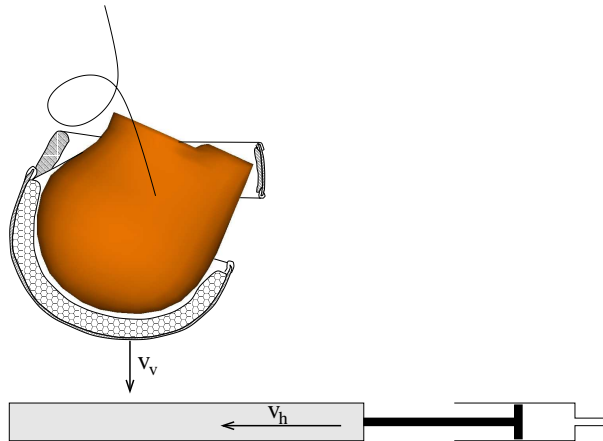
Figure 1.8: Oblique test setup, used by Halldin *et al.* [2001]. V_h is the horizontal plate velocity and V_v is the perpendicular impact velocity.

the whole body drop tests than in the drop tests with the standard headform and the head-neck unit. This indicates a transformation of translational kinetic energy into rotational kinetic energy instead of an absorption of kinetic energy. The head's rotational motion was observed from images which were recorded during the drop tests. This rotational motion was not quantified.

Willinger *et al.* [2001] used helmeted head drop tests, using the Bi-mass 150 headform (see Section 1.2.3), and reconstructed real motorcycle accident data [Chinn *et al.*, 1999] as input for FE calculations with the Bi-mass 150 headform. They found a correlation between the computed maximum values of the brain-skull relative acceleration and the AIS value of the victim from the real accident. It should be noted, that the graphical representation of this correlation showed a group of data-points with one data-point away from this group, which could unjustifiably increase the already poor correlation factor (R^2=0.54). The authors also found a correlation between brain rotational acceleration and concussion, and between relative skull-brain motion and subdural haematoma, but these correlations were not quantified.

Halldin *et al.* [2001] also recognise rotational accelerations to be a major cause for head injury in motorcycle accidents, in particular subdural haematoma (SDH) and diffuse axonal injury (DAI). Since oblique impacts, with a significant tangential force on the helmet, are more common than radial (normal) impacts [Otte *et al.*, 1999], they developed an oblique test procedure to assess the helmet's ability to reduce rotational acceleration of the head during impact. In this test, a free falling helmeted headform impacts a horizontally moving steel plate covered with grinding paper (Figure 1.8).

They tested one helmet type with three different interfaces between outer shell and protective padding liner:

- In the 'BONDED' helmet, the outer shell and the protective padding liner were glued together;

- In the 'FREE' helmet, the outer shell and the protective padding liner were only held together by a flexible joint at the bottom edge. No countermeasures for reducing the friction, between outer shell and protective padding, were taken;

- In the Multi-direction Impact Protection System (MIPS) helmet, which was designed to reduce the head's rotational acceleration, a low-friction Teflon film is placed between the outer shell and the protective padding liner.

The MIPS helmet reduced the peak rotational acceleration significantly (up to 50%) in all oblique tests, compared to the FREE and the BONDED helmets. Furthermore, the presence of a horizontal plate velocity, for tests with the same perpendicular impact velocity, reduced the peak translational acceleration for the FREE and MIPS helmets slightly. It should be noted that the comfort foam was removed from the helmet. This may have influenced the results significantly, since one of the functions of the comfort foam is to provide a better fit, which is believed to be especially important in oblique impacts.

1.4   Problem and Objective

The foregoing has shown that many researchers have investigated the performance of motorcycle helmets and have tried to find ways to improve helmet performance on the basis of various criteria. It is suggested that helmets, in particular the protective padding liner, should be made softer to reduce the risk of (severe) head injury. These conclusions are drawn from experimental as well as numerical studies of standard drop tests in which only (functions derived from) translational accelerations are considered.

Over the years, helmet standards have evolved to be an effective means to assure helmet quality in terms of minimal performance. In general, helmet testing standards are the result of often rather pragmatic compromises in meetings of technical experts, more than scientific research. As helmet quality improved, the criteria of shock absorption tests were raised and impact severities were increased. This strategy has resulted in helmets that reduce the chances of a fatal accident up to 57% [Hurt Jr. *et al.*, 1981].

The shock absorption test of the ECE Regulation 22 (ECE-R.22) will be the focal point of this thesis. In this test, the **load** onto the helmeted head is generated by dropping a helmeted headform, instrumented with a triaxial accelerometer, onto an anvil at a velocity 7.5 m/s. The helmet quality is **assessed** by measuring the acceleration time history of the headform during the impact and is expressed in terms of the injury parameters: *maximum resultant translational headform acceleration* ($a_{\max}$) and *Head Injury Criterion* (HIC). The HIC is currently the leading head injury parameter in automotive research, however the ECE standard is still the only helmet standard that has implemented it in its shock absorption test. The **head model** used in this test, is an aluminium, "rigid" headform. Compared to the first issue of the BS 1869:1952, the application of the **load** on the head and the **assessment** of injury have greatly improved in the ECE-R.22. The **headform** has remained essentially unchanged.

1.4.1   Problem: Limitations of the Current Shock Absorption Tests for Motorcycle Helmets

The shock absorption test of the ECE-R.22 has two main limitations with respect to injury assessment. The first concerns the choice of the headform in the test method. The progress in finite element modelling of the head and brain as we see today allows more detailed analyses of injury mechanisms associated with different types of head injury. As a result, more attention is being given to strain- and stress-based head injury criteria. Application of such criteria for helmet assessment is impossible with a rigid headform, as it requires skull and brain deformations to occur in order to properly mimic helmet-head interactions as well as brain deformations. Furthermore, the use of accelerations assessed with rigid headforms to drive FE models of the head could be inadequate due to improper helmet-head interaction.

The second limitation of current shock absorption tests concerns the measurement of the injury parameters. The injury parameters a_{max} and HIC are subject to criticism and may not be adequate or sufficient parameters to predict injury, since they are both based on translational acceleration only (see Section 1.2.2). This ignores the fact that in reality almost always external load results in both translational and rotational head accelerations, and both determine the total deformation pattern of the brain. In addition, the effects of rotational acceleration are believed to be the main cause for specific types of traumatic brain injury, such as DAI and (A)SDH [Adams *et al.*, 1983; Gennarelli *et al.*, 1987; Holbourn, 1945]. The ECE-R.22 shock absorption test allows for rotation of the headform during impact, but rotational accelerations are not measured. Whereas the ECE-R.22 shock absorption test represents a free-fall in which rotational head accelerations could be assessed, the projection-and-friction-test calls for measuring tangential force on the helmet as measured on the anvil. The rationale for measuring this tangential load appears to be more a design restrictive requirement for crash helmets related to external projections, rather than having a biomechanical basis to assess risk of injury related to brain deformations.

1.4.2 Objective: Improving Helmet Design by Advanced Shock Absorption Assessment

A better understanding on how the application of different head injury criteria in the shock absorption tests effects helmet design, is expected to help the process of adopting progressions in the field of biomechanics into helmet safety standards. This should ultimately improve head protection offered to motorcyclists. To date, however, little has been done to explore how helmet designs may change as a result of applying these different criteria. This thesis deals specifically with the question:

How could motorcycle helmet designs change as a result of applying new and different head injury criteria in the shock absorption test of ECE-R.22?

To implement these criteria in these tests, more quantitative data must be available from the drop test, like rotational accelerations and strains inside the brain. This requires an anatomically more detailed headform or at least a numerical model of such a headform. This holds especially for the strain-based injury criteria, since strains cannot be assessed using a conventional, rigid headform. Furthermore, the interaction between headform and helmet is likely to influence the outcome of the test. To better model the head-helmet interaction, the headform must at least have a deformable skull and brain. This reasoning leads to the following objectives of this study:

- Developing an anatomically more detailed, deformable headform that will allow more realistic helmet-head interaction and will allow the assessment of helmet performance using more and different types of head injury criteria, compared to the standard ECE-R.22 rigid magnesium alloy headform.

- Studying the effects of the anatomically more detailed headform on helmet-head interactions and assessment of head injury risk in the shock absorption test of ECE-R.22 in terms of the currently applied head injury criteria (a_{max} and HIC).

- Develop guidelines for changing crash helmet design to integrate the effects as described above.

- Studying if and how the use of other (e.g. strain-based) injury criteria in the shock absorption test has additional effects on helmet design compared to the use of a_{max} and HIC.

It is not the goal of this research to develop new injury criteria or to develop a new type of helmet evaluation test.
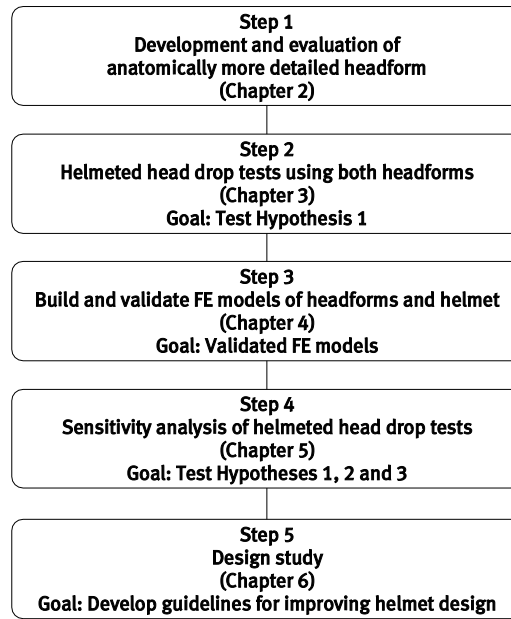
Figure 1.9: Schematic overview of the strategy of this research.

1.4.3   Hypotheses and Research Strategy

The objectives of this study as presented in Section 1.4.2 and the reasoning for requiring an anatomically more detailed headform are formulated into the following hypotheses:

1. An anatomically more detailed, deformable headform, allowing more realistic helmet-head interaction and allowing brain deformation, will provide more relevant information on helmet performance.

2. Peak acceleration ($a_{\max}$) and HIC are insufficient to quantify helmet performance. Also, rotational response should be included to assess helmet performance.

3. The application of the new headform and associated head injury criteria will lead to significant changes in helmet design.

To investigate whether to accept or reject these hypotheses, the research strategy in this thesis is based on combined experimental and numerical modelling of helmeted head impacts. The impact configuration studied is exactly as described in ECE-R.22, hence this study does not address whether or not this impact configuration is a correct and sufficient representation of head impacts in real world motorcycle accidents. The focus of this research is on improved assessment of helmet performance and its effects on helmet design. Figure 1.9 shows a schematic of the research approach. The figure also shows which hypotheses will be tested in which chapters.

Step 1: The first, and necessary, step is the development of a new, anatomically more detailed, deformable headform [Chapter 2]. A set of design and performance criteria is established on the basis of published biomechanical (post mortem human subject) data. The headform is built and evaluation experiments are conducted to establish the new headform's response characteristics.

Step 2: An experimental drop test program is conducted according to the shock absorption test of ECE-R.22 on a series of helmets with both the conventional headform and the new deformable headform [Chapter 3]. This test program incorporates:

- advanced measurement of headform responses, necessary to consider performance of the helmets in terms of several injury criteria;
- the analysis of the effects of using a deformable headform on helmet performance expressed in several criteria;
- the analysis of the differences and similarities between responses of helmets of different design (size and structure).

Step 2 specifically addresses Hypothesis 1.

Step 3: Finite Element models of the helmet, the conventional headform and the anatomically more detailed headform are built and validated using data from Step 1 and 2 [Chapter 4]. Finite Element simulations enable the computation of field parameters like deformations and stresses inside the helmet and head. This enables the use of injury criteria that can not currently be evaluated in experiments.

Step 4: A sensitivity analysis shows how the values for the different injury criteria will change as a result of changes in helmet design [Chapter 5]. Differences in sensitivity between drop tests with the conventional headform and the anatomically more detailed headform will be explored. This step addresses all three hypotheses.

Step 5: Finally, results from this research are used to try and develop guidelines for improving the helmet design and for improving the headforms used in helmet certification tests [Chapter 6].

This thesis will be concluded with an overview of the conclusions with respect to the objectives and hypotheses, and with recommendations on how to proceed in future research based on the conclusions and limitations of this research [Chapter 7].

Chapter 2

The Deformable Headform

2.1 Introduction

Current crash helmet drop tests can only predict the protective capacity of a crash helmet in a limited way. It is hypothesised that the use of a rigid headform does not model the dynamics of the real, flexible human head correctly. Saczalski *et al.* [1976] compared helmeted head impacts using the conventional rigid headform and a "human-responding" headform and found that unrealistic (rigid) headforms can not properly evaluate the protective capacities of a helmet.

An anatomically more detailed, deformable headform will probably be more sensitive to parameters that predict injury risk. In contrast to the conventional headform, it can also be made sensitive to the latest, strain-based head injury criteria, related to SDH and DAI, when designed accordingly. Thus, it is to be expected that such a headform predicts more types of head injury more reliably.

The way in which the headform can predict head injury depends not only on the design of the headform, but also on the measurement taken. Currently, only translational accelerations of the headform are measured, which is insufficient to predict various types of head injury. Translational accelerations may be a valid indicator for skull fracture and contusion, but they do not predict other types of head injury like diffuse brain injury and acute subdural haematoma. These two types of injury are believed to be closer correlated to brain deformations and rotational accelerations, respectively.

This chapter describes the development and evaluation of an anatomically more detailed, deformable headform that will allow more realistic helmet-head interaction and will allow the assessment of helmet performance using more and different types of head injury criteria, compared to the standard ECE-R.22 rigid magnesium alloy headform [UN, 2000]. Thus, the third factor in injury assessment, the load (see Chapter 1), is chosen in accordance with the drop test in ECE-R.22 and remains unchanged in this research. This drop test will be elaborated on in Chapter 3.

When developing a new dummy, in this case a headform, there are eight factors to be considered [Wismans *et al.*, 1994]: Simplicity, anthropometry, biofidelity, repeatability, reproducibility, sensitivity, durability and cost.

Simplicity (anatomical detail), anthropometry and sensitivity concern the design requirements and are discussed in Section 2.2. Biofidelity and repeatability are response requirements and are discussed in Section 2.3. Reproducibility is not tested, since only one headform is built. Since this headform is mainly developed for research purposes, the factors cost and durability are considered less important. Section 2.4 and Section 2.5 discuss the development and the biofidelity and repeatability of the resulting headform, respectively.
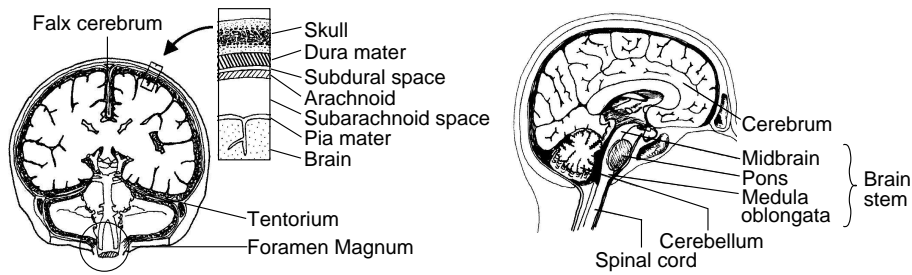
Figure 2.1: Overview of anatomical components of the head (based on Pike [1990]). *Left:* Coronal section of the meninges of the brain. *Right:* Principal parts of the brain in sagittal section.

2.2 Design Requirements for the Physical Headform

Designing a headform that diverts drastically from the standard conventional headform, will most probably not be accepted in future drop test regulations. In this study, it is therefore chosen not to build an entirely new headform, but to use the conventional headform, as defined in ECE-R.22 UN [2000], as the base of the design and increase the level of anatomical detail of that headform.

2.2.1 Anatomical Requirements

The human head is a complex structure with complex materials. The main components of the head are shown in Figure 2.1. The brain, consisting of cerebrum, cerebellum and brain stem, is a fragile soft visco-elastic material. The brain is the most important component of the head, with respect to head injury. To protect it, it is covered by a strong and stiff skull. The level of anatomical detail of the headform should correspond with the objective of the research. Too much detail makes the headform unnecessarily complex. However, the headform should be detailed enough to be able to measure the parameters of all relevant injury criteria.

Brain and Skull-Brain Interface

The most important modification of the conventional headform refers to the brain. Brain injury is found to correlate with strain and strain rate [Lee & Haut, 1989; Viano & Lövsund, 1999]. To make brain deformations measurable, the brain must be modelled as a deformable medium. It is difficult, if not impossible, to model the brain anatomically correct with respect to its geometry as well as with respect to its boundary conditions. The falx and tentorium cerebelli, the two most important meninges in the head, inhibit the movements of the brain inside the head and thus influence the dynamics of the human head as a whole. However, the falx and tentorium cerebelli are complex structures with unknown interface conditions. For practical and reproducibility considerations, the falx and tentorium cerebelli are left out of the model and the skull-brain interface is modelled as a stick condition. With respect to its geometry, the model is chosen to be hemispherical. This means it is flat on the side of the skull base. This approach has the advantage that it does not bring too many constructional problems. It is recognised that the various simplifications may have a significant influence on the outcome of the drop tests. This type of geometrical simplification is also used in the NHTSA Finite Element model [Bandak & Eppinger, 1994].

The brain model material should mimic the dynamic material properties of the human brain. The mechanical properties of brain tissue have been subject of many investigations [e.g.: Brands *et al.*, 1999;
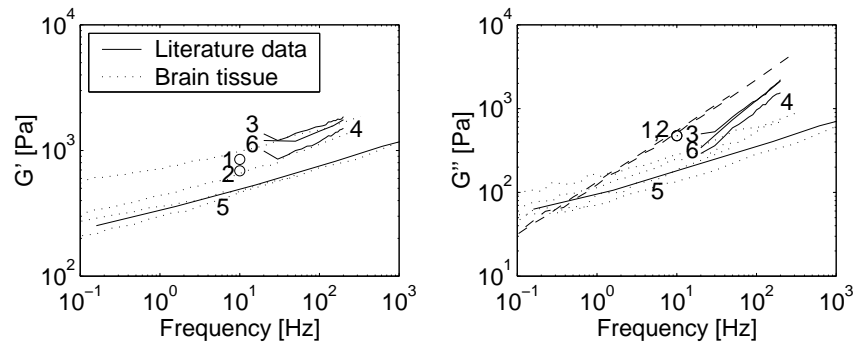
Figure 2.2: Storage modulus G' (*left*) and loss modulus G'' (*right*) of measured results (brain tissue (n=4)), and literature data (numbered): 1. human white matter[Fallenstein *et al.*, 1969], 2. human cerebrum[McElhaney *et al.*, 1972], 3. porcine brain stem [Arbogast & Margulies, 1997], 4. porcine cerebrum [Thibault & Margulies, 1996], 5. calf cerebrum [Peters *et al.*, 1997], 6. porcine cerebrum [Thibault & Margulies, 1998]. (Figure extracted from Brands *et al.* [1999])

Fallenstein *et al.*, 1969; McElhaney *et al.*, 1972; Arbogast & Margulies, 1997; Thibault & Margulies, 1996; Peters *et al.*, 1997; Thibault & Margulies, 1998]. Brands *et al.* [1999] compared their results with those reported by others (Figure 2.2). Furthermore, the density of the model material should be close to 1.04 kg/m^3, the average density of brain tissue. Since the human brain has a complex structure as well as material properties, it is difficult to synthesize such a material. Therefore, it is also hard to give tolerance criteria on the material properties of the brain model material.

The ECE-R.22, uses five headform sizes with a head circumference ranging from 500 mm to 620 mm. In this research, a headform of size M (head circumference: 600 mm) is chosen, since it is the appropriate headform for the helmet used in this research. This headform is larger than the average human head, which has a head circumference of 572 mm and a brain volume of about 1.3 l [Blinkov & Glezer, 1968]. The desired brain volume of the headform should be scaled accordingly, to realistically mimic inertial effects. However, data on brain volume in relation to head size was not found in literature. In order to find an indication on the brain volume of a head this size, the HUMOS head model [Thollon *et al.*, 2002] is scaled to a head circumference of 600 mm. The HUMOS model is a Finite Element model of a 50th percentile male human, built from MRI data. It is larger than the average human head, yet smaller than the headform in this study. Scaling the head model to a head circumference of 600 mm results in a brain volume of 1700 ml.

Skull

The cranial skull should be modelled as a deformable medium, since deformations to the cranial skull can influence the head helmet interaction significantly [Gilchrist & Mills, 1993]. The thickness of the human cranial skull is 6.91±1.19 mm and Young's modulus of cranial bone is 5.6±3 GPa [McElhaney *et al.*, 1970]. The skull design of the headform of ECE-R.22 may not be very humanlike in the chin area , however it is left uncompromised, since the injury mechanisms due to chin impact are not well understood and injury parameters are not available.

Table 2.1: Desired principal moments of inertia of the physical head model and their orientations.

I_{xx} [kg·cm^2]	I_{yy} [kg·cm^2]	I_{zz} [kg·cm^2]
317	316	197
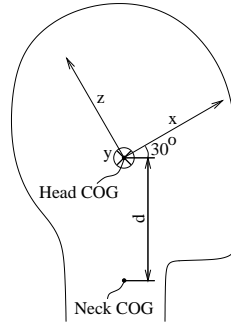
Scalp

The scalp consists of several layers of soft tissue covering the skull. Including the scalp into the model would jeopardise the reproducibility of the headform. Not only is it difficult to find a correct model material, but including the scalp in the model would also change the design of the headform drastically, and thus divert too much from the conventional headform. Therefore, the scalp is not included in the model. Furthermore, it is expected that the scalp is of little influence in helmeted head impact. This will be elaborated on in Section 2.5.2.

2.2.2 Anthropometry

Inertial Properties

The ECE regulations have no requirements as to the moments of inertia of the head model. However, since this research also discusses rotational injury parameters, the need for a correct modelling of the moments of inertia is obvious. Average inertial properties of the human head are published by Chandler [1975]. The mass of the size M headform is 5.60±0.15 kg, according to ECE-R.22, which is 1.5 kg heavier than the average human head. This is not only due to its larger size, but also due to the fact that the headform includes the neck. Therefore, the values for the moments of inertia of the average human head need to be scaled to the correct size, and the influence of the neck on these values has to be accounted for. The scaling method and the adding of the neck is elaborated on in Appendix C. The results are shown in Table 2.1. The moments of inertia of the newly developed headform shall deviate no more than 25 kg·cm^2. This is a rather coarse and arbitrary tolerance, based on what is practicably achievable, since the headform's moments of inertia are already largely determined by the geometry of the headform in combination with the materials used. Still, these tolerances are about half the standard deviation of the principal moments of inertia of the human head (50 kg·cm^2, [Chandler, 1975]). The principal moments of inertia I_{xx}, I_{yy} and I_{zz} of the size M conventional headform are 370, 440 and 300 kg·cm^2, respectively[1], which deviate up to 50% from the desired values.

---

[1]These values are computed using an already existing model in MADYMO of the conventional headform, that is based on the ECE-R.22 requirements on mass, outer geometry and material,.

Geometry

Of course the most detailed geometry of the headform would yield the most biofidelic results, and thus result in a highly sensitive headform. However, the human head shows great biodiversity. Furthermore, a detailed outer geometry may be hard to manufacture and jeopardises reproducibility and repeatability. Therefore, the outer geometry remains unchanged with respect to the conventional headform as defined in ECE-R.22. This includes the neck, which is rigidly attached to the head.

2.2.3 Instrumentation

A new dummy should be sensitive to parameters that directly relate to injury mechanisms. In Section 1.2.2, three types of injury criteria, that are considered to relate to various injury mechanisms, were discussed: translational acceleration based, combined translational and rotational acceleration based, and stress and strain based injury criteria. To evaluate all three types, translational and rotational accelerations must be measured as well as brain deformations.

Headform accelerations are measured at the headform's centre of gravity using a triaxial accelerometer (Entran Devices, model EGCS3-A). Each acceleration signal is filtered with a CFC 1000 filter.

Three angular rate sensors (ATA Sensors, model ARS01) are mounted at the headform's centre of gravity to measure the rotational velocity ω of the headform. The axes of the three angular rate sensors coincide with the three axes of the triaxial accelerometer. The rotational velocity is filtered with a CFC 1000 filter. Differentiation of the rotational velocity yields the rotational acceleration α.

Measuring the brain deformations during helmeted head impact is not trivial. In fact, the only viable way to measure those, is by tracking radiopaque markers inside the brain using high-speed X-rays. Therefore, the skull and brain model materials must be chosen such that markers inside the brain can be detected using X-ray technique. Section 3.2.1 elaborates on how these markers are visualised.

2.3 Response Requirements

2.3.1 Biofidelity

When the headmodel meets all the anthropometry requirements, it does not mean that it represents the human head sufficiently well. To investigate whether the physical head model is really biofidelic (i.e. sufficiently mimics the dynamics of the human head in impact situations), it has to be evaluated on the basis of biological experiments found in literature. Several researchers investigated the mechanical response of cadaver heads. The most relevant studies are discussed below.

Impulse Tests

The resonance frequencies of human cadaver heads are reported in literature [e.g.: Hodgson *et al.*, 1967; Hodgson & Patrick, 1968]. Design requirements for the resonance frequencies of the headform based on these studies are shown in Table 2.2. Considering the large biological spread in human skull stiffness and thickness (see Section 2.2.1), the maximum tolerable deviation from these resonance frequencies is set at 100 Hz. In the present study, the resonance frequencies of the headform will be determined using impulse tests.

Table 2.2: Resonance frequency requirements for the head model for different impact directions, based on the work of Hodgson & Thomas [1975].

Impact direction	Resonance frequency
Frontal	360 ± 100 Hz
Side Parietal	450 ± 100 Hz
Top Parietal	300 ± 100 Hz

Hodgson Test

The European Enhanced Vehicle-safety Committee [EEVC, 1999] has reviewed several drop and impactor tests in relation to appropriateness for defining side impact dummy biomechanical targets. They found that Hodgson & Thomas [1975] performed tests with sample size and energy level appropriate to be used for definition of a side impact head performance requirement. These tests involve a 200 mm head only drop test on a rigid horizontal surface (impact velocity: 1.98 m/s). The head is positioned so that its a-p axis is horizontal and its mid-sagittal plane makes an angle of 35° with the impact surface. The head is dropped using a quick-release mechanism. During impact, head peak resultant acceleration of the head model must be between 100 g and 150 g, with g the gravitational acceleration (9.81 m/s^2). This experiment will be further referred to as the Hodgson test.

Other Tests

Nahum *et al.* [1977] and Hodgson *et al.* [1972] also reported evaluation experiments for biofidelity testing. However, these could not be used to validate the headform. For the sake of completeness, these experiments will be discussed as well as the reason why they could not be used in the research:

Nahum *et al.* [1977] performed two series of blunt head impacts on stationary unembalmed human cadavers. They used a rigid impactor covered with a variety of padding materials to provide a means of altering the duration of load application. Unfortunately, they did not mention padding thickness and density, which plays a crucial role when these experiments are to be used for evaluation purposes.

Hodgson *et al.* [1972] developed a physical head model for use in evaluation of impact attenuation properties of football helmets. They evaluated their head model in helmeted cadaver head experiments. They reproduced these experiments with their head model, so that evaluation experiments exactly matched the cadaver experiments. However, the type of helmet used in their experiments is no longer available. The influence of a different type of helmet on the outcome of the experiments could be quite drastic. Due to these uncertainties, these experiments can not be used to properly evaluate the physical head model.

2.3.2 Repeatability

The quality of a physical model depends on the repeatability of its behaviour. If a certain drop test is performed twice using the same headform, the results should not differ too much. A repeatability error of 5% (peak values) is generally accepted in automotive impact safety tests. The repeatability of the headform will be tested by comparing maximum resultant headform acceleration during consecutive

Hodgson tests. The Hodgson test is well defined and the magnitude of the load is comparable to the load in helmeted head impacts, which makes the test suitable for repeatability testing.

2.4 Design of the New Headform

2.4.1 Brain and Skull-Brain Interface

As a brain model material, the Dow Corning Sylgard 527 A&B dielectric silicone gel is used. This material models the dynamic properties of brain tissue in a sufficient manner [Brands *et al.*, 1999]. It resembles brain tissue at low frequencies, but becomes stiffer and more viscous at higher frequencies. Using this material as a brain model material limits the evaluation of brain deformations during impact to a qualitative rather than a quantitative evaluation. Despite this disadvantage, this material is still one of the best and most widely applied brain model materials [e.g.: Viano *et al.*, 1997; Ivarson *et al.*, 2000]. Furthermore, the gel is very adhesive. This means the boundary conditions between the brain and the skull are well defined (no-slip condition), which means it can easily be modelled numerically. A disadvantage is that the cerebrospinal fluid (CSF) can not be modelled without using a lubricant.

During the helmeted head drop tests, brain deformations are measured using a bi-plane X-ray setup. Therefore, spherical markers are put inside the gel. The size and density of the markers should be large enough to be recorded, yet small enough not to disturb the brain deformations. Markers that are too small get overradiated by the high intensity of the radiation and leave no shade on the image intensifiers. On the other hand, markers that are too large are too heavy and thus disturb the brain deformations too much. Steel spherical markers of 4 mm diameter are a good compromise between visibility and low weight.

2.4.2 Skull

To model the dynamic properties of cranial bone correctly, a composite material is chosen. Composites are fiber reinforced polymers or resins. These materials are known for their strength in combination with low weight, much like bone material. The stiffness of the material can be adjusted by varying the fiber volume fraction. More fibers result in a stiffer material. Using composite theory [Peijs, 1998], a polyester resin with a glass fiber volume fraction of 0.15 yields a composite with a Young's modulus of 5.6 GPa. In Section 4.2.2 static skull compression experiments are compared with Finite Element simulations to validate the composite's stiffness.

For the lower part of the skull, the requirements on the stiffness are less strict, because in helmet crash tests this part of the head is not impacted. This part is made of Poly-Oxy-Methylene (POM). The outer geometry is in conformity with the ECE regulations. The internal structure can be milled to adjust the inertial properties of the total head model and to provide space for the placement of the sensors. A numerical model of the physical headform is used for tuning the inertial properties of the headform (see Section 4.2).

The composite cranial skull model is glued to the POM part of the head, after sanding the connecting surfaces, using a two component epoxy adhesive (Bison ™Epoxy Metal). This provides a liquid tight connection between the two components and thus prevents the gel from squeezing out of the cranial vault during impact. Furthermore, stresses are equally distributed over the glued surfaces, which reduces the chance of failure.
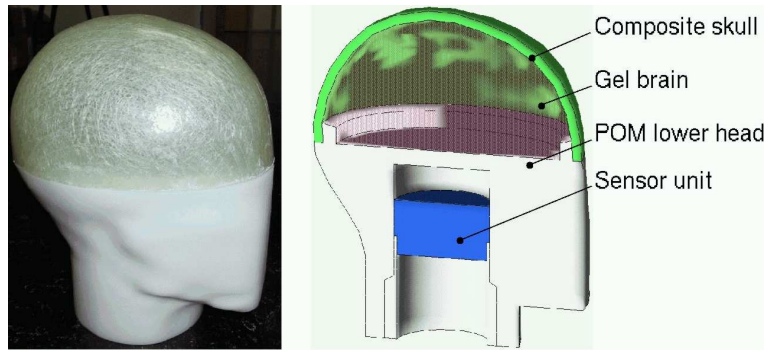
Figure 2.3: Anatomically improved headform. *Left:* Picture. *Right:* Schematic cross-section.

Table 2.3: Principal moments of inertia of the physical head model.

	Mass [kg]	I_{xx} [kg·cm^2]	I_{yy} [kg·cm^2]	I_{zz} [kg·cm^2]
Physical model	5.61	286	338	209
Requirements	5.6±0.15	317±25	316±25	197±25

2.5   Testing the New Headform

The complete headform was built by turning the composite skull upside-down and filling it partly with the silicone gel. After the gel has hardened sufficiently, 4 mm steel spherical markers were placed on the gel. After that the head was filled a little more with the gel and another set of markers was placed on the hardened gel. This process was repeated until the cranial cavity was almost completely filled. Then, the milled POM lower part of the headform was glued onto the composite skull. After the composite skull is firmly attached to the lower part of the head, the cranial cavity is filled up with the gel through a hole in the skull base. Through this hole, air can escape while the gel is hardening out. This prevents air inclusions in the gel. When the gel is fully hardened, the hole in the skull base is closed using a bolt. Figure 2.3 shows a picture and a schematic cross-section of the completely assembled anatomically improved headform. In this section, it is investigated whether it meets the design criteria.

2.5.1   Anthropometry

The mass of the physical model is 5.61 kg, which was measured on an electronic scale. This result is within the required range of 5.6 ±0.15 kg. The principal moments of inertia were computed using a numerical model of the headform (see Section 4.2). The results of this computation are compared to the requirements in Table 2.3. The results are within the range of the requirements, except for I_{xx} which is 2% lower than the minimum required value. This will not interfere with the results, since rotational accelerations around the x-axis are negligible in the impact configurations considered in this research.
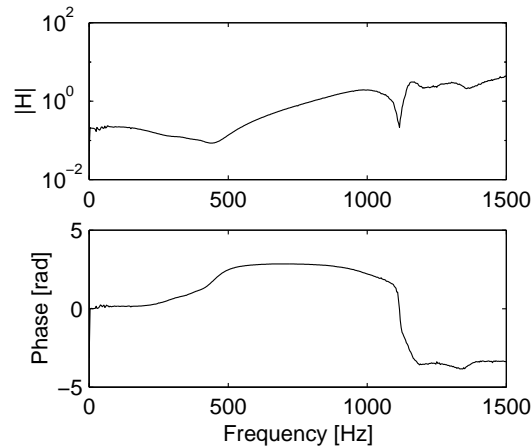
Figure 2.4: Frequency response function of the head model in frontal impact.

Table 2.4: Anti-resonance frequencies of the head model different impact directions.

Impact direction	Experiment	Literature
Frontal	440 Hz	360 Hz
Side Parietal	350 Hz	450 Hz
Top Parietal	330 Hz	300 Hz

2.5.2 Biofidelity

Impulse Test

The resonance frequency of the head model was determined from the frequency response function (FRF). The FRF was measured with a standard impulse test method, where the acceleration was measured near the point of impact, and computed with DIFA data acquisition software (DSA200). This software has a built-in anti-aliasing filter (-90 dB). A PCB piezoelectric impact hammer (model 208A05) was used in combination with a Kistler piezoelectric force transducer (model 8704B50). The results of the impulse test for frontal impact are depicted in Figure 2.4. The figure shows an antiresonance at a frequency of about 440 Hz. The antiresonance shows that the resonance mode has a node at the measured location. Other impact locations were also measured and compared with the literature data. The results are summarised in Table 2.4. Considering the large differences in human skull stiffness and thickness [McElhaney *et al.*, 1970], the differences between experiments and literature data [Hodgson & Thomas, 1975; Hodgson *et al.*, 1967] are considered acceptable.

Hodgson Test

The head model does not contain a scalp, because it is expected to be of little influence in helmeted head impact. In the Hodgson test evaluation experiments, there is direct hard-surface contact, on which the scalp most probably is of influence. Therefore, the influence of the scalp was accounted for by using a padding on the anvil. The most widely used skin substitute material in dummy heads for
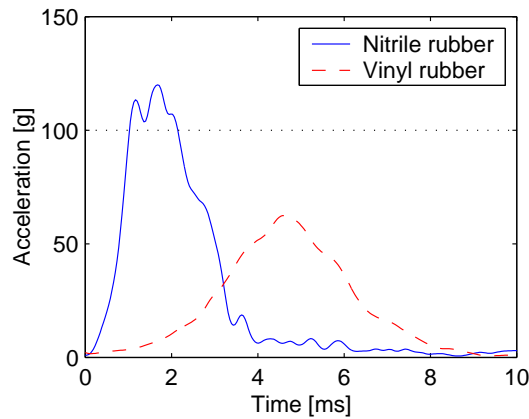
Figure 2.5: Resultant translational head acceleration resulting from the Hodgson test.

hard contact is vinyl rubber. The Hybrid III dummy head, currently the most widely applied dummy head in the automotive environment, uses such a skin substitute. The thickness of this skin is about 12 mm. Vinyl rubber is also softer than the human skin. The reason for this is that, in the Hybrid III headform, all of the flexibility of the human head is modelled in the skin. The flexible headform used in this research has a flexible skull and brain. Therefore, a stiffer, rubber skin substitute material of 12.6 mm thickness is used (Butadiene Acrylonitrile, also called nitrile rubber), in order to still meet the requirements of the Hodgson test (maximum resultant headform acceleration between 100 and 150 g).

The evaluation experiments were carried out on the same drop test setup as used for the helmeted head drop tests (Chapter 3). In Figure 2.5, the resultant translational headform acceleration during the Hodgson test, for both the nitrile rubber and the vinyl rubber, are depicted. The maximum resultant translational headform accelerations are 120 and 63 g, respectively. It is clear that in case the headform would be equipped with a vinyl rubber skin, it would be lower than the minimum required acceleration of 100 g and thus would not have passed the test. But with the rubber skin, the resultant acceleration is well within the required interval of 100-150 g.

Skin Importance

In the Hodgson drop test experiments, the maximum resultant translational head acceleration of the headform meets the requirement of the Hodgson test quite well, provided that the headform is padded with a nitrile rubber skin. To verify whether the skin is important in helmeted head impact, the Hodgson tests were repeated with Expanded Polystyrene (EPS) foam padding on the anvil, to simulate the effect of the helmet. EPS, the material of which the protective padding liner in crash helmets is made, has excellent shock absorbing capacities. Figure 2.6 shows the resultant translational head accelerations of the Hodgson tests with and without the nitrile rubber padding on the EPS foam padded anvil. The figure shows hardly any difference between the drop tests with and without rubber padding, because the EPS foam (the helmet substitute) is much softer in compression than the rubber padding (the skin substitute).

The drop tests were repeated at a velocity of 7.5 m/s, the same impact velocity as in the ECE regulations. Figure 2.7 shows the results of these tests on an EPS-foam padded anvil, with and without the rubber skin substitute. The tests were repeated on three different densities of EPS foam: 20, 30 and 50 kg/m^3, respectively. The test on the 30 kg/m^3 and the 50 kg/m^3 EPS foam, are similar in shape and size. The
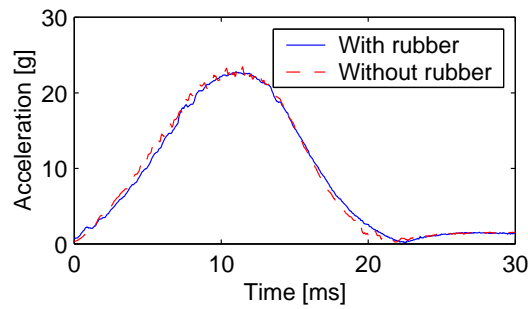
Figure 2.6: Comparison of the Hodgson tests with and without the nitrile rubber padding on an EPS foam padded anvil.
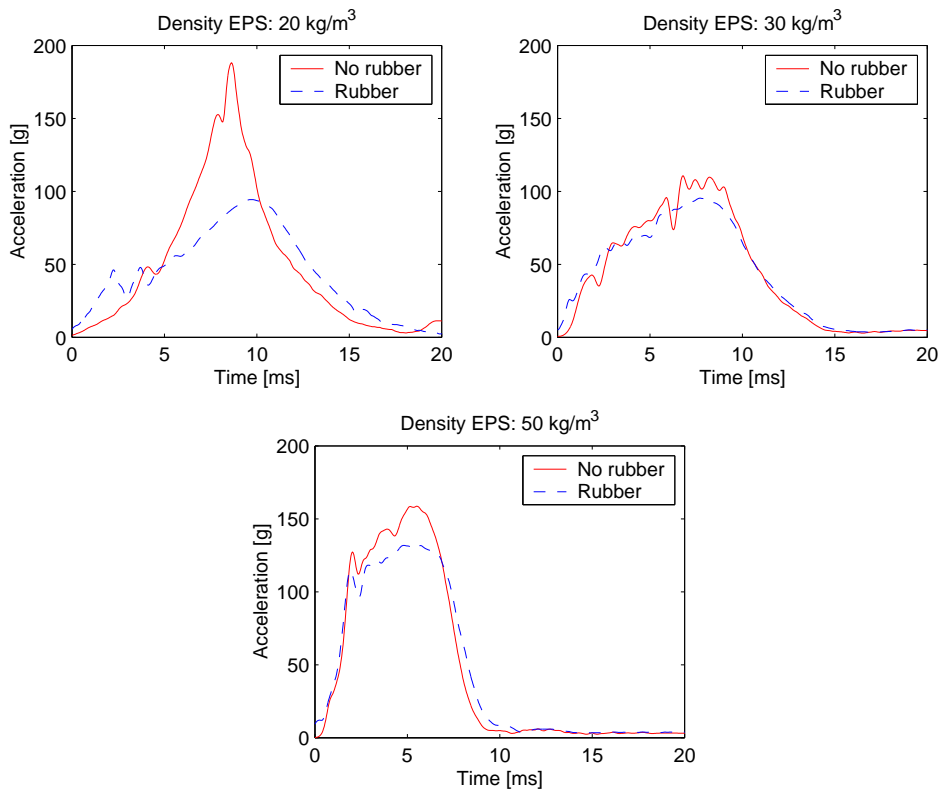
Figure 2.7: Comparison of the Hodgson tests at 7.5 m/s, with and without the nitrile rubber padding on an EPS-foam padded anvil.

maximum difference between the experiments without the rubber skin and those with the rubber skin are 14% and 17% for the tests on the 30 kg/m^3 and the 50 kg/m^3 EPS foam, respectively. However, the test on the 20 kg/m^3 EPS foam shows a different result, especially the experiment without the rubber. This is due to the bottoming-out of the EPS foam. Bottoming-out is a typical phenomenon which occurs when a foam is compressed beyond its energy absorbing capacity. During bottoming-out, the load increases rapidly upon increasing deformation. This phenomenon will be further explained in Chapter 3. A good helmet will not bottom out within the range of loads for which it was designed,
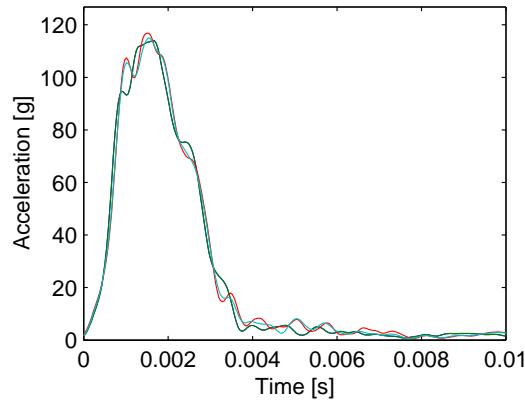
Figure 2.8: Resultant translational head acceleration resulting from four successive Hodgson tests.

since this would increase the load on the head dramatically, which is unacceptable. Therefore, it can be stated from the results in Figure 2.7 that the skin is of little importance in helmeted head impact as long as no bottoming-out occurs in the protective padding liner of the helmet. However, as long as no helmeted head tests are actually conducted, this result is inconclusive. Therefore, the effect of the skin in helmeted head impact will be further elaborated on in Chapter 5.

2.5.3   Repeatability

Figure 2.8 shows the results from four successive Hodgson tests. The figure shows that the headform shows a good repeatability. At the maximum, the average deviation is less than 2%, which is well within the requirement of 5%. This provides confidence for performing and comparing multiple helmeted head drop tests.

2.6   Discussion

An anatomically improved physical headform for use in helmeted head drop tests is developed according to selected biomechanical requirements and is evaluated against these requirements. The moments of inertia of the physical headform are well within the range of the requirements. This is important when the load on the headform is eccentric, which is often the case. When the moments of inertia are too high, the rotational accelerations will be too low. In this case, less translational kinetic energy from the drop test is transformed into rotational kinetic energy, the helmet must absorb more energy, resulting in higher resultant translational head accelerations. Since the injury mechanisms for rotational and translational accelerations differ, it remains uncertain whether the magnitude of predicted injury is the same.

The dynamics of the physical headform is evaluated by means of impulse testing. For top parietal impact the antiresonance frequency of the physical head model matches the literature data very well (330 Hz vs. 300 Hz). For side parietal, frontal and especially occipital impact, the differences are somewhat larger. These regions are close to the lower part of the head, which is made of solid material (POM). Therefore, that part of the head is modelled less accurate, which is probably the cause of these differences.

The duration of helmeted head impact T is 5-10 ms. Thus, the head and the helmet experience loads at a frequency f of at least $\frac{1}{2T} = \frac{1}{2 \cdot 0.005} = 100$ Hz. This frequency is close to the antiresonance frequency of both the headform (± 300 Hz) and the helmet (90 Hz and higher [Cappon, 1997]). Since both headform and helmet are excited in their resonance frequencies, it is expected that a dynamic interaction between the two will occur. Thus the dynamics of the helmet will affect the response of the headform and vice versa.

The physical headform satisfies the criteria of the Hodgson test, provided that the headform is padded with 12 mm of nitrile rubber. Additional experiments make it plausible, but do not prove, that the skin would not be important in helmeted head impact. This statement holds as long as the protective padding liner does not bottom out. Chapter 5 will elaborate more on the importance of the skin in helmeted head impact.

The headform specifications in the impact absorption test of the ECE-R.22 are limited to head geometry, mass and location of the centre of gravity. Mass distributions (i.e. moments of inertia) are not specified. Therefore, in practice a large range of headforms are possible, including the conventional headform developed in this study. Such deviations will particularly effect the rotational motions (and consequently the rotational accelerations) of the headform. Therefore, it is recommended that the specifications for the headform are extended with mass distribubtion requirements.

The design of the headform makes it possible to measure various injury parameters, related to various injury mechanisms. Besides a_{max} and HIC, other relevant injury parameters, such as Head Impact Power and rotational headform velocity/acceleration, can be measured using this headform. Potentially, also the Cumulative Strain Damage Measure can be measured using internal visualisation techniques such as X-rays.

Chapter 3

Helmeted Head Drop Test Experiments

3.1 Introduction

In this chapter, helmeted head drop tests according to ECE-R.22 are performed and extended with measurements of rotational accelerations and brain deformations, to find an answer to the question:

Are injury criteria currently used in helmet certification tests adequate for predicting expected injury severity?

Furthermore, the interaction between head and helmet during impact is largely unknown. Therefore, this research will try to answer the question:

How are helmet fit and headform flexibility related to headform response?

The effect of helmet fit is tested using two helmets that only differ in comfort foam thickness. The comfort liner is very soft and thus absorbs little energy. Therefore, it is hypothesised here that the comfort liner has little effect on the helmet performance. The main effect on helmet performance is expected to be caused by the flexibility of the headform.

An additional goal of this chapter is to obtain validation data for the Finite Element models of the helmet and the anatomically more detailed headform (Chapter 4).

3.2 Experimental Setup

Helmeted head drop test experiments were performed on a drop tower using the conventional headform and the anatomically more detailed headform. This section discusses the drop test setup, the headforms, the helmets and the experimental protocol.

3.2.1 Drop Test Setup

The experiments were carried out on a drop test setup which meets the requirements of the European standard for energy absorption testing of helmets, ECE Regulation 22.04 [UN, 2000]. The test setup is depicted in Figure 3.1. The helmeted head is dropped onto an anvil using a guided free fall. The anvil is mounted on a rigid, vibration-free floor to prevent external vibrations from influencing the measurements.
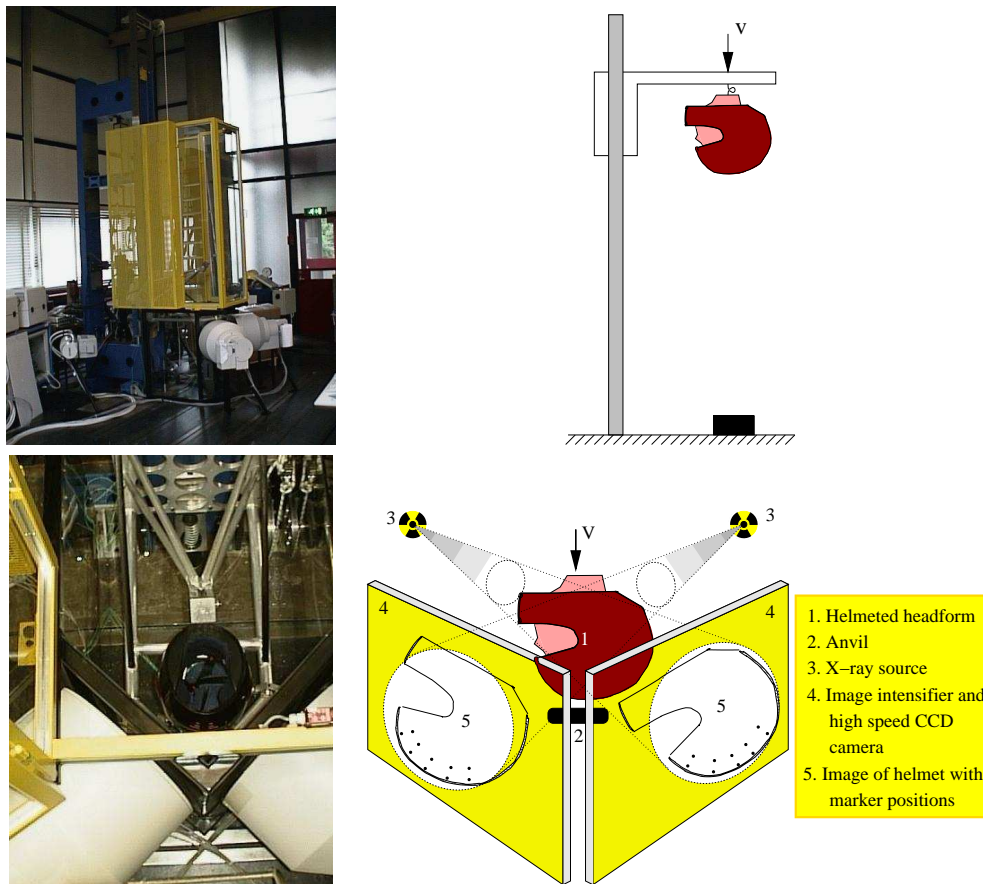
Figure 3.1: Drop test setup. *Upper left*: Photograph of overview. *Upper right*: Schematic of drop tower. *Lower left*: Top view photograph of cart with helmet. *Lower right*: Schematic of X-ray setup.

Sensors

Resultant headform accelerations are measured at the headform's centre of gravity using a triaxial accelerometer (Entran Devices, model EGCS3-A). The acceleration signals are filtered with a CFC1000 filter [ISO-6487, 2002].

Besides the triaxial accelerometer, three angular rate sensors (ATA Sensors, model ARS01) are mounted at the headform's centre of gravity to measure the rotational velocity ω of the headform. The axes of the three angular rate sensors coincide with the three axes of the triaxial accelerometer. The rotational velocity is filtered with a CFC1000 filter.

The impact velocity is measured shortly before impact using an optic sensor (MAIS-Matsushita opto sensor, model UZJ-101) and a triggering instrument attached to the cart. The optic sensor produces an on/off signal when an object approaches it. The shape of the triggering instrument causes the sensor to produce two pulses in the interval Δt as shown in Figure 3.2. The impact velocity is calculated using:

$$v = \frac{\Delta L}{\Delta t} \tag{3.1}$$

in which v is the velocity of the cart, in metres per second; Δt is the interval between two pulses, in seconds; and ΔL is the distance travelled by the cart within the interval Δt, in metres. The velocity is
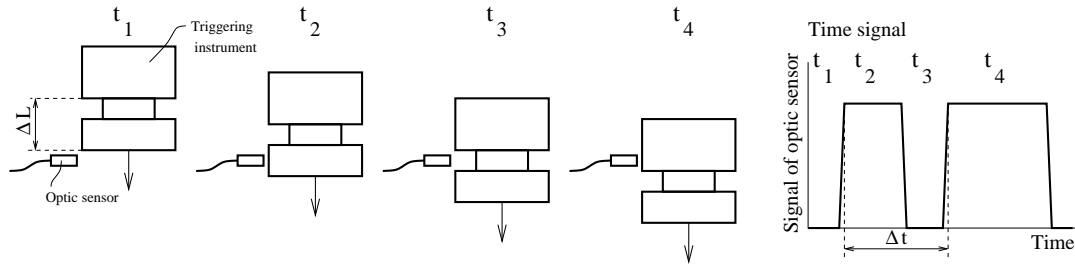
Figure 3.2: Measurement of the cart velocity
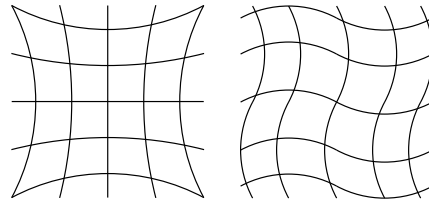
Figure 3.3: Spatial distortion in X-ray imaging. *Left*: Pincushion distortion. *Right*: Spiral distortion.

measured at a distance between 1 cm and 6 cm from the anvil surface, as required by the ECE-R.22.

The first of the two pulses is used as a trigger signal for all data acquisition. A DIFA Dynamic Signal Analyser (DSA) records the outputs of the optic sensor, the triaxial accelerometer and the three angular rate sensors with a sample frequency of 102.4 kHz. The DIFA DSA (model 230) is a high-performance PC-based data-acquisition system. DIFA's Transfer, Analysis and Control software (D-TAC 200) is used to control all the acquisition functions [DIFA, 1994].

X-ray Setup

The drop test setup is also equipped with a high-speed bi-plane X-ray setup which provides a unique means of determining the 3D deformations of the helmet and the inside of the head during impact. As discussed in Chapter 2, steel spherical markers are inserted into the brain of the deformable headform. To determine helmet deformations, steel markers are also glued to the outer shell of the helmet and inside the protective padding liner. All markers are located in the mid-sagittal plane, to facilitate the post-processing of the X-ray images. The X-ray setup consists of two Philips 38 cm image intensifiers (the white tubes in Figure 3.1) and two Philips SRO2550 ROT350 X-ray tubes which are powered by two CREOS 330 ESU generators. The bi-plane X-ray images are recorded at a rate of 1000 frames per second by two high-speed cameras: a Kodak Motion Corder Analyzer Monochrome, model SR-1000 (Unit 1) and a Kodak Ektapro HS Motion Analyser (Unit 2). Unit 1 and Unit 2 record the images at a resolution of 256×240 and 256×256 pixels, respectively.

The marker positions (in pixels) were computed from contour plots of the images using a circle fit method based on a least squares approximation. With this method, sub-pixel accuracy is obtained. However, image intensifiers introduce two types of spatial distortion: pincushion and spiral distortion (see Figure 3.3). These distortions can easily be compensated for by calibrating each unit first. This is done by generating an X-ray image of a grid of known coordinates. Figure 3.4 shows the metal grid and an X-ray image of the grid. Since both the coordinates of the markers of the metal grid (mm)
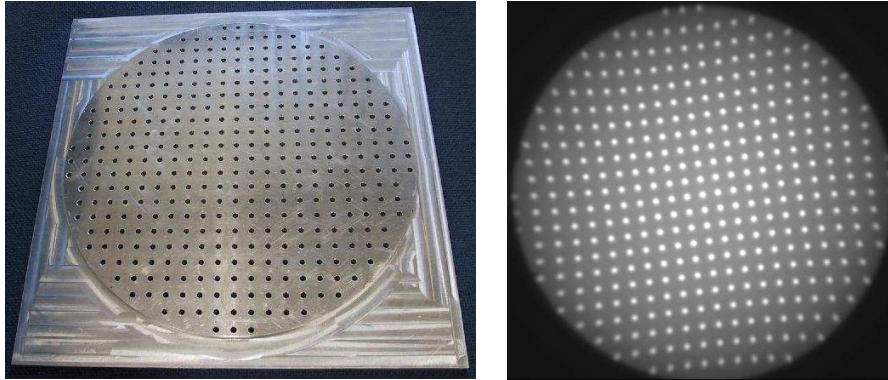
Figure 3.4: Picture (*left*) and X-ray image (*right*) of the metal grid.

Figure 3.5: Images of the headforms. *Left:* Conventional headform. *Right:* Anatomically more detailed, deformable headform.

and of the X-ray image (pixels) are known, all 2D X-ray coordinates in pixels can be transformed into 2D real coordinates in millimeters. X-ray coordinates that do not coincide with coordinates on the grid are transformed to real coordinates using linear interpolation between the four nearest marker coordinates on the grid.

The 3D coordinates of the markers are computed from the 2D coordinates in millimeters using a standard technique called *Direct Linear Transformation* (DLT) which is implemented in the KineMat Toolbox [Reinschmidt & van den Bogert, 1997] in MATLAB [MATLAB, 1999]. All markers are located in the mid-sagittal plane.

3.2.2   Headforms

Two headforms are used in this research: the conventional, rigid headform and the deformable head-form (Figure 3.5).

The conventional, rigid headform is made of polymethyl acrylate (PMA). The lowest resonance frequency of the conventional headform is higher than 3000 Hz, in agreement with the rigidity requirement of the ECE-R.22. The headform weighs 5.605 kg in agreement with ECE-R.22. The ECE-R.22

Table 3.1: Desired and realized principal moments of inertia.

	Desired	Conventional headform	Anatomically more detailed headform
I_{xx}	317 kg·cm²	283 kg·cm²	286 kg·cm²
I_{yy}	316 kg·cm²	332 kg·cm²	338 kg·cm²
I_{zz}	197 kg·cm²	219 kg·cm²	209 kg·cm²

has no requirement on the headform's rotational inertial properties. The rotational inertial properties should be close to those of the deformable headform to compare the drop tests using the conventional headform with those using the deformable headform. The inertial properties of both headforms were computed using a Finite Element model of the particular headform. Since principal moments of inertia are defined for rigid structures only, the headforms are both considered rigid in the computation. The results of the computations are given in Table 3.1, as well as the desired principal moments of inertia as presented in Chapter 2. The realized moments of inertia of the conventional headform are close to the desired ones and are within 5% of those of the anatomically more detailed headform.

The development of the anatomically more detailed, deformable headform is described in Chapter 2. In the following, this headform will be called the flexible headform.

Beusenberg & Happee [1993] found that a helmet with a fibre reinforced outer shell, such as the Arai helmet used in the current research, deforms from the inside (see Section 1.3). The performance of this helmet type is therefore expected to be influenced by the skull geometry, which changes during impact.

The flexibility of the brain is not expected to affect translational accelerations, since the brain is almost incompressible. However, it is expected to affect rotational accelerations more, since the brain has a low shear modulus and is a visco-elastic material. On the one hand, the low shear modulus will result in large shear strains. In rotational motion, this means that the brain will lag behind, resulting in lower 'effective' moments of inertia. On the other hand, the visco-elastic properties of the brain will attenuate the impact.

3.2.3 Helmets

The investigated helmet is an Arai Quantum, which has a fibre reinforced outer shell (Figure 3.6) and has a multi-density protective padding liner, which makes it interesting to investigate. Two sizes of this helmet were tested: Size M and Size L. These helmets are designed for a head circumference of 57-58 cm and 59-60 cm, respectively. They differ in comfort liner thickness, which are 12 mm and 9 mm, respectively, while outer shell and protective padding design are identical.

3.2.4 Experimental Protocol

Both helmet sizes were tested using the conventional headform and using the flexible headform. The ECE-R.22 requires tests at five points of impact, three of which are tested in this research. The points of impact are named and located as follows (for exact definition and location: see UN [2000]):

- Top impact (in the crown area),
- Front impact (in the frontal area), and
- Rear impact (in the rear area).

Figure 3.6: Picture of an Arai Quantum helmet.

Table 3.2: Number of drop tests series (n) for each configuration.

Helmet size	Headform	
	Conventional	Flexible
Size M	n=2	n=3
Size L	n=2	n=1

The ECE-R.22 also requires a side and a chin impact. The first side impact test resulted in a failure of the glued connection of the cranial skull of the flexible headform because of too high tensile stresses at the contre-coup site. Therefore, this impact site was not tested any further. In the chin area of the helmet, there is only little protective padding, which could also result in an overload of the headform. Therefore only the Top, Front and Rear impact will be discussed in this research. If a new headform is to be used in future helmet testing regulations, it should be able to withstand side and chin impact as well.

Each series of three tests was performed on a single helmet and in the order as the standard requires: firstly Front impact, then Rear impact and finally Top impact. Each new series of three impacts was performed on a new helmet without removing the helmet in between two consecutive drop tests. In total, eight series of three drop tests were performed as shown in Table 3.2. The number of available helmets was limited. Therefore, only one test on the Size L helmet using the flexible headform was performed.

Before the drop test, the helmeted headform is positioned on the cart in such a way that it will hit the anvil at the desired point of impact. The cart is then pulled up to such a height that the helmet will hit the anvil with a velocity of $7.5^{+0.15}_{-0}$ m/s, in accordance with ECE-R.22.

According to the ECE-R.22 energy absorption test, the helmets energy absorption is considered sufficient if the following criteria are met:

- The resultant translational acceleration measured at the headform's centre of gravity shall, at no time, exceed 275 g (g = 9.81 m/s^2);

- The Head Injury Criterion (HIC) shall not exceed 2400.
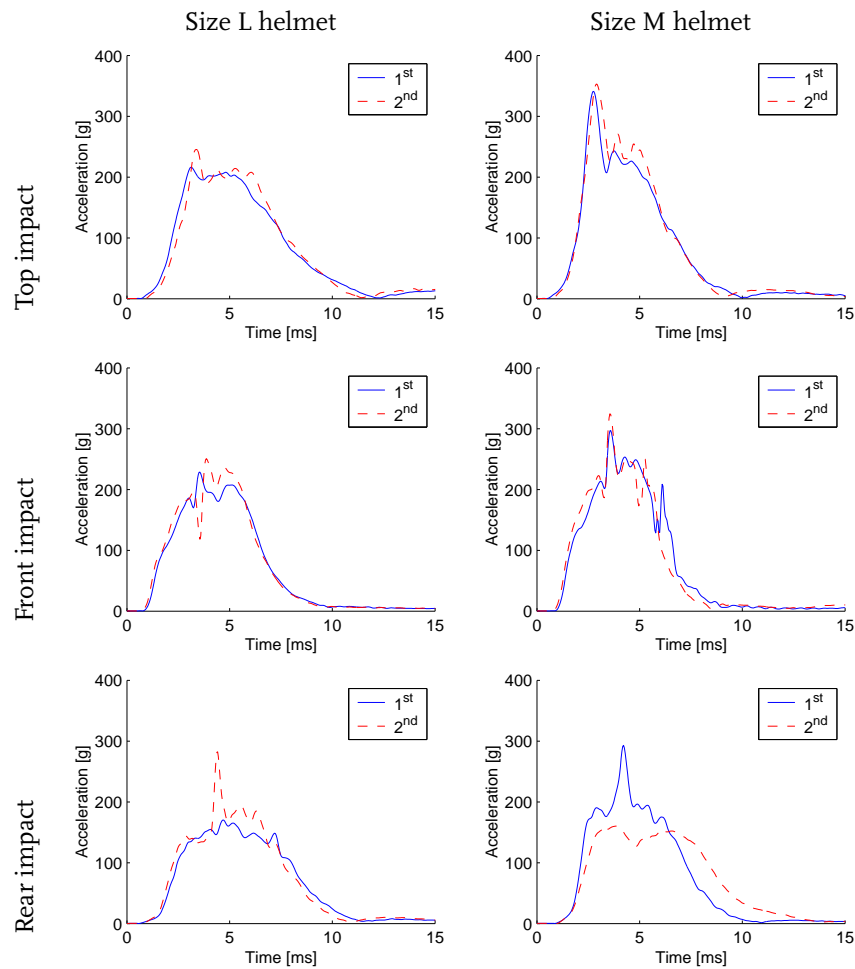
Figure 3.7: Resultant translational headform accelerations of the drop tests using the conventional headform.

Besides HIC and maximum resultant translational accelerations, maximum resultant rotational velocity and Head Impact Power (HIP) will be determined. Several studies aimed to find thresholds for the maximum rotational acceleration [e.g.: Gennarelli, 1983; Ommaya, 1984; Löwenhielm, 1975; Margulies & Thibault, 1992]. The thresholds found in these studies range from 4.5 to 13.6 $krad/s^2$, corresponding to AIS 3+ (SDH and DAI). Newman *et al.* [2000a] found a threshold for HIP of 12.8 kW, corresponding to AIS 1 (concussion). No helmet testing regulations so far specify thresholds for rotational accelerations or HIP.

3.3 Results: Helmeted Head Drop Test Experiments

3.3.1 Drop Tests Using Conventional Headform

Sensor Data

Figure 3.7 shows the resultant translational headform accelerations of the drop tests using the conventional headform. Except for two Rear impact experiments — the spike in the middle of the experiment
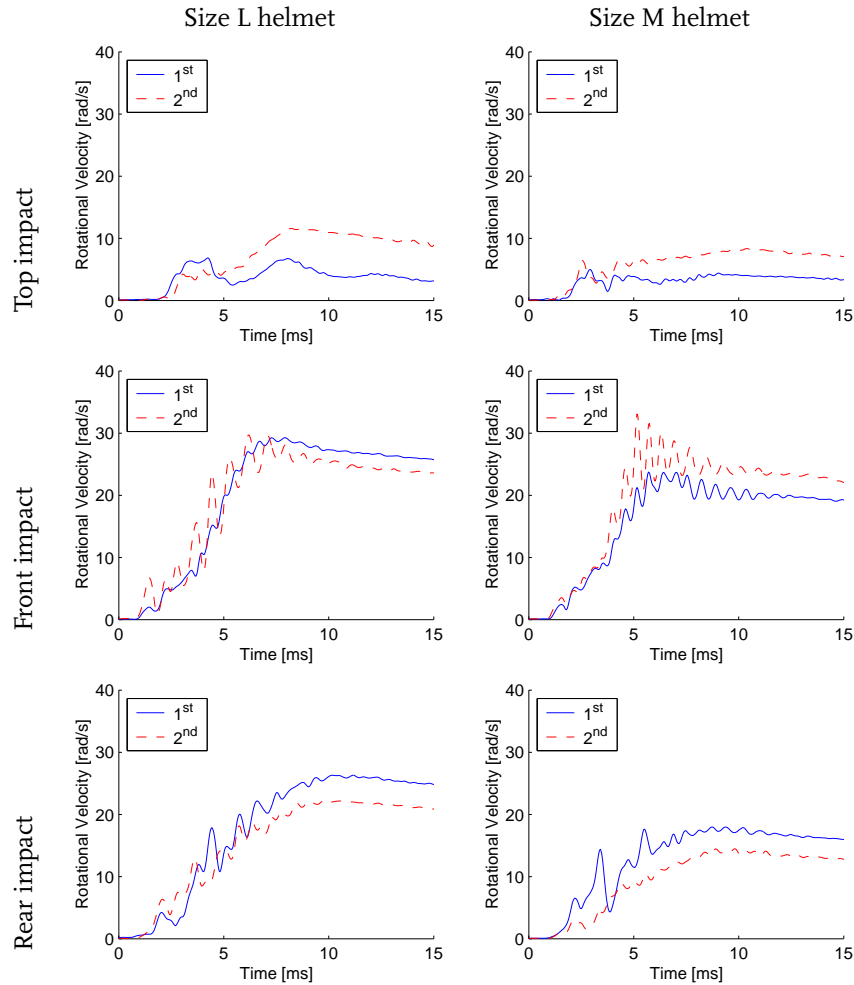
Figure 3.8: Resultant rotational headform velocities of the drop tests using the conventional headform.

is probably due to loosening of the sensor module[1] — the figure shows quite reproducible results. The repeatability of the drop tests is quantified in Appendix D. Repeatability of the resultant headform acceleration is best for Top and Front impact ($\pm$ 5% deviation).

The resultant translational headform accelerations for the drop tests with the Size M helmet are higher than those of the Size L helmet for all impact sites. For both the drop tests with the Size M helmet and with the Size L helmet, Rear impact shows the lowest maximum resultant headform accelerations. There is no statistical significant difference in maximum resultant headform acceleration between Front and Top impact.

Figure 3.8 shows the resultant rotational velocities of the drop tests using the conventional headform. Repeatability of these results is somewhat less than for the translational accelerations, but still acceptable (see also Appendix D). For the drop tests with the Size L helmet, resultant rotational headform velocities are generally higher than for those of the drop tests with the Size M helmet for all impact sites. The Front impact drop tests show the highest resultant rotational headform velocities and the

---

[1]It is unlikely that this behaviour is caused by the dynamics of the headform, since it consist of only one spike instead of an oscillating behaviour; and the spike is of high amplitude and very short duration. Bottoming-out is also unlikely, since energy is also absorbed after the spike, whereas the helmet would have lost all of its energy absorbing capacities after bottoming-out.
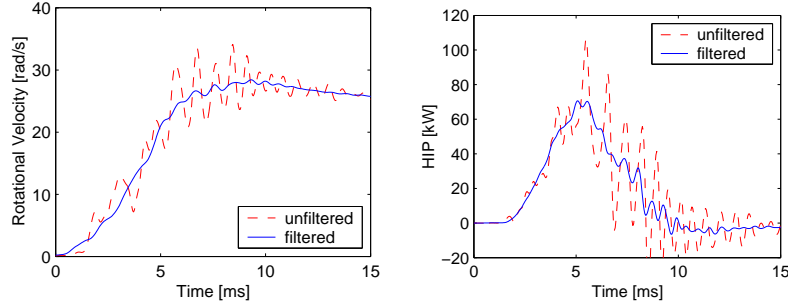
Figure 3.9: Effect of applying a moving average filter. *Left:* Rotational velocity. *Right:* HIP.

Table 3.3: Summary of the results of the drop tests using the conventional headform. Underlined numbers are values which exceed the thresholds for the ECE-R.22

	Size L helmet							
	HIC		a_{max} [g]		ω_{max} [rad/s]		HIP_{max} [kW]	
	1st	2nd	1st	2nd	1st	2nd	1st	2nd
Top impact	2233	2400	216	246	6.8	11.6	73.6	86.5
Front impact	1899	2161	229	251	29.3	29.7	77.3	90.24
Rear impact	1317	1723	170	<u>282</u>	26.3	22.4	60.6	72.4

	Size M helmet							
	HIC		a_{max} [g]		ω_{max} [rad/s]		HIP_{max} [kW]	
	1st	2nd	1st	2nd	1st	2nd	1st	2nd
Top impact	<u>3017</u>	<u>3632</u>	<u>341</u>	<u>353</u>	5.0	8.4	87.2	106.7
Front impact	<u>2701</u>	<u>2792</u>	<u>297</u>	<u>324</u>	23.7	33.1	95.9	111.6
Rear impact	2263	1410	<u>293</u>	160	18.0	14.5	76.1	57.2

Top impact drop tests show the lowest.

From the translational accelerations, the injury parameters HIC and a_{max} are computed. To compute HIP, the rotational accelerations are needed. These are obtained by differentiating the rotational velocities. Since the rotational velocities contain small high-frequency components, differentiating them results in large fluctuations in the rotational accelerations. Therefore, the rotational velocities are first filtered using a mid-point moving average filter, before computing HIP. The time-span of the filter should be chosen large enough to largely remove the high-frequency components, yet small enough not to disturb the trend of the signal. A 2 ms moving average filter was found to be a suitable compromise. Figure 3.9 shows the effect of this filtering operation on the rotational velocity and on HIP. It can be seen that filtering has a major effect on the maximum HIP value, HIP_{max}, yet the trend of the signal remains largely the same. This makes it easier to compare the HIP with other tests, since it is less burdened by the erratic oscillations of the rotational accelerations.

Table 3.3 shows the computed HIC, a_{max}, ω_{max} (maximum resultant rotational headform velocity) and HIP_{max} for all drop tests using the conventional headform. All values that exceed the thresholds of the ECE-R.22 are underlined. The ECE-R.22 does not require evaluation of HIP_{max}. The only threshold

for $\text{HIP}_{\max}$ found in literature is 12.8 kW [Newman *et al.*, 2000a]. However, this is a threshold (50% probability) for Mild Traumatic Brain Injury and is not applicable here. $\text{HIP}_{\max}$ and $\omega_{\max}$ were never validated for more severe brain injuries. Therefore, no threshold are specified for $\text{HIP}_{\max}$ and $\omega_{\max}$ and no values are underlined.

For the Size L helmet drop tests, there is only one test that exceeds the ECE thresholds, namely the second test for Rear impact. In Figure 3.7 it is seen that there is only one spike and that did not occur in the first test. It is unknown what causes this spike. The spike is of such a short duration (< 1 ms) that it is unlikely to cause injury. The HIC, which takes into account magnitude as well as duration of the acceleration, predicts that no injury will occur in this particular case. The same phenomenon also occurred in the first Rear impact test with the Size M helmet.

For the Top and Front impact drop tests on the Size M helmet, all HIC and $a_{\max}$ values exceed the thresholds of the ECE-R-22. The Size L and the Size M helmet differ only in comfort liner thickness. Apparently, the comfort liner is, in contrast to what was expected, of great influence on the drop test results, despite its low stiffness compared to the protective padding liner.

Considering HIC and $a_{\max}$, Table 3.3 makes clear that Top impact is the most severe impact and Rear impact is the least severe impact. However, considering HIP, the most severe impact is Front impact instead of Top impact. Based on the HIC and $a_{\max}$ values from the injurious and non-injurious drop tests and the corresponding $\text{HIP}_{\max}$ values, the threshold for $\text{HIP}_{\max}$ for the conventional headform is expected to be somewhere around 90 kW. For $\omega_{\max}$ this threshold is less clear.

The difference in HIP between the drop tests with both helmet sizes is smaller (up to 21%) than for HIC (up to 35%). Also the difference in HIP between the Top and Front impact drop tests is not large (up to 10%), but the HIP in both these drop test configurations is larger than the HIP in the Rear impact drop tests (up to 50%).

Maximum Deformation

In the ECE drop test regulation, the impact velocity is 7.5 m/s. In real life accidents, the impact velocity may become much higher. If the protective padding liner is not entirely compressed during impact, the helmet still has some 'reserves', to protect the head against even higher impact velocities, i.e. the maximum deformation has not yet occurred. The additional protection is measured in terms of minimum distance $\Delta L_{\min}$ between headform and anvil, which is determined from the X-ray images. The larger $\Delta L_{\min}$, the more reserves the helmet has after impact. This parameter is not an injury criterion, however it may reveal more on the protective capacities of the helmet.

To measure $\Delta L_{\min}$, the image where the headform is closest to the anvil is extracted from the series of images of the entire drop test. In this image, two points are carefully marked manually (see Figure 3.10). The first point is the center of the anvil contact area, the second point is the point on the headform closest to the anvil. Both points are marked manually. The error of each point is estimated to be less than two pixels. Converting the pixel coordinates to real coordinates using the method discussed in Section 3.2.1, the real distance between the two marked points is computed.

Figure 3.11 shows $\Delta L_{\min}$ for the drop tests with both helmet sizes, using the conventional headform. The figure shows that the Unit 2 measurements show less deformation of the foam than the Unit 1 measurements, even though the Unit 1 and Unit 2 images were captured from the same drop test. The reason for this difference is that on Unit 2 higher X-ray voltages and currents are used than for Unit 1. This results in a smaller image of the headform, because the edges of the headform are over-radiated, and thus $\Delta L_{\min}$ appears to be larger. This effect is of the same magnitude in all drop
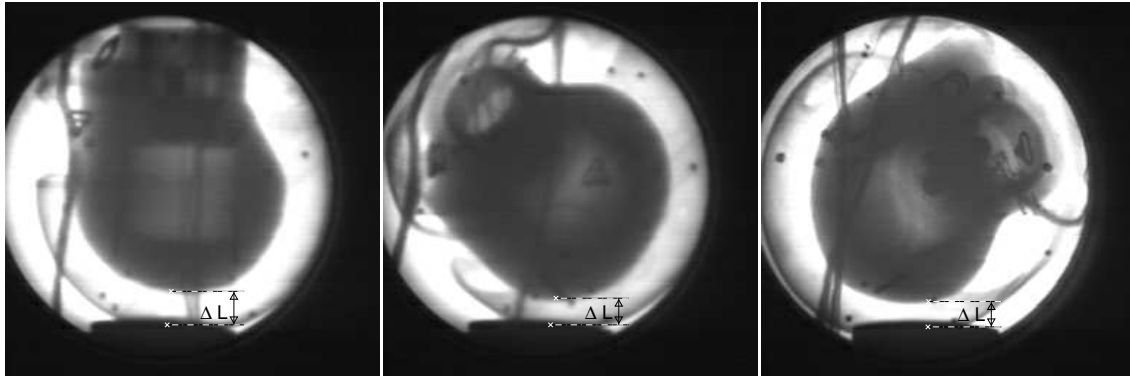
Figure 3.10: Selected image with the two marked locations '×'. *Left:* Top impact. *Middle:* Front impact. *Right:* Rear impact.
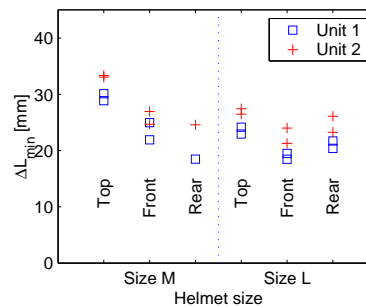
Figure 3.11: Minimum distances between anvil and headform for drop tests with both helmet sizes, using the conventional headform.

tests, so a qualitative comparison is still possible. As far as the difference between the helmet sizes is concerned, for Top impact, the Size L helmet deforms roughly 30% more than the Size M helmet. For the other impact sites, the difference between the helmet sizes is 0-10%. Front impact yields the smallest ΔL_{min}. In Top impact, this distance is the largest. It should be noted that the protective padding liner thickness in the frontal region is also less thick than in the crown area.

Marker Tracking

Unique in this experimental setup is the use of a bi-plane high-speed X-ray setup which enables tracking markers not only on the outside of the helmet, but also inside the helmet. Figure 3.12 shows the marker tracks of a Top impact drop test on a Size L helmet using the conventional headform (Appendix E includes all X-ray data of all helmeted head drop tests). The circles indicate the marker positions prior to impact. The question is, how to obtain useful information from this data, other than the general motion of the helmet. Principal Component Analysis (PCA) breaks up the motion into a summation of *modes* to visualise the main motions of the markers, while removing noise in both the time and the spatial domain. The theory on PCA is elaborated in Jolliffe [1986] and will only be briefly discussed here. Firstly, all coordinates of the markers are placed in a matrix of shape vectors $\boldsymbol{S}$:
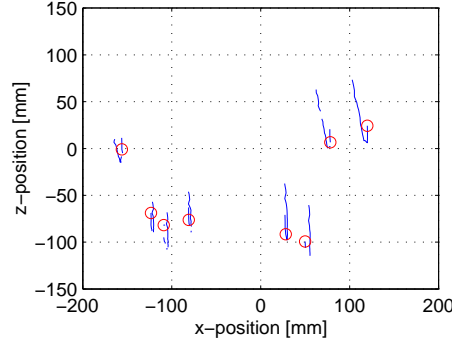
Figure 3.12: Marker tracks of a Top impact drop test on a Size L helmet using the conventional head-form.

$$
\boldsymbol{S} = \begin{bmatrix}
x_1(t_1) & y_1(t_1) & z_1(t_1) & x_2(t_1) & y_2(t_1) & z_2(t_1) & \cdots & x_m(t_1) & y_m(t_1) & z_m(t_1) \\
x_1(t_2) & y_1(t_2) & z_1(t_2) & x_2(t_2) & y_2(t_2) & z_2(t_2) & \cdots & x_m(t_2) & y_m(t_2) & z_m(t_2) \\
\vdots & \vdots & \vdots & \vdots & \vdots & \vdots & \ddots & \vdots & \vdots & \vdots \\
x_1(t_n) & y_1(t_n) & z_1(t_n) & x_2(t_n) & y_2(t_n) & z_2(t_n) & \cdots & x_m(t_n) & y_m(t_n) & z_m(t_n)
\end{bmatrix}
\tag{3.2}
$$

where $x_i(t_j)$, $y_i(t_j)$ and $z_i(t_j)$ are the x-, y- and z-coordinate, respectively, of marker i ($i = 1, \ldots, m$) at time t_j ($j = 1, \ldots, n$) and m and n are the number of markers and the number of time steps, respectively. Secondly, the covariance matrix $\boldsymbol{C}$ of $\boldsymbol{S}$ is calculated. Finally, the eigenvectors Φ_i and corresponding eigenvalues λ_i ($i = 1, \ldots, n$) of $\boldsymbol{C}$ are calculated. The largest variation from the mean position is in the direction of the eigenvector corresponding to the largest eigenvalue.

PCA requires that all positions are known at all points in time. However, most markers could not be tracked during the entire impact. Some markers were not tracked at all. This results in a partly filled matrix $\boldsymbol{S}$. Figure 3.13 shows the process of preparing $\boldsymbol{S}$ in such a way that PCA can be applied, by finding the largest data set that contains only 'known' marker positions.

Figure 3.14 shows the marker tracks and the direction of the first and second mode eigenvectors of the two Top impact drop tests on a Size L helmet using the conventional headform. The lengths of the eigenvectors are normalised to unit length and multiplied by 200 for visibility. The PCA results for all drop tests are displayed in Appendix E. For Top impact, the main direction of the motion (1st mode) of the helmet is a translational motion along the z-axis. The 1st mode eigenvectors show much similarity with the marker tracks. The 2nd mode eigenvectors show that there's also some rotation involved in the impact. In the first impact, the rotation is clockwise, in the second, the rotation is counter clockwise.

The magnitude of the eigenvalue of a mode compared to the total sum of eigenvalues, indicates how much of the energy is concentrated along the eigenvector corresponding to that particular mode. The absolute values of the eigenvalues have only little meaning since the analysis could not be performed on the same set of markers in each individual drop tests. Table 3.4 shows the eigenvalues of the first three modes of each drop test, and the part of the energy that is concentrated in the corresponding mode. It is clear that over 81.3% up to 99% of the energy is concentrated in the first mode. This mode describes the general motion: Translational motion for Top impact and rotational motion for Rear and Front impact (see also Appendix E). The second mode still contains up to 18.1% of the total energy. The third and higher modes can be neglected in this analysis. Even though the second mode does
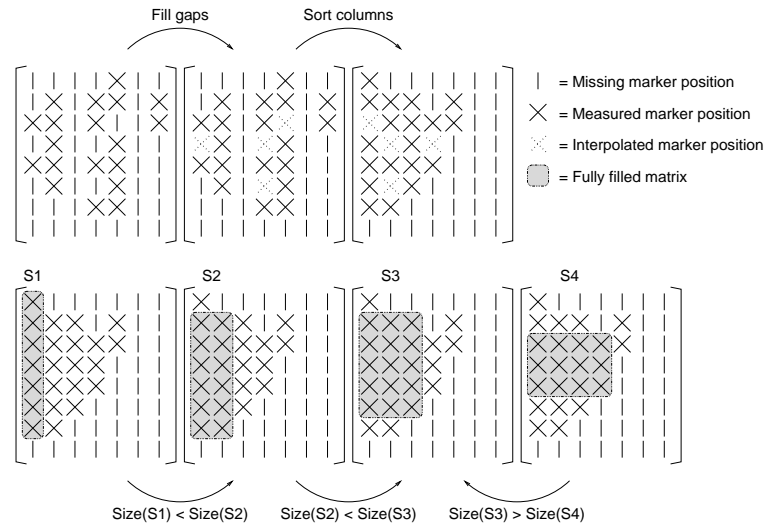
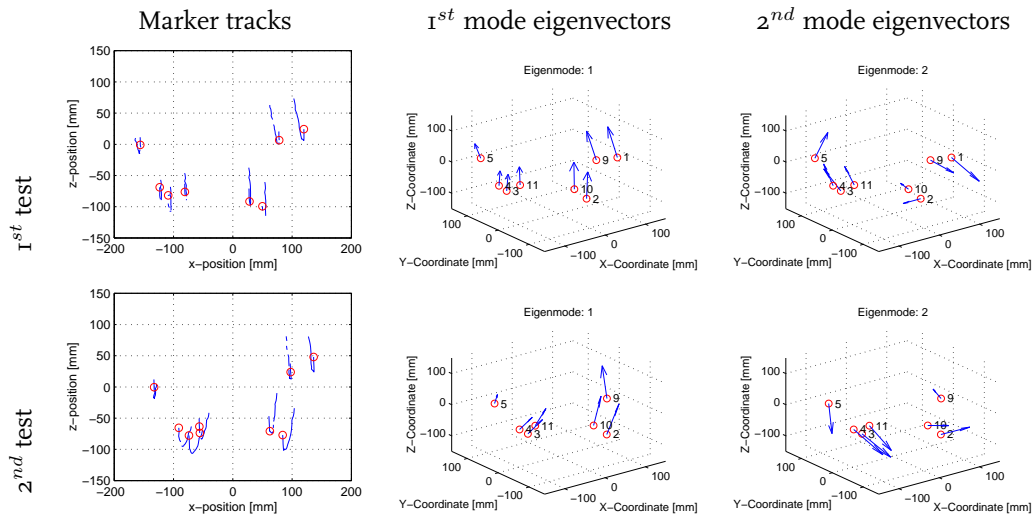Figure 3.13: Finding the largest, fully filled, matrix of shape vectors.

Figure 3.14: Marker tracks and first and second mode eigenvectors for the drop tests on a Size L helmet using the conventional headform.

Table 3.4: Eigenvalues corresponding to the first three modes of the Principal Component Analysis, for each drop test using the conventional headform.

Helmet size		Top impact		Front impact		Rear impact	
		λ_i	$\frac{\lambda_i}{\Sigma\lambda_i}*100\%$	λ_i	$\frac{\lambda_i}{\Sigma\lambda_i}*100\%$	λ_i	$\frac{\lambda_i}{\Sigma\lambda_i}*100\%$
	Mode 1	1442.6	93.9	2372.6	81.6	2208.2	96.7
Size L (1st)	Mode 2	87.5	5.7	509.3	17.5	68.9	3.0
	Mode 3	1.9	0.2	13.7	0.5	4.8	0.2
	Mode 1	1827.5	91.6	2632.9	97.4	1613.9	81.3
Size L (2nd)	Mode 2	163.2	8.2	23.6	2.4	359.3	18.1
	Mode 3	0.3	0.1	3.6	0.1	6.7	0.3
	Mode 1	1618.3	98.5	1097.7	92.7	—	—
Size M (1st)	Mode 2	16.5	1.0	81.2	6.9	—	—
	Mode 3	5.8	0.4	3.2	0.3	—	—
	Mode 1	781.8	96.5	892.9	94.9	1388.9	99.0
Size M (2nd)	Mode 2	20.7	2.6	38.6	4.1	11.9	0.9
	Mode 3	7.0	0.9	8.6	0.9	0.1	0.1

not yield reproducible results, the amount of energy in that mode indicates that this mode is not to be neglected. Since the results of the first mode of all drop tests, which express the general motion, are quite similar, this second mode, which expresses the more detailed motion, may be responsible for the differences between the individual drop tests.

3.3.2 Drop Tests Using Flexible Headform

Sensor Data

Figure 3.15 shows the resultant translational headform accelerations of the drop tests using the flexible headform. The drop tests with the Size L helmet were only performed once, so no conclusions on repeatability can be drawn here. The results from the drop tests with the Size M helmet show good reproducibility for Top and Rear impact. For Front impact, the repeatability is somewhat less, but still acceptable (see also Appendix D). Repeatability of the drop tests using the flexible headform is comparable to that of the drop tests using the conventional headform. The results from the former are generally more fluctuant, whereas the results from the latter are more often burdened by outliers.

Like the results from the drop tests using the conventional headform, these results also show the largest accelerations in Top impact and the smallest for Rear impact. Also the drop tests with the Size M helmet yield higher results than the drop tests with the Size L helmet.

Figure 3.16 shows the resultant rotational velocities of the drop tests using the flexible headform. The result from the Top impact drop test with the Size L helmet will be omitted in further analyses, due to a sensor cable break during the drop test.[2] The repeatability of the rotational velocity results from the drop tests with the Size M helmet is somewhat less than for the translational accelerations, but still

---

[2]The result from the Top impact drop test with the Size L helmet shows erratic behaviour. After a closer inspection of the drop test setup, a break in one of the sensor cables was found. After replacing the cable, the problem was solved and the other tests were performed. Unfortunately, this particular test could not be repeated on this particular helmet, since each drop test deforms the helmet irreversibly. Therefore, this particular test could not be repeated.
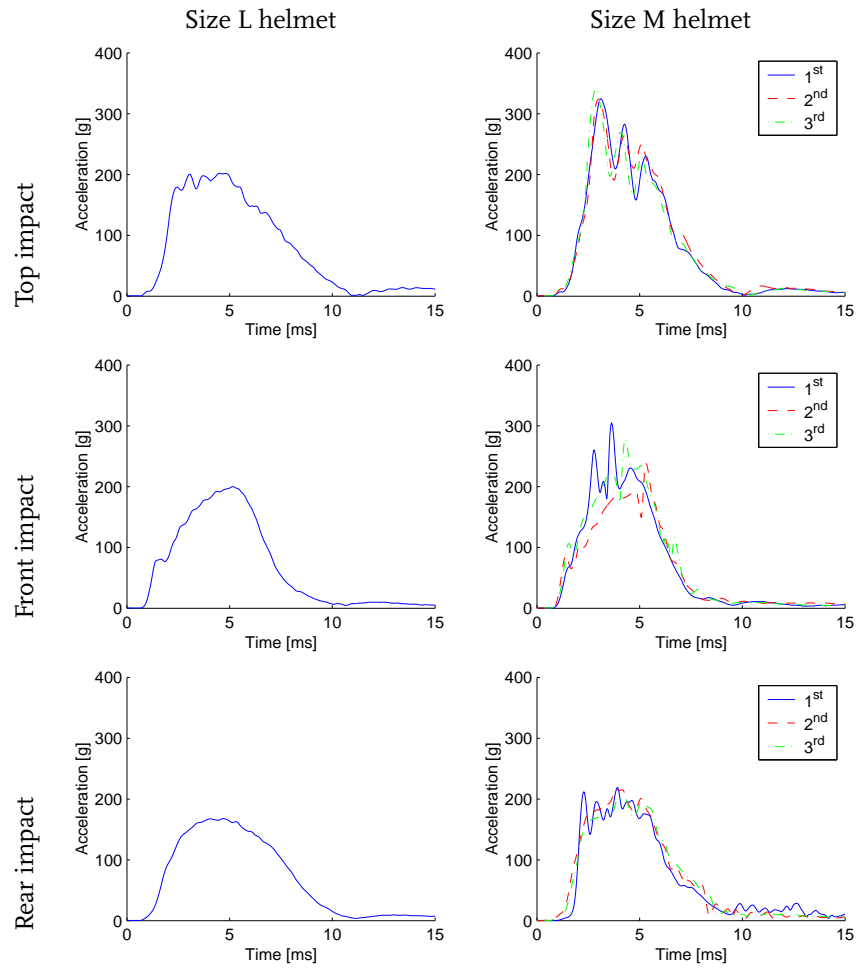
Figure 3.15: Resultant translational headform accelerations of the drop tests using the flexible headform.
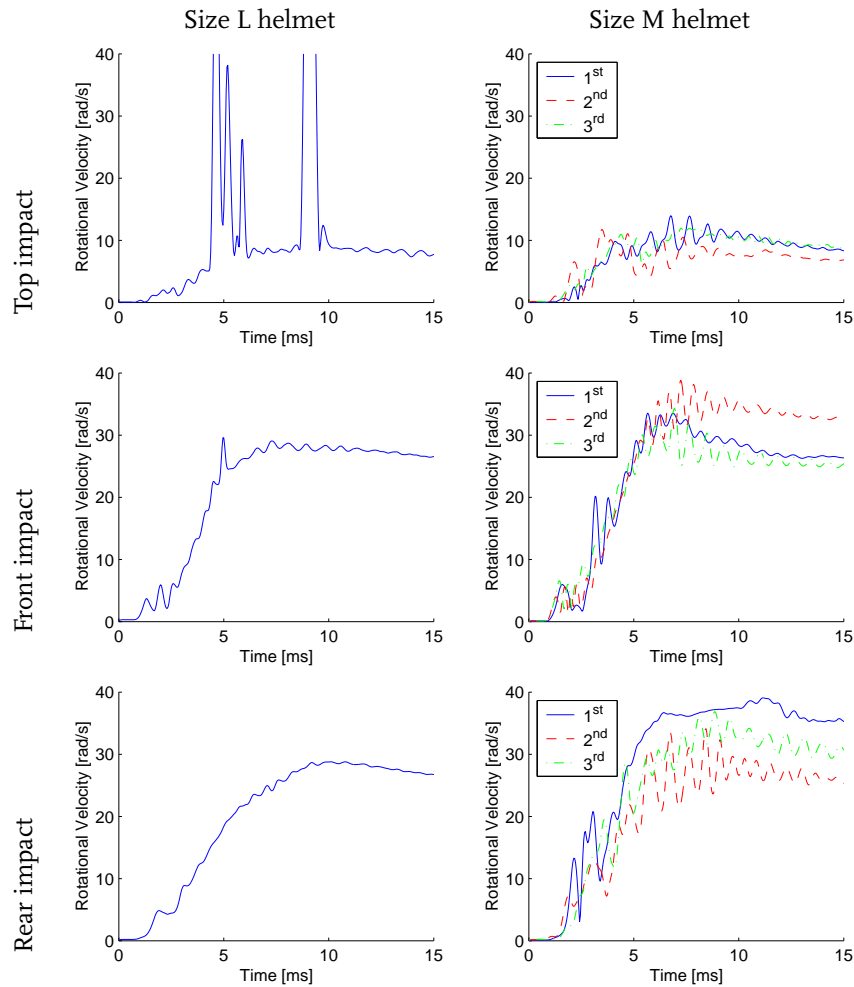
Figure 3.16: Resultant rotational headform velocities of the drop tests using the flexible headform.

acceptable. This is similar to the results from the drop tests using the conventional headform (see also Appendix D).

Front and Rear impact show the highest and Top impact shows the lowest resultant rotational head-form velocities. The results from the drop tests with the Size L helmet are not significantly little lower than those of the drop tests with the Size M helmet.

Table 3.5 shows the computed HIC, $a_{\max}$, $\omega_{\max}$ and $HIP_{\max}$ for all drop tests using the flexible head-form. The time histories of HIP were again computed after filtering the rotational velocity with the moving average filter (see Section 3.3.1). All HIC and $a_{\max}$ values that exceed the thresholds of the ECE-R.22 are underlined. For the Size L helmet drop tests, all values are below the ECE thresholds. For the Size M helmet drop tests, two out of three $a_{\max}$ values for the Front impact exceed the ECE thresholds, but these excesses are of such a small duration (see Figure 3.15) that the HIC threshold is not exceeded. In the Top impact drop tests, all values of both $a_{\max}$ and HIC exceed their thresholds.

Considering HIC and $a_{\max}$, Table 3.5 makes clear that Top impact is the most severe impact and Rear impact is the least severe impact. However, considering HIP, the most severe impact is Front impact instead of Top impact. These conclusions were also drawn from the drop tests using the conventional

Table 3.5: Summary of the results of the drop tests using the flexible headform. Underlined numbers are values which exceed the thresholds for the ECE-R.22

	Size L helmet			
	HIC	$a_{\max}$ [g]	$\omega_{\max}$ [rad/s]	$HIP_{\max}$ [kW]
	1st	1st	1st	1st
Top impact	2051	202	—	—
Front impact	1619	200	29.6	70.5
Rear impact	1413	168	28.8	54.7

	Size M helmet											
	HIC			$a_{\max}$ [g]			$\omega_{\max}$ [rad/s]			$HIP_{\max}$ [kW]		
	1st	2nd	3rd	1st	2nd	3rd	1st	2nd	3rd	1st	2nd	3rd
Top impact	3094	3170	2977	325	324	341	14.0	11.7	12.0	96.2	98.9	91.3
Front impact	2218	1438	2178	305	238	278	33.5	38.8	34.3	84.0	80.9	91.5
Rear impact	1682	1834	1674	219	217	204	39.1	34.1	36.9	66.1	70.7	70.6
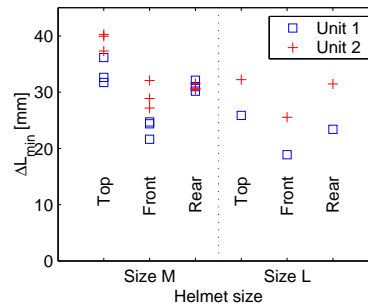
Figure 3.17: Minimum distances between anvil and headform for drop tests with both helmet sizes, using the flexible headform.

headform. Also similar to the drop tests using the conventional headform, the threshold for injury for $HIP_{\max}$ for the flexible headform is approximately 90 kW, based on the HIC and $a_{\max}$ values of the corresponding drop tests.

Maximum Deformation

In Figure 3.17, the minimum distance between headform and anvil $\Delta L_{\min}$ is compared for drop tests with both helmet sizes using the flexible headform. The drop tests with the flexible headform show the same trends in $\Delta L_{\min}$, as the drop tests using the conventional headform. The minimum distance for the Unit 1 measurements is again smaller than for the Unit 2 measurements as explained in Section 3.3.1. Particularly for Top impact, the Size L helmet deforms more than the Size M helmet (25-30%). Again, Front impact yields the smallest values for $\Delta L_{\min}$. In Top impact, this distance is the largest.

Higher currents and voltages were used in the drop tests using the flexible headform to make the markers inside the headform visible (see also next paragraph), which results in larger values for $\Delta L_{\min}$ as already explained in Section 3.3.1. Therefore, a comparison with respect to $\Delta L_{\min}$ between drop tests using the conventional headform and those using the flexible headform is not possible.

Table 3.6: Eigenvalues corresponding to the first three modes of the Principal Component Analysis, for each drop test using the flexible headform.

Helmet size			Top impact		Front impact		Rear impact	
			λ_i	$\frac{\lambda_i}{\Sigma\lambda_i}*100\%$	λ_i	$\frac{\lambda_i}{\Sigma\lambda_i}*100\%$	λ_i	$\frac{\lambda_i}{\Sigma\lambda_i}*100\%$
		Mode 1	1246.6	99.7	1438.6	99.2	1518.6	99.6
Size L (1st)		Mode 2	2.1	0.2	9.6	0.7	4.1	0.3
		Mode 3	1.1	0.1	1.7	0.1	1.7	0.1
		Mode 1	85.9	96.5	495.1	95.1	5312.9	99.1
Size M (1st)		Mode 2	2.2	2.5	24.0	4.6	29.1	0.5
		Mode 3	0.9	1.0	1.1	0.2	8.9	0.2
		Mode 1	611.8	98.9	1577.8	99.1	4541.8	99.4
Size M (2nd)		Mode 2	4.9	0.8	14.2	0.9	16.7	0.4
		Mode 3	0.7	0.1	0.4	0.0	4.9	0.1
		Mode 1	1308.4	99.7	2076.3	99.6	5279.7	99.4
Size M (3rd)		Mode 2	1.5	0.1	5.2	0.3	30.5	0.6
		Mode 3	0.7	0.0	3.6	0.2	0.2	0.0

Marker Tracking

Using the flexible headform, the bi-plane high-speed X-ray setup now enables marker tracking not only inside the helmet, but also inside the headform. However, the flexible headform absorbs a reasonable amount of X-ray energy. Therefore, a higher current and voltage had to be used to make the markers inside the headform visible. Consequently, the markers in and on the helmet were only rarely visible due to over-exposure.

Appendix E shows all the marker tracks and the 1st and 2nd mode eigenvectors from the PCA for all drop tests using the flexible headform. Like the drop tests using the conventional headform, the 1st mode eigenvectors (general motion) show much similarity with the marker tracks. However, the results of the 2nd mode eigenvectors are more erratic than in the drop tests using the conventional headform. The relative amount of energy of the second mode (Table 3.6) is considerably less (4.6% max.) than in the drop tests using the conventional headform, which may explain the more erratic behaviour. If a particular mode contains only little energy, it is more difficult to estimate its parameters. It should be noted that the results from the drop test using the conventional headform were based on the helmet markers only, whereas the results of the flexible headform are based mainly on the markers inside the headform. Apparently, the second mode is more prominent in the helmet motion than in the motion of the brain.

3.4   Discussion

3.4.1   Research Question 1: Are the Injury Criteria Currently Used in Helmet Certification Tests Adequate for Predicting Injury Severity?

In this research, the ECE-R.22 drop tests are extended with measuring rotational velocities, to investigate whether it would be useful to also implement other injury criteria. From the drop test results, it has become clear that the rotational response can reach injurious magnitudes of ω >30 rad/s and
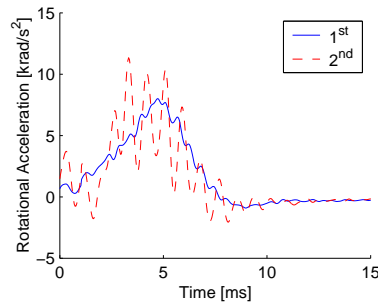
Figure 3.18: Derivative of the resultant rotational velocity during a Front impact drop tests on Size L helmets using the conventional headform.

$\alpha >$ 5 krad/s^2 [Ommaya, 1984; Ommaya *et al.*, 1967], depending on the impact location. Top impact results in the highest values for HIC and $a_{\max}$, whereas maximum resultant rotational velocities and maximum protective padding deformations are lowest for this impact configuration. For Front and Rear impact it is exactly the other way round, because of the more eccentric impact configuration. Even though Front and Rear impact are both eccentric impacts, the HIP$_{\max}$ for Front impact is significantly higher than for Rear impact. It even exceeds the HIP$_{\max}$ for Top impact. To compute HIP$_{\max}$, rotational velocities and accelerations must be determined. Therefore, headform rotations must be allowed for in shock absorption tests, just like in real motorcycle accidents. In the ECE-R.22, the neck is rigidly mounted to the headform and body mass is neglected. Depending on the impact configuration, Vincze-Pap & Áfra [2001] showed that rotational accelerations could further increase, and translational accelerations could further decrease, as the entire human body is modelled. However, modelling the entire human body, could make the shock absorption test needlessly complicated.

In the results presented in this chapter, rotational motion is expressed in terms of rotational velocities. However, rotational velocities as such have never been found to be correlated with injury, but rotational accelerations have, since they result in shear strains inside the brain. If these rotational accelerations approach critical values ($\alpha >$ 4.5 krad/s^2, see Appendix B), countermeasures should be taken. Figure 3.18 shows the time histories of the derivative of the resultant rotational velocity (i.e. the rotational acceleration) during a Front impact drop tests on Size L helmets using the conventional headform. The figure shows that rotational accelerations of over 8 krad/s^2 can occur, which may cause injury (see Section 3.2.4). This means that a helmet that passed the criteria for $a_{\max}$ and HIC may still not provide sufficient protection. Even the more so, the maximum resultant rotational velocity generally increases as $a_{\max}$ and HIC decrease for the various impact points. This probably also holds for the maximum resultant rotational acceleration, but this is hard to prove because of the erratic nature of the rotational velocity measured here. So, for Front and Rear impact an evaluation of a rotational injury parameter is needed. However, the rotational parameters show large spreads in the results. Thus, the repeatability of the test with respect to rotational parameters must be increased. This may be achieved by using a different way to measure rotational accelerations, for instance using a 9-accelerometer array [Padgaonkar *et al.*, 1975]. In this method, no differentiation is needed, however the calibration procedure is more critical.

Also for Top impact, measuring rotational acceleration may prove to be beneficial. Possibly, the helmet could be designed in such a way that translational kinetic energy is transformed into rotational kinetic energy during impact. This results in a decrease of HIC and $a_{\max}$ and an increase in rotational accelerations, while keeping all the injury parameters below their critical values. It is shown that the

eccentricity of the impact does exactly that.

HIP_{max} supports this conclusion, since it shows injurious values (> 90 kW) for both Top and Front impact, whereas HIC and $a_{max}$are significantly lower for Front impact than for Top impact. It should be noted that HIP_{max} was never validated for these impact severities and the threshold of 90 kW is solely based on HIC and a_{max}, which are translational acceleration based criteria, obtained from the drop tests performed in this research. Even though both a_{max} and HIC are currently implemented in the ECE-R.22, HIC is preferred over a_{max} since it is better correlated with injury and it is less affected by spikes in the acceleration signal. The same holds for HIP_{max}.

Currently, ECE-R.22 includes an oblique test. However, the rotational accelerations of the headform are not measured. Instead, reaction forces of the anvil are measured, since the objective of the oblique test is to ensure that:

- projections shear off easily;

- shear forces acting on the outer shell should be below 3500 N.

The outcome of these tests is greatly dependent on the moments of inertia of the headform. However, ECE-R.22 does not include requirements for these moments of inertia. This may result in acceptance of a helmet in one test and rejection of the same helmet in another test with a different headform, even when both headforms meet the requirements of the test. This test originates from the BS 6658 [BSI, 1985]. Back then, measuring shear force was preferred over measuring rotational accelerations, because the latter could only be measured at high costs. The relation between shear force and rotational acceleration in helmeted head impact is never investigated. Nowadays, measuring rotational accelerations is relatively cheap and should therefore be preferred.

3.4.2 Research Question 2: How Are Helmet Fit and Headform Flexibility Related to Helmet-head Interaction?

To investigate the effect of helmet fit and headform flexibility on the results of the drop tests, a statistical analysis is performed based on the injury parameters HIC, a_{max}, ω_{max} and HIP_{max} of all drop tests presented in Table 3.3 and 3.5. This statistical analysis involves a *three-factor analysis of variance* including first-order interaction terms to determine which factors (headform used, helmet size and impact site) have a significant effect on the parameters HIC, a_{max}, ω_{max} and HIP_{max}. It also tests for significant interactions amongst the factors. For details on how to perform a multi-factor analysis of variance, see Chatfield [1994]. The results of the analysis of variance for HIC, a_{max}, ω_{max} and HIP_{max} are presented in Table 3.7.

The P-value indicates the significance level of the particular factor. The factors with corresponding P-values less than 0.05 (underlined in the table) have a significant effect on the particular parameter at the 95% confidence level. There are two values which are larger than 0.05, but still close to 0.05 (underlined with a dashed line in the table) and should therefore not be discarded. These factors still have a significant effect on the particular parameter at the 90% confidence level. More tests need to be performed to yield a definite answer.

Helmet Fit

The Size L helmet and the Size M helmet only differ in comfort liner thickness. From Table 3.7 it becomes clear that the comfort liner thickness has a significant effect on HIC, a_{max} and HIP_{max}. Drop

Table 3.7: Analysis of variance for HIC, $a_{\max}$, $\omega_{\max}$ and $HIP_{\max}$.

Source	P-value			
	HIC	$a_{\max}$	$\omega_{\max}$	$HIP_{\max}$
Main effects:				
Headform	<u>0.0231</u>	<u>0.0678</u>	<u>0.0064</u>	<u>0.0195</u>
Helmet size	<u>0.0002</u>	<u>0.0006</u>	0.2884	<u>0.0005</u>
Impact site	<u>0.0000</u>	<u>0.0115</u>	<u>0.0000</u>	<u>0.0003</u>
Interactions:				
Headform × Helmet size	0.6351	0.5507	<u>0.0043</u>	0.3175
Headform × Impact site	0.1888	0.9108	<u>0.0063</u>	0.2681
Helmet size × Impact site	0.1018	<u>0.0670</u>	0.5581	0.1969
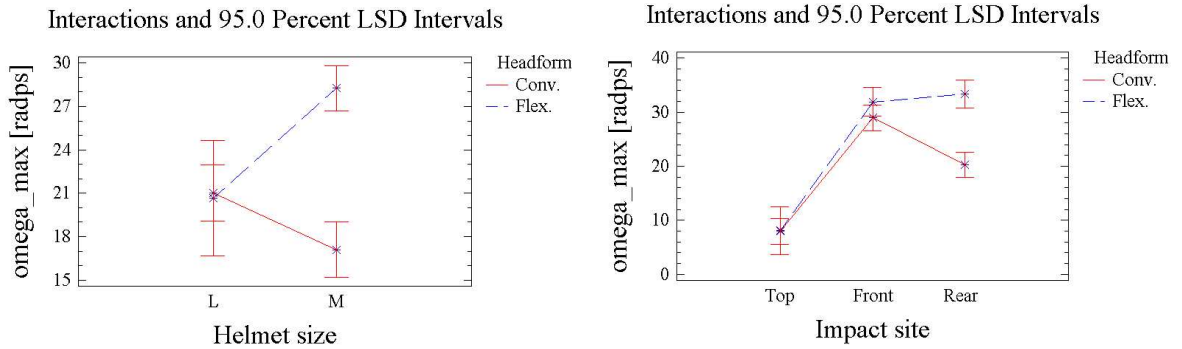
Figure 3.19: Interaction plots of $\omega_{\max}$. *Left:* Headform-helmet interaction. *Right:* Headform-impact site interaction.

tests on the Size M helmet yield significantly larger results. The maximum resultant rotational head-form velocity does not seem to be affected by the comfort liner thickness. However, the interaction terms do play a significant role for $\omega_{\max}$. This is visualised in Figure 3.19. On average, $\omega_{\max}$ is not affected by the helmet tested. However, the result does depend on the combination of helmet tested and headform used. For the conventional headform, the Size M helmet yields favourable results in terms of maximum resultant rotational headform velocity, whereas for the flexible headform, the Size L helmet should be preferred. Thus, the wrong choice of headform may lead to an incorrect evaluation of protective capacities of the helmet. This holds especially for Rear impact, where the rotational velocities are large and the translational accelerations are small (see the right graph of Figure 3.19). One must bear in mind that the comparisons with the flexible headform are based on only one test with the Size L helmet. Nevertheless, the phenomenon is striking.

It is concluded that, even though the comfort liner absorbs only little energy and has a low stiffness, compared to the other parts of the helmet, the comfort liner, and thus the helmet fit, still accounts for a considerable part of the protective function of the helmet in terms of resultant translational headform acceleration. Therefore, one should not use a helmet that is too tight. The effect of a helmet which fits too loosely was not investigated, but this is also likely to have an effect on the protective capacities of the helmet. The effect of the comfort liner on the protective capacities of the helm may be caused by the fact that the connection between the headform and a tight helmet is stiffer, because of the pre-

stressed comfort foam. Another factor may be the increased friction between headform and helmet, which also loads parts of the helmet that are located further away from the impact point. Both causes makes the the helmet and headform behave more as a whole. Thus, more mass is involved in the rotation, resulting in a lower rotational velocity change which in turn results in higher translational acceleration.

However, for the drop tests using the flexible headform, both translational acceleration and rotational velocity are higher for the drop tests with the Size M helmet, compared to those with the Size L helmet. A possible explanation for this may be found in the flexibility of this headform. The flexible brain lags behind during a rotational load on the head, which results in lower effective moments of inertia and thus in higher rotational accelerations. However, why this effect is larger on the smaller sized helmet is unknown.

Conventional Headform vs. Flexible Headform

In Table 3.7 it has become clear that the choice of headform has a significant influence on HIC, $\omega_{\max}$ and $\text{HIP}_{\max}$. The P-value for $a_{\max}$ is only slightly larger than 0.05. Therefore, more tests are needed to investigate whether or not this parameter plays a significant role in the drop tests. The parameters HIC and $\text{HIP}_{\max}$ are larger for the drop tests using the conventional headform than for those using the flexible headform. The conventional headform is considered rigid and does not contribute to the attenuation of the impact. Therefore it is concluded that, besides the helmet of course, the flexible headform significantly contributes to the attenuation of the impact. The hypothesis that skull deformations lead to a larger contact area with the helmet, resulting in higher translational headform accelerations, seems not true. At least the effect is less significant than the attenuation of the headform.

The results for $\omega_{\max}$ are larger for the drop tests using the flexible headform than for those using the conventional headform. The higher rotational velocities are mainly caused by the flexibility of the brain which results in lower effective moments of inertia.

The headform is the only factor that is present in both significant interaction terms presented in Table 3.7. The difference in impact attenuation and effective moments of inertia is probably the cause for the headform to behave structurally different, as a result of a change in impact site or helmet size, than the conventional headform.

When comparing the resultant rotational headform velocities of the drop tests using the conventional headform with those using the flexible headform for Front and Rear impact, the higher rotational velocities of the flexible headform immediately strike the eye. The differences are bigger for Rear impact than for Front impact and bigger for the Size M helmet than for the Size L helmet.

In the current ECE-R.22 only translational accelerations are measured. This means, would the flexible headform be used with the current injury criteria, it would result in more favourable results than with the conventional headform. In Chapter 5, it will be shown that a stiffer protective padding liner increases the translational accelerations during a drop test. This stiffer helmet is better suited for higher impacts, since bottoming-out of the protective padding liner is less likely to occur. However, a stiffer protective padding liner results in higher rotational accelerations. So, this 'safer' helmet may actually lead to injury more easily. Therefore, an assessment of injury with respect to rotational accelerations should also be included in the test.

Conclusions on the effects of the headform on the helmet and head response could not be drawn from the X-ray data, since only helmet markers were tracked in the drop tests using the conventional

headform, whereas mainly headform markers were tracked in the drop tests using the flexible head-form. However, the results showed that the second mode of the response clearly affected the helmet response, whereas it was only little prevalent in the brain response. In terms of injury parameters, this means the second mode response affects acceleration based injury parameters (translational as well as rotational), whereas stress and strain based injury parameters are only affected to a little extent by the second mode response of the helmet.

As to whether or not brain deformations should also be determined in helmet certification tests, the results from the X-ray data were inconclusive, since they do not offer a quantitative evaluation of strains inside the brain. It appears that strains inside the brain are more prevalent for Front impact, than in Rear and Top impact, since the average amount of energy in the second mode is the largest. The average amount of energy of the second mode for Front impact is 1.6 %, whereas for Top and Rear impact these are only 0.9 % and 0.5 %, respectively. It should be noted, that Front impact, as well as Rear impact have a total amount of energy, that is significantly larger than that of Top impact. It is not clear which of these parameters relates to injury. However, these figures indicate that measuring brain deformations may yield a different evaluation of helmet performance. Further research is needed to investigate the validity of this.

3.5 Conclusions

This research concludes that determining only the injury criteria, HIC and a_{max}, in helmet certification tests is not sufficient to evaluate helmet performance. Especially in eccentric loading conditions, the translational response is significantly less than in centric loading conditions, whereas the rotational response in these loading conditions can reach injurious magnitudes. Therefore, the test protocol should be extended with measurement of the rotational acceleration. To implement this, headform rotations must be allowed for in shock absorption tests.

As far as the comfort liner is concerned, it is more than a matter of bringing comfort to the user. It also provides the fit of the helmet. The fit also accounts for a considerable part of the protective function of the helmet. A helmet should not be too tight, since it results in an increase of the injury probability. It should neither be too loose, since it increase the risk of seperation of head and helmet during impact, which increases the risk of injury drastically.

The fit of the helmet on the headform during impact is not determined by the flexibility of the skull of the flexible headform. However, the flexible headform attenuates a considerable part of the impact energy, causing lower values of the injury parameters. To compensate for the attenuation when using the conventional headform, the thresholds for the injury parameter HIC is raised from 1000 for the human head to 2400 for the conventional headform. However, the flexible headform behaves structurally different to a change in impact configuration than the conventional headform. Simply scaling the threshold for HIC when using the conventional headform may therefore lead to an incorrect assessment of injury. To overcome this problem, the experiments in this chapter suggest that the conventional headform should be replaced by a more biofidelic, flexible headform in helmet certification tests.

The numerical simulations in the following chapters can be used to further investigate the hypotheses. The results from this chapter can only partly be used to validate the numerical models. The sensor data (translational acceleration and rotational velocity) is of sufficient quality, that it can be used for this purpose. However, the X-ray data do not offer quantitative results that can properly be used for validation purposes.

Chapter 4

Numerical Modelling of Helmeted Head Drop Tests

4.1   Introduction

The experiments in the previous chapter resulted in some interesting conclusions. However, they do not enable the computation of field parameters like deformations and stresses inside the helmet and head. For that, Finite Element simulations are needed, which enable the use of injury criteria that can not be evaluated in experiments. This chapter discusses the development and validation of the Finite Element models of the helmet, the conventional headform and the anatomically more detailed headform. Most attention goes out to the helmet model, especially in terms of material parameters which turned out to be critical for a validated helmet model. After individually validating the helmet and headform models, numerical drop test simulations are performed, to validate the response of the helmeted headform numerical models, compared to the experiments. The Finite Element models of the helmet and headforms are later used to perform a sensitivity analysis (Chapter 5) and to investigate the effect of helmet design changes (Chapter 6).

4.2   Numerical Model of the Flexible Headform

Firstly, the development and validation of the flexible headform is elaborated. The main advantage of the numerical model over the physical head model is that it enables the investigation of the effect of more, and maybe more relevant, parameters like stresses and strains. All mechanical and geometrical parameters of the headform's components are known (Chapter 2), which makes it fairly easy to construct a Finite Element model. All numerical simulations in this research were performed using the Finite Element package MADYMO [TNO Automotive, 2001]. MADYMO uses an explicit integration code.

4.2.1   Realization of the Model

Figure 4.1 shows a cross-section of the model. The model consists of 22998 nodes that define 20976 brick elements (8-node reduced integration elements). In Table 4.1 an overview of the number of elements and of the material models is given for the numerical model. With E being Young's modulus, ρ the density, G_∞ the elastic shear modulus and K the bulk modulus. For the viscoelastic material
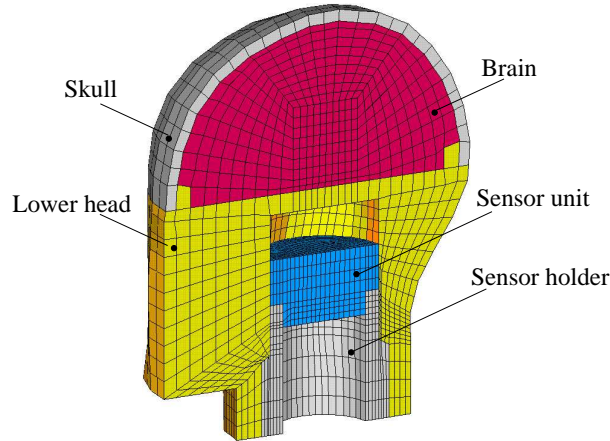
Figure 4.1: Numerical model of the physical head model.

Table 4.1: Overview of the numerical head model.

Component	#elements	material model	material parameters
Cranial skull	628	Linear elastic	$E = 5.3$ MPa, $\rho = 1300$ kg/m^3
Brain	7040	Visco-elastic	$G_\infty = 216.4$ Pa, $K = 1.065$ MPa, $\rho = 970$ kg/m^3 $G_{d,1} = 27.6$ kPa, $\tau_1 = 9.7434 \cdot 10^{-5}$ s^{-1} $G_{d,2} = 1.72$ kPa, $\tau_2 = 2.1563 \cdot 10^{-3}$ s^{-1} $G_{d,3} = 379$ Pa, $\tau_3 = 2.4705 \cdot 10^{-2}$ s^{-1} $G_{d,4} = 122$ Pa, $\tau_4 = 3.0977 \cdot 10^{-1}$ s^{-1}
Lower head	8220	Rigid	$\rho = 1410$ kg/m^3
Sensor unit	3632	Rigid	$\rho = 1890$ kg/m^3
Sensor holder	1456	Rigid	$\rho = 2710$ kg/m^3

model of the silicone gel, a 4-mode Maxwell model is used [Brands *et al.*, 1999]. $G_{d,i}$ and τ_i are the dynamic shear modulus and time constant, respectively, of the i-th mode. Figure 4.2 shows that this model describes the silicone gel material behaviour quite well. .

The lower head, sensor unit and sensor holder were modelled using MADYMO's RIGID material model. So, no deformations were allowed in these parts. This speeds up the simulations considerably, but it is also necessary for obtaining smooth acceleration signals. In Finite Element simulations, nodes are subject to extreme high frequency vibrations with low amplitude. These nodal vibrations are caused by the limited numerical accuracy of the nodal positions (10^{-16} m) and almost uncorrelated with neighbouring nodes. Since the elements are small (< 1 cm^3) and stiff, their individual eigenfrequencies are large (> 1 MHz), resulting in nodal accelerations that overshadow the global acceleration of the headform by magnitudes. Modelling these parts as rigid eliminates this problem and does neither change the overall kinematics of the headform nor the behaviour of the flexible parts of the headform in terms of stresses and strains (less than 0.01 %).
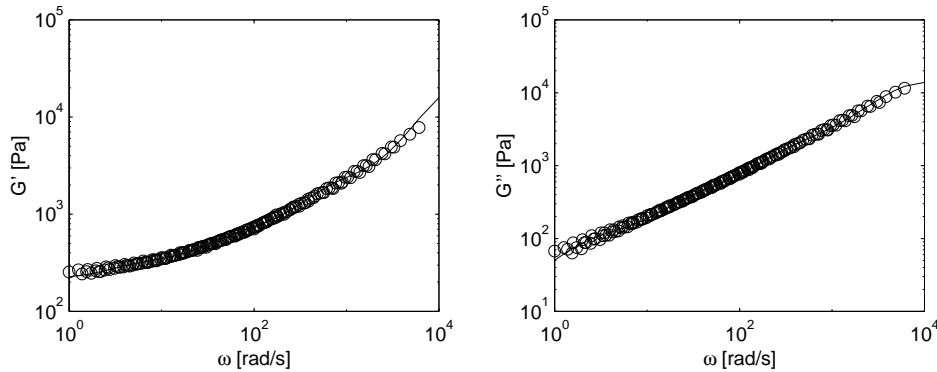
Figure 4.2: Fit of 4-mode Maxwell model (·) on experimental data (○) of silicone gel from Brands *et al.* [1999]. *Left*: Elastic modulus G'. *Right*: Loss modulus G".

4.2.2 Validation of the Model

The numerical model of the headform represents a powerful means of investigating a wide range of physical and engineering parameters such as velocity, acceleration, pressure, stress and strain. However the numerical model has to be validated against experiments on the physical head model first. Two experiments, performed on the physical headform in Chapter 2, are used for the validation of the numerical model: the Hodgson test and the impulse test. Additional validation data originate from static compression tests performed on the physical headform. These three tests will be discussed in the following.

Hodgson Test

These experiments have been discussed in Section 2.5. The corresponding simulations were performed with the numerical model. The head was positioned above the anvil in the same way as in the experiments. Since gravity was not modelled, the headform was given an initial velocity of 1.98 m/s. This configuration is equivalent to a free fall of 200 mm in gravity. The experiment and the simulation were synchronised at the moment the anvil reaction force starts to increase. The translational acceleration at the center of gravity was obtained from the node closest to the head's center of gravity. The rubber padding was modelled with two layers of 169 brick elements each. The anvil was modelled as a fixed rigid plane (see Figure 4.3).

Figure 4.4 shows the resultant acceleration for the Hodgson drop test experiment compared with the simulation. The difference between simulation and experiment is considered acceptable, both in shape and in magnitude (less than 10 %).

Static Compression

As an extra means of validation for the numerical model, static compression tests were performed on the physical headform. The headform was placed in a hydraulic compression test device (MTS 858 Tabletop Test System), in which the force-deflection characteristic was recorded. Four compression tests were performed. The headform was compressed to a maximum load of about 700 N. Higher loads may damage the headform because of the localised nature of the load. In the numerical model, the load is applied at the top node, while keeping the bottom nodes supported. Figure 4.5 shows the
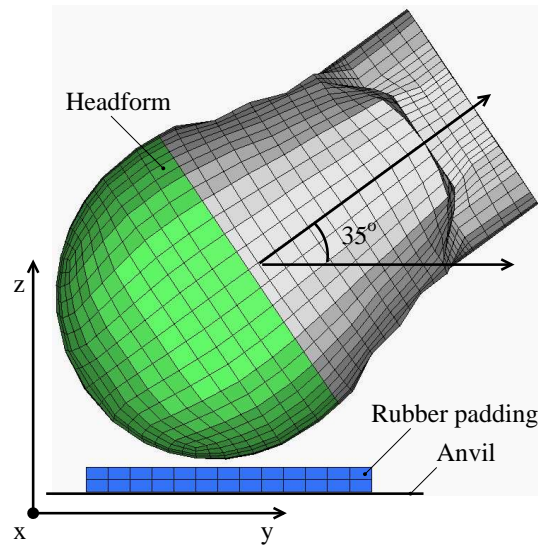
Figure 4.3: Hodgson drop test simulation.
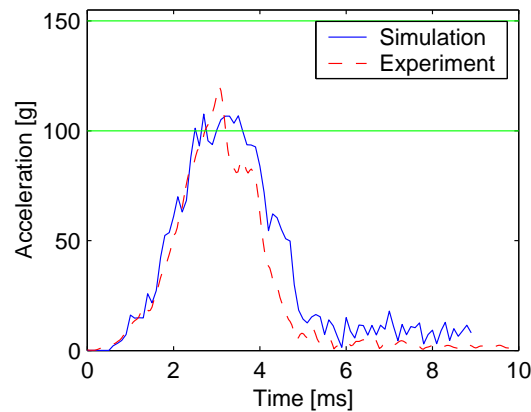
Figure 4.4: Hodgson drop test experiment compared with the simulation.

results of the experiments and the simulation. The results of the experiments show that the numerical model of the headform also responds acceptably in static compression (average deviation: less than 7 %).

Impulse Test

This test is not suitable for validating the numerical model. On the one hand, MADYMO uses an explicit time integration scheme, which does not allow for output as a function of frequency. On the other hand, comparison of time responses between experiment and simulation is not possible, since the output of the numerical simulation contains very high frequency components, because of the stiffness of the skull in combination with the small element size (as explained in Section 4.2.1). Several attempts have been made to allow for a sound comparison, but with no success. This means that the numerical model of the flexible headform can not be used in comparing nodal skull accelerations.
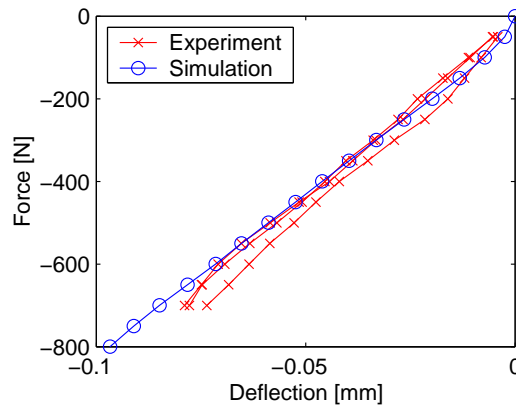
Figure 4.5: Static compression of the headform.

4.3 Conventional Headform Model

The numerical model of the conventional headform is geometrically identical to the model for the flexible headform. The only difference is that the entire model, including brain and skull, is now modelled as rigid. As a measure for rigidity, ECE-R.22 requires the lowest eigenfrequency of the headform to be larger than 3000 Hz. This way the dynamics of the headform does not affect the results of the drop tests. In the simulations, the eigenfrequency of the conventional headform is infinite, since the model is infinitely stiff.

4.4 Helmet Model

In a preparatory study by Brands *et al.* [1997], a Finite Element model of an existing certified full-face motorcycle helmet of consumer size 59-60 (L) was built and validated on the basis of resultant headform acceleration time history. This helmet model will be used as a basis of this study. The model consists of an outer shell, a protective padding liner and a chin strap. Furthermore, they claim to have modelled the comfort padding liner by leaving a gap between the headform model and the helmet model, assuming that this zero stiffness approximates the low stiffness of the polyurethane foam. In Chapter 3, it is shown that the thickness of the comfort foam has a significant effect on the outcome of the drop test. Furthermore, the helmet of Brands *et al.* was modelled with an incompressible protective padding, whereas in practice, the protective padding is highly compressible. Nowadays, more realistic material models, that model the complex nature of these materials more accurately, are available and will be used in this study.

4.4.1 Protective Padding Liner

The protective padding liner is the helmet part that absorbs the most energy. It is made of a closed-cell structural foam, often Expanded Polystyrene (EPS), which is a complex material with excellent shock-absorbing qualities. The helmet in this research also has an EPS protective padding liner. EPS is known to be strain-rate independent for strain rates up to 233 s^{-1} [Happee, 1993; Thunnissen, 1995]. However, higher strain rates occur in crash-helmet drop tests. Furthermore, the local deformation behaviour of EPS foam at high strain rates is unknown. For a correct modelling of the helmeted
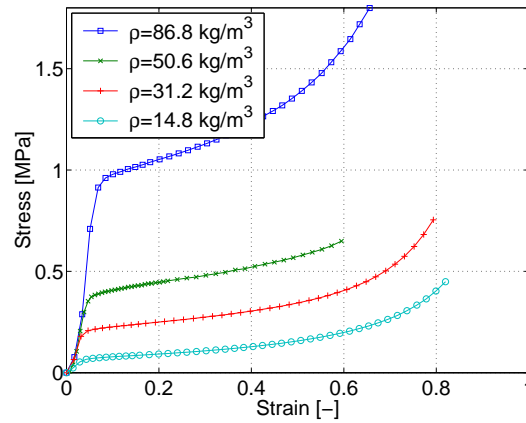
Figure 4.6: Low-rate compression experiments on EPS foam samples.

headform drop tests, the mechanical behaviour of EPS foam must be known up to a strain rate of at least 300 s^{-1}. Since the protective padding liner is the most important part of the helmet, its material properties are investigated quite extensively.

Low-rate Compression Tests

Low-rate unconfined-compression experiments on EPS foam samples of four different densities (14.8, 31.2, 50.6 and 86.8 kg/m^3) were performed as a reference. The cylindrical EPS foam samples (Ø 80× 50 mm) were compressed at a velocity v of 0.5 mm/s using a Karl Frank GmbH draw-bench (model 891565). Compressive forces were measured using a Wägezelle force transducer (model U2A). The built-in displacement transducer of the draw-bench was used to measure the clamp displacement. The compressive stress is calculated by dividing the force by the initial area of the sample. The strain is calculated by dividing the displacement by the initial thickness of the sample.

Figure 4.6 shows the results of low-rate compression experiments ($\dot{\varepsilon} < 0.01$ s^{-1}). Initially, the material shows non-linear elastic behaviour. When the yield stress is exceeded, the material starts to behave almost as an ideally plastic material, with a Poisson ratio of zero. This is the 'crush' stage. In this stage, the cells in the material start to collapse. When the cells have collapsed completely, the gradient of the stress-strain curve increases rapidly. This phenomenon is termed 'bottoming out'.

To obtain a rough indication of the initial stiffness of the material, an estimate of Young's modulus E was computed from the measurements. Young's modulus is, by definition, a linear material parameter, whereas the elastic behaviour of EPS foam is initially non-linear, probably due to sample inaccuracies (setting of the sample between the two compression plates). Therefore, a region of fairly linear elastic behaviour is selected from the stress-strain curves and Young's modulus of this region is computed as $E = \frac{\Delta\sigma}{\Delta\varepsilon}$. Figure 4.7 shows the stress-strain curves together with the graphical representation of the estimates of Young's moduli. Table 4.2 shows the estimates of Young's moduli of EPS foam for different foam densities.

Clearly, high-density EPS foam is stiffer than low-density EPS foam. This effect is directly related to the structure of the material. EPS foam is a so-called closed-cell structural foam, which means the material has a cellular structure. The higher the density of the foam, the more cells per unit of volume the material contains and the smaller, and thus stiffer, these cells are.
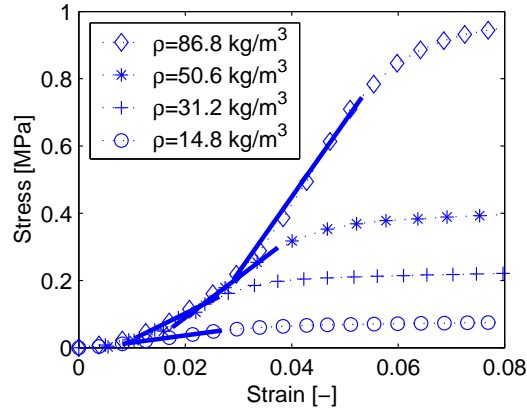
Figure 4.7: Graphical representation of Young's moduli of EPS foam during elastic compression.

Table 4.2: Young's moduli of EPS foam.

ρ [kg/m^3]	E [MPa]
14.8	2.1
31.2	7.8
50.6	12.0
86.8	22.4

High-rate Compression Tests

To investigate the mechanical behaviour of the material up to a strain rate of 320 s^{-1}, high-rate compression experiments were conducted on 25 mm thick EPS foam samples of four different densities (14.8, 31.2, 50.6 and 86.8 kg/m^3) using a drop mass experimental setup. Figure 4.8 shows a schematic representation of the drop mass apparatus. A drop mass m falls down, guided by a plastic tube, and hits the foam sample positioned on the anvil. Air holes in the tube reduce drag and prevent the sample from being blown away by the air, flowing out of the lower end of the tube. Two series of drop mass experiments were performed on cylindrical foam samples of 65 mm diameter and 25 mm thickness. The samples were compressed at three different impact velocities (4, 6 and 8 m/s), each using three different drop masses (2.990, 3.805 and 4.608 kg), resulting in 2×36 different experiments. The sequence of the experiments was randomized to reduce the effect of possible environmental changes between the experiments.

The way in which the samples are prepared turned out to be critical. In pilot experiments, cubic foam samples were compressed. Two sides of each sample were cut thermally and two sides were not. Figure 4.9 shows the differences in residual deformation of these sides after compression. The thermal cutting technique probably altered the chemical structure of the material, resulting in a non-cubic sample after compression. Therefore, the samples used in the drop mass experiments were cut mechanically using a cylindrical drill.

Impact velocities are measured in the same way as with the helmeted head drop test experiments (see Section 3.2.1). Forces acting on the anvil are measured using a tri-axial force transducer (Kistler 9067)
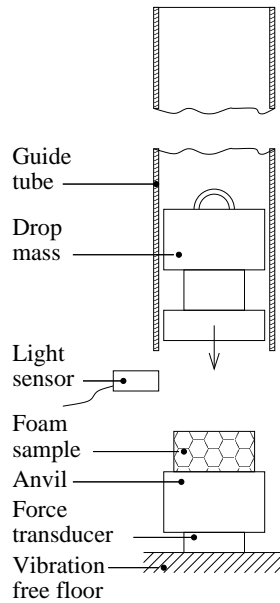
Figure 4.8: Drop mass apparatus for high-rate compression testing of the EPS foam samples.
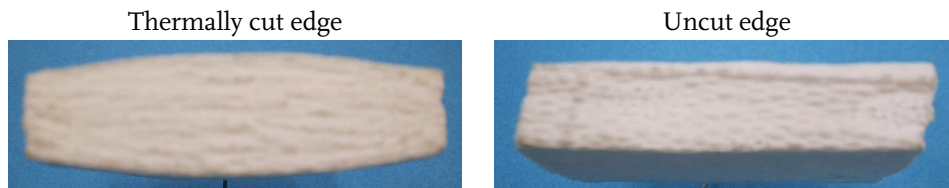
Figure 4.9: Differences in residual deformations on different edges.

positioned underneath the anvil. The transducer signals are amplified by a charge amplifier (Hottinger Baldwin Messtechnik AB22A). The DIFA Dynamic Signal Analyser (DSA, model 230) records the outputs of the optical sensor and the force transducer at a sample frequency of 102.4 kHz.

The anvil and the force transducer are mounted on a rigid, vibration-free floor to prevent external vibrations from influencing the measurements. However, at these impact severities, the anvil itself starts to vibrate, resulting in oscillations in the force signal of about 2.5 kHz. These oscillations do not correspond to the load on the sample and should therefore be removed in a proper manner as a first and necessary step in the postprocessing of the data. Since the oscillations contain frequencies of the same order as the force acting on the foam sample, ordinary low-pass filters or moving average filters are not appropriate.

The best way to obtain the load on the sample and thus remove the oscillations is by means of the deconvolution technique [Harrigan *et al.*, 1998], which accounts for the flexibility of the anvil (Figure 4.10). This technique transforms an output signal to a (possibly unknown) input signal. The Frequency Response Function (FRF) must be known for this technique to be applied. The FRF is measured using the DIFA data acquisition system, a hammer with force transducer (PCB Piezotronics, model 208 A05) to impact the anvil, and the tri-axial force transducer (Kistler, model 9067). Figure 4.10 shows the FRF of the anvil with a resonance frequency of about 2.5 kHz. The figure also shows that this method effectively removes the oscillations from the measured force signal.
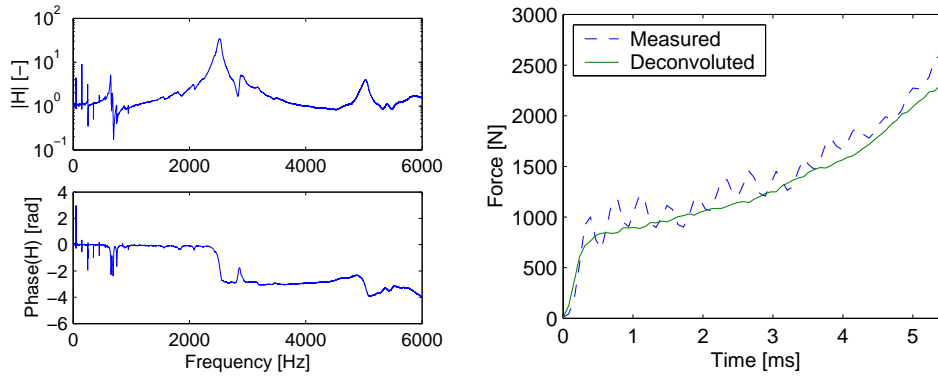
Figure 4.10: Deconvolution technique. *Upper left:* Magnitude of the Frequency Response Function of the anvil. *Lower left:* Phase angle of the Frequency Response Function of the anvil. *Right:* Measured and deconvoluted impact force signals.
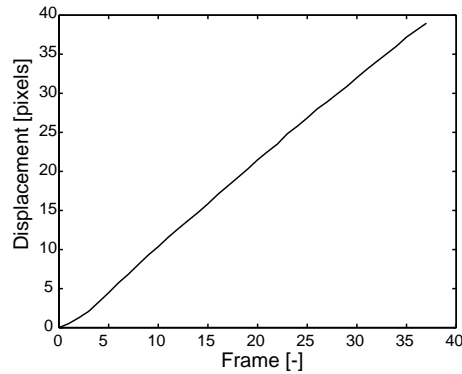
Figure 4.11: Displacement of the drop mass.

Global stress-strain curves are derived from the force and the impact velocity. The stress is calculated by dividing the force by the initial area of the foam sample. Drop mass displacements are calculated by multiplying the impact velocities by time. After that, the strains are calculated by dividing the displacements by the initial thickness of the foam samples. This computation is only valid if the compression velocity is constant over time. Figure 4.11 shows that the drop mass displacement, which is measured using high-speed video, is linear as a function of time (the frame rate is constant). Thus, the deceleration of the drop mass during impact is negligible and the velocity during compression is considered as being constant. In the final stage of the compression, the mass is decelerated rapidly.

Figure 4.12 shows the stress-strain curves for different impact velocities, drop masses and foam densities. Another set of 31 measurements was performed[1] for a closer investigation of the local deformation patterns. The results turned out not to be useful for that purpose, however stress-strain curves could still be determined from the transducer signals.

All measurements $(36 + 36 + 31 = 103)$ were subjected to a statistical analysis, using STATGRAPHICS Plus Version 4, to investigate the influence of the strain rate, the foam density and the drop mass

---

[1]Five measurements were omitted to prevent overloading of the force transducer. It concerns the following measurements: 31.2 kg/m^3, 8 m/s, 4.608 kg; 14.8 kg/m^3, 8 m/s, 3.805 kg; 14.8 kg/m^3, 8 m/s, 2.990 kg; 14.8 kg/m^3, 8 m/s, 4.608 kg and 14.8 kg/m^3, 6 m/s, 4.608 kg.
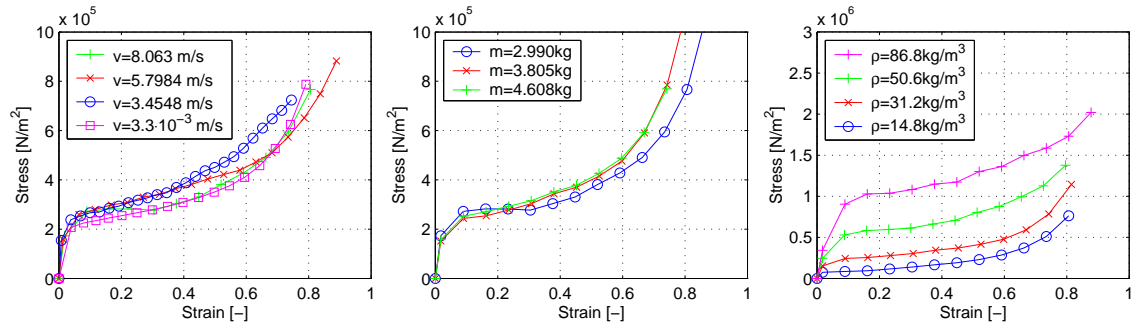
Figure 4.12: Stress-strain curves for: *Left:* different impact velocities (ρ=31.2 kg/m^3, m=2.990 kg); *Middle:* different drop masses (ρ = 31.2 kg/m^3, v $\approx$ 8 m/s); and *Right:* different foam densities (m = 3.805 kg, v $\approx$ 8 m/s).
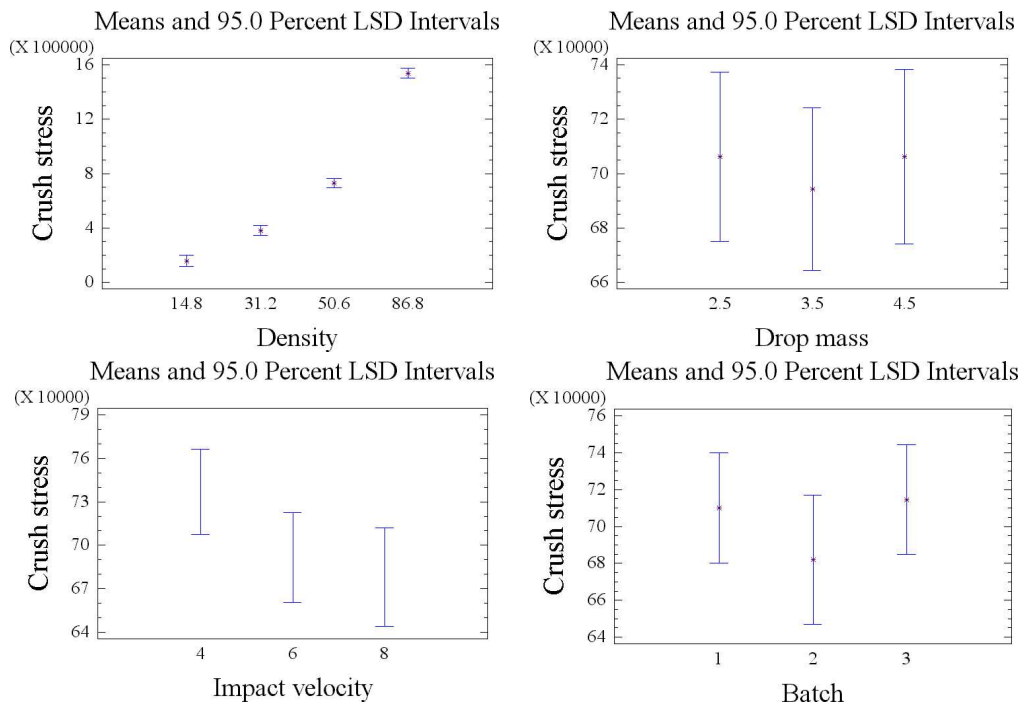
Figure 4.13: Statistical influence of the density of EPS foam (*upper left*), the drop mass (*upper right*), the impact velocity (*lower left*), and of the series of experiments (*lower right*) on the crush stress.

on the mechanical properties of EPS foam. The crush stress is used as a parameter to compare the measurements. The crush stress is the stress in the material during the crush stage. Since this parameter is not constant over time, it is defined as the mean value of the stress between 0.0025 and 0.0125 seconds. During this interval, the elastic phase has ended and the bottoming out phase has not yet started.

Four factors were considered: the foam density, the drop mass, the series of measurements and the impact velocity. The influence of these factors on the crush stress is quantified by the least significant difference (LSD, [Chatfield, 1994]). Figure 4.13 shows the 95% LSD intervals for these factors.

Residual Plot for Crush stress
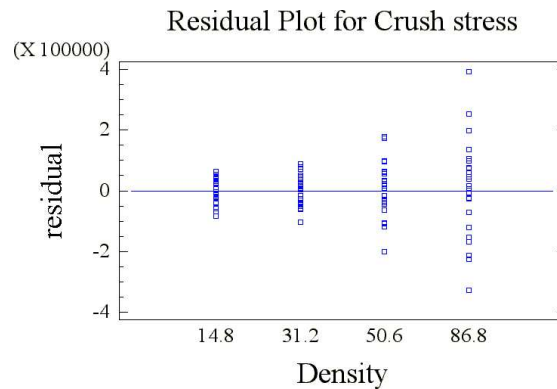
Figure 4.14: Residual plot for the crush stress as a function of density.

The following example explains the use of the LSD intervals. In Figure 4.13, the mean crush stress of EPS foam with a density of 14.8 kg/m³ is about 0.15 MPa. This value does not occupy the LSD intervals of the crush stress of EPS foams with a higher density. Therefore, the crush stress of EPS foam with a density of 14.8 kg/m³ is, with 95% certainty, 'significantly different' from the crush stress of EPS foam with one of the other densities. This effect also occurred in the low-rate compression tests.

Figure 4.13 also shows that the series of experiments and the drop mass do not significantly influence the crush stress. Therefore, other factors — such as environmental circumstances, sample shape and sample preparation — either did not differ between the series of experiments or they have no influence on the crush stress. This was to be expected. However, the figure also shows a decreasing crush stress for an increasing impact velocity. One would expect the opposite in the case of strain-rate dependency, since strain rate dependency in foams often originates from material damping and airflow within the cells on deformation. This effect is on the edge of what is statistically significant (the intervals only just overlap). A closer investigation of the scatter in the data (Figure 4.14) shows that the residuals for the crush stress of the samples with the highest density (86.6 kg/m³) are much larger than the other residuals, indicating a much lower accuracy or a much lower reproducibility of these experiments. Thus it is not proven whether or not the crush stress depends on the impact velocity.

Scatter in the data for high foam-densities could be caused by the deconvolution technique. The FRF, required for this technique, only holds for linear systems. However, the anvil may not respond as a linear system for high loads. Yet, these high loads do occur at high impact-velocities in combination with high-density foam samples. This non-linearity might introduce errors into the reconstruction of the force signal, and thus introduce a higher level of scatter.

Therefore, the statistical analysis is repeated without the measurements on the foam samples with the highest density. Figure 4.15 shows the results of this analysis. Now, the influence of the impact velocity on the crush stress is no longer significant. EPS is therefore considered to be strain rate independent.

Figure 4.16 shows the interaction between the impact velocity and the density, computed using the Multi-factor Analysis of Variance (MAV) in STATGRAPHICS. Again, in this figure the measurements on the foam samples with the highest density were not considered. The results of the MAV show a significant contribution of the interaction terms at the 5% level. If no interaction between the density and the impact velocity was present, the three lines would be parallel, since the density would not influence the change in mechanical behaviour due to changes in impact velocity. In Figure 4.16, the
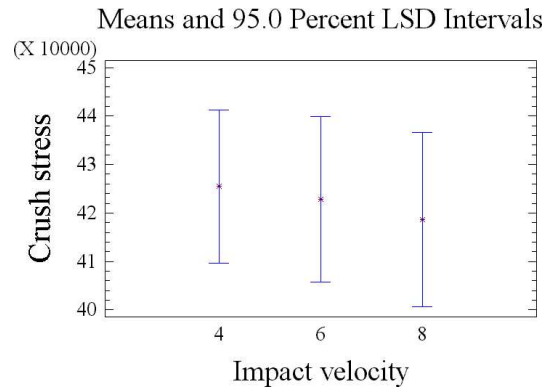
Figure 4.15: Statistical influence of the impact velocity on the crush stress.
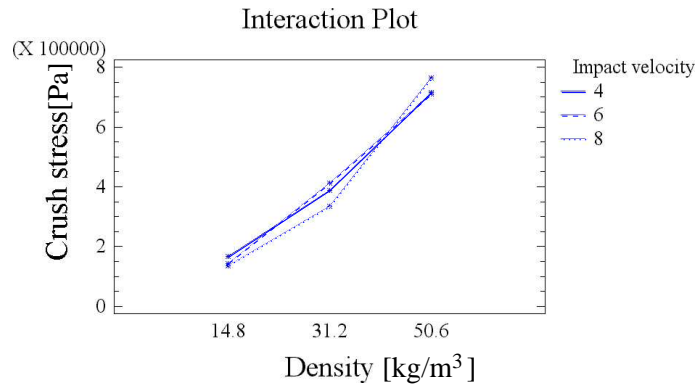
Figure 4.16: Interaction plot for the crush stress as a function of density and impact velocity.
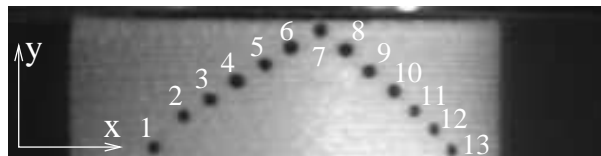
Figure 4.17: Foam sample with thirteen ink markers.

lines cross over. The crush stress of the foam with density 31.2 kg/m^3 *increases* with increasing impact velocity, whereas the crush stress of the foam with density 50.6 kg/m^3 *decreases* with increasing impact velocity. Both effects cancel each other out, when only strain rate dependency is considered. That is why the material showed no impact-velocity dependency.

Local Deformations

Local deformations of the foam samples were measured using high-speed video capturing in combination with a marker tracking algorithm. A high-speed monochrome CCD camera (Kodak Ektapro HS 4540) captures 18000 frames per second at a resolution of 256×64 pixels. Figure 4.17 shows an undeformed foam sample with the thirteen markers. The marker distribution is Λ-shaped, which al-
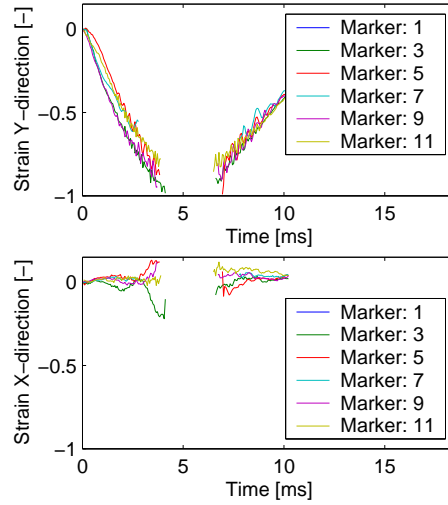
Figure 4.18: Local strains of a sample during impact (v≈6 m/s, m=4.608 kg, ρ=31.2 kg/m^3).
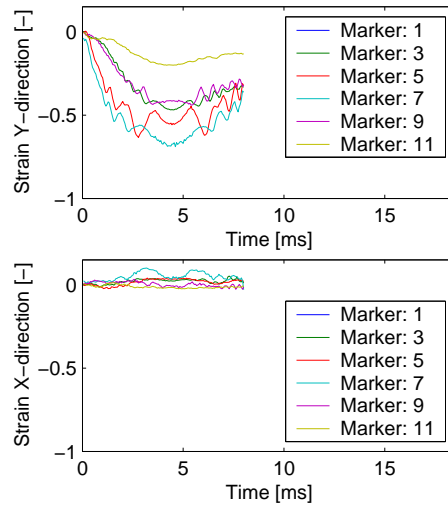
Figure 4.19: Local strains of a sample during impact (v≈4 m/s, m=3.805 kg, ρ=86.8 kg/m^3).

lows the marker tracking algorithm to track the markers more easily. Otherwise, the marker tracking algorithm cannot tell the markers apart at large deformations, when the distance between markers becomes less than one pixel.

The markers were tracked using MATLAB's Image Processing Toolbox [MATLAB, 1999]. This toolbox allows computing of the marker positions from contour plots of the images using the circle fit method [de Kraker, 1993]. The local strains were computed from the relative displacements of two neighbouring markers.

Figure 4.18 and Figure 4.19 show two typical strain distributions. Figure 4.18 shows a uniform strain field in the y-direction and hardly any deformation in the x-direction, which means the Poisson ratio is almost zero. Between four and seven milliseconds, the deformations were too large for single markers to be distinguished. Consequently, the marker tracking algorithm was unable to track the markers

during this period. At about 80% strain in the y-direction, just before the markers are lost, there is an increase in the strain in the x-direction, which means the Poisson ratio is no longer zero. There is no more room for the cells to crush into, so they have to push out neighbouring material. This behaviour is typical for the bottoming out phase. In the rebound phase, after about seven milliseconds, the markers became distinguishable again and the marker tracking algorithm was reactivated.

Some experiments showed inhomogeneous strain fields as shown in Figure 4.19. These inhomogeneous strain fields occurred mainly on high-density foam samples ($\rho = 50.6$ kg/m^3 and $\rho = 86.8$ kg/m^3) deformed at a high rate (v $\approx$ 8 m/s). The foam sample deformation occurs mainly at the upper side, at which the drop mass impacts the foam sample. Instead of a homogeneous deformation, a crush front occurs at the side of the drop mass. The lower part of the material only deforms as the crush front reaches this part of the material. As a result, the lower side of the sample remains almost undeformed. As mentioned before, attempts to further investigate the local deformation patterns failed.

Besides these inhomogeneous strain fields, high-density EPS foam also showed strange strain-rate dependent behaviour when loaded at high impact-velocities. These effects could be correlated. The high-energy impact may locally weaken the material. A weaker material buckles more easily and as a result leaves the other part of the material unharmed until local bottoming out occurs. Then the neighbouring material starts to buckle. A micro-mechanical analysis of the material may reveal the true nature of this phenomenon. However, this is beyond the scope of this research.

Modelling the EPS Foam

EPS foam samples of different densities were tested at strain rates up to 320 s^{-1}. The bulk material behaviour of EPS foam in high-velocity impact does not significantly differ from the behaviour at low-velocity impact. Therefore, modelling strain-rate dependency is not required. The crush front, that appears in some experiments can not be modelled with the current material models available in MADYMO, and will thus not appear in the simulations. The crush front did not appear to affect the global material behaviour and will probably not affect the headform's response in helmeted head impact. The MADYMO material model FOAM [TNO Automotive, 2001, Reference Manual, p. 251] is used to model EPS using the compression curves from the static compression tests (Figure 4.6) and Young's moduli from Table 4.2. This material model correctly models the compressive behaviour of foams, but is less suited in shear loading conditions. In helmeted head impact, the main deformation is compression.

4.4.2   Comfort Padding Liner

The comfort padding of the helmet is made of Polyurethane (PU) foam. PU foam is a soft, low-density, open-celled flexible foam. As seen in Chapter 3, the comfort padding liner can have a significant impact on the results of the drop tests and should therefore also be modelled. The compression curves were measured on 47.3×44.0×39.6 mm (l×w×h) foam samples using an MTS 858 Mini Bionix draw-bench. The loading and unloading results for various compression velocities (up to 1.2 m/s) are shown in Figure 4.20. This material also shows no strain-rate dependency and will also be modelled using MADYMO's FOAM material model. Young's modulus of PU foam is 470 kPa.
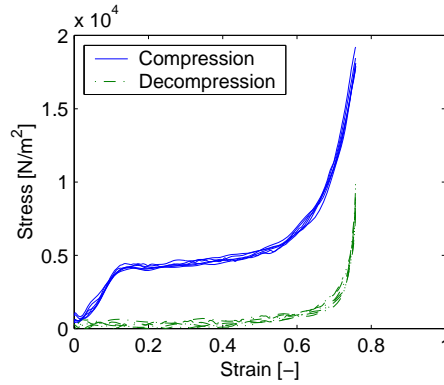
Figure 4.20: Compression experiments on PU foam samples at different compression velocities (initial strain rate: 6.7 - 40 s^{-1}).

Table 4.3: Material properties of the outer shell [Brands *et al.*, 1997].

Young's modulus	Poisson ratio	Density
E = 8.54*10^9 N/m^2	0.325	2.08*10^3 kg/m^3

4.4.3 Outer Shell

The outer shell consists of 3520 4-node shell elements. The outer shell material properties were copied from the helmet model used by Brands *et al.* [1997]. They used a linear-elastic material model with the material properties displayed in Table 4.3. There is no reason to doubt that a linear elastic material model does not suffice for this material.

4.4.4 Assembly of the Helmet Model

During an impact, the comfort foam can be compressed to less than 5% of its initial thickness. This lead to instability in the simulations. To overcome this problem, the comfort foam and protective padding liner are modelled as one material. The combined compression curve of the material is derived from compression curves of both materials. Since the materials are compressed in the same direction, the stresses (and thus the forces) are always equal for both materials. The combined material is derived by simply adding up the displacements (see Figure 4.21). The curve is dependent on the ratio between the thicknesses of both layers, which is not constant over the entire helmet. Therefore, the helmet is divided into sections of almost constant thickness ratio. Furthermore, the density of the protective padding is not constant over the helmet. Therefore the helmet is also divided into sections with equal protective padding liner density. Figure 4.22 shows the combination of these two distributions into one helmet model. The comfort foam and protective padding liner consist of 7656 8-node reduced-integration brick elements.

The contact interface between helmet and headform is modelled using a penalty force method. In reality, the helmet is somewhat clamped onto the headform by the comfort foam. This means that internal stresses are already present in the helmet before the drop test. A pre-simulation is run to
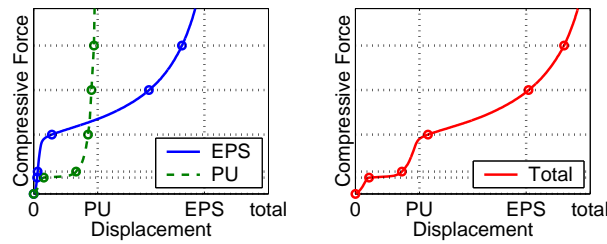
Figure 4.21: Deriving the global deformation curve of the combined foam material from the EPS and PU deformation curves.
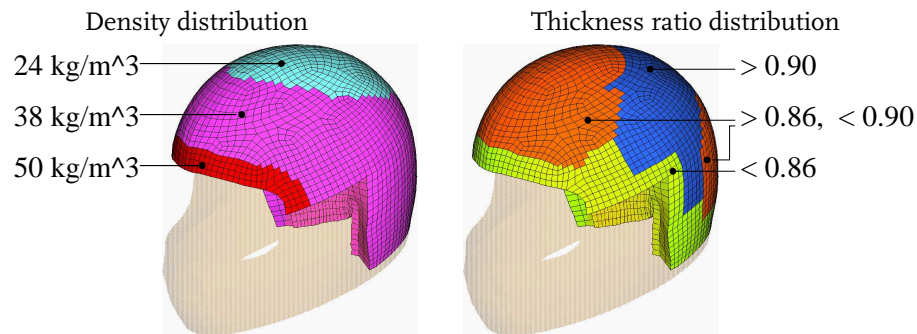
Figure 4.22: Density distribution (*left*) and thickness ratio distribution (*right*) of the numerical helmet model.

place the helmet onto the headform, however this simulation is too time consuming to run before each simulation. Also, since MADYMO does not offer the possibility to pre-stress the material, no stresses are present prior to the start of the simulation.

Now that both headform models and the helmet model are complete, helmeted head drop test simulations can be performed and the results are compared to those of drop test experiments.

4.5   Helmeted Head Drop Test Simulations with Conventional Head-form

The helmet model is rather complex and has a rather fine mesh compared to other Finite Element helmet models [e.g.: Köstner & Stöcker, 1987; Yettram *et al.*, 1994; Brands *et al.*, 1997; Chang *et al.*, 2000]. Even though some of these models are validated against linear acceleration data from helmeted headform drop tests, they are not subjected to a convergence study. However, in this study it is found that an increase in mesh density is required to obtain reliable results. Since this model is more reliable, it is also more sensitive to modelling inaccuracies. The protective padding liner density and outer shell thickness distributions, as discussed in Section 4.4.4 do not only, make the model more in accordance with reality, but without those, the model does not yield satisfactory results.

Figure 4.23: Comparison of the conventional headform Top impact drop test simulation results with drop test experiment results. *Left:* Resultant translational headform acceleration (a_r). *Center:* Resultant rotational headform velocity (ω_r). *Right:* Head impact power (HIP).

Figure 4.24: Comparison of the conventional headform Front impact drop test simulation results with drop test experiment results. *Left:* Resultant translational headform acceleration (a_r). *Center:* Resultant rotational headform velocity (ω_r). *Right:* Head impact power (HIP).

4.5.1 Top Impact

Figure 4.23 shows a comparison of the conventional headform Top impact drop test simulation results with the results of the drop test experiments. The resultant translational headform acceleration of the numerical model shows good resemblance with the one obtained in the experiment. However, its maximum value is 10-15% lower than the one measured in the experiment. Opposite to that, the unloading part of the curve, after about 7.5 ms, is a bit overestimated by the simulation. This is acceptable, since it is unlikely to affect HIC, $a_{\max}$, $\omega_{\max}$ and $\text{HIP}_{\max}$.

The resultant rotational headform velocity showed a large spread in the experiments (over 50 %). Therefore, no conclusions can be drawn here, except that the simulation results follow roughly the experimental results, both in shape and in magnitude. The amount of energy transferred to the headform is fairly accurately predicted by the numerical model.

4.5.2 Front Impact

Figure 4.24 shows a comparison of the conventional headform Front impact drop test simulation results with the results of the drop test experiments. In this particular impact site, the numerical results show quite large deviations from the experimental results. The resultant translational headform acceleration is underestimated by the model and the duration is too long. As a result, the resultant

Figure 4.25: Comparison of the conventional headform Rear impact drop test simulation results with drop test experiment results. *Left:* Resultant translational headform acceleration (a_r). *Center:* Resultant rotational headform velocity (ω_r). *Right:* Head impact power (HIP).

rotational headform velocity of the simulation continues to increase a bit longer than the one in the experiments, resulting in an overestimate of about 50 %. Thus, in the simulation more energy is transformed into rotational kinetic energy, whereas in the experiments, the changes in translational kinetic energy are larger. Looking at HIP, the translational energy outweighs the rotational energy, resulting in higher values and shorter duration of the HIP time history for the experiments.

4.5.3   Rear Impact

Figure 4.25 shows a comparison of the conventional headform Rear impact drop test simulation results with the results of the drop test experiments. The best results were obtained from the rear impact simulations. Both resultant translational headform acceleration and HIP are predicted quite well. Up to the duration of the impact, the resultant rotational headform acceleration shows acceptable results. However, when the impact is over, the rotational velocity in the simulation keeps increasing some 3 ms longer, resulting in an overestimate of about 30 %.

4.6   Helmeted Head Drop Test Simulations with Flexible Headform

4.6.1   Top Impact

Figure 4.26 shows a comparison of the flexible headform Top impact drop test simulation results with the results of the drop test experiment. The result for the Top impact simulation using the flexible headform show closer correlation with the experiment than those using the conventional headform (see Section 4.5.1). The resultant translational headform acceleration is of the same magnitude, but the duration is somewhat longer than in the experiment. The resultant rotational headform velocity of the simulation matches the experiment quite well, ignoring the erratic spikes in the experimental signal (see also Section 3.3.2). These spikes are the result of a cable failure and has already been discussed in Section 3.3.2. As a result of the longer duration of the resultant translational headform acceleration, HIP has also a longer duration and is also overestimated by the model (up to 25%).

4.6.2   Front Impact

Figure 4.27 shows a comparison of the flexible headform Front impact drop test simulation results with the results of the drop test experiment. Like the drop tests using the conventional headform
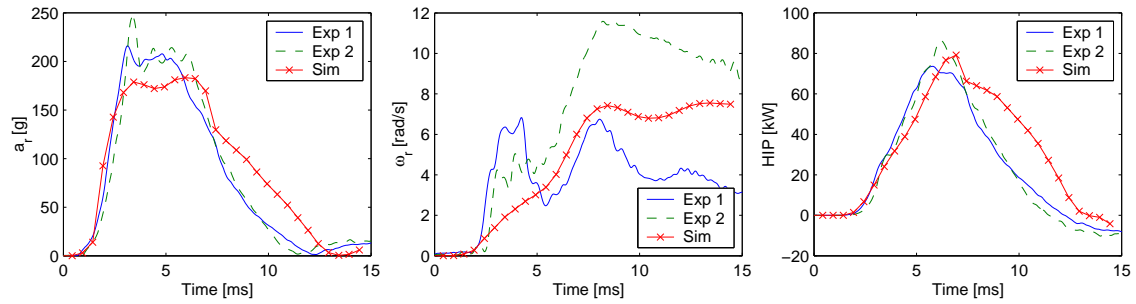
Figure 4.26: Comparison of the flexible headform Top impact drop test simulation results with drop test experiment results. *Left:* Resultant translational headform acceleration (a_r). *Center:* Resultant rotational headform velocity (ω_r). *Right:* Head impact power (HIP).
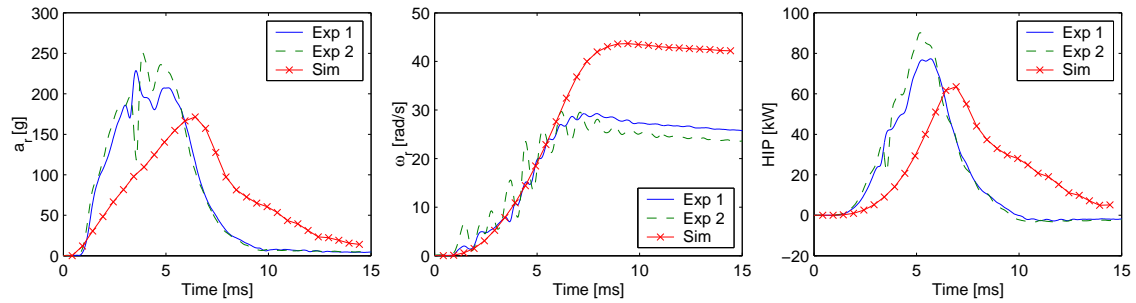

Figure 4.27: Comparison of the flexible headform Front impact drop test simulation results with drop test experiment results. *Left:* Resultant translational headform acceleration (a_r). *Center:* Resultant rotational headform velocity (ω_r). *Right:* Head impact power (HIP).

(Section 4.5.2), the numerical results for this impact site also show quite large deviations from the experimental results. However, the differences between the numerical results and experimental results are smaller than when the conventional headform is used. Again, the resultant translational headform acceleration is underestimated by the model and the duration is too long; the resultant rotational headform velocity of the simulation continues to increase a bit longer than the one in the experiment, resulting in an overestimate of about 50 %; and the translational energy outweighs the rotational energy, resulting in ± 15 % higher values for HIP_{max} and shorter duration of HIP for the experiment.

4.6.3 Rear Impact

Figure 4.28 shows a comparison of the flexible headform Rear impact drop test simulation results with the results of the drop test experiment. Except for the mismatch of the resultant rotational headform velocity after about 10 ms, all three simulation results show close correlation with the experimental results similar to what was found with the drop tests using the conventional headform (Section 4.5.3).
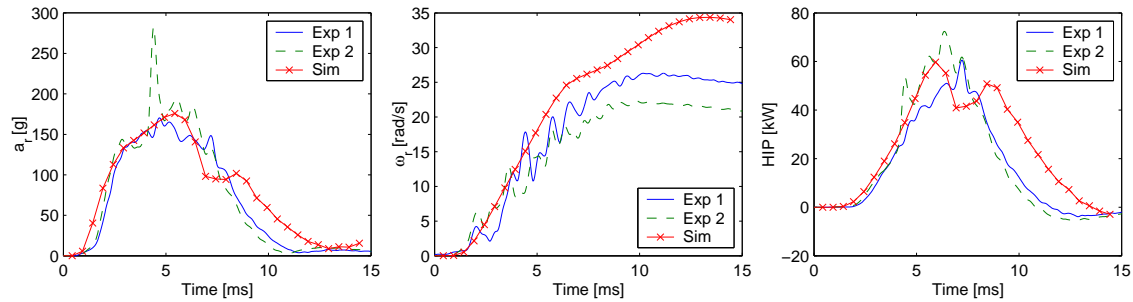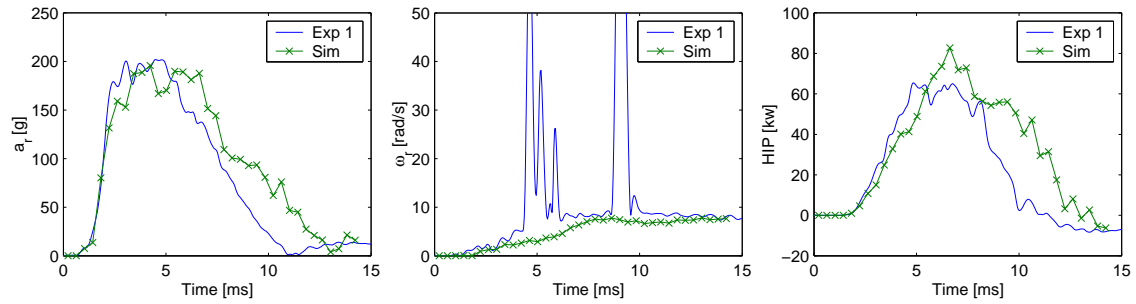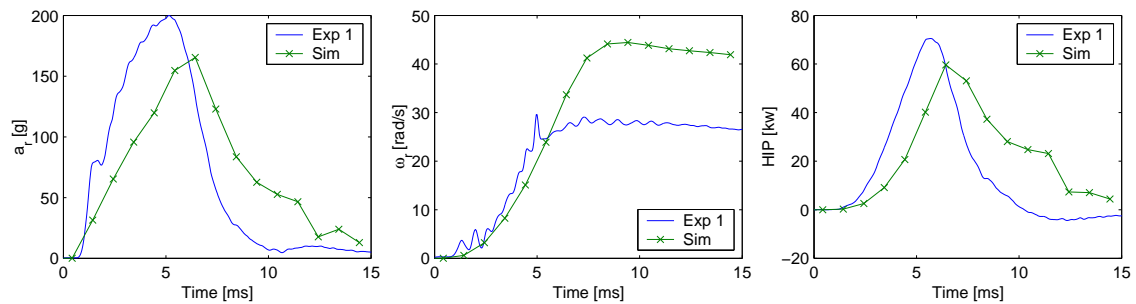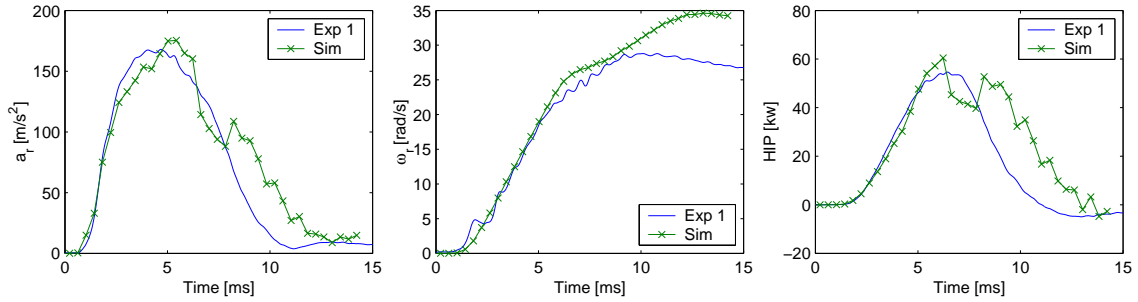
Figure 4.28: Comparison of the flexible headform Rear impact drop test simulation results with drop test experiment results. *Left:* Resultant translational headform acceleration (a_r). *Center:* Resultant rotational headform velocity (ω_r). *Right:* Head impact power (HIP).

4.7   Conclusions on Model Validity

A Finite Element model of the flexible headform is built and validated using the experimental results from the Hodgson test, the impulse test and a static compression test. The model matches the Hodgson test and the static compression test very well, both in shape (duration deviation < 9%) and in magnitude (maximum acceleration deviation < 10%). The impulse test could not be used to validate the model, because of numerical artifacts. The Finite Element model of the conventional headform is not validated, since it is modelled as a rigid structure.

The Finite Element helmet model, developed by Brands *et al.* [1997] has been further improved. The major enhancement is the use of a compressible and more realistic material model for the protective padding. Other recommendations of the study by Brands *et al.* [1997] are also implemented. These are: The modelling of comfort foam, the density distribution of the protective padding liner and the thickness distribution of the outer shell. Especially the latter two turned out to significantly improve the simulation results, compared to the experimental results, which confirms the conjecture of Brands *et al.* [1997]. The Finite Element model of the helmet is only validated in helmeted head drop tests, and not in helmet-only tests.

Despite these major model enhancements, the FOAM material model still has two shortcomings: It is too compliant in shear and it remains fully compressible during the bottoming-out stage. These limitations should be considered when drawing conclusions from the helmeted head drop test simulations.

When comparing the simulations of the helmeted head drop tests with the experiments, the drop tests using the flexible headform matched the experiment slightly better than the drop test using the conventional headform. Since the model of the conventional headform is less complex than the model of the flexible headform, one would expect the opposite. Apparently, the modelling assumptions of the helmet and the flexible headform cancel each other out.

The simulations yielded the best results in Top impact. In Rear impact the results are also acceptable. Only the Front impact drop tests could not be predicted very well by the model. The shear strains in the FOAM material are not the cause of the deviation between simulation and experiment, since they are equally small for all three impact configurations and should therefore cause deviations in all three impact configurations, instead of only in Front impact. The compressibility in the bottoming out phase is neither the cause of the deviation, since bottoming out would occur only at compressive strains over 75% (after about 5 ms). However, the simulation for Front impact deviates from the

experiment already at the start of the impact. The only remaining difference with the Top and Rear impact is that in Front impact the impact site is close to the edge of the outer shell, where the visor is located. So, at this point, there is less material on one side of the impact location. Even though this is also the case in the experiment, it is unknown what the effects of neighbouring material are on the material behaviour of the used material model in the Finite Element calculations.

Despite the differences for Front impact between the results from the simulations and those from the experiments, the helmet and headform models yield sufficiently acceptable results, to continue with a sensitivity analysis (Chapter 5) and to investigate the effect of helmet design changes (Chapter 6).

The accuracy of the X-ray is insufficient to directly compare marker trajectories in terms of global coordinates. A transformation to local coordinates with respect to the headform's centre of gravity lacked the positions of markers attached to the rigid part of the headform. However, the brain material model used in the simulations showed accurate results in confined tests, performed by Brands *et al.* [1999]. Therefore, an analysis on strains inside the brain, in terms of CSDM, will be included in the following chapter.

Chapter 5

Helmet Design Sensitivity Analysis Using Simulated Helmet Drop Tests

5.1 Introduction

With the validated models from Chapter 4, a sensitivity analysis is performed to investigate what parameters will in what way determine the outcome of a drop test. The analysis will provide insight in the dynamic behaviour of the helmet and in the interaction between headform and helmet.

The analysis is based on the injury parameters $a_{\max}$, HIC, $HIP_{\max}$, $\omega_{\max}$ and CSDM for various impact and material parameters. The impact and material parameters under consideration are:

- Impact site: Top, Front and Rear impact helmeted head drop tests, as defined in ECE-R.22, represent three categories of general motion (translational, rearward rotational and forward rotational, respectively). This parameter investigates the effects of the eccentricity of the load.

- Headform type: This part will focus on the effect of the presence of skin on the outcome of the drop test simulations.

- Boundary conditions: To what extent does the support of the neck change the simulation results. Guided free fall (ECE-R.22) is compared to guided fall, where headform rotations are suppressed (e.g. Snell M2000, DOT FMVSS 218).

- Helmet material parameters: This section will provide insight in the change in headform response with respect to a change in the various material parameters. The varied parameters are outer shell stiffness and protective padding liner density, and various combinations of the two.

- Impact velocity: In the ECE-R.22 only one impact velocity needs to be tested. Higher or lower impact velocities also provide insight in the helmet's performance for more severe and less severe impacts, respectively.

With the results, the hypotheses stated in Chapter 1, p. 20, will be tested, resulting in conclusions on the added value of the flexible headform with respect to the conventional headform.
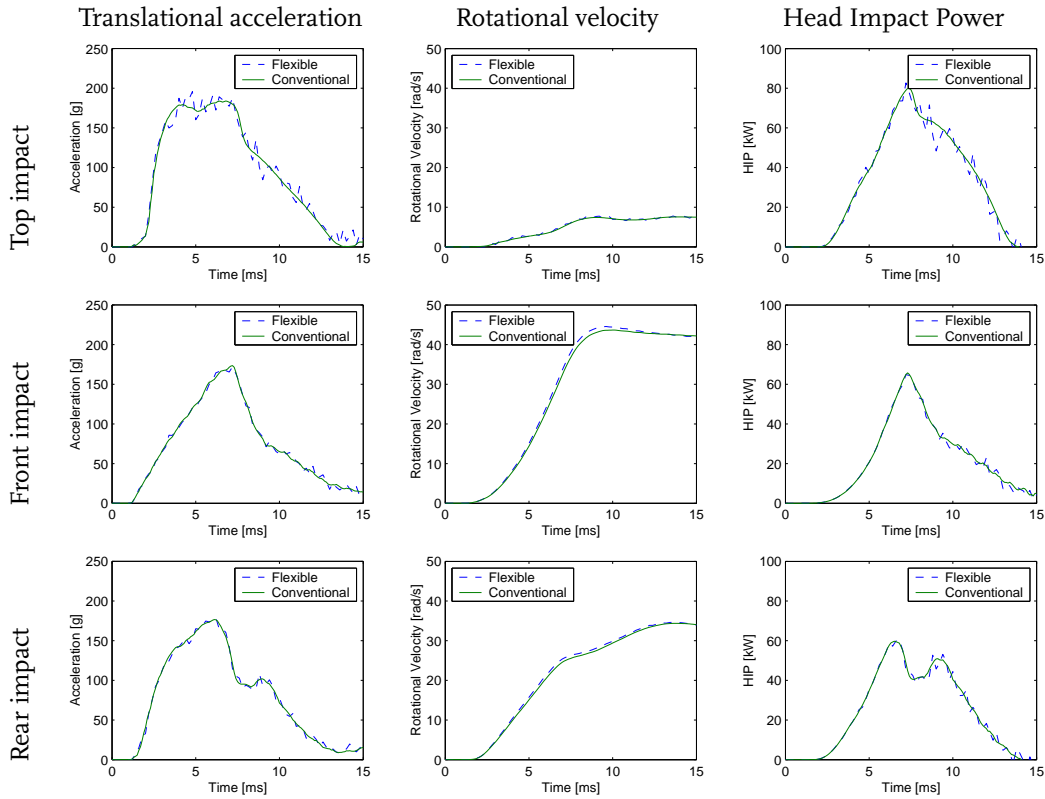
Figure 5.1: Resultant translational headform acceleration, resultant rotational headform velocity and Head Impact Power for the drop test simulations of the various impact sites compared between headform used.

5.2 Effect of Impact Site

The effect of the impact site on the headform response is already investigated with the experiments discussed in Chapter 3, but this discussion will be briefly repeated and extended with a discussion on CSDM. Figure 5.1 shows the results of the drop test simulations for the various impact sites. The same trends as in the experiments can be observed. Top impact results in the highest resultant translational acceleration, whereas resultant rotational velocities are lowest for this impact configuration. For Front and Rear impact it is exactly the other way around due to the eccentricity of the impact as explained in Section 3.4.1.

In contrast to the experimental results, the differences between the results for the conventional headform and those for the flexible headform are negligible, whereas in the experiments there was a small but statistically significant difference between the two. Apparently, the model is not capable of explaining the deviations between the two. In the experiments, friction between headform and helmet was thought to be one of the causes for the difference between the results for the drop tests with the Size L helmet and with the Size M helmet. The friction forces acting between the helmet and the headform in the experiments are less prevalent in the simulations due to the reduced capacity of the FOAM material model to withstand shear forces. Furthermore, in the experiments the helmet is somewhat clamped onto the headform, due to the compression of the comfort foam while putting on the helmet. Thus, the comfort padding is already somewhat compressed before the actual drop test, which also

Table 5.1: Injury criteria compared for the various impact sites.

	$a_{\max}$ [g]	HIC	$\omega_{\max}$ [rad/s]	$\text{HIP}_{\max}$ [kW]	CSDM [-]
Top impact	195	2121	7.8	82.7	0.052
Front impact	172	1052	44.6	64.9	0.879
Rear impact	179	1377	34.6	60.5	0.753

contributes to an increased friction between head and helmet. In the simulations it is not possible to model this pre-stressing of the material, which also contributes to low friction forces. Nevertheless, the numerical results match those of the drop test experiments quite well. There is a better match for the drop tests using the flexible headform, than for those using the conventional headform.

Since the differences between the drop test simulations using the conventional headform and those using the flexible headform are small, these will no longer be compared. Henceforth, only the drop tests using the flexible headform will be discussed, since they allow for brain deformations to be quantified.

Table 5.1 shows the values for $a_{\max}$, HIC, $\text{HIP}_{\max}$, $\omega_{\max}$ and CSDM for the Top, Front and Rear impact drop test simulations. CSDM is computed for a critical strain level of 0.15 in accordance with the work of Bandak *et al.* [2001] as described in Section 1.2.2. These results confirm what was found previously. Even though Top impact yields the highest values for the translational induced head injury parameters $a_{\max}$ and HIC, the rotational induced head injury parameter CSDM indicates that Front and Rear impact are actually more hazardous. $\text{HIP}_{\max}$, which accounts for both translational and rotational induced head injury, indicates that Top impact is the most severe impact. It should be noted that each injury parameter is based on a different type of head injury and can therefore not easily be compared.

5.3 Skin

In Section 2.5.2, it is made plausible that the skin does not have to be modelled in helmeted head impact, provided that no bottoming-out occurs. This conclusion is based on the padded Hodgson test. It is still to be investigated, whether this also holds in helmeted head impact simulations. In this section, the skin is modelled using the same flexible headform model. In order not to change the headform's mass and geometry, the skin is modelled with the elements of the former skull and the skull is modelled as shell elements between the skin and the brain (see Figure 5.2). Both the skin and the skull are now 7 mm thick, which is comparable to the average human skull and skin thickness. To compensate for the added mass of the inserted shell elements of the skull, the skull density is reduced to 100 kg/m^3.

Hendriks *et al.* [2003] investigated the mechanical properties of the skin and found that an extended Mooney material model matched their experimental results best. The strain energy function they used was:

$$W = C_{10}(I_1 - 3) + C_{11}(I_1 - 3)(I_2 - 3) \tag{5.1}$$
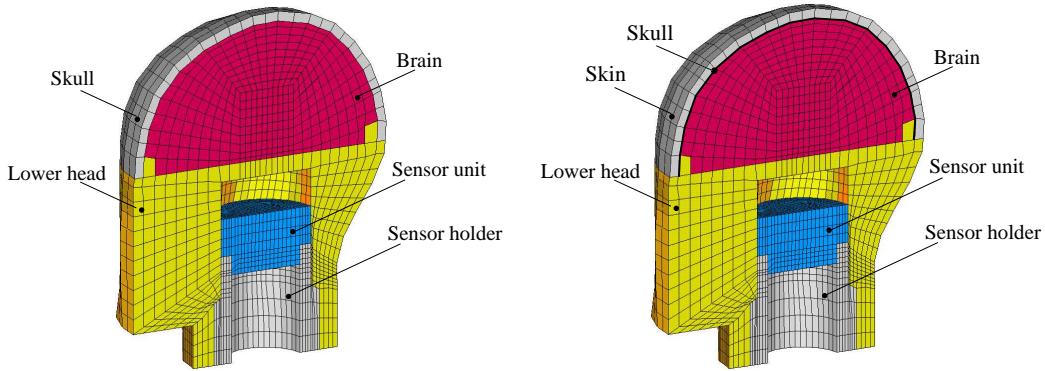
Figure 5.2: *Left:* Original flexible headform model. *Right:* Flexible headform model with skin.

Table 5.2: Injury criteria compared for the various impact sites.

Impact site		$a_{\max}$ [g]	HIC	$\omega_{\max}$ [rad/s]	$\mathrm{HIP}_{\max}$ [kW]	CSDM [-]
Top impact	Without skin	196	2121	7.8	82.7	0.052
	With skin	224	2247	8.6	81.2	0.067
Front impact	Without skin	172	1052	44.6	64.9	0.879
	With skin	166	983	47.4	62.4	0.891
Rear impact	Without skin	179	1377	34.6	60.5	0.753
	With skin	179	1405	35.5	65.4	0.771

where W is the strain energy, C_{10} and C_{11} are constants, and I_1 and I_2 are the first and second invariant of the right Cauchy-Green strain tensor $\boldsymbol{B}$, respectively. In MADYMO, this model is only available in the form:

$$W = A(I_1 - 3) + B(I_2 - 3) + C(I_3^{-2} - 1) + D(I_3 - 1)^2 \qquad (5.2)$$

where W is again the strain energy, A, B, C and D are constants, and I_1, I_2 and I_3 are the first, second and third invariant of the right Cauchy-Green strain tensor $\boldsymbol{B}$, respectively. For small strains, the second-order term in Equation (5.1) can be neglected and both models are equivalent when $A = C_{10}$ (= 9.4 kPa) and $B = C = D = 0$ kPa. For larger strains, these models cannot be made equivalent. Therefore, the same parameters will be used.

Figure 5.3 shows the results of the drop test simulations using the flexible headform with and without modelling the skin. Based on these simulations, the hypothesis that the skin is not important in helmeted head impact is accepted. Table 5.2 also shows that the values for $a_{\max}$, HIC, $\mathrm{HIP}_{\max}$, $\omega_{\max}$ and CSDM for the Top, Front and Rear impact drop test simulations with and without modelling the skin do not differ much. In the following simulations, the skin is no longer included in the model of the flexible headform.

Figure 5.3: Resultant translational headform acceleration, resultant rotational headform velocity and Head Impact Power of the drop test simulations using the flexible headform with and without modelling the skin.

5.4 Effects of Boundary Conditions

Generally there are two types of helmet drop test standards. The first is a drop test in which the headform and helmet are free to move during impact, such as ECE-R.22. The second type is a drop test in which the headform is not allowed to rotate, such as the Snell M2000 and the DOT FMVSS 218 (see also Appendix A).

Figure 5.4 shows the results of the standard ECE-R.22 drop test simulations compared with those where the rotation of the headform was not allowed. It should be noted that all other parameters of the drop test remain unchanged (headform, impact velocity, etc.). For Top impact, there is no difference between the two configurations, since the headform already showed little rotation during the Top impact drop test (see Figure 5.1). For Front and Rear impact however, the resultant headform accelerations significantly increase by 30% for Front impact and by 10% for Rear impact. For HIP, these increases are 53 and 18 percent, respectively. The shape of the time histories of the resultant translational headform acceleration and of HIP do not change.

Table 5.3 shows the values for a_{max}, HIC, HIP_{max}, ω_{max} and CSDM for the Top, Front and Rear impact drop test simulations. The table shows that for HIC, the consequences are even more drastic. HIC increases by almost 90% for Front impact and 36% for Rear impact. Still, the a_{max} and HIC values are all below their thresholds. And even without rotation, the HIC values for Front and Rear impact do not exceed the HIC value for Top impact. However, the shape of the acceleration time history for
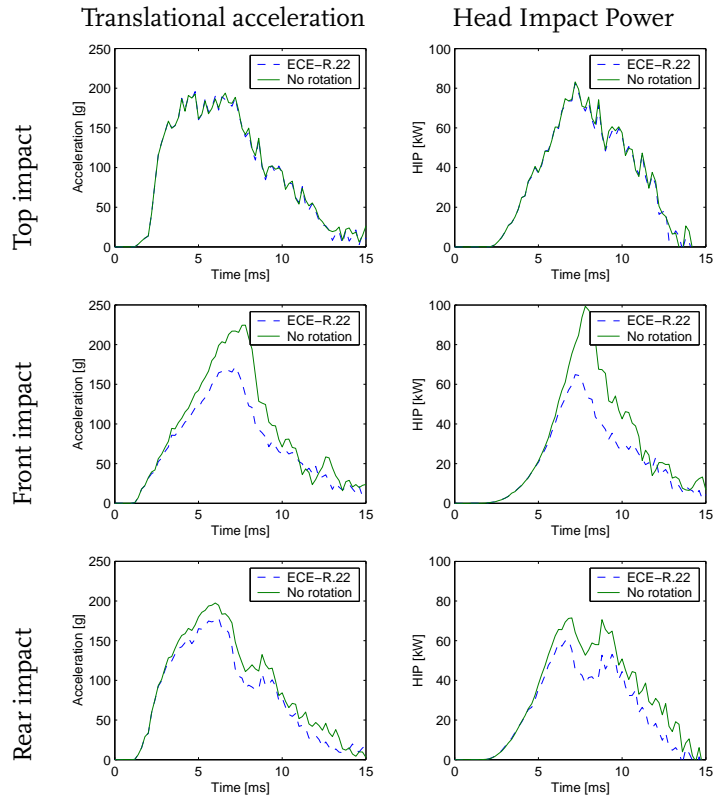
Figure 5.4: Resultant translational headform acceleration and Head Impact Power of the standard ECE-R.22 drop test simulations compared with those where the rotation of the headform was not allowed.

Table 5.3: Injury criteria compared for the various impact sites.

Impact site		a_{max} [g]	HIC	ω_{max} [rad/s]	HIP_{max} [kW]	CSDM [-]
Top impact	ECE-R.22	196	2121	7.8	82.7	0.052
	No rot.	194	2151	0.0	83.2	0.004
Front impact	ECE-R.22	172	1052	44.6	64.9	0.879
	No rot.	225	1997	0.0	99.4	0.011
Rear impact	ECE-R.22	179	1377	34.6	60.5	0.753
	No rot.	197	1873	0.0	71.5	0.006

Front and Rear impact is less favourable than that for Top impact, resulting in a higher maximum acceleration. The same holds for HIP, especially in Front impact. It should be noted however that the results of the Front impact simulation did not match those of the experiments as well as the Top and Rear impact did. These results should therefore be considered with caution.

CSDM was already low for Top impact, but it seems when the rotation of the headform is completely suppressed, CSDM almost equals zero. Also for Front and Rear impact, CSDM approaches zero when headform rotation is suppressed.
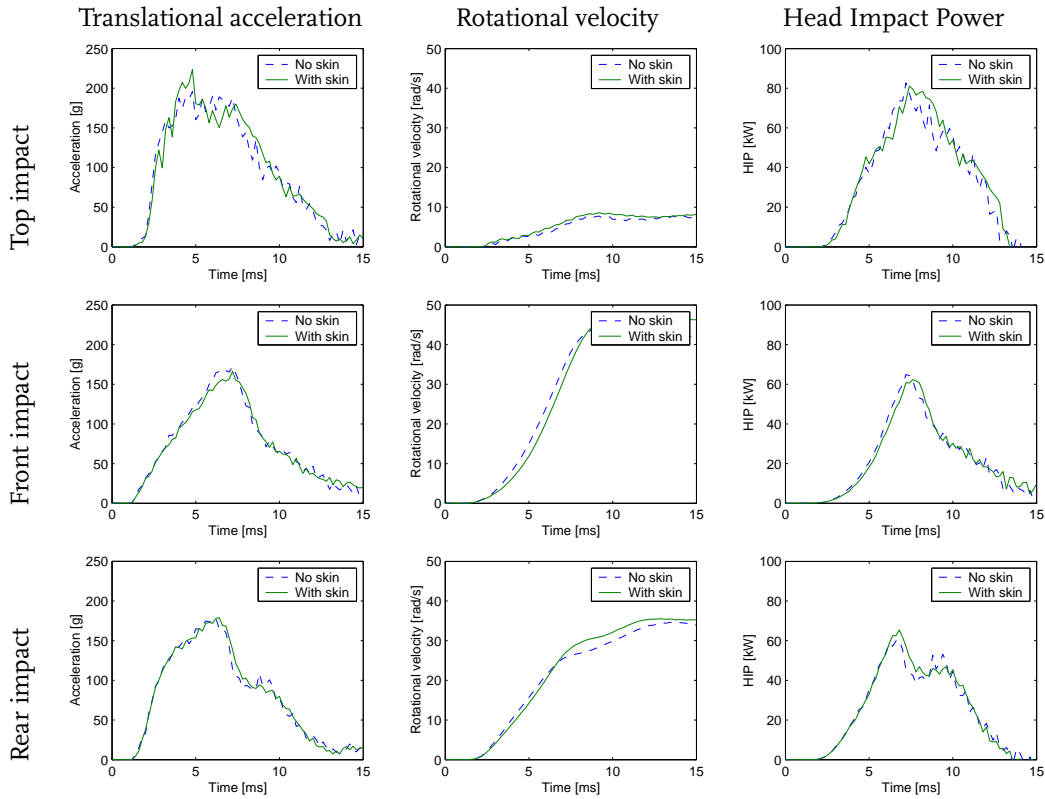
Figure 5.5: Resultant translational headform acceleration, resultant rotational headform velocity and Head Impact Power of the drop test simulations with a standard helmet compared with those with a helmet with a 20% thicker and a 20% thinner outer shell.

In practice, a rotationally suppressed headform probably yields more reproducible results. However, it also less resembles the real world situation and it ignores the human head's assumed sensitivity for different impact directions. The injury mechanism for translational motion differs from that for rotational motion. The CSDM is insensitive for translational motion, which makes it only applicable in unsuppressed helmeted headform drop tests.

5.5 Effects of Material Parameters.

The helmet's two main components are the outer shell and the protective padding liner. The effect of outer shell stiffness is investigated in Section 5.5.1 by changing its thickness. The material properties of the protective padding liner are all combined in its density. The higher the density, the stiffer the material (see also Section 4.4.1). The effect of the protective padding liner density is investigated in Section 5.5.2.

5.5.1 Outer Shell

Figure 5.5 shows the results of the drop test simulations for a 1 mm variation in outer shell thickness. Since the bending stiffness of a thin shell is proportional to the third power of the thickness, the outer shell is up to 70% more compliant and up to 137% stiffer for a 1 mm shell thickness decrease and

Table 5.4: Injury criteria compared for the various impact sites.

Impact site	Shell thickness	$a_{\max}$ [g]	HIC	$\omega_{\max}$ [rad/s]	$\text{HIP}_{\max}$ [kW]	CSDM [-]
Top impact	-1 mm	198	2130	7.2	76.7	0.033
	Standard	196	2121	7.8	82.7	0.052
	+1 mm	207	2162	9.4	83.9	0.066
Front impact	-1 mm	170	944	46.8	59.3	0.884
	Standard	172	1052	44.6	64.9	0.879
	+1 mm	191	1139	41.5	71.2	0.859
Rear impact	-1 mm	175	1368	32.9	65.0	0.735
	Standard	179	1377	34.6	60.5	0.753
	+1 mm	172	1546	36.2	66.0	0.782

increase, respectively. Except for the Top impact simulation with the 1 mm thicker outer shell, the variation of outer shell thickness seems to have only little effect on the headform response. The Top impact simulation for the helmet with the thicker outer shell shows a little more erratic behaviour. The outer shell thickness changes the shape of the translational acceleration and rotational velocity time histories more than its magnitude. In terms of helmet performance, a smooth headform acceleration is favourable over an erratic one, since it reduces maximum headform accelerations and improves comfort to the wearer.

Table 5.4 shows the values for $a_{\max}$, HIC, $\text{HIP}_{\max}$, $\omega_{\max}$ and CSDM for the Top, Front and Rear impact drop test simulations. Again, the effect of the outer shell thickness is small. It mostly affects HIC, which is not strange since HIC itself is, more than the other parameters, a function of acceleration time history. A thicker outer shell leads to higher HIC values.

5.5.2 Protective Padding

Only four different protective padding liner densities are measured (see Section 4.4.1). The compression curves for other protective padding liner densities are obtained by interpolation between the measured compression curves of the next lower and next higher density EPS foam. Figure 5.6 shows the results of the drop test simulations for a 20% variation in protective padding density. The density distribution is still according to Figure 4.22. In contrast to the outer shell thickness, the protective padding liner density changes the magnitude of the acceleration time history, rather than its shape. The same conclusion can be drawn for the HIP time history. Except for the Front impact simulation, a lower protective padding liner density leads to a lower headform acceleration with a longer duration. For Front impact however, the protective padding liner is already compressed to the limits of its shock absorbing capacities. Reducing the protective padding liner density any further leads to bottoming-out of the EPS foam, resulting in a rapid increase of the forces acting on the head and thus in an increase of the acceleration.

The rotational velocity changes only little with a change in protective padding liner density. The changes that do occur are in accordance with previous findings that an increase in translational acceleration leads to a decrease in rotational velocity.

Table 5.5 shows the values for $a_{\max}$, HIC, $\text{HIP}_{\max}$, $\omega_{\max}$ and CSDM for the Top, Front and Rear impact drop test simulations. In accordance with the previous findings for Top and Rear impact, $a_{\max}$, HIC
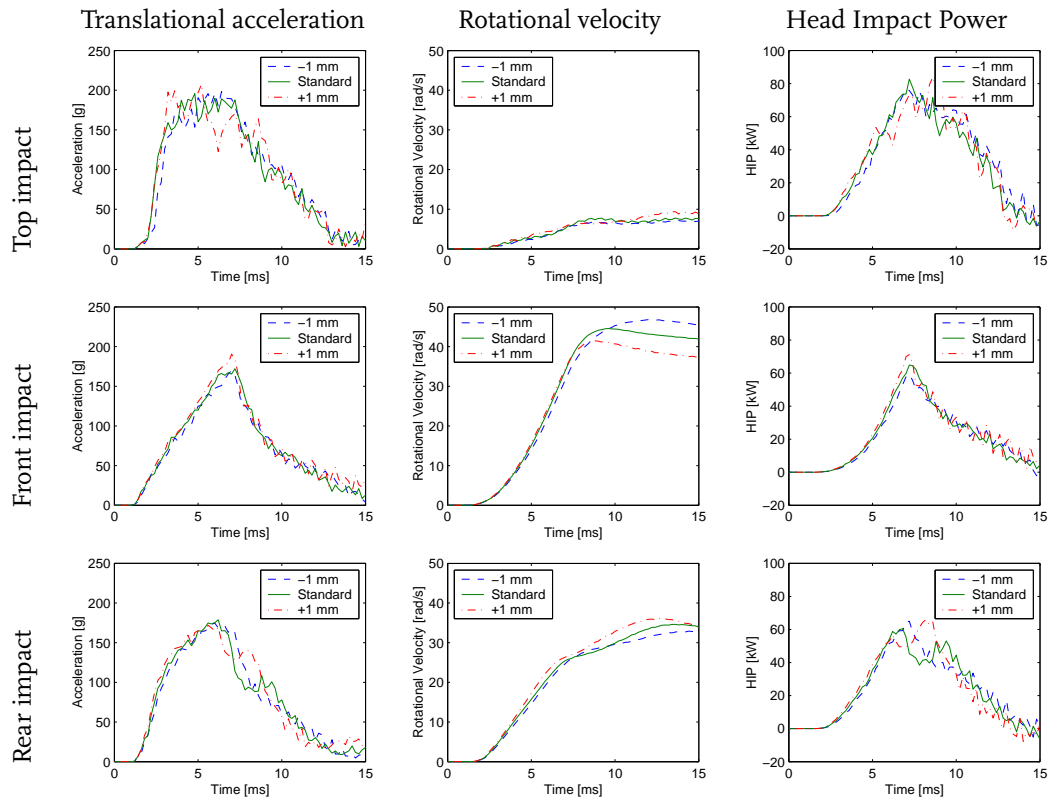
Figure 5.6: Resultant translational headform acceleration, resultant rotational headform velocity and Head Impact Power of the drop test simulations with a standard helmet compared with those with a helmet with a 20% more dense (stiffer) and a 20% less dense (less stiff) protective padding liner.

Table 5.5: Injury criteria compared for the various impact sites.

Impact site	EPS density	a_{max} [g]	HIC	ω_{max} [rad/s]	HIP_{max} [kW]	CSDM [-]
Top impact	-20%	175	1734	8.1	76.1	0.037
	Standard	196	2121	7.8	82.7	0.052
	+20%	236	2554	7.0	93.8	0.039
Front impact	-20%	186	1141	43.5	70.7	0.865
	Standard	172	1052	44.6	64.9	0.879
	+20%	172	1100	45.0	64.4	0.888
Rear impact	-20%	153	1196	37.4	58.2	0.758
	Standard	179	1377	34.6	60.5	0.753
	+20%	205	1646	31.4	75.4	0.734

and HIP_{max} increase and ω_{max} decreases with increasing padding liner density. CSDM follows the trend of ω_{max}, but to a lesser extent.
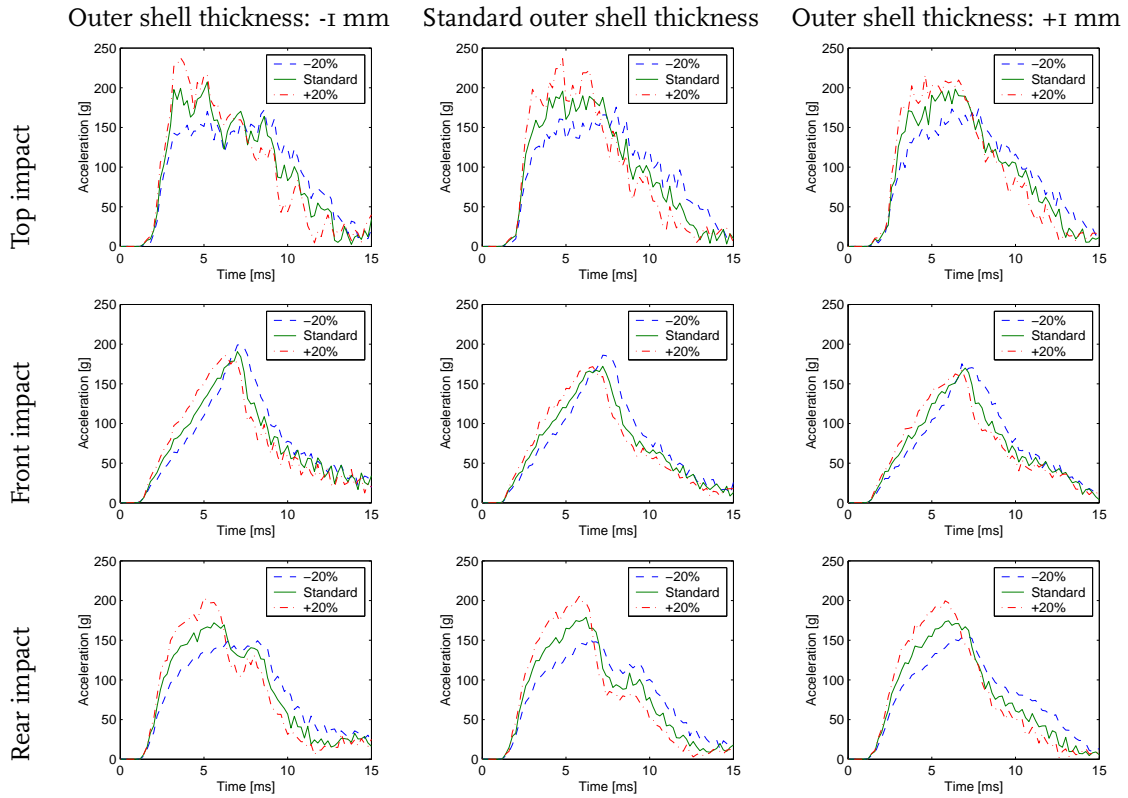
Figure 5.7: Resultant translational headform acceleration of the drop test simulations for a 20% variation in protective padding density (each graph) and a 1 mm variation in outer shell thickness (left to right).

5.5.3   Interaction Between Outer Shell and Protective Padding

The outer shell thickness and the protective padding liner density both determine the outcome of the drop test. Chances are that changing one parameter (e.g. the outer shell thickness) may influence the response with respect to changes in another parameter (e.g. the protective padding liner density). In other words, an interaction between the two may exist. To investigate this interaction, simulations with all combinations of the outer shell thickness and protective padding liner density as discussed in Section 5.5.1 and 5.5.2 are also performed.

Figure 5.7 shows the resultant translational headform acceleration of the drop test simulations for a 20% variation in protective padding density and a 1 mm variation in outer shell thickness. The figure shows that an outer shell thickness variation does not affect the way the protective padding liner density changes the resultant headform acceleration. The same holds for the rotational velocity (Figure 5.8).

5.6   Impact Velocity

Studies of Harms [1981]; Hurt Jr. *et al.* [1981] and Otte *et al.* [1981] show that the average impact velocity in real world motorcycle accidents is about 30 km/h, which is about 1 m/s higher than the currently used 7.5 m/s in ECE-R.22. To investigate the effect of the impact velocity in helmeted head drop tests,
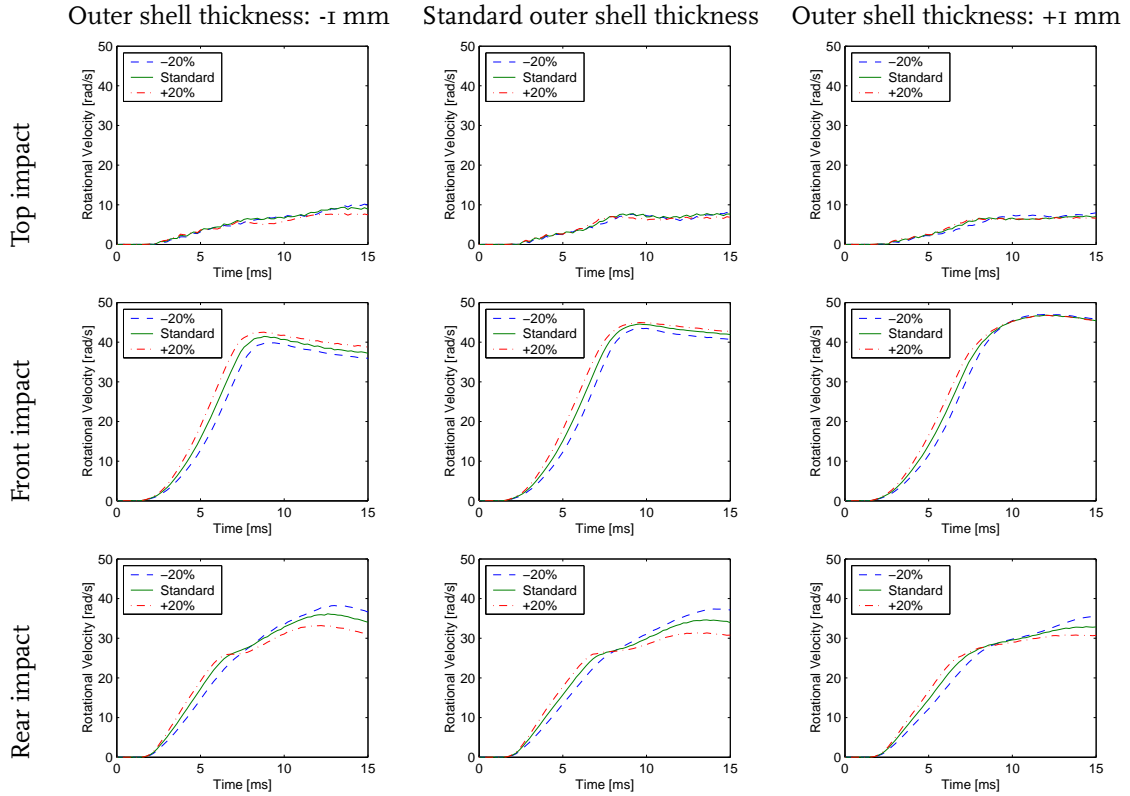
Figure 5.8: Resultant rotational headform velocity of the drop test simulations for a 20% variation in protective padding density (each graph) and a 1 mm variation in outer shell thickness (left to right).

drop test simulations are performed at 5.5, 7.5 and 9.5 m/s. Figure 5.9 shows the results of the drop test simulations at the three different impact velocities. As expected, all parameters increase when the impact velocity is increased. Also the magnitude of the increase is almost equal for all parameters. The shapes of the curves remain unchanged, which leads to the conclusion that, for Top and Rear impact, bottoming-out of the protective padding liner has not yet occurred. For Front impact, the increase in maximum resultant acceleration is larger than for the other two impact configurations. Remarkably, the shape of the responses does not change with increasing impact velocity, which indicates that bottoming-out has not yet occurred.

Table 5.6 shows the values for a_{max}, HIC, HIP_{max}, ω_{max} and CSDM for the Top, Front and Rear impact drop test simulations. Now that the increase in rotational velocity is large with increasing impact velocity, the increase in CSDM is also more apparent. Even though the protective padding of the helmet is still not bottoming-out, most HIC and HIP_{max} exceed their respective tolerance of 2400 and 90.

5.7 Discussion and Conclusions

In the helmeted head drop test experiments (Chapter 3), a difference was found between drop tests with a Size L helmet and those with a Size M helmet. Except for the comfort padding liner thickness, the Size L and the Size M helmet are identical. Since the stiffness of the comfort padding liner is
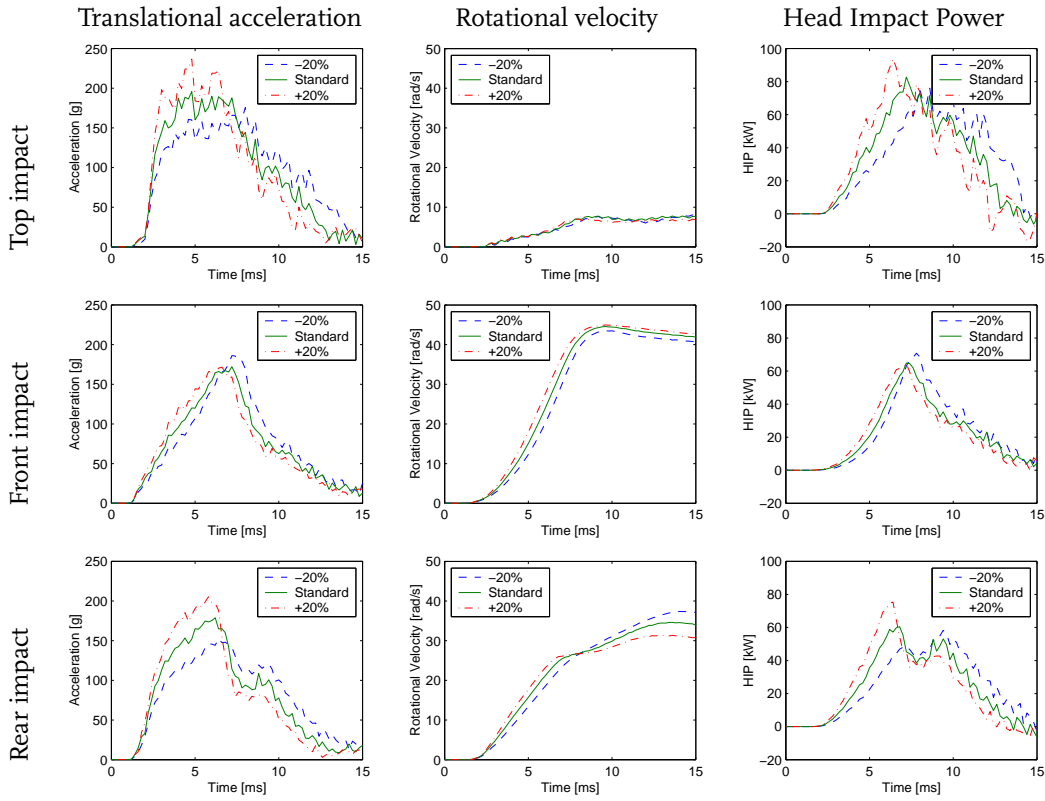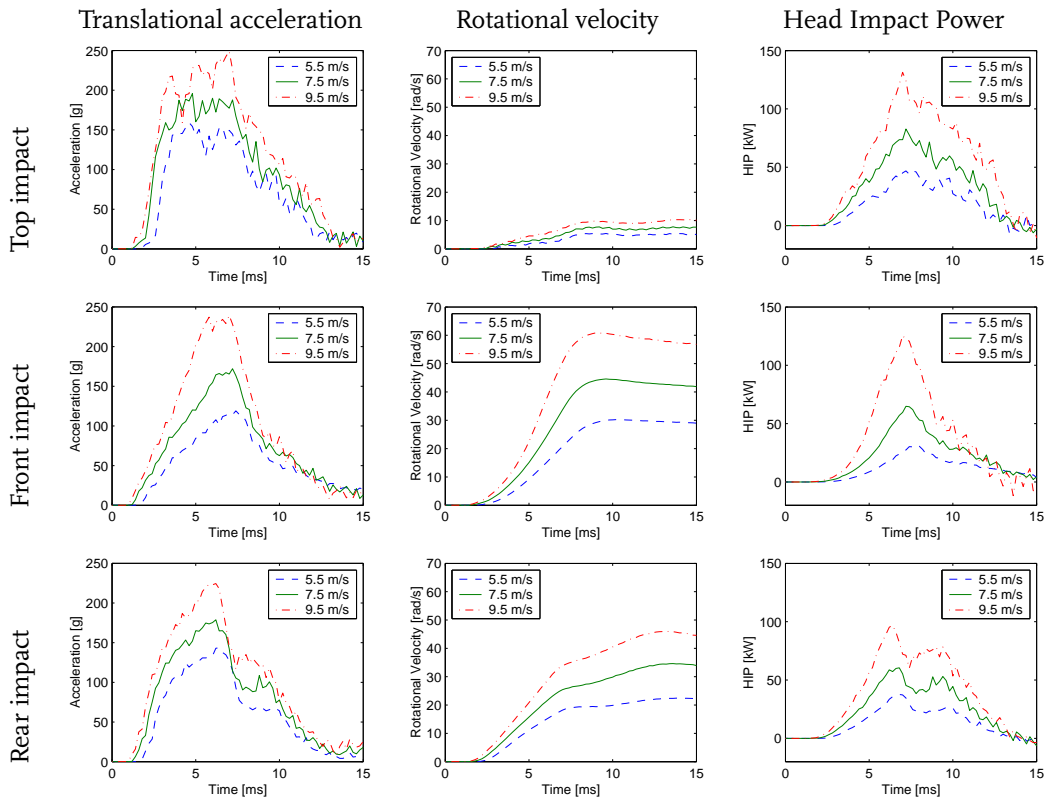
Figure 5.9: Resultant translational headform acceleration, resultant rotational headform velocity and Head Impact Power of the drop test simulations at three different impact velocities.

Table 5.6: Injury criteria compared for the various impact sites.

Impact site	Impact velocity	a_{max} [g]	HIC	ω_{max} [rad/s]	HIP_{max} [kW]	CSDM [-]
Top impact	5.5 m/s	159	1174	5.6	46.8	0.006
	7.5 m/s	196	2121	7.8	82.7	0.052
	9.5 m/s	249	3587	10.3	131.3	0.152
Front impact	5.5 m/s	119	445	30.2	31.8	0.701
	7.5 m/s	172	1052	44.6	64.9	0.879
	9.5 m/s	239	2552	60.9	125.6	0.956
Rear impact	5.5 m/s	144	726	22.4	37.6	0.481
	7.5 m/s	179	1377	34.6	60.5	0.753
	9.5 m/s	225	2357	46.0	96.9	0.870

negligible compared to the protective padding liner stiffness, friction between the head and the helmet is the most probable cause for this difference. However, the foam model used in the simulations has a low resistance to shear compared to the real foam. Since the surface shear stress as a result of the friction forces can never exceed the shear forces in the foam material, the friction forces in the model are also very small.

Furthermore, the absence of friction between the helmet and the headform in the model is probably

	$a_{\max}$	HIC	$\omega_{\max}$	$\text{HIP}_{\max}$	CSDM
$a_{\max}$	1	0.9610	0.2250	0.9223	0.0409
HIC	0.9610	1	-0.0036	0.9228	-0.1690
$\omega_{\max}$	0.2250	-0.0036	1	0.1697	0.9604
$\text{HIP}_{\max}$	0.9223	0.9228	0.1697	1	-0.0229
CSDM	0.0409	-0.1690	0.9604	-0.0229	1

Table 5.7: Correlation between various injury parameters.

also the cause for not being able to discriminate between the two headforms. However, the simulations are not far off and are therefore still very useful in sensitivity and optimisation studies.

One of the effects studied in this chapter is the effect of modelling the skin. The skin did not have a significant influence on the outcome of the drop test simulations. The assumption that the skin is of no significant importance in helmeted head impact is herewith accepted, provided that no bottoming-out occurs in the protective padding liner.

In Chapter 3, it was already found that the standard drop tests measurements should be extended with measuring rotational velocity/acceleration. These findings were confirmed by the results of the simulations. In the experiments, strain-based injury parameters were not investigated, since they can only be evaluated in numerical models. In this chapter, the Cumulative Strain Damage Measure (CSDM) is also evaluated. It was thought that CSDM would be a good parameter for both translational and rotational motion induced injuries. However, this headform model does not support that conclusion. Table 5.7 shows the correlation coefficients between the various injury parameters. A correlation coefficient close to +1 or -1 represents a close correlation, whereas a correlation coefficient close to zero represents no correlation at all. Table 5.7 shows that CSDM is strongly correlated to $\omega_{\max}$ and poorly correlated to any of the other (translational motion based) injury criteria. Therefore, the CSDM adds no value to the assessment of injury in helmeted headform impacts, compared to $\omega_{\max}$, when using this headform.

In an attempt to compare the ECE-R.22 with the Snell M2000 and the DOT FMVSS 218, headform rotation was suppressed in the simulations. As a result, the helmet needs to absorb more energy, since no energy can be transformed into rotational kinetic energy. For Front and Rear impact, this effect was seen in an increase of all (partly) translational injury criteria $a_{\max}$, HIC and $\text{HIP}_{\max}$. The shape and duration of the resultant translational headform acceleration and of HIP time history did not change. This indicates that suppressing the rotational motion of the headform only quantitatively effects the outcome of the drop tests and not qualitatively. This means that both methods of helmet performance evaluation are equivalent, but different thresholds for the injury criteria should be chosen in order to evaluate the helmets for the same performance. However, the ECE-R.22 method should be preferred over the method of Snell and DOT, since it also allows for a helmet evaluation based on rotational motion induced injury.

Even when rotational motion is suppressed, Top impact yields the highest values for HIC even though the resultant translational headform acceleration time history is the most favourable because of its flat and smooth course. The shape of the acceleration time history is mainly determined by the outer shell stiffness, whereas its amplitude is mainly determined by the protective padding liner density. A lower protective padding liner density decreases the resultant translational headform acceleration. This means that for Top impact, the helmet may be improved by using a lower density protective padding liner, whereas for Front and Rear impact, the helmet may be improved by changing the outer

shell stiffness. Chapter 6 deals with the optimization of the helmet for the various impact sites and injury criteria.

Drop test simulations were also performed at different impact velocities. As expected, a higher impact velocity leads to an increase in the values for the injury parameters. At 9.5 m/s the HIC values for Top and Front impact exceeded the threshold of 2400, indicating a high risk of injury. Just like the tests with different protective padding liner densities, the impact velocity only changes the magnitude of the signals, not their shape. This indicates that bottoming-out has not yet occurred and lower density padding liners may also improve the outcome of the test at higher impact velocities. This will also be investigated in Chapter 6.

Chapter 6

Helmet Design Optimisation

6.1 Introduction

This chapter deals with the optimisation of the helmet, to find out how helmet design can be improved. This is done by trying to find the answer to the following question:

Do the various injury criteria lead to the same 'optimal' helmet design?

The helmet is defined by its material parameters, its geometry and its construction. All of which have a large number of degrees of freedom. Optimising for all degrees of freedom is practically impossible. Therefore, the design space is limited to those design changes that can be directly implemented into the manufacturing methods of helmets and are therefore directly applicable, of course within certain boundaries. The question above is answered for three basic design changes:

- Protective padding liner density optimisation (Section 6.3.1)

- Outer shell configuration (Section 6.3.2)

- Protective padding liner density distribution (Section 6.3.3)

For comfort and aerodynamic reasons, the geometry of the helmet is left unchanged and an increase of helmet mass by more than 5% is not allowed .

Most researchers (see Section 1.3) have concluded that reducing the protective padding liner density results in lower values for the various injury criteria. Therefore, they concluded that such a helmet also reduces the injury risk and severity. However, this conclusion only holds for one particular impact velocity. Because of bottoming-out of the protective padding liner, the same helmet will probably result in higher values for the injury criteria, compared to helmets with a higher density protective padding liner, when tested at a higher impact velocity. Therefore, the impact velocity should also be considered when searching for the optimal helmet. The same reasoning is applied in helmet testing standards. Over the years, the criteria set by the helmet standards have raised, however the tolerance levels of the human head have not! Therefore, the strategy of this chapter is not to find the helmet that yields the lowest values for the various injury criteria at a given impact configuration, but to find that helmet offers the best protection for the human head. These two strategies are closely related since they use injury parameters as measure for the level of protection, but they are essentially different.

In the Finite Element simulations in Chapter 4 it is found that the kinematics of the conventional headform do not significantly differ from those of the flexible headform under the same impact conditions. Therefore, only the drop tests simulations using the conventional headform are used in this

chapter. Furthermore, Chapter 4 reports that CSDM is closely and only related to ω_{max}. Therefore, a discussion on CSDM is not included in this chapter.

Two impact configurations are discussed: Top impact, representing centric loading conditions, and Rear impact, representing eccentric loading conditions.

6.2 Methodology

6.2.1 Protective Padding Liner Density Optimisation

In this research, the strategy is to minimise several different injury parameters in several different impact configurations using the protective padding liner density as optimisation parameter. The protective padding liner of the helmet investigated in this research contains three different densities of EPS foam (see Figure 4.22). To reduce the computation time, the ratio between the densities is chosen fixed, leaving only parameter λ for the optimisation. Here, λ is defined as the ratio between the EPS foam density of the helmet being optimised and the EPS foam density of the original helmet. Thus, $\lambda = 1$ characterises the original helmet. In this strategy, the optimal helmet is defined as the helmet that minimises a particular injury parameter (a_{max}, HIC, HIP$_{\mathrm{max}}$ or ω_{max}). Since the result is only optimal for one particular impact velocity, the procedure is performed for the standard impact velocity of 7.5 m/s and for an increased impact velocity of 9.5 m/s. A tailor-made second-order optimisation routine is developed, to reduce the number of simulations to a minimum. This requires three startup simulations, before running the optimisation routine.

When the optimal protective padding liner density is found for a particular impact configuration, the maximum impact velocity is found for which the threshold for a particular injury parameter is not exceeded. For this, the same algorithm is applied, using the impact velocity as optimisation parameter and using the thresholds for the injury parameters as boundary conditions. The thresholds for a_{max} and HIC are set to 275 g and 2400, respectively, in accordance with ECE-R.22; the threshold for HIP$_{\mathrm{max}}$ is set to 90 kW and is based on the results in Chapter 3; and the threshold for ω_{max} is set to 30 rad/s [Ommaya *et al.*, 1967].

The minimum and maximum protective padding liner density are limited to 14.8 and 86.8 kg/m^3, which are the lowest and the highest density measured in the compression tests (see Section 4.4.1). Changing the density beyond these limits only affects those parts which have not yet reached their limit value. To speed up the process, the minimum parameter change $\Delta\lambda$ between two iterations is 0.02, meaning a minimum initial density variation of 2% between each iteration of the optimisation process. Figure 6.1 graphically represents all admissible combinations of densities. A maximum parameter variation is also implemented to ensure convergence of the optimisation. The maximum parameter variations are 0.2 and 0.3 for impact velocities of 7.5 and 9.5 m/s, respectively.

6.2.2 Variations to the Outer Shell Configuration

In 1976, Bastiaanse & Brockhoff made a study of the protective properties of a coconut. They reasoned that nature is perfectly capable of protecting itself. If that is the case, they reasoned, the construction of a coconut may be a good alternative to the current day helmet design. In a coconut, the delicate contents is protected by a hard coconut shell, surrounded by a soft tissue outer shell. This is exactly the opposite to current day helmets. They compared the protective capacity of a motorcycle helmet with that of a coconut. They found that the coconut was 20% more efficient in absorbing impact energy than the motorcycle helmet.
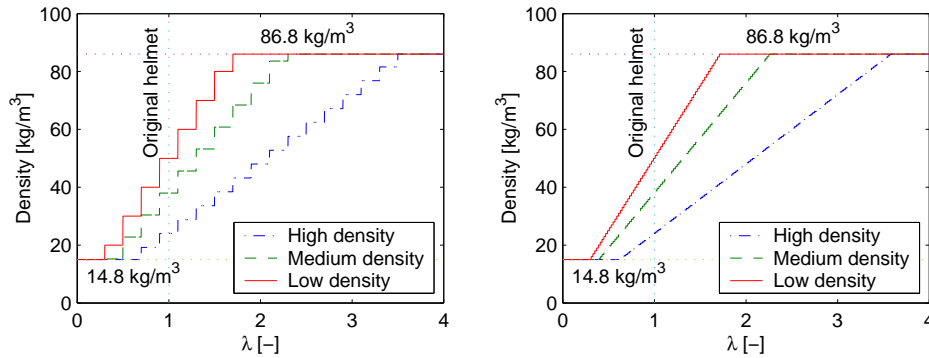
Figure 6.1: Admissible combinations of protective padding liner densities. *Left:* For a minimum parameter variation of 0.2. *Right:* For a minimum parameter variation of 0.02.

Configuration 1:	Configuration 2:	Configuration 3:	Configuration 4:
layer 1	layer 1	layer 1	layer 1
layer 2	layer 2	layer 2	layer 2
layer 3	layer 3	layer 3	layer 3
FRP shell: most outer shell	FRP shell: between 1st and 2nd layer	FRP shell: between 2nd and 3rd layer	FRP shell: most inner shell
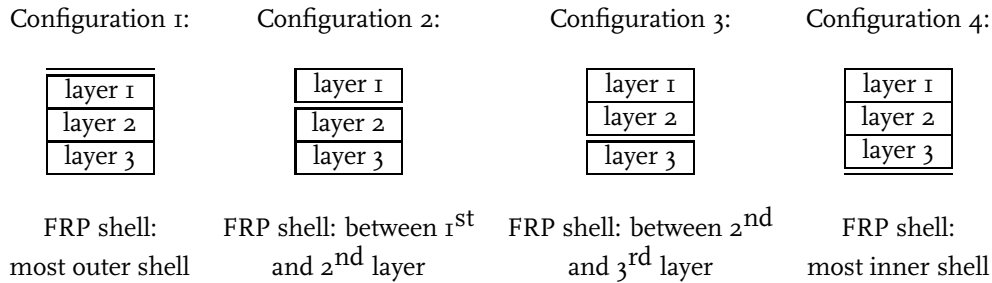
Figure 6.2: Various helmet configurations in FRP shell position.

In this section, the effects of various helmet configurations with respect to the outer shell position are investigated. This section also elaborates on the effects of multiple shells used in a helmet. In fact, the term outer shell does not really apply, since it will be placed on the inside of the helmet as well as in between two layers of protective padding liner. Therefore, the outer shell will be called Fibre Reinforced Plastic or FRP shell, since the outer shell of the helmet studied here is made of this material. However, the outer shell can be made of several other materials (see Section 1.3.1). The material properties of the FRP shell remain fixed in this chapter, since they have already been elaborated on in Chapter 5.

The protective padding liner distribution and material parameters are the same as in the original helmet (see Figure 4.22). The protective padding liner in the helmet model consist of three layers of brick elements. Between these layers, the FRP shell is modelled as a layer of shell elements, using the same nodes as the brick elements. Figure 6.2 shows the four configurations considered in this study. Note that Configuration 1 equals the original helmet and Configuration 4 resembles the coconut configuration of the study by Bastiaanse & Brockhoff [1976].

6.2.3 Variation of Protective Padding Liner Configuration

Based on the assumption that the helmet's protective padding liner does not deform uniformly, there may be some benefit in varying the protective padding liner density over the thickness of the liner. Two scenarios emerge from this principle:

Higher density protective padding liner deforms as the impact continues. The low-density protective padding liner absorbs the low-energy impacts and the high-density protective padding deforms only when needed. This results in a helmet that is efficient in both low-energy as high-energy impacts.

Lower density protective padding liner deforms as the impact continues. The idea behind this is that at high impact velocity, a high-density EPS foam is deformed, and as the impact continues, the impact velocity decreases and a lower density EPS foam suffices to absorb the remaining part of the impact.

Question is how to get the higher density EPS foam to deform before the lower density foam does. This may be possible using the principle that FRP shelled helmets predominantly deform from the inside (see Figure 1.6). Using a higher density EPS foam on the inside of the protective padding liner and a lower density EPS foam on the outside, may cause the higher density EPS foam to deform firstly and vica versa. This hypothesis is tested using a helmet with three different padding liner densities (15, 38 and 60 kg/m^3): one density for each layer of elements (see Figure 6.2). Two helmets are compared: one helmet with an increasing and one helmet with a decreasing padding liner density from the outside to the inside of the helmet. The simulations are repeated for helmets with multiple FRP shells. This may enhance the effect of consecutive deformation of the EPS foam layers, rather than simultaneous deformation.

6.3   Results

6.3.1   Protective Padding Liner Density Optimisation

Figure 6.3 shows the history of the optimisation process for a Rear impact drop test simulation at 7.5 m/s. Since a second order optimisation routine is used, the results of at least three different values for λ, need to be computed (startup values 1, 2 and 3) for the routine to compute its optimisation result (i =1 to n). The minimum value for $a_{\max}$ in this impact configuration is 134 m/s^2. The optimum is reached for $\lambda = 0.56$. Thus, the respective values for the different protective padding liner densities are ($\lambda \times \rho$): $0.56 \times 50 = 28\,\text{kg/m}^3$, $0.56 \times 38 = 21.3\,\text{kg/m}^3$ and $14.8\,\text{kg/m}^3$ ($0.56 \times 24 = 13.4 < 14.8$).

Table 6.1 shows the optimal parameters λ_{opt} for the minimum values for the various injury criteria at 7.5 and 9.5 m/s. Considering the translational acceleration based injury parameters $a_{\max}$ and HIC, it appears that the reduction of the padding liner density has a larger effect on HIC than on $a_{\max}$. This holds for both impact configurations as well as for both impact velocities. For Rear impact, the optimal padding liner density is equal for both HIC and $a_{\max}$, whereas for Top impact, the optimal padding liner density for HIC is about 10% lower than for $a_{\max}$. The maximum achievable reduction for $a_{\max}$ and HIC at an impact velocity of 7.5 m/s is 22-33%. To obtain this reduction, the protective padding liner density should be reduced by 38-50% compared to the original helmet. At an impact velocity of 9.5 m/s, the maximum achievable reduction of HIC and $a_{\max}$ is only 7-14%, requiring a reduction of the protective padding liner density of 12-20%.

In Chapter 5, the injury parameters $a_{\max}$ and HIC showed significantly higher values for Top impact than for Rear impact. It was concluded that at least in Top impact, the helmet's performance could be improved, in terms of these injury parameters, by reducing the protective padding liner density. Table 6.1 shows that this is indeed the case. Furthermore, it was also expected that this effect would not be as large for Rear impact. However, the table proves this statement to be wrong. The gains
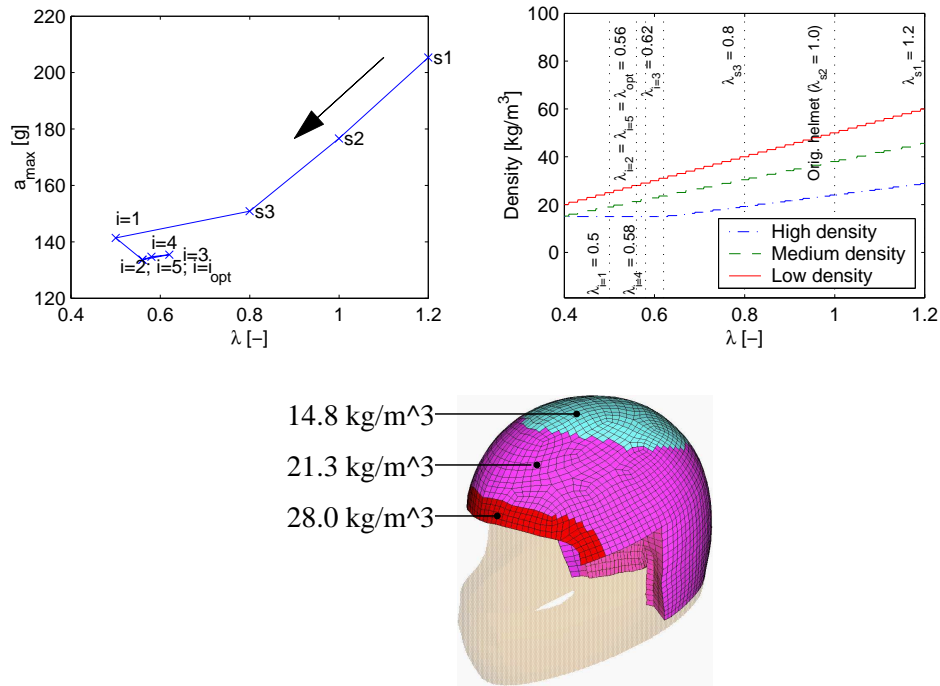
Figure 6.3: Example of an optimisation history (Rear impact drop test simulation at 7.5 m/s using the conventional headform). *Top left:* Optimisation history of maximum acceleration. *Top right:* Optimisation history of density. *Bottom:* Final result of optimisation.

for Rear and Top impact are almost equally large. Thus, Top impact drop tests yield higher values for a_{max} and HIC than Rear impact drop tests, even when these injury parameters are minimised for their particular impact configuration. Surprisingly, the λ value for the optimal helmet for Top impact is close to the λ value for the optimal helmet for Rear impact, when considering a_{max} and HIC.

For the rotational velocity based injury parameter ω_{max} at Top impact, the results are not shown in Table 6.1. In Chapter 5 it was found that, for Top impact, ω_{max} is not very sensitive for variations in the material parameters of the helmet. This causes bad convergence of the optimisation routine. At an impact velocity of 7.5 m/s, a reduction for ω_{max} of 12%, requires an increase of the protective padding liner density of 50%. This would result in inadmissibly high translational accelerations. Since the rotational velocity never reaches critical values in Top impact, the results for ω_{max} in Top impact will not be discussed further.

For the Rear impact drop test simulations at an impact velocity of 7.5 m/s, the padding liner density of the original helmet is already close to optimal with respect to ω_{max}. At an impact velocity of 9.5 m/s, a reduction of ω_{max} of 29% is achievable by reducing the padding liner density by 28%. This also means that bottoming-out has not yet occurred in the Rear impact drop test simulations at 9.5 m/s, where the padding liner density was only reduced up to 14%.

In contrast to the results for HIC and a_{max}, where the largest reduction is achieved at 7.5 m/s, the results for ω_{max} show a larger reduction at 9.5 m/s. The results for HIP_{max}, which depends on both translational and rotational accelerations, are found between the two types of injury parameters.

In general, a reduction of the padding liner density leads to a reduction of all injury parameters. However, a reduction of the padding liner density also limits the protective function of the helmet at

Table 6.1: Optimisation results for various injury criteria for Rear and Top impact at two different impact velocities.

Impact	Velocity	a_{max}		λ_{opt}	HIC		λ_{opt}
		$\lambda = 1$	$\lambda = \lambda_{opt}$		$\lambda = 1$	$\lambda = \lambda_{opt}$	
Rear impact	7.5 m/s	177	134	0.56	1377	1013	0.58
		-24%			-26%		
	9.5 m/s	239	222	0.86	2552	2188	0.86
		-7%			-14%		
Top impact	7.5 m/s	195	153	0.62	2121	1418	0.5
		-22%			-33%		
	9.5 m/s	249	232	0.88	3587	3093	0.8
		-7%			-14%		

Impact	Velocity	HIP_{max}		λ_{opt}	ω_{max}		λ_{opt}
		$\lambda = 1$	$\lambda = \lambda_{opt}$		$\lambda = 1$	$\lambda = \lambda_{opt}$	
Rear impact	7.5 m/s	64.9	53.7	0.88	34.6	32.5	0.94
		-17%			-6%		
	9.5 m/s	125.6	94.8	0.8	60.9	43.1	0.72
		-25%			-29%		
Top impact	7.5 m/s	82.7	60.9	0.6	–	–	–
		-26%			–		
	9.5 m/s	131.3	122.1	0.9	–	–	–
		-7%			–		

Table 6.2: Maximum impact velocities at the thresholds of the various injury criteria.

Impact	Helmet	$a_{max} = 275$	HIC = 2400	$HIP_{max} = 90$ kW	$\omega_{max} = 40$ rad/s
Rear impact	original ($\lambda = 1$)	10.5 m/s	9.75 m/s	9.3 m/s	9.0 m/s
	optimal ($\lambda = 0.6$)	9.9 m/s	9.3 m/s	8.85 m/s	8.7 m/s
Top impact	original ($\lambda = 1$)	10.65 m/s	8.7 m/s	8.4 m/s	–
	optimal ($\lambda = 0.6$)	9.6 m/s	8.7 m/s	8.25 m/s	–

higher impact velocities, since bottoming-out occurs already at lower impact velocities. To investigate to what extent the helmet still properly protects the head (i.e. the thresholds for the injury parameters are not exceeded), the maximum impact velocities at which the helmet reaches the thresholds of the injury parameters are calculated. Table 6.2 shows the results of these computations for the original helmet ($\lambda = 1$) and for the 'optimal' one ($\lambda = 0.6$). The value of 0.6 is chosen, based on the results in Table 6.1.

Table 6.2 shows that the optimal helmet provides less protection at higher velocities, because bottoming-out is occurring at a lower impact energy for a lower density of the protective padding liner. For Rear impact the maximum admissible velocities are generally higher than for Top impact. Since the previous results showed that Top impact generally yields higher values for the various injury parameters, these parameters are likely to reach their limit values already at lower impact velocities. These trends hold for all four injury parameters, except for a_{max} for the original helmet.
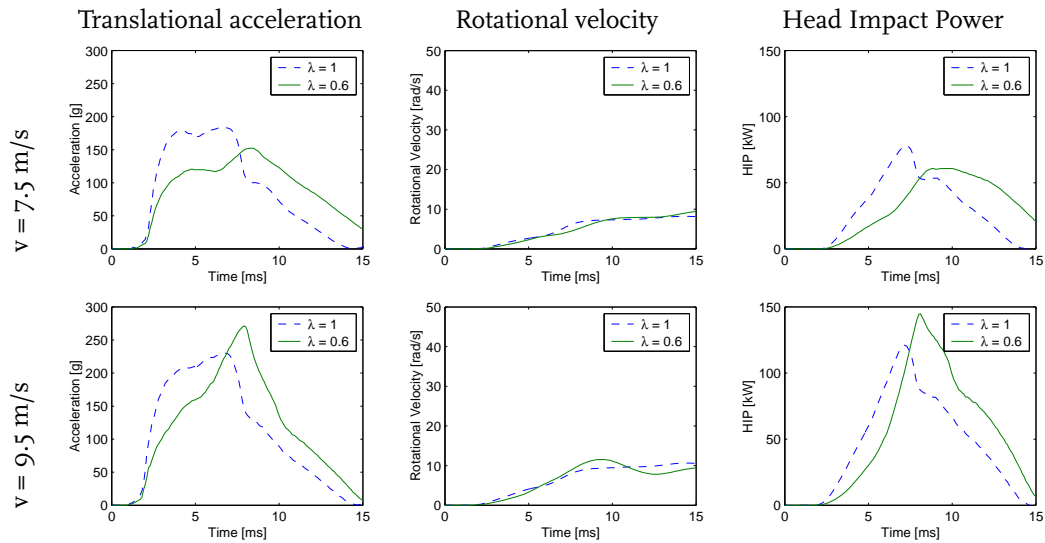
Figure 6.4: Resultant translational headform acceleration, resultant rotational headform velocity and Head Impact Power of the Top impact drop test simulations with the original helmet compared with those with the optimal helmet at two different impact velocities.

The higher the velocity at which the particular injury parameter reaches its threshold value, the higher the amount of residual protection at the standard impact velocity of 7.5 m/s. For Rear impact, the amount of residual protection is largest when considering a_{max} as the injury parameter, followed by HIC and HIP_{max}. The least residual protection is offered when considering ω_{max} as the injury parameter. For Top impact, ω_{max} is not investigated. Here, HIP_{max} offers the least residual protection.

Figure 6.4 shows the various time histories of the Top impact drop test simulations with the original ($\lambda = 1$) helmet and with the optimal helmet ($\lambda = 0.6$) at two different impact velocities. The same results for Rear impact are displayed in Figure 6.5

Both Top and Rear impact simulations yield the same trends. The largest differences between the original helmet and the optimal helmet occur in the time histories of the translational acceleration and of the Head Impact Power. Since the optimal helmet is optimised for an impact velocity of 7.5 m/s, the behaviour of the optimal helmet is favourable over that of the original helmet at this impact velocity. At 9.5 m/s the protective padding liner of the optimal helmet starts to bottom out after about 5 ms, resulting in a rapid increase of the acceleration. This behaviour explains the different behaviour between a_{max}, HIC and HIP_{max} in Table 6.2. A short duration peak acceleration immediately affects a_{max}, but HIC, which takes into account the duration of the peak, is less affected. And HIP, which is a product of acceleration and velocity, translational as well as rotational, is even less affected as the velocity decreases more rapidly with increasing acceleration.

6.3.2 Variations to the Outer Shell Configuration

Position of the FRP Shell

The results in terms of translational acceleration, rotational velocity and HIP are depicted in Figure 6.6. It is seen that Configuration 4 yields high-frequency components in the responses for the resultant translational headform acceleration and HIP. This means that, even though these responses
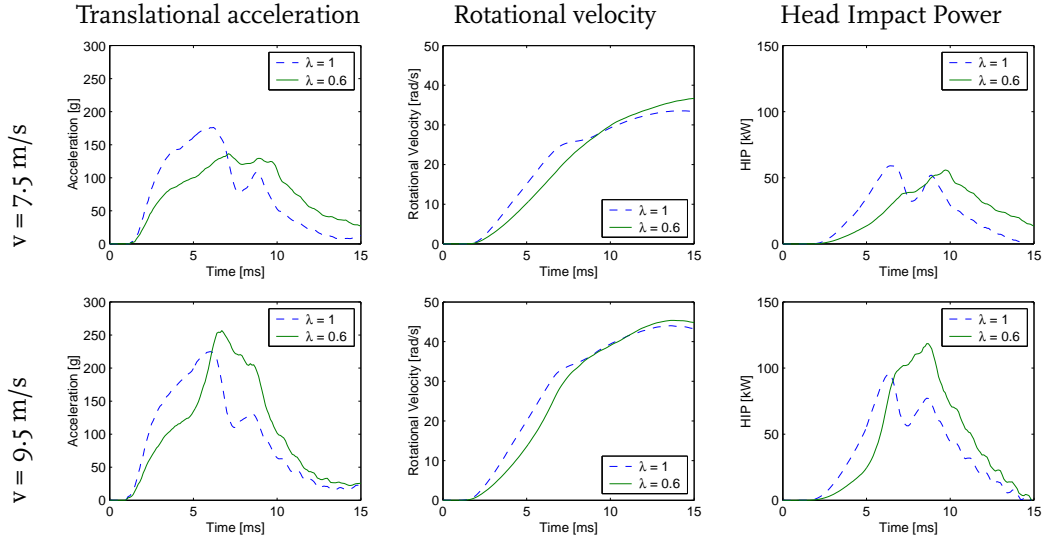
Figure 6.5: Resultant translational headform acceleration, resultant rotational headform velocity and Head Impact Power of the Rear impact drop test simulations with the original helmet compared with those with the optimal helmet at two different impact velocities.

Table 6.3: Injury criteria for the various FRP shell configurations.

	a_{max} [m/s^2]	HIC	HIP$_{max}$ [kW]	ω_{max}[rad/s]
Configuration 1	230	2806	97.0	8.9
Configuration 2	224	2194	88.6	8.5
Configuration 3	199	1423	77.1	7.2
Configuration 4	394	1223	136.2	15.1

in this configuration are lowest on average, they are unpredictable and may even include very high spikes. This is caused by the hard contact between the FRP shell and the headform. Furthermore, the resultant rotational headform velocity is almost twice that of Configuration 1. Configuration 3 seems to yield the best of both worlds: There is no hard contact between the FRP shell and the headform, which eliminates the high-frequency components in the results for the resultant translational headform acceleration and HIP, yet the FRP shell is still relatively close to the headform, which reduces the resultant translational headform acceleration and HIP, as well as resultant rotational headform velocity, significantly.

The injury criteria from the simulation results are given in Table 6.3. The table confirms that Configuration 3 is the best helmet of the four configurations in terms of the injury parameters under consideration. Only the HIC of Configuration 4 is lower than that of Configuration 3. However, the other injury parameters in Configuration 4 are almost twice those of Configuration 3.
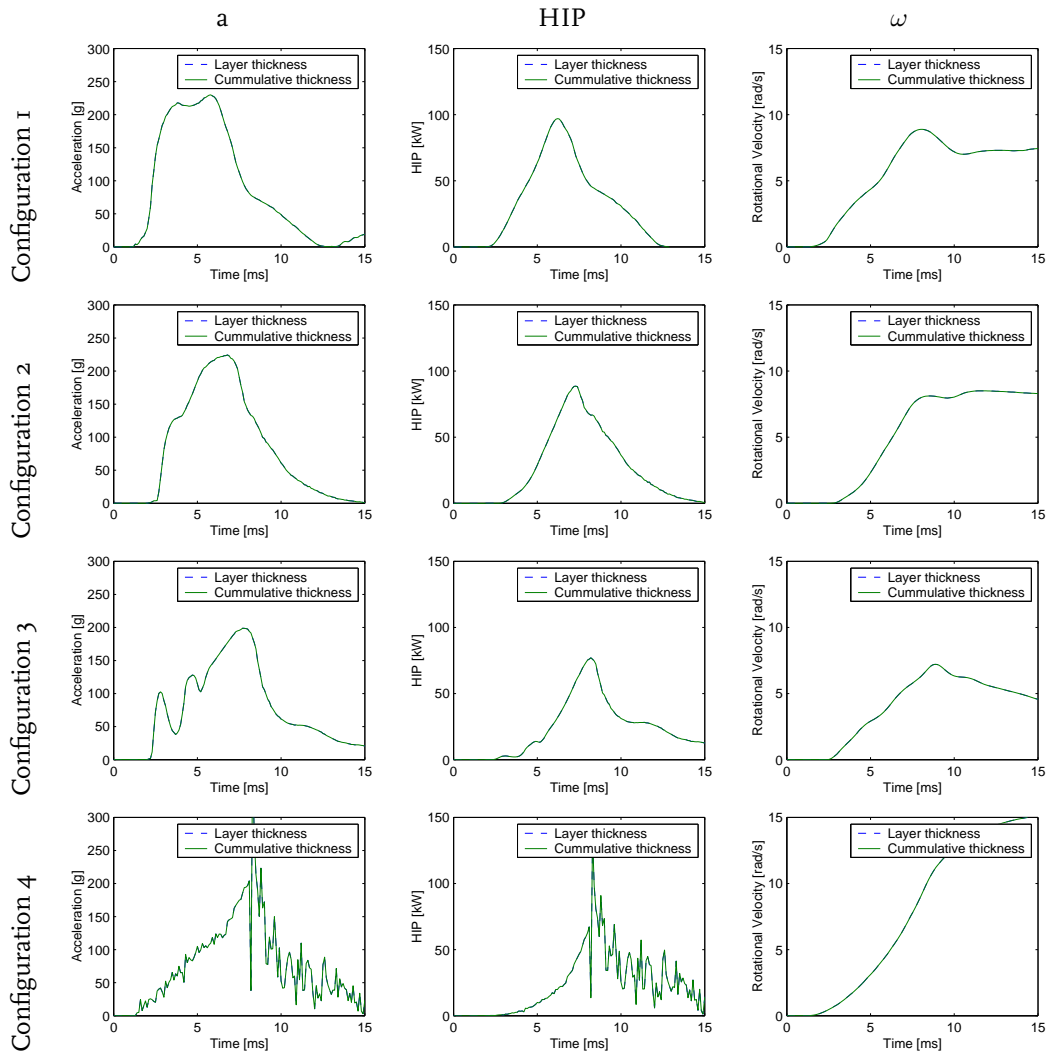
Figure 6.6: Results of the drop test simulations with helmets with different FRP shell position.

Multiple FRP Shells

Configuration 3 of the previous section yields favourable results over the other configurations. However, the absence of an outer shell makes the helmet more vulnerable to wear and abrasion. In this section, several combinations of Configuration 1 to Configuration 4 are investigated, to determine whether multiple FRP shells yield even more favourable results. Each combination of configurations is considered with two different shell thicknesses. In the first case, each FRP shell is 3 mm thick, the outer shell thickness of the original helmet. This results in an increase of the helmet mass of up to 40%, which is unacceptable. Therefore, the simulations are repeated for a helmet of which each FRP shell thickness is such that the total shell thickness is 3 mm. Table 6.4 shows the results of all drop test simulations with helmets with two and three FRP shells. For a_{max}, HIC and HIP_{max}, the values for the tests on helmets with a total shell thickness of 3 mm are, with only one exception, lower than those on helmets with an individual layer thickness of 3 mm. This is consistent with the results from Chapter 5, that a thicker outer shell leads to higher values for the various injury parameters.

Table 6.4: Injury criteria for the various FRP shell configuration combinations.

	a_{max} [m/s^2]		HIC		HIP$_{max}$ [kW]		ω_{max}[rad/s]	
Shell thickness*:	t_{ind}	t_{tot}	t_{ind}	t_{tot}	t_{ind}	t_{tot}	t_{ind}	t_{tot}
Configuration 1-2	243	226	2866	2587	86.5	94.6	6.3	8.1
Configuration 1-3	361	242	3881	2664	112.6	101.2	10.3	7.9
Configuration 1-4	229	228	2574	2090	97.0	84.2	8.0	9.5
Configuration 2-3	304	252	3083	2268	110.2	101.5	9.5	9.1
Configuration 2-4	235	232	2072	1726	94.2	87.9	10.1	9.6
Configuration 3-4	232	215	1448	1394	86.6	82.7	9.0	9.4
Configuration 1-2-3	328	229	3935	2520	112.7	91.3	11.6	6.7
Configuration 1-2-4	248	224	2704	1953	92.9	87.2	7.0	8.5
Configuration 1-3-4	404	246	3557	2093	133.9	97.0	9.8	7.5
Configuration 2-3-4	294	267	2944	2059	111.0	100.8	10.2	9.3

* t_{ind}: Each layer is 3.0 mm thick. t_{tot}: Total shell thickness is 3.0mm
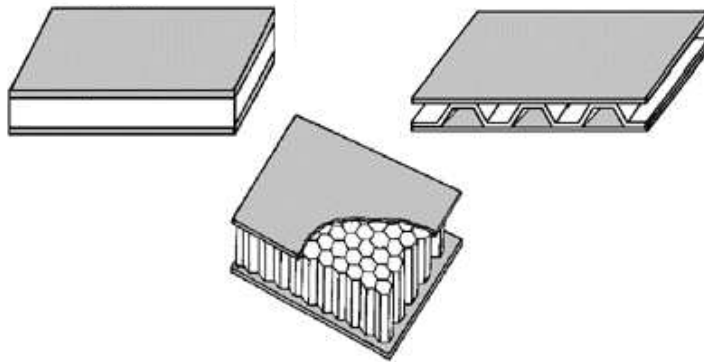

Figure 6.7: Principle of a various sandwich constructions.

Apparently, this also holds when the FRP shell is split into more than one layer.

However, when comparing these results to the single layer results, the results are less consistent. For example, the average values for a_{max}, HIC and HIP$_{max}$ for Configuration 1 and Configuration 3 are 215, 2115 and 87.1, respectively. One would expect the result of Configuration 1-3 to be close these values, at least between those of Configuration 1 and Configuration 3. However, the values for a_{max} and HIP$_{max}$ for Configuration 1-3 even exceed those for Configuration 1. When considering Configuration 1-2, the values for a_{max}, HIC and HIP$_{max}$ are all between those for Configuration 1 and Configuration 2, conforming to expectation. Overall, the results of these simulations show that none of these combinations improve the helmet's performance in terms of the injury criteria, compared to the Configuration 3 helmet. Combining the Configuration 3 helmet with the Configuration 1 helmet to improve the helmet's resistance to wear and abrasion, results in an increase of a_{max} of 25% (t_{tot}) and values for HIC and HIP$_{max}$ that even exceed the proposed threshold values of 2400 and 90, respectively. This increase can be explained by the principle of a so-called sandwich construction. Sandwich constructions typically consist of two face sheets and a core as shown in Figure 6.7. The face sheets are

Table 6.5: Injury criteria for the various FRP shell configuration and protective padding liner density combinations.

	a_{max} [m/s^2]		HIC		HIP_{max} [kW]		ω_{max}[rad/s]	
Padding density*:	incr.	decr,	incr.	decr.	incr.	decr.	incr.	decr.
Configuration 1	216	244	2261	2599	81.7	79.3	6.4	7.7
Configuration 1-2	227	240	3062	2666	103.0	92.4	10.0	6.3
Configuration 1-3	258	412	3335	3738	108.0	103.3	10.1	14.4
Configuration 1-2-3	279	396	4148	4109	139.7	152.0	10.2	13.6

* incr.: increasing padding density. decr.: decreasing padding density

the noble material in the sandwich and they must resist the in-plane and bending loads (like the FRP shells). The core is made of light, inexpensive and/or easily compressible material (like the EPS foam) depending on the application of the sandwich construction. It must keep the face sheets supported, separated, and working as a single unit. It must also resist the transverse shear and transverse normal loads. This is exactly what happens in a multi-shelled helmet.

For further investigation, the time histories of the resultant acceleration, the HIP and rotational velocity are depicted in the following figures: Figure 6.8 shows the results of all drop test simulations with helmets with two FRP shells and Figure 6.9 shows the simulation results for three shelled helmets. It shows that the thicker shelled helmets result in higher curves of shorter duration, because of the higher overall stiffness of the helmet.

It also shows that the response of the helmeted headform is dominated by the outer most shell of each particular configuration. When Configuration 1 is part of the combination of configurations, the response of the headform is quite similar in shape as Configuration 1. When Configuration 2 is the outer most shell, thus Configuration 1 is not part of the combination of configurations, than the response of the headform is quite similar in shape as Configuration 2. The same holds for Configuration 3 in combination with only Configuration 4. Since the outer most shell of each configuration determines the shape of the response, this shell dominates the load distributing capacities of the helmet, since it carries the most of the load.

6.3.3   Variation of Protective Padding Liner Configuration

In Section 6.3.1, it was found that the protective padding liner density distribution over the *surface* of the helmet, as present in the helmet of this study, is chosen such that the protective padding liner density compensates for the reduced structural protection as a result of the edge and visor opening of the helmet. In this section, the effects of a protective padding liner density distribution over the *thickness* of the helmet are investigated using two configurations. The first configuration uses an increasing protective padding liner distribution, meaning that the outside of the helmet has a lower protective padding liner density (15 kg/m^2) than the inside of the helmet (60 kg/m^2). The second configuration uses a decreasing protective padding liner distribution in which the distribution is the other way round. Table 6.5 shows the result of the simulations. First of all, most results of the multi-shelled helmets exceed the threshold values, since the stiffness of the helmets is increased, resulting in higher response values. For a_{max}, which is highly sensitive for fluctuations, the helmet with decreasing padding liner density yields lower results than the helmet with increasing padding liner density. For HIC and HIP_{max}, no trend emerges from these results, yet differences can be quite large.
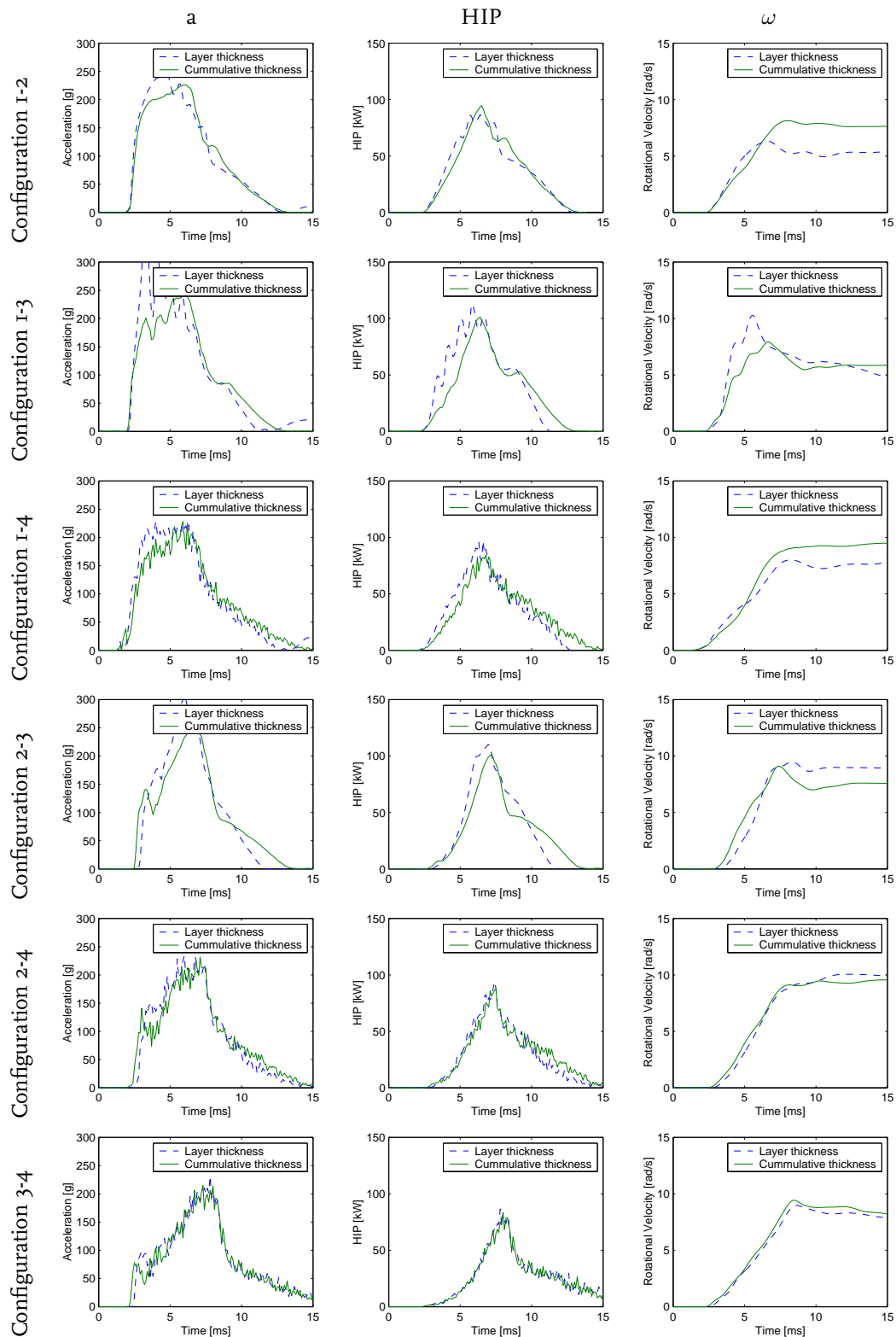
Figure 6.8: Results of the drop test simulations with helmets with two FRP shell configurations.
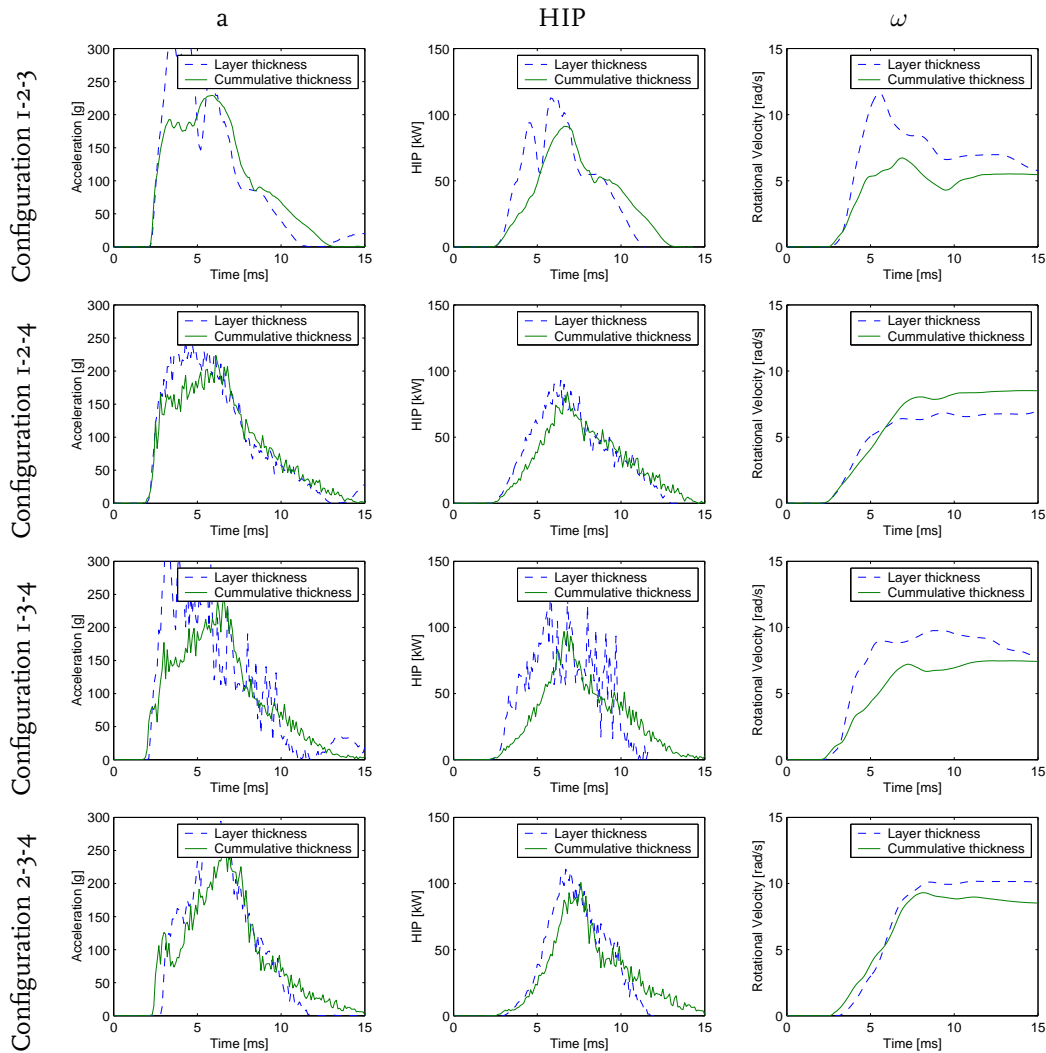
Figure 6.9: Results of the drop test simulations with helmets with three and four FRP shell configurations.

However, more insight in the structural behaviour of the helmet may be gained by investigating the time histories of the various injury parameters (see Figure 6.10). From the results of Table 6.5 it is concluded that the higher values for a_{max} are caused by fluctuations. However, the time histories of Figure 6.10 show that this is not exclusively the case. For Configuration 1, the helmet with decreasing protective padding liner density has a more smooth characteristic, yet it still has a higher maximum value for the resultant translational headform acceleration. When the same amount of energy is absorbed, flat long-duration accelerations result in a lower injury risk than high-peak short-duration accelerations, since they result in lower values for the various injury parameters. Therefore, the translation acceleration time histories of the helmet with increasing protective padding liner density are generally favourable over those of the helmet with decreasing protective padding liner density.
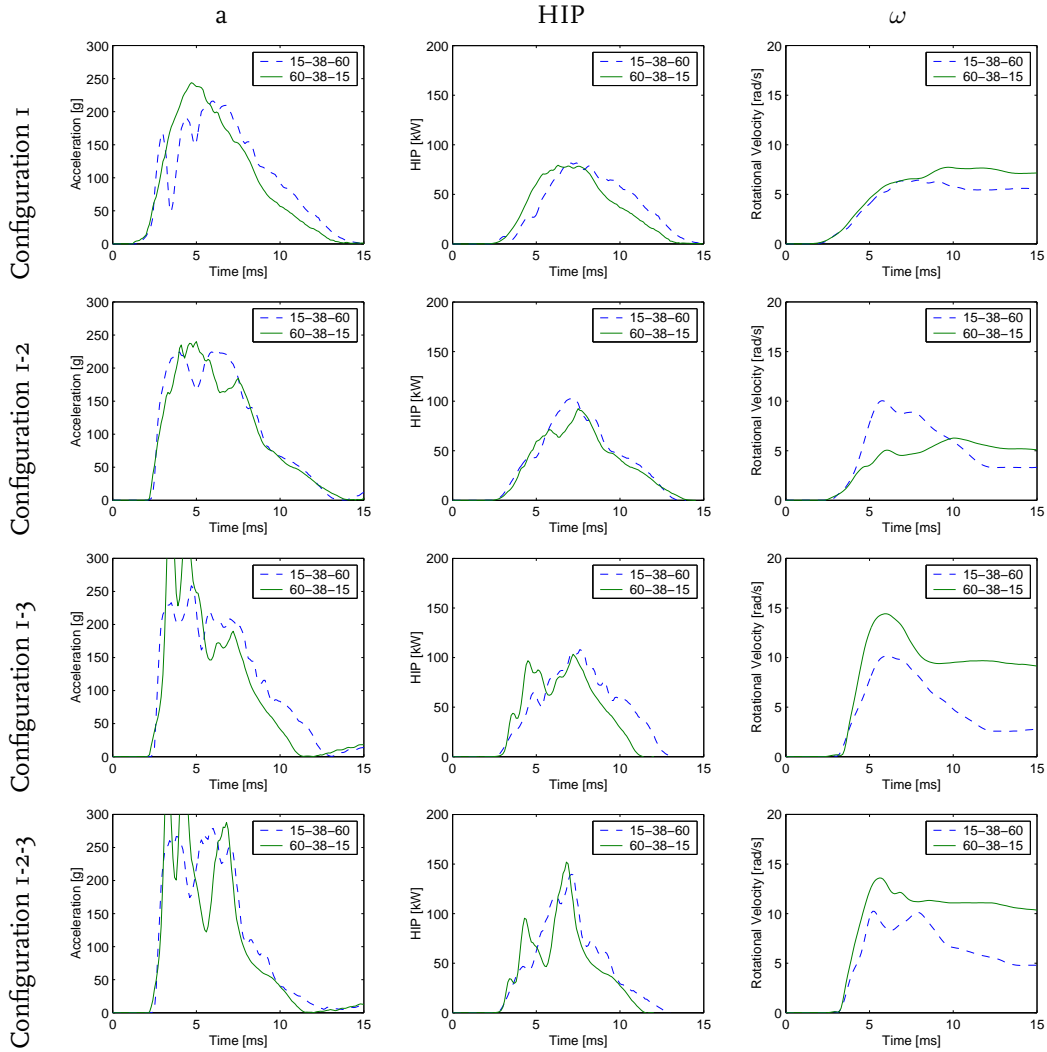
15-38-60 =   Outer layer EPS density of 15 kg/m^3, middle layer EPS density of 38 kg/m^3 and inner
             layer of EPS density of 60 kg/m^3
60-38-15 =   Outer layer EPS density of 60 kg/m^3, middle layer EPS density of 38 kg/m^3 and inner
             layer of EPS density of 15 kg/m^3

Figure 6.10: Results of the drop test simulations with helmets with three different layers of EPS foam density and various FRP shell configurations.

6.4   Discussion and Conclusions

The results presented in this chapter show that not all injury parameters yield the same optimal helmet design in terms of protective padding liner density. The protective padding density that minimises $a_{\max}$ and HIC is lower than that that minimises $\text{HIP}_{\max}$ and $\omega_{\max}$. When the helmet is designed such that the injury parameters are minimised, then that helmet is highly sensitive, in terms of $a_{\max}$, to an increase in drop velocity in helmeted headform drop tests because of bottoming-out of the protective padding liner. HIC is less sensitive in this case, since the increase in translational headform acceleration is of short duration.
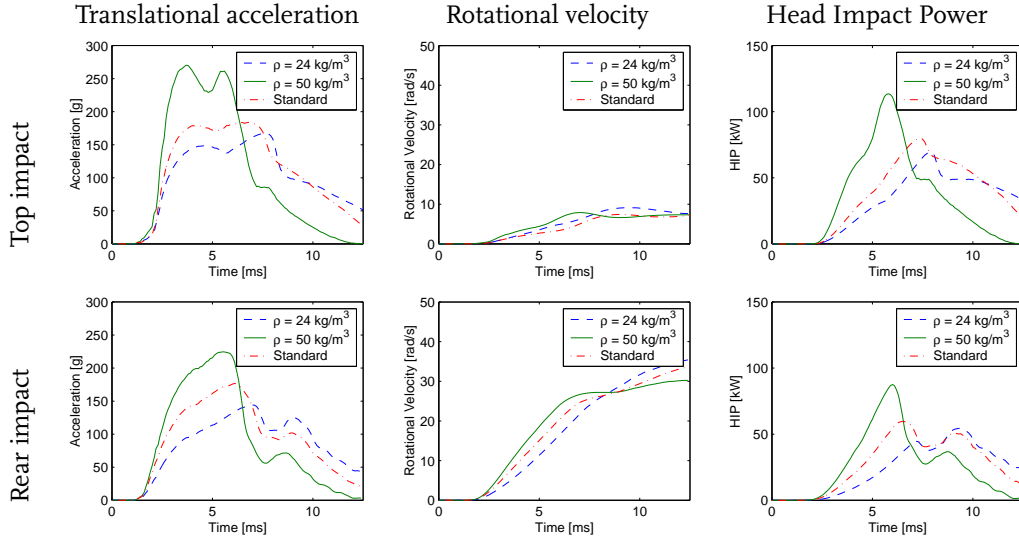
Figure 6.11: Resultant translational headform acceleration, resultant rotational headform velocity and Head Impact Power of the drop test simulations with two uniform protective padding density helmets and with the original helmet.

Considering the drop test simulations, with the helmet considered in this research, at various impact sites, Rear impact yields lower values for a_{max} and HIC than Top impact. The ratio between them does not change when optimising the helmet for these injury parameters for both impact sites. This leads to the conclusion that the protective padding density distribution as used in this helmet is chosen such that it minimises a_{max} and HIC for both impact sites for a particular drop velocity. Protective padding liner density optimisation is less useful for minimising ω_{max} and HIP_{max}.

Most helmets have a uniform density protective padding liner. Figure 6.11 shows the results of the drop test simulations for two helmets with a uniform protective padding liner density and for the original helmet. For Top impact, the results of the original helmet are closer to those of the low-density helmet (24 kg/m^3) than to those of the the high-density helmet (50 kg/m^3). For Rear impact, the results of the original helmet are almost in the middle of both uniform density helmets. Thus, a uniform density helmet shows relatively higher resultant accelerations for Top impact than for Rear impact, when compared to the original helmet. The values for the injury parameters confirm this conclusion (Table 6.6). All injury parameters show larger differences between the two uniform density helmets for Top impact, than for Rear impact. This confirms that a density distribution of the protective padding liner, as used in the original helmet, is to be preferred over a uniform protective padding density distribution.

In this research, the optimal helmet is found by minimising the different injury parameters. This helmet will result in an increased risk of injury at higher impact velocities, compared to helmets that use a higher density protective padding liner. To overcome this problem, helmets can also be optimised by finding that protective padding density for which the different injury parameters just reach their threshold values.

The current drop test regulations allow for both strategies. Some helmets, like the helmet investigated in this research, barely pass the test, but provide more protection at higher impact velocities, whereas other helmets yield much lower values for the various injury parameters, but loose their protective capabilities at higher impact velocities. In real-world motorcycle accidents, there is a wide spread

Table 6.6: Injury criteria for the drop test simulations with two uniform protective padding density helmets and with the original helmet.

Impact site	EPS density	$a_{\max}$ [g]	$\frac{[a_{\max}]_{\rho_2}}{[a_{\max}]_{\rho_1}}$	HIC	$\frac{[\mathrm{HIC}]_{\rho_2}}{[\mathrm{HIC}]_{\rho_1}}$	$\mathrm{HIP}_{\max}$ [kW]	$\frac{[\mathrm{HIP}_{\max}]_{\rho_2}}{[\mathrm{HIP}_{\max}]_{\rho_1}}$
Top	$\rho_1 = 24$ kg/m^3	168	1.61	1542	2.25	69.7	1.63
	$\rho_2 = 50$ kg/m^3	270		3484		113.5	
	Original	196	-	2121	-	82.7	-
Rear	$\rho_1 = 24$ kg/m^3	144	1.56	1032	1.96	54.4	1.61
	$\rho_2 = 50$ kg/m^3	225		2026		87.6	
	Original	179	-	1377	-	60.5	-

in impact velocity [Hurt Jr. *et al.*, 1981]. To offer protection in both high-impact and in low-impact situations, helmets should be tested in both these situations. This means that less severe injuries should be allowed in low impact velocities, meaning that injury criteria must be reduced at an impact velocity of 7.5 m/s. This study shows that values up to 153 m/s^2 and 1418 are achievable for $a_{\max}$ and HIC in Top impact at 7.5 m/s. Yet, the current levels of the injury criteria $a_{\max} = 275$ m/s^2 and HIC = 2400, which represent the thresholds of the human head, should be maintained but at a higher impact velocity. This study shows that these values are achievable in Top impact at an impact velocity up to 8.7 m/s, which is an increase in impact energy of 35 %.

In the optimisation for Top and Rear impact, it is found that for both impact sites the benefits are equal. Considering the fact that the helmet already has a lower protective padding liner density at the top of the helmet, than at the rear, this leads to the conclusion that the helmet's current protective padding liner density distribution accounts for the differences in local structural design of the helmet (e.g. the edge and visor opening). Would the helmet have had a uniform protective padding liner density distribution, then the optimisation would probably have resulted in different values for λ_{opt} as a result of these local structural design differences. In Section 5.2, it was found that the translational acceleration in Top impact most resembles a rectangular shape. Since, the optimal protective padding liner density is higher for the other impact sites, it is concluded that the higher protective padding liner density is required to compensate for the loss of helmet effectiveness as a result of edges and the visor opening.

As far as the position of the FRP shell is concerned, the injury criteria yield lower values as the FRP shell is positioned closer to the headform. In this case, the helmet deforms from the outside. Because of the spherical shape of the helmet, a larger area is compressed as the impact progresses (see also Figure 1.6), resulting in a the triangular shape of the acceleration time history, which is a less efficient way of absorbing energy. The most efficient way of absorbing energy is when the acceleration is constant during the impact and no rebound occurs. This situation is best approximated when the FRP shell is positioned on the outside of the helmet.

For Rear and Front impact, the helmet's efficiency may be improved by using an increasing protective padding liner density over the thickness of the helmet. The results of Section 6.3.3 show that this has a positive effect on the shape of the acceleration time history.

Chapter 7

Conclusions and Recommendations: Towards a Safer Motorcycle Helmet

The underlying question of this research has been:

How could motorcycle helmet designs change as a result of applying new and different head injury criteria in the shock absorption test of ECE-R.22?

To answer this question, the following three hypotheses have been formulated:

1. An anatomically more detailed, deformable headform, allowing more realistic helmet-head interaction and allowing brain deformation, will provide more relevant information on helmet performance.

2. Peak acceleration (a_max) and HIC are insufficient to quantify helmet performance. Also, rotational response should be included to assess helmet performance.

3. The application of the new headform and associated head injury criteria will lead to significant changes in helmet design.

To test whether or not these hypotheses are true, helmeted head drop tests, and numerical simulations thereof, have been conducted using both a conventional (rigid) headform and an anatomically more detailed (flexible) headform. The flexible headform has been built and validated to suit the specific needs of this research.

7.1   Conclusions

Hypothesis 1: An anatomically more detailed, deformable headform, allowing more realistic helmet-head interaction and allowing brain deformation, will provide more relevant information on helmet performance. The flexible headform is equipped with a flexible brain, to allow for brain deformations to be measured. In this research, the brain deformations are quantified in terms of the Cumulative Strain Damage Measure (CSDM). It was thought that CSDM would be a good parameter for both translational and rotational motion induced injuries. However, in this research, CSDM is correlated to maximum rotational velocity only. Since the maximum rotational velocity is far more easy to determine in both experiments and simulations, there is no need to measure brain deformations. Hypothesis 1 is therefore rejected with respect to the flexible brain,

based on the numerical simulations. However, it should be noted, that a clear link between experimental results and numerical results is not established in the research. Furthermore, this conclusion does not mean that Hypothesis 3 is also rejected, since the flexible brain yields a more realistic headform-helmet interaction. This results in more relevant information on the protective capacities of a crash helmet.

Hypothesis 2: Peak acceleration ($a_{\max}$) and HIC are insufficient to quantify helmet performance. Also, rotational response should be included to assess helmet performance. This research concludes that determining only the injury criteria, HIC and $a_{\max}$, in helmet certification tests is not sufficient to evaluate helmet performance. Especially in eccentric loading conditions, the translational response is significantly less than in centric loading conditions, whereas the rotational response in these loading conditions can reach injurious magnitudes. Therefore, the test protocol should be extended with measurement of the rotational acceleration. To implement this, headform rotations must be allowed for in shock absorption tests. Hypothesis 2 is herewith accepted.

The consequences of this conclusion go beyond just an extra parameter to be measured, since most drop test regulations suppress headform rotations in their shock absorption tests (e.g. Snell and DOT). Both methods are equivalent (except for the thresholds for the injury criteria), since suppressing the rotational motion of the headform only quantitatively affects the outcome of the drop tests and not qualitatively. However, the rotational motion induced injury criteria can only be measured indirectly, for instance by measuring the bending moment at the joint, which neglects the dynamical effects during impact. Therefore, the ECE-R.22 method should be preferred over the methods of Snell and DOT, since it also allows for a correct helmet evaluation based on rotational motion induced injury.

Hypothesis 3: The application of the new headform and associated head injury criteria will lead to significant changes in helmet design. This hypothesis is partly true. The head injury criteria associated with the flexible headform, such as CSDM, do not lead to significant changes in helmet design, since their responses follow the trends of injury parameters that can also be measured with the conventional headform. However, the flexible headform attenuates a considerable part of the impact energy, causing lower values of the injury parameters. To compensate for the attenuation when using the conventional headform, the thresholds for the injury parameter HIC is raised from 1000 for the human head to 2400 for the conventional headform. However, the flexible headform behaves structurally different to a change in impact configuration than the conventional headform. Simply scaling the threshold for HIC when using the conventional headform may therefore lead to an incorrect assessment of injury. To overcome this problem, the experiments in this research suggest that the conventional headform should be replaced by a more biofidelic, flexible headform in helmet certification tests. Therefore, Hypothesis 3 should not be rejected: More biofidelity = better safety.

This conclusion concerns the flexibility of both the skull and the brain. However, it does not concern the skin. It is found in this study, that the skin does not have a significant influence on the outcome of the drop test simulations, provided that no bottoming out occurs in the protective padding liner.

7.2 Recommendations for the Flexible Headform

This study has proven that the biofidelity of the conventional headform can be improved and that doing so may change the way helmets are designed. However, the headform presented in this research is not suitable as a replacement for the conventional headform, since it still has some shortcomings that can be improved in future studies. In such studies, the following considerations need to be addressed. Firstly, the headform must be made more robust, since the flexible headform in this study is particularly vulnerable to side impact. Secondly, the headform needs to be validated for the rotational motion induced injury parameters (such as HIP, $\omega_{\max}$ and CSDM), when it is to be implemented in shock absorption test regulations. Furthermore, the thresholds for the existing injury parameters HIC and $a_{\max}$ can not simply be copied from the conventional headform, but they need to be redetermined for this particular headform by calibration with real-world accident data. Finally, the results of the drop tests show large spreads in rotational velocities. Consequently even larger spreads are to be expected in rotational accelerations. To overcome this, the boundary and initial conditions of the drop tests need to be defined more accurately with respect to the positioning of the headform inside the helmet and with respect to the accuracy of the impact location. One way of doing so may be by locking the headform to the cart of the drop tower and releasing it only just before impact by means of quick release mechanism.

When considering CSDM, the numerical headform must be validated on the basis of experiments on the physical headform. The current numerical model lacks this validation, since marker trajectories in the experiments could not be compared one-on-one with the nodal displacements in the numerical model. To do so, markers fixed to the rigid parts of the headform need to be tracked, simultaneously with markers inside the brain. Due to the amount of X-ray energy needed to penetrate the brain, this was not possible. By changing the settings of the X-ray equipment, only either one of those marker sets could be visualised. In this research, it was chosen to visualise the markers inside the brain. Unfortunately, no good quantitative data resulted from these experiments. From the simulations however, it is concluded that $\omega_{\max}$ has a strong correlation with CSDM. Therefore, there is no need to measure CSDM in drop test experiments.

7.3 Helmet Design Optimisation

The design study in this research is based on numerical modelling of helmeted head impacts. However, there is also one conclusion with respect to helmet design, drawn from the experiments: As far as the comfort liner is concerned, it is more than a matter of bringing comfort to the user. It also provides the fit of the helmet. The fit also accounts for a considerable part of the protective function of the helmet. This study shows that using a helmet that is smaller in size than the headform results in an increase of the injury probability (see Section 3.4.2). This conclusion contradicts general belief, that a helmet must be tight to fit. One should not use a helmet that is too tight. Unfortunately, this conclusion could not be backed up by simulations, since current explicit FE codes are not yet applicable in low-stiffness, large-deformation situations.

Unless stated otherwise, the discussion below refers only to the numerical simulations with a helmet that includes the modelling of comfort foam, the density distribution of the protective padding liner and the thickness distribution of the outer shell. Especially the latter two turned out to significantly affect the simulation results, compared to the experiments, which confirms the approach proposed by Brands *et al.* [1997].

Many researchers have tried to investigate the protective capacities of current day motorcycle helmets in numerical simulations. Without exception, they all concluded that reducing the protective padding liner density leads to lower translational accelerations. Of course this conclusion is only valid when bottoming out does not occur. This study also confirms that conclusion. Besides controlling the magnitude of the translational acceleration, its shape can be influenced by changing the outer shell stiffness. This can be used to design helmets with a smooth and mostly rectangular shaped acceleration curve which minimises HIC.

As far as the position of the FRP shell is concerned, the injury criteria yield lower values when the FRP shell is positioned closer to the headform. In this case, the helmet deforms from the outside. The impacted surface is never the same as the outer geometry of the helmet, especially in real accident situations. Because the FRP shell is not positioned on the outside of the helmet and the protective padding liner possesses only little load distributing capacities, load distribution over the surface of the helmet does not occur. Because of the spherical shape of the helmet, a larger area is compressed as the impact progresses. This results in a contact force that increases as the impact progresses, resulting in a the triangular shape of the acceleration time history. This is a less efficient way of absorbing energy. The most efficient way of absorbing energy is when the acceleration is constant during the impact and no rebound occurs. This situation is best approximated when the FRP shell is positioned on the outside of the helmet. Due to the load distribution over the surface of the helmet, the load is then spread over a larger area of the helmet and the area of deformation remains more constant throughout the impact.

Since the load distributing capacities of the the outer shell are not infinite, the contact force still increases as the impact progresses. The helmet's efficiency can be further improved by using a higher protective padding liner density on the outside than on the inside of the helmet. This way the contact force can be further tuned to be constant, thus resulting in a positive effect on the shape of the acceleration time history.

This study does not only consider HIC and $a_{\max}$, it also considers other injury criteria. Even though reducing the protective padding liner density leads to a reduction of all injury criteria, the results presented in this study show that not all injury parameters yield the same optimal helmet design in terms of protective padding liner density. The protective padding density that minimises $a_{\max}$ and HIC is lower than the one that minimises $HIP_{\max}$ and $\omega_{\max}$. Since the optimal protective padding liner in these cases is close to bottoming out, that helmet is highly sensitive, in terms of $a_{\max}$, to an increase in drop velocity. HIC is less sensitive in this case, since the increase in translational headform acceleration is of a short duration. Therefore, one should carefully consider the desired level of protection at higher impact velocities, when designing a helmet. A higher protective padding liner density results in higher values for the injury criteria, but it also ensures increased protection against higher velocity impacts. However, in most helmets, the level of protection is not the same for each impact configuration as a result of differences in local structural design of the helmet. A higher protective padding liner density is required to compensate for the loss of helmet effectiveness as a result of edges and the visor opening. To ensure the same level of protection in all impact configurations, the protective padding liner density should be determined for each particular impact configuration. Rear impact yields lower translational accelerations as a result of increased rotational motion, even though this conclusion also holds for drop tests in which rotational motion is suppressed.

As stated before, helmets that are optimised to yield minimum values for the injury parameters in standard drop tests, will result in an increased risk of injury at higher impact velocities, as a result of bottoming out. However, helmets can also be optimised by finding that protective padding liner

density for which the different injury parameters just reach their threshold values and thus offer protection at higher impact velocities. The current drop test regulations allow for both strategies. To overcome this ambiguity and to offer protection in both high-impact and in low-impact situations, helmets should be tested in both these situations. This means that less severe injuries should be allowed in low impact velocities, meaning that injury criteria must be reduced at an impact velocity of 7.5 m/s. This study shows that values up to 153 m/s^2 and 1418 are achievable for a_{max} and HIC in Top impact at 7.5 m/s. Yet, the current levels of the injury criteria $a_{max} = 275$ m/s^2 and HIC = 2400, which represent the thresholds of the human head, should be maintained but at a higher impact velocity. This study shows that these values are still achievable in Top impact at an impact velocity up to 8.7 m/s, which is an increase in impact energy of 35 %.

7.4 Future Research

Numerical modelling plays an increasing role in the design stage of almost every product. Designers want to know whether their product will likely pass the certification tests, before a prototype is built. Despite the fact that the numerical models presented in this research show acceptable results, current day Finite Element codes are not accurate enough to predict rotational motion sufficiently well in drop test simulations. The main reason for that is found in the material model used for the comfort and for the protective padding liner. In compression, this material model is very accurate. However, in shear it is too compliant. In order to be able to predict also rotational motion sufficiently well in helmeted head impact simulations, this material model needs further improvement. When this problem is solved, it is likely that the model can discriminate between drop tests using the Size L helmet and those using the Size M helmet, since it is assumed that the shear forces in the comfort foam are responsible for this difference in the helmeted headform drop test experiments. Furthermore, the interaction between helmet and type of headform, found in the experiments (see Section 3.4.2), may then also be found in the simulations.

Another shortcoming of this material model, is that it remains fully compressible during the bottoming out stage. However, this is not critical, since bottoming out should not occur in helmeted head impact, because it results in unacceptably high headform accelerations.

These shortcomings are likely to be responsible for the models not being able to discriminate between the drop tests with the flexible headform and those with the conventional headform. In this study it is shown, that in the experiments the flexible headform is to be preferred over the conventional. Yet, the differences are small, since it is chosen to model the flexible headform much alike the conventional headform. A headform which is anatomically and geometrically more like the human head will probably lead to larger differences between the two. A perfect model of the human head is far too complex to build, let alone to yield reliable and reproducible results. Therefore, further research is needed to investigate to what extent the headform should be made more biofidelic, to find a compromise between model complexity and biofidelity on the one hand, and reproducibility, repeatability and cost on the other.

As far as the drop test itself is concerned, it can be concluded from this research that the test should be extended with at least a second drop test at a different impact velocity. From the simulations, it has become clear that helmet investigated in this research can withstand higher impacts, when the protective padding liner density is reduced. Doing so, also reduces the values for the injury parameters at the standard impact velocity. Other studies demonstrate that some helmets show lower values for the injury parameters in the standard drop test than the helmet in the present study does. Adding

a second criterion at a higher impact velocity, may require these helmets to be designed somewhat stiffer. This would then most likely result in higher values for the injury parameters in the drop test at the standard impact velocity, and thus in a higher injury risk for these helmets. Therefore, the impact velocity and the injury criteria at the higher impact velocity should be chosen with care and requires additional research.

The author of this thesis hopes that this research and its results motivates other researchers to continue to increase the knowledge on head injury and to find ways to implement it in helmet testing standards for a better protection to the human head.

Bibliography

ACEM, 1997. 'Homepage of the Motorcycle In-Depth Accident Study (MAIDS) project, http://www.acembike.org/html/maids.htm.'

Adams, J.H., Graham, D.I. & Gennarelli, T.A., 1983. 'Head injury in man and experimaental animals: neuropathology.' *Acta Neurochirurgica*, **32**, 15–30.

Advani, S., Ommaya, A.K. & Yang, W.J., 1982. *Head injury mechanisms: Characterizations and clinical evaluation*, pp. 1–37. Clarendon Press, Oxford.

Al-Bsharat, A.S., Hardy, W.N., Yang, K.H., Khalil, T.B., Tashman, S. & King, A.I., 1999. 'Brain/Skull Relative Displacement Magnitude Due to Blunt Head Imapact: New Experimental Data and Model.' In: *Proceedings of the 43rd Stapp Car Crash Conference*, pp. 321–332. Paper No. 99SC22.

ANSI, 1991. *Standard for protective headgear — for motor vehicle users.* Tech. Rep. ANSI Z90.1-1991, American National Standard Institute. Originated in 1966 as Z90.1-1966.

Arbogast, K.B. & Margulies, S.S., 1997. 'Regional Differences in Mechanical Properties of the Porcine Central Nervous System.' In: *Proceedings of the 41st Stapp Car Crash Conference*, pp. 293–300. Society of Automotive Engineers. SAE Paper No. 973336.

Bandak, F.A., 1995. 'On the Mechanics of Impact Neurotrauma: A Review and Critical Synthesis.' *Journal of Neurotrauma*, **12**(4), 635–649.

Bandak, F.A., 1997. 'Impact Traumatic Brain Injuries: A Mechanical Perspective.' In: *Neurotraumatology: Biomechanic Aspects, Cytologic and Molecular Mechanisms* (Edited by Oehmichen, M. & König, H.G.), pp. 58–83. Schmidt-Römhild.

Bandak, F.A. & Eppinger, R.H., 1994. 'A three-dimensional finite element analysis of the human brain under combined rotational and translational accelerations.' In: *Proceedings of the 38th Stapp Car Crash Conference*, pp. 145–163. Society of Automotive Engineers. SAE Paper No. 942215.

Bandak, F.A., Zhang, A.X., Tannous, R.E., DiMasi, F., Masiello, P. & Eppinger, R., 2001. 'SIMon: A Simulated Injury Monitor; Application to Head Injury Assessment.' In: *Proceedings of the 17th International Technical Conference on Enhanced Safety of Vecicles*, Amsterdam.

Bastiaanse, J.C. & Brockhoff, H.S.T., 1976. 'The Natural Crash-Helmet.' In: *International IRCOBI Conference on the Biomechanics of Impacts*, pp. 375–384.

Bednar, Frank, Billheimer, John W., McRea, Keith, Sabol, Scott A., Syner, Joey & Thom, David R., 2000. *Motorcycle Safety*. Tech. rep., The National Academies, Transportation Research Board, Washington, DC (USA).

Beusenberg, M.C. & Happee, R., 1993. 'An experimental evaluation of crash helmet design and effectiveness in standard impact tests.' In: *International IRCOBI Conference on the Biomechanics of Impacts*, pp. 307–323, Eindhoven.

Blinkov, S.M. & Glezer, I.I., 1968. *The Human Brain in Figures and Tables - A Quantitative Handbook.* Plenum Press, New York.

Brands, D.W.A., Bovendeerd, P.H.M., Peters, G.W.M., Paas, M.H.J.W., van Bree, J.L.M.J. & Wismans, J.S.H.M., 1999. 'Comparison of the Dynamic Behaviour of Brain Tissue and Two Model Materials.' In: *Proceedings of the 43rd Stapp Car Crash Conference*, pp. 313–320. Society of Automotive Engineers. Paper No. 99SC21.

Brands, D.W.A., Thunnissen, J.G.M. & Wismans, J.S.H.M., 1997. 'Modelling Head Injury Counter-measures: a 3D helmet model.' In: *Proceedings of the AGARD Specialists' Meeting on Impact Head Injury*, no. 597, pp. 26–2 – 26–9, Mescalero, NM (USA). Advisory Group for Aerospace Research & Development.

BSI, 1952. *Specification for protective helmets for racing motorcyclists.* Tech. Rep. BS 1869:1952, British Standards Institution.

BSI, 1985. *Specification for protective helmets for vehicle users.* Tech. Rep. BS 6658:1985, British Standards Institution.

Cappon, H.J., 1997. *Experimental and numerical modal analysis of a motor cycle helmet.* Master's thesis, Eindhoven University of Technology.

Chandler, R.F., 1975. *Investigation of Inertial Properties of the Human Body*, pp. 68–69. Aerospace Medical Research Laboratory, Ohio, USA.

Chang, Chih-Han, Chang, Li-Tung, Chang, Guan-Liang, Huang, Shyh-Chour & Wang, Chiou-Hua, 2000. 'Head Injury in Facial Impact — A Finite Element Analysis of Helmet Chin Bar Performance.' *Journal of Biomechanical Engineering*, **122**(6), 640–646.

Chatfield, C., 1994. *Statistics for Technology: A Course in Applied Statistics.* Chapman & Hall, London, 3rd edn.

Chinn, B.P., Doyle, D., Otte, D. & Schuller, E., 1999. 'Motorcyclists head injury: Mechnisms identified from accident reconstruction and helmet damage replication.' In: *International IRCOBI Conference on the Biomechanics of Impacts*, pp. 53–71.

DIFA, 1994. *DSA200 Getting Started Manual.* DIFA Measuring Systems B.V., Breda, The Netherlands.

EEVC, 1993. *Report in motorcycle safety.* Tech. rep., European Experimental Vehicles Committee ad-hoc group.

EEVC, 1999. *Summary of Side Impact Response Requirements.* Tech. rep., European Experimental Vehicles Committee — WG-12.

Eiband, A., 1959. *Human tolerance to rapidly applied accelerations: a summary of the literature.* Report no. 5-19-59e, NASA Memorandum.

Evans, L., 1986. 'Double Pair Comparison – A new method to determine how occupant characteristics affect fatality risk in Traffic crashes.' *Accident Analysis & Prevention*, **18**(3), 217–227.

Evans, L. & Frick, M.C., 1986. *Helmet Effectiveness in Preventing Motorcycle Driver and Passenger Fatalities.* General motors research publication no. gmr-5602.

Fahlbusch, G., 1984. *Die Aufstellung von vollständigen Übertragungsmatrizen für Kreiskegelschalen und die durch Grenz/"ubergang daraus ableitbaren Platten, Scheiben und Zylinderschalen.* Tech. rep., Technische Akademie, Wuppertal, Germany.

Fallenstein, G.T., Hulce, V.D. & Melvin, J.W., 1969. 'Dynamic Properties of Human Brain Tissue.' *Journal of Biomechanics*, **2**, 217–226.

Gadd, C.W., 1966. 'Use of a weighted-impulse criterion for estimating injury hazard.' In: *Proceedings of the 10th Stapp Car Crash Conference*, pp. 164–174.

Gadd, C.W., 1971. 'Tolerable Severity Index in whole-head nonmechanical impact.' In: *Proceedings of the 15th Stapp Car Crash Conference*, pp. 809–816.

Gennarelli, T.A., 1981. 'Mechanistic approach to the head injuries: Clinical and experimental studies of the important types of injury.' In: *Head injury criteria - A consensus workshop*, pp. 20–25, Washington D.C., USA. U.S. Government printing office.

Gennarelli, T.A., 1983. 'Head Injury in Man and Experimental Animals: Clinical aspects.' *Acta Neurochirurgica, Supplement*, **32**, 1–13.

Gennarelli, T.A., 1985. 'The state of the art of head injury biomechanics - A review.' In: *Twenty-Ninth Conference of the Association for the Advancement of Automotive Medicine*, pp. 47–63.

Gennarelli, T.A., Thibault, L.E., Tomei, G., Wiser, R., Graham, D. & Adams, J., 1987. 'Directional dependence of axonal brain injury due to centroidal and non-centroidal acceleration.' In: *Proceedings of the 31st Stapp Car Crash Conference*, pp. 49–53. SAE Paper No. 872197.

Gilchrist, A. & Mills, N.J., 1993. 'Deformation analysis for motorcycle helmets.' In: *International IRCOBI Conference on the Biomechanics of Impacts*, pp. 269–281, Eindhoven, The Netherlands.

Goldstein, J., 1988. *Review of Helmet and Helmet Law Effectiveness Studies.* http://www.bikersrights.com/statistics/goldstein/reviews/reviews.html, Dowdoin college, Department of Economics, Brunswick, ME (USA).

Gurdjian, E., 1975. *Impact Head Injury – Mechanistic, Clinical and Preventive Correlations.* Charles C Thomas Publisher, Springfield, Illinois (USA).

Gurdjian, E.S., Lissner, H.R. & Evans, F.G., 1961. 'Intracranial pressure and acceleration accompanying head impacts in human cadavers.' In: *Surgery, Gynecology, and Obstetrics*, vol. 112, pp. 185–190.

Gurdjian, E.S. *et al.* , 1953. 'Quantitative determination of acceleration and intracranial pressure in experimental head injury.' *Neurology*, **3**, 417–423.

Halldin, P., Gilchrist, A. & Mills, N.J., 2001. 'A new oblique impact test for motorcycle helmets.' *International Journal of Crashworthiness*, **6**(1), 53–64.

Happee, R., 1993. *The behaviour of foam material in crash conditons: Experiments with polystyrene foam, and predictions with one-dimensional models.* Internal Report TNO-report 751210176, TNO Automotive, The Netherlands.

Hardy, W.N., Foster, C.D., King, A.I. & Tashman, S., 1998. 'Update on the study of headinjury kinematics.' In: *Symposium Proceedings, Centers for Disease Control*, pp. 177–184.

Hardy, W.N., Foster, C.D., Mason, M.J., Yang, K.H., King, A.I. & Tashman, S., 2001. 'Investigation of Head Injury Mechanisms Using Neutral Density Technology and High-Speed Biplanar X-Ray.' *Stapp Car Crash Journal*, **45**, 337–368.

Harms, P.J., 1981. *Injury patterns of motorcyclists involved in accidents.* Supplementary report SR 651, TRRL, Crowthorne.

Harms, P.L., 1993. *Crash injury investigation and injury mechanisms in road traffic accidents.* Trl state of the art review, HMSO, London.

Harrigan, J.J., Reid, S.R. & T.Y., Reddy, 1998. 'Accurate measurement of impact force pulses in deforming structural components.' In: *Experimental Mechanics: Advances in Design, Testing and Analysis (Proceedings of the 11th International Conference on Experimental Mechanics)* (Edited by Allison, I.M.), vol. 1, pp. 149–154, Oxford, UK. BSSM, EPCEM.

Hendriks, F.M., Brokken, D., van Eemeren, J., Oomens, C.W.J., Baaijens, F.P.T. & Horsten, J.B.A.M., 2003. 'A numerical-experimental method to characterize the non-linear mechanical behaviour of human skin.' *Skin Research and Technology*, **to be published.**

Hodgson, V.R., 1976. 'Head injury criteria and evaluation of protective head gear.' In: *Measurement and Prediction of Structural and Biodynamic Crash-Impact Response* (Edited by Saczalski, K.J. & Pilkey, W.D.), pp. 121–135. ASME-WAM, New York.

Hodgson, V.R., Gurdjian, E.S. & Thomas, L.M., 1967. 'The determination of response characteristics of the head with emphasis on mechanical impedance techniques.' In: *Proceedings of the 11th Stapp Car Crash Conference*, pp. 125–138. Society of Automotive Engineers. SAE Paper No. 670911.

Hodgson, V.R., Mason, M.W. & Thomas, L.M., 1972. 'Head Model for Impact.' In: *Proceedings of the 16th Stapp Car Crash Conference*, pp. 1–13. Society of Automotive Engineers. SAE Paper No. 720969.

Hodgson, V.R. & Patrick, L.M., 1968. 'Dynamic response of the human cadaver head compared to a simple mathematical model.' In: *Proceedings of the 12th Stapp Car Crash Conference*, pp. 280–301. SAE Paper No. 680784.

Hodgson, V.R. & Thomas, L.M., 1975. *Head Impact Response.* VRI report 7.2, SAE.

Holbourn, A.H.S., 1945. 'The mechanics of brain injuries.' *British Medical Bulletin*, **3**, 147–149.

Hopes, P.D. & Chinn, B.P., 1989. 'Helmets: A new look at design and possible protection.' In: *International IRCOBI Conference on the Biomechanics of Impacts*, pp. 39–54, Stockholm.

Hurt Jr., H.H., Ouellet, J.V. & Thom, D.R., 1981. *Motorcycle accident cause factors and identification of countermeasures. Vol. 1.* Technical report DOT HS-5-01160, US Department of Transportation NHTSA.

Hurt Jr., H.H. & Thom, D.R., 1992. 'Motorcyclist head injury mechanisms- with and without helmets.' In: *36th Conference of the Association for the Advancement of Automotive Medicine*, pp. 235–250.

IIHS, 2001. *Special Issue: Motorcycle Deaths.* Status Report Newsletter, Vol. 37, No. 1, Insurance Institute for Highway Safety.

ISO-6487, 2002. *Road vehicles – Measurement techniques in impact tests – Instrumentation.* Tech. rep., International Standards Organisation.

ISO-R1511, 1970. *Protective Helmets for Road Users.* Tech. rep., International Standards Organisation.

Ivarson, D.C., Viano, D.C. & Lövsund, P.L., 2000. 'The Influence of the Irregular Skull Base on Brain Kinematics during head Impact — an experimental study.' *Journal of Biomechanics*, **33**(2), 181–189.

Jolliffe, I.T., 1986. *Principal component analysis.* Springer, Berlin. ISBN 3-540-96269-7.

Köstner, H. & Stöcker, U.W., 1987. 'Mathematische Analyse der Stoßabsorption im Schutzhelm-material.' In: *VDI-bericht Nr. 657*, pp. 211–244.

de Kraker, A., 1993. *Numeriek-Experimentele Analyse van Dynamische Systemen.* Lecture notes, nr. 4668. Eindhoven University of Technology, The Netherlands (Dutch).

Lee, M.C. & Haut, R.C., 1989. 'Insensitivity of tensile failure properties of human bridging beins to strain rate: Implications in biomchanics of subdural hematoma.' *Journal of Biomechanics*, **22**(6/7), 537–542.

Lissner, H.R., Lebow, M. & Evans, F.G., 1960. 'Experimental studies on the relation between acceleration and intracranial pressure changes in man.' In: *Surgery, Gynecology, and Obstetrics*, vol. 111, pp. 320–338.

Löwenhielm, C.G.P., 1974. 'Dynamic properties of the parasagittal bridging veins.' In: *Zeitschrift für Rechtsmedizin*, vol. 74, pp. 55–62.

Löwenhielm, P., 1975. 'Mathematical simulation of gliding contusions.' *Journal of Biomechanics*, **8**, 351–356.

Margulies, S.S. & Thibault, L.E., 1992. 'A proposed tolerance criterion for Diffuse Axonal Injuries in man.' *Journal of Biomechanics*, **25**, 917–923.

MATLAB, 1999. *User's Guide.* Mathworks, Inc., South Natick, MA, USA.

McElhaney, J.H., Fogle, J.L., Melvin, J.W., Haynes, R.R., Roberts, V.L. & Alem, N.M., 1970. 'Mechanical Properties of Cranial Bone.' *Journal of Biomechanics*, **3**, 495–511.

McElhaney, J.H., Melvin, J.W., Roberts, V.L. & Portnoy, H.D., 1972. 'Dynamic characteristics of tissue of the head.' *Symposium Perspectives in Biomedical Engineering*, pp. 1–8.

Mills, N.J. & Gilchrist, A., 1988. 'Mathematical modelling of the effectiveness of helmets in head protection.' In: *International IRCOBI Conference on the Biomechanics of Impacts*, pp. 215–226, Bergisch Gladbach, Germany.

Mooi, H.G. & Galliano, F., 2001. 'Dutch in-depth accident investigation: First experiences and analysis results for motorcycles and mopeds.' In: *17th International Technical Conference on the Enhanced Safety of Vehicles*, Amsterdam, The Netherlands.

Nahum, A.M., Smith, R. & Ward, C.C., 1977. 'Intracranial pressure dynamics during head impact.' In: *Proceedings of the 21st Stapp Car Crash Conference*, pp. 339–366. SAE Paper No. 770922.

Newman, J.A., 1980. 'Head Injury Criteria in Automotive Crash Testing.' In: *Proceedings of the 27th Stapp Car Crash Conference*, pp. 701–747. SAE Paper No. 801317.

Newman, J.A., 1986. 'A Generalized Acceleration Model for Brain Injury Threshold (GAMBIT).' In: *Proceedings of the 1986 International IRCOBI Conference*, Bron, France. IRCOBI Secr.

Newman, James A., Barr, Cameron, Beusenberg, Marc, Fournier, Ed, Shewchenko, Nicholas, Welbourne, Eric & Withnall, Christopher, 2000b. 'A New Biomechanical Assessment of Mild Traumatic Brain Injury: Part 2 — Results and Conclusions.' In: *International IRCOBI Conference on the Biomechanics of Impacts*, pp. 223–233, Montpellier (France).

Newman, James A., Shewchenko, Nicholas & Welbourne, Eric, 2000a. 'A Proposed New Biomechanical Head Injury Assessment Function — The Maximum Power Index.' *Stapp Car Crash Journal*, **44**, 215–222. Paper No. 2000-01-SC16.

NHTSA, 1972. *Occupant crash protection — Head Injury Criterion.* Report No. FMVSS 208, Docket Number 69-7, Notice 17, US Department of Transportation.

NHTSA, 1988. *Federal Motor Vehicle Safety Standards: Standard No. 218; Motorcycle helmets.* Tech. Rep. 49 CFR 571.218, U.S. Department of Transportation, National Highway Traffic Safety Administration.

NHTSA, 2000. *Federal Motor Vehicle Safety Standards: Standard No. 208; Occupant crash protection.* Tech. Rep. 49 CFR 571.208, U.S. Department of Transportation, National Highway Traffic Safety Administration.

NOCSAE, 2002. *Standard drop test method and equipment used in evaluating the performance of protective headgear.* Tech. Rep. NOCSAE DOC.001-00, National Operating Committee on Standards for Athletic Equipment, Overland, KS, USA.

Ommaya, A.K., 1984. 'Biomechanics of Head Injuries: Experimental aspects.' In: *Biomechanics of Trauma* (Edited by Nahum, A. & Melvin, J.W.), East Norwalk (CT, USA). Appleton-Century-Crofts.

Ommaya, A.K., 1988. 'Mechanisms and Preventive Management of Head Injuries, a Paradigm for Injury Control.' In: *Proc. 32nd AAAM Conference.*

Ommaya, A.K., Thibault, L. & Bandak, F.A., 1994. 'Mechanisms of Impact Head Injury.' *International Journal of Impact Engineering*, **15**(4), 535–560.

Ommaya, A.K., Yarnell, P., Hirsch, A.E. & Harris, E.H., 1967. 'Scaling of experimental data on cerebral concussion in sub-human primates to concussion threshold for man.' In: *Proceedings of the 11th Stapp Car Crash Conference*, pp. 47–52, New York (USA). Society of Automotive Engineers.

Otte, D., Chinn, B., Doyle, D., Sturrock, K. & Schuller, E., 1999. *Accident Description and Analysis of Motorcycle Safety Helmets.* Final report, COST 327 Project – Task Group: Accident Data.

Otte, D., Jessl, P. & Suren, E.G., 1984. 'Impact points and resultant injuries to the head of motorcyclists involved in accidents, with and without crash helmets.' In: *Proc. Int. Conf. on the Biomechanics of Impact (IRCOBI)*, pp. 47–64.

Otte, D., Kalbe, P. & Suren, E.G., 1981. 'Typical injuries to the soft body parts and fractures of the motorised 2-wheelers.' In: *6th IRCOBI Conference on Biomechanics of Impacts*, pp. 148–165, Salon de Provence, France.

Otte, D., Kühnel, A., Suren, E.G., Weber, H., Gotzen, L. & Schockenhoff, G., 1982. 'Erhebungen am Unfallort; Unfall- und Sicherheitsforschung Strassenverkehr.' *Heft 37*, pp. 7–10.

Padgaonkar, A.J., Krieger, K.W. & King, A.I., 1975. 'Measurement of angular acceleration of a rigid body using linear accelerometers.' *Journal of Applied Mechanics*, **42**, 552–556.

Patrick, L.M., Lissner, H.R. & Gurdjian, E.S., 1965. 'Survival by design — head protection.' In: *Proceedings of the 7th Stapp Car Crash Conference*, pp. 483–499.

Peijs, T., 1998. *Composieten.* College Diktaat Module 9. Eindhoven University of Technology, The Netherlands (Dutch).

Peters, G., Meulman, H. & Sauren, A., 1997. 'Application of the Time Temperature Superposition Theory on Brain Tissue.' *Biorheology*, **34**, 127–138.

Pike, J.A., 1990. *Automotive safety - Anatomy, Injury, Testing and Regulation.* Society of Automotive Engineers, Inc., Warrendale, PA (USA).

Prasad, P., Melvin, J.W., Huelke, D.F., King, A.I. & Nyquist, G.W., 1985. *Review of biomechanical impact response and injury in the automotive environment*, chap. 1 - Head. report no. DOT HS 807 042. U.S. Department of transport - NHTSA, Washington D.C., USA.

Ramet, M., Cesari, D. & Dedoyaw, A., 1981. 'Two weeler accidents.' In: *6th IRCOBI Conference on Biomechanics of Impacts*, pp. 193–205, Salon de Provence, France.

Ran, A., Koch, M. & Mellander, H., 1984. 'Fitting injury versus exposure data into a risk function.' In: *9th IRCOBI Conference on Biomechanics of Impacts*, Delft, The Netherlands.

Reinschmidt, C. & van den Bogert, T., 1997. *KineMat: A /nounMATLAB Toolbox for Three-Dimensional Kinematic Analyses.* http://www.isbweb.org/software/movanal/kinemat/, Human Performance Laboratory, The University of Calgary.

Saczalski, K.J., States, J.D., Wagar, I.J. & Richardson, E.Q., 1976. 'A critical assessment of the use of non-human responding surrogates for safety evaluation.' In: *Proceedings of the 20th Stapp Car Crash Conference*, pp. 161–187. SAE Paper No. 760805.

SAE, 1986. *Human Tolerance to Impact Conditions as related to Motor Vehicle Design.* Tech. Rep. SAE J885 JUL86, Society of Automotive Engineers, Inc. (USA).

Schuller, E. & Beier, G., 1981. 'Satety helmets shell material and head injury incidence in motorcycle accidents.' In: *6th IRCOBI Conference on Biomechanics of Impacts*, pp. 184–192, Salon de Provence, France.

Slattenschek, A. & Tauffkirchen, W., 1970. 'Critical evaluation of assessment methods for head impact applied in appraisal of brain injury hazard, in particular in head impact on windshields.' In: *1970 International Automobile Safety Conference Compendium*, pp. 1084–1112.

SMF, 2000. *Standards for Protective Headgear: For Use with Motorcycles and other Motorized Vehicles.* Tech. rep., Snell Memorial Foundation, Inc., North Highlands, CA, USA. Originated in 1959.

Sporner, A., Langwieder, K. & Polauke, J., 1990. 'Passive safety for motorcyclists — From the leg protector to the airbag.' In: *SAE International Congress and Exposition*, pp. 197–206, Detroit. SAE Paper No. 900756.

Swearingen, J.J., 1965. *Tolerances of the human face to crash impact.* Tech. rep., Oklahoma: Office of Aviation Medicine, FAA, Civil Aeromedical Research Institute.

Tarriere, C., 1981. *Head and Neck Injury Criteria – A Consencus Workshop*, pp. 218–228. U.S. Dept. of Transport, NHTSA, Washington D.C. (USA).

Thibault, K.L. & Margulies, S.S., 1996. 'Material Properties of the Developing Porcine Brain.' In: *International IRCOBI Conference on the Biomechanics of Impacts*, pp. 75–85, Dublin (Ireland).

Thibault, K.L. & Margulies, S.S., 1998. 'Age-dependent material properties of the porcine cerebrum: effect on pediatric inertial head injury criteria.' *Journal of Biomechanics*, **31**, 1119–1126.

Thibault, L.E., Gennarelli, T.A., Margulies, S.S., Marcus, J. & Eppinger, R., 1990. 'The strain dependent pathophysiological consequences of inertial loading on central nervous system tissue.' In: *International IRCOBI Conference on the Biomechanics of Impacts*, pp. 191–202.

Thollon, L., Arnoux, P.J., Kayvantash, K., Cavallero, C. & Brunet, C., 2002. 'Human Injury Evaluation Using HUMOS RADIOSS Finite Element Model.' In: *International IRCOBI Conference on the Biomechanics of Impacts*, pp. 369–373, Munich, Germany.

Thomas, P. & Bradford, M., 1992. 'Vehicle Design for Secondary Safety.' In: *Proceedings of Road Safety in Europe, VTI, No. 380A, Part 4.*

Thunnissen, T.G.M., 1995. *The behaviour of foam material in crash conditons: Experiments with a spring impactor, and predictions with MADYMO.* Internal Report TNO-report 95.OR.BV.002.1/JTH, TNO Automotive, The Netherlands.

TNO Automotive, 2001. *MADYMO Manuals.* TNO Road-Vehicles Research Institute, Delft, The Netherlands, 6th edn.

UN, 2000. *Regulation No. 22: Uniform provisions concerning the approval of protective helmets and of their visors for drivers and passengers of motorcycles and mopeds.* Tech. rep., United Nations, Economic Commission for Europe (working party 29), Geneva, SUI. Initially passed, 1958; amendment 04, 1995; amendment 05 1999.

Vallée, H., Thomas, C., Sacreste, J., Henry, C., Tarrière, C., Got, C. & Patel, A., 1981. 'Characteristics of objects struck by the head of moped riders or motorcyclists.' In: *6th IRCOBI Conference on Biomechanics of Impacts*, pp. 99–109, Salon de Provence, France.

Versace, J., 1971. 'A review of the Severity Index.' In: *Proceedings of the 15th Stapp Car Crash Conference*, pp. 771–796. Also (MVSS208).

Viano, D., Aldman, B., Pape, K., van Hoof, J. & von Holst, H., 1997. 'Brain Kinematics in Physical Model Tests with Translational and Rotational Acceleration.' *International Journal of Crashworthiness*, 2(2), 191–205.

Viano, D.C. & Lövsund, P., 1999. 'Biomechanics of brain and spinal-cord injury: Analysis of neuropathologic and neurophysiologic experiments.' *Journal of Crash Prevention and Injury Control*, 1, 35–43.

Vincze-Pap, Sándor & Áfra, Zsombor, 2001. 'Comparative Impact Tests on Helmets.' In: *Lecture notes of the ICB Seminars*, Warsaw, Poland.

Willinger, R., Baumgarten, D., Chinn, B. & Schuller, E., 2001. 'New dummy head prototype: development, validation and injury criteria.' *International Journal of Crashworthiness*, 6(3), 281–293.

Willinger, R. & Cesari, D., 1990. 'Determination of cerebral movement at impact through mechanical impedance measurement.' In: *International IRCOBI Conference on the Biomechanics of Impacts*, pp. 203–213.

Wismans, J.S.H.M., Janssen, E.G., Beusenberg, M., Koppens, W.P. & Lupker, H.A., 1994. *Injury biomechanics.* nr. 4552. Eindhoven University of Technology, The Netherlands, 2nd edn.

Yettram, A.L., Godfrey, N.P.M. & Chinn, B.P., 1994. 'Materials for motorcycle crash helmets — a finite element parametric study.' In: *Plastics rubber and composites: processing and applications, Vol 22(Issue4)*, pp. 215–222.

Appendix A

Helmet Testing Standards

A.1 Introduction

This appendix discusses the history of helmet testing standards. Furthermore, differences and similarities between the current versions of the DOT, Snell and ECE standards are discussed. These standards apply to transport only and do not cover sport or leisure activities. The DOT and the Snell standard apply largely to helmets intended for the United States and Canada. The ECE standard is the de-facto European standard. The ECE standard is discussed in more detail, since this standard is the base of this thesis.

A.2 History

Motorcycle helmets have improved greatly in comfort and convenience since the first patent for the modern protective helmet was issued in 1953 [Bednar *et al.*, 2000]. The first full-facial-coverage helmet was built in 1967. Several standards for testing motorcycle helmets exist worldwide to assess the quality of the helmets. Most standards are raised roughly every five years when the level of development (e.g. knowledge on head injury, improved energy absorbing materials) allows better head protection. Since helmets are built to pass a certain standard, helmet performance increases accordingly.

The first standard tests for motorcycle helmets was the British Standard 1869:1952 [BSI, 1952], issued by the British Standard Institution (BSI). This test applied shock loadings to a helmeted headform. The test technicians would drop a hardwood block weighing ten lbs. (4.5 kg) from a height of nine feet (2.7 m) onto a helmeted headform. The output consisted of dynamic force measurements recorded from a gauge mounted between the base of the headform and a massive reaction block. The test criterion required that the output force not exceeded 5000 lbs. (22.2 kN). Only qualified helmets were to be sold in Great Britain.

This standard served two immediate purposes: it was a tool for the evaluation of available headgear and it also served as a guide for the design of new headgear. It set performance levels that every crash helmet should satisfy. In the early 1960's, the Snell Memorial Foundation (SMF) began to administer a helmet certification programme [SMF, 2000] similar to the programs of the BSI. However, the performance levels were set to higher levels that only the best helmets would meet and were raised as more and more helmets would meet the standard. In contrast to the British Standard, passing the Snell standard was not mandatory. However, manufacturers were eager to comply with the standard, because Snell certified helmets were easier to sell than non-certified helmets.

In 1966, the American Standards Association (ASA), later the American National Standards Institute (ANSI), published the first standard for protective headgear, Z90.1-1966 [ANSI, 1991], which every helmet sold in the United States should pass. From this standard, the current Federal Motor Vehicle Safety Standard 218 (FMVSS 218) [NHTSA, 1988] originated, which became effective in 1973 and is

issued by the U.S. Department of Transport (DOT). The FMVSS 218 is also mandatory. However, both standards do not administer any corresponding certification programmes. Manufacturers who claim to comply with the DOT are obliged to label their products with the DOT emblem, but are not required to inform the government about it or even test the helmet. The only driving force to comply with DOT is to avoid legal conflicts in case the manufacturer is held responsible for the sustained injury.

In 1970 the first European standard, ISO R 1511 [ISO-R1511, 1970], became effective. Currently, ECE Regulation 22 [UN, 2000] is the leading standard in Europe. Both standards arose from a United Nations effort to promote international trade and were recommended as models for governments and others to use in developing national standards. The administration is done by 'notified bodies', agencies throughout Europe empowered to consider applications for acceptance and to award the 'CE' mark which identifies each product meeting the standard. ECE Regulation 22 is, like the Snell and the DOT standard, heavily influenced by the standard of the BSI [1985].

A.3   Summary of Helmet Testing Standards

Each standard specifies tests for several different aspects of helmet performance, such as:

Shock absorption tests involve a drop test in which a headform is placed inside a helmet and then dropped onto an anvil. The acceleration measured inside the headform is related to the helmet's ability to reduce the risk of a head/brain injury from impact forces.

Resistance to penetration tests evaluate the helmet's ability to resist an impact with objects which cause localised loads, possibly leading to penetration of the helmet and head.

Rigidity tests involve application of a quasi-static, compressive force to evaluate the ability of a helmet to withstand compressive loads.

Friction tests can be divided into two categories:

- tests in which the loads are generated by abrasion; and
- tests in which the loads are generated by contact with protrusions.

Both tests will tend to impart rotational motion to the helmet and headform, which is to be minimised.

Retention system effectiveness tests examine the helmet's retention system on its ability to withstand external loads and to hold the helmet on the head during an accident. These tests can include a roll-off test, in which the helmet shall not release from the headform and the retention system shall remain functioning.

Visor safety tests can include a test for minimal peripheral view or optical qualities. The user's view on the road shall not be impeded by the helmet.

Flamability tests investigate the helmet's ability to withstand a fire. These tests are only for helmets that are used in racing. No standard for helmets that are used in traffic requires such a test.

Table A.1 gives an overview of which standard tests are required for the ECE, Snell and DOT standards. The ECE and the DOT standard are the legally approved standards for Europe and the USA, respectively. The Snell standard is also discussed, because it is a highly respected standard and it is more stringent than the DOT standard. From this table, it seems that the ECE standard is the most stringent one. However, in most tests, the requirements for the M2000 are more strict and more extensive. In the following sections, Table A.1 will be elaborated further.

A.3.1 Shock Absorption Tests

Impact protection is the primary consideration of almost every helmet standard. Although the general term for tests to assess impact protection is shock absorption tests, helmet quality is not assessed by measuring the amount of absorbed energy. Instead, the acceleration time history of a helmeted head-form is measured during an impact. From these measurements, injury parameters such as maximum acceleration in the headform, HIC (Chapter 1) and possibly other criteria which can be related to the potential for injury, are determined. The severity of the test, in terms of kinetic energy of the headform and helmet prior to impact and the anvil profile, varies between standards. Table A.2 compares the test conditions and requirements of the Snell, DOT and ECE standards.

The table shows the impacts prescribed for the various impact anvils. There are four different anvils: the flat, used in all the standards; the hemispherical anvil, with a diameter of about 4 inches, used in M2000 and DOT; the kerbstone anvil which resembles pavement curbing used in R.22; and the edge anvil, which is a 6 mm wide beam, used in M2000.

Impact

M2000 requires at least five impacts on one helmet in random order: two impacts on the flat anvil on a single site, two impacts on the hemispherical anvil on a site at least 120 mm from the previous site and one impact on the edge anvil on a site at least 120 mm from the previous two sites. The severity is described in terms of the kinetic energy of the falling headform and headform guidance system without the helmet. The mass of the headform and headform guidance system does not vary with headform size. The first drop is always 150 J, which is equal to an impact velocity of 7.7 m/s, and the

Table A.1: Overview of helmet standards.

Standard	Shock Sec. A.3.1	Penetration Sec. A.3.2	Retention Sec. A.3.3	Visor Sec. A.3.4	Rigidity Sec. A.3.5	Friction Sec. A.3.5
ECE-R.22	X	X	X	X	X	X
Snell M2000	X	X	X	X		
DOT FMVSS 218	X	X	X	X		

Table A.2: Shock absorption requirements of helmet standards.

Standard	Anvil Shape	Impact		Criterion
		1st Impact	2nd Impact	
ECE R.22	flat or kerbstone*	7.5 [m/s]	-	$a_{r,\,max} < 275$ [g], HIC < 2400
Snell M2000	flat	150 [J]	110 [J]	$a_{max} < 300$ [g]
	hemisphere	150 [J]	110 [J]	
	edge	150 [J]	-	
DOT FMVSS 218	flat	6.0 [m/s]	6.0 [m/s]	$a_{max} < 400$ [g], $a_{[2ms]} < 200$ [g], $a_{[4ms]} < 150$ [g]
	hemisphere	5.2 [m/s]	5.2 [m/s]	

* = depending on the conditioning (see paragraph 'Conditioning'):

Ambient: Flat and kerbstone anvil
Hot: Kerbstone anvil
Cold: Flat anvil
Wet: Flat or kerbstone (to be selected by the laboratory)

second drop, if required, is always 110 J, which is equal to an impact velocity of 6.6 m/s. The impact procedures leave considerable margin to the helmet tester regarding impact site and anvil selection. It is expected that the tester will use his experience to arrange each test series in such a way that potential weaknesses and likely failure modes are exercised.

The DOT standard also requires two impacts at each site tested against the flat and hemispherical anvils. There are no impact requirements against other anvils. Each helmet receives eight impacts, two on each anvil. The impact sites must be at least one sixth of the headform circumference apart. The severity is described in terms of the headform velocity just prior to impact. The velocity required depends on the anvil but is the same for both the first and the second impact. However, the kinetic energy prior to impact is not the same for all headforms, since a large headform, including guidance system, is, in contrast to the M2000, heavier than a small headform with guidance system. Thus, the helmet size determines the headform to be used and hence determines the kinetic energy of the headform and headform guidance system prior to impact. The kinetic energy prior to impact of the small, medium and large headform, including the guidance system, are 63, 90 and 110 J, respectively, for the tests on the flat anvil and 47, 68 and 82 J, respectively, for the tests on the hemispherical anvil.

The ECE standard requires only single impacts against the flat and kerbstone anvils. As with DOT, the impact severity is described in terms of the impact velocity: 7.5 m/s for both anvils. The ECE standard uses eight differently sized ISO headforms, indicated by the letters A, C, E, G, J, K, M and O. The impact energies for the E, J and M ISO headforms, which are comparable to the small, medium and large headform of the DOT, are 115, 132 and 158 J, respectively. The single impact approaches the M2000 first impact levels and actually exceeds it for the large size headform.The impact sites of the ECE standard are predefined on the front, side, top and rear of the helmet.

The main difference between the ECE standard and the Snell and DOT standards is the way in which the headform is supported during a drop test. In both the DOT and the Snell drop test, the headform's rotational motion is suppressed during the test. The headform is only allowed to move in the impact direction, whereas, in the ECE drop test, the motion of the headform and helmet are not suppressed in any way, allowing for movement in all six degrees of freedom during the impact. In the latter case, the guidance system for the headform and helmet releases upon impact, so it does not contribute to the load on the helmet.

Conditioning

All three standards apply similar sorts of conditioning to the helmet before performing the drop tests. The conditioning is always preceded by a treatment with a solvent mixture, to simulate wear and use of the helmet. Then there are four kinds of conditioning, to simulate different weather conditions: ambient, hot, cold and wet. The ECE standard requires a full series of drop tests with all four conditions to be tested on different helmets, whereas DOT and Snell leave the choice of conditioning to the tester. The tester chooses the conditions in which he thinks the helmet will perform the least well. If he decides to test also one of the other conditions, he may do so before the end of the testing protocol. These tests should then be performed on the same helmet, following the rest of the protocol.

Chin Bar

The majority of helmets sold in Europe are full-face helmets. Full-face helmets are equipped with a chin bar, also called a chin guard, that protects the head against chin impact. The Snell and ECE standards specify a test for chin impact, if the helmet is equipped with such a chin bar. The ECE standard uses a standard drop test with impact at the chin at a velocity of 5.5 m/s on the flat anvil, whereas the Snell standard uses a different approach. The Snell standard allows for a maximum deflection of 60 mm, when a mass of 5 kg is dropped vertically onto the chin bar at a velocity of 3.5 m/s. If this deflection is exceeded, the helmet is rejected. The ECE standard requires the maximum resultant acceleration not to exceed 275 g and a HIC below 2400. If one of these thresholds is exceeded in the chin bar test, the helmet is not rejected, but a warning sign must be applied to the helmet to inform the user that the helmet does not protect the chin from impact.

Discussion

The above standards measure and calculate only translational accelerations. Rotational effects should also be taken into consideration in a new helmet standard, because rotational acceleration is believed to be the most important cause for severe head injury: SDH and shearing injury [Gennarelli, 1981; Ommaya, 1988]. However, rotational movements are suppressed by the guidance system of the DOT and the Snell standard. In this case, the rotational kinetic energy which would have been released when the headform was not supported, is now absorbed by the helmet and the restraint system. The ECE standard allows for rotational movements, because the headform and helmet are not supported upon impact, however these movements are not measured. In real accidents, the movement of the head is neither completely suppressed nor completely free, since it is limited by the neck which connects the head to the torso. In other words, the torso is neither massless (ECE) nor of infinite mass (DOT and Snell), with respect to rotational motion.

Full-face helmets offer better protection for the face and chin area than open-face helmets. Thus, any chin bar, meeting or not meeting the drop test requirements, is probably better than none at all. Therefore, the ECE standard does not reject the helmet if the requirements are not met, since this may encourage the helmet designer to remove the chin bar in a next design of the helmet. That helmet may then pass the test, but it will offer less protection.

A.3.2   Resistance to Penetration Tests

Penetration is an infrequent cause of injury. Therefore, the ECE does not require a test for penetration anymore. It was dropped when the 04 series of amendments became effective. The penetration tests described in the DOT and the Snell standards are virtually identical. The headform is fixed to the ground and a metal punch, with a conical tip, of mass 3 kg is dropped onto the helmeted headform from a height of 3 m (impact energy is 88.3 J). If the metal punch touches the headform during the impact, the helmet is rejected. Even though injuries as a result of penetration are rare, a resistance to penetration test should remain included in the standard. Otherwise, helmets manufacturers will reduce priority with respect to this particular quality and injuries as a result of penetration may increase in frequency and severity.

A.3.3   Retention System Tests

All three standards require a test for the retention system's ability to withstand external loads. The DOT standard applies a static load on a headform of 250 lbs (1.11 kN), whereas the ECE and the Snell standards apply a dynamic load using a mass, dropped from a certain height (10 kg from 0.75 m and 6 kg from 0.6 m, respectively). The retention system must withstand the load and not increase in length by more than 30 mm.

The Snell and ECE standard also require a positional stability test, also called a roll-off test. This test tries to pull the helmet of the headform, without opening the retention system (Figure A.1) by applying a dynamic load by means of a drop mass (ECE: 10 kg from 0.5 m; Snell: 5 kg from 0.6 m). To pass the test, the helmet should remain on the headform.

The ECE standard also includes additional tests for micro-slip, resistance to abrasion, inadvertent release, ease of release and durability. With respect to the retention system it can be concluded that the ECE standard is the most stringent standard of the three.

A.3.4   Visor Tests

The test for peripheral vision is virtually the same for all three standards. The field of view must at least be $210°$. The ECE standard also has a requirement on transmittance of light. If the transmittance is below 80%, the helmet should be marked 'for daytime use only'. If it is below 50%, the helmet should

be rejected. After an extensive abrasive treatment, the transmittance should still be above 20% as a measure for resistance to wear and (mis)use.

The Snell and ECE standard also require a resistance to penetration test for the visor. For the ECE standard this test is similar to the helmet resistance to penetration tests of the other standards (Section A.3.2). For the Snell standard, a projectile of 1 gram, with a diameter of 5.5 mm, is fired at the visor at a velocity of 500 km/h . The helmet is rejected when the projectile shatters the visor or penetrates to the interior of the helmet.

A.3.5   Other Tests

The most important additional test is included in the ECE standard. It is a test for projections and friction, which is based on the BS 6658 standard. The rotation-inducing forces caused by projections on the helmet and friction against the outer surface of the helmet which occur in an accident when the motorcyclists falls and slides over a (rough) surface are simulated in a drop test. It is intended to test whether projections shear off easily and whether friction is low. In this test a helmeted headform (size small) is dropped onto two different, inclined anvils at a velocity of 8.5 m/s. The bar anvil consists of a series of at least five horizontal bars, 6 mm high and 40 mm apart. The abrasive anvil is a sheet of abrasive paper. The drop test is of the same principle as the impact tests of the ECE standard. During the test, anvil forces are measured. For the bar anvil and the abrasive anvil, these shall not exceed 2.5 kN and 3.5 kN, respectively, nor shall the integral with respect to time over the duration of the impact exceed 12.5 Ns and 25 Ns, respectively. This integral indicates a change in impulse. Since the mass of the headform and helmet (about 6.1 kg) does not change during impact, the change in impulse is actually a change in velocity (ΔV). In other words, ΔV should not exceed 2.0 m/s for the bar anvil and ± 4.1 m/s for the abrasive anvil.

The Snell standard includes an additional test for removability. A technician must be able to remove a properly adjusted helmet on a headform within 30 s, using common hand tools, without accessing any of the helmet's retention mechanisms. The helmet removability test determines whether the helmet can be removed from an unconscious victim without using the retention system which may be rendered non-functional by the impact.
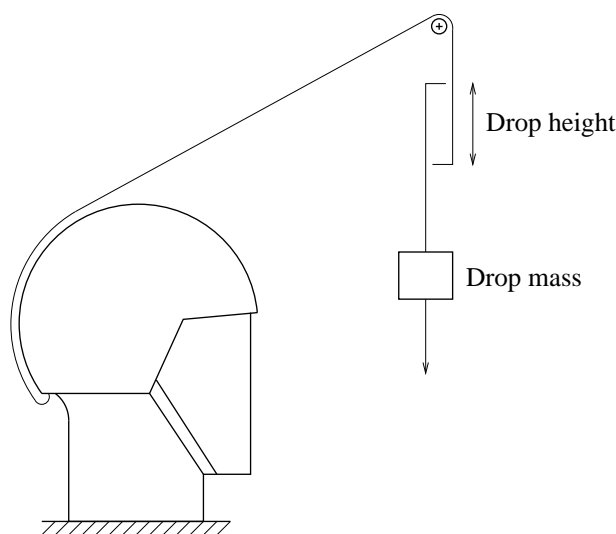

Figure A.1: Positional stability test.

A.4   The ECE Standard Drop Test

To improve the current test methodology of motorcycle helmets, it is sensible to study the existing standards and try to improve them, rather than formulate a new standard from scratch. This research is restricted to the shock-absorption test of the ECE R22-04 standard. The ECE standard is chosen as research object for two reasons. Firstly, because it is the de-facto European standard. And secondly, because it is one of the few standards in which the headform, in the shock-absorption test, is not supported in any way during impact. In most standards, the headform is supported in such a way that only translations in one direction are permitted. Therefore, these standards are not suitable to study rotational motion during impact.

The R.22 requires four types of conditioning: ambient, wet, cold and hot. In this research, no conditioning is applied. This means that all tests were performed at room temperature at normal humidity. These conditions are comparable to the ambient conditioning.

A drop tower was built to meet the requirements of the R.22. In this experimental setup, a helmeted headform is dropped, guided by a cart, onto an anvil with a velocity of 7.5 m/s. The anvil is mounted on a rigid, vibration-free floor to prevent external vibrations from influencing the measurements. Resultant headform accelerations are measured at the headform's centre of gravity using a triaxial accelerometer. The standard requires the resultant headform acceleration not to exceed 275 g (g = 9.81 m/s^2) and the Head Injury Criterion not to exceed 2400.

Headform accelerations alone give insufficient information on the protective capacities of helmets. Therefore, the experimental setup is extended with three angular rate sensors, a triaxial force transducer and a bi-plane high-speed X-ray setup.

The three angular rate sensors are mounted at the headform's centre of gravity to measure the rotational velocity ω of the headform. The axes of these sensors coincide with the three axes of the triaxial accelerometer. The rotational velocity is filtered with a CFC1000 filter. Differentiation of the rotational velocity yields the rotational acceleration α. The triaxial force transducer is mounted below the anvil, to measure anvil reaction forces in three perpendicular directions. Deformations of the helmet and headform can be measured using the X-ray setup. The experimental setup is discussed in more detail in Chapter 3. With these additional measurements, more insight is gained into the dynamic behaviour of the headform and helmet during impact.

A.5   Discussion

Over the years, helmet standards have evolved to be an effective means to assure helmet quality. In general, helmet testing standards are the result of experience, more than research. As helmet quality improved, helmet standards were raised and extended with new tests. Except for the shock absorption tests, helmets rarely fail a test. This does not mean that the remaining tests are useless. If they would be dropped from the standard, helmet manufacturers may take the opportunity to change the helmet design to cut the costs, which may make the helmets less safe.

The Snell standards are known as the worlds toughest standards, but the ECE standard is closing in and in some cases already exceeds the Snell standard. This is expressed not only in the severity of the criteria, but also in the diversity of the tests. Furthermore, only the ECE standard requires an assessment against HIC, which is a time dependent criterion and widely accepted as the best injury criterion currently available. However, HIC is based on translational accelerations only. None of the standards has implemented a test to evaluate the helmet's ability to reduce injury as a result of rotational motion. The standards measure and calculate only the translational accelerations in the impact tests and also in the projections and friction test of the ECE standard. Rotational effects should also be taken into consideration in a new helmet standard, because rotational acceleration is believed to be the most important cause for severe head injury: SDH and shearing injury [Gennarelli, 1981; Ommaya, 1988].

As knowledge about head injury increases, standards are improved. However, the process of improving is slow. The main reason for this is the globalization of the industry. There are many advantages in building a helmet according to one global standard over building a helmet that has to comply with many national standards. However, the larger the area for which the standard applies, the more the affiliated countries have to compromise, which hampers the development of the standards.

The HIC is a nice example of the slow process of the development of helmet testing standards. The HIC was developed in 1971, however it was introduced in the ECE standard only in 1995. Even then the threshold for the certification of the helmet was set to the current value of 2400, whereas a value of 1000 is specified for the HIC as concussion tolerance level for concussion in frontal (contact) impact. Still, the ECE standard is the only standard which incorporates the HIC. In Chapter 1 several injury criteria are discussed. Even though some of these criteria seem promising, it will take some time before any of those will be introduced in helmet testing standards. Firstly, because the validation of these criteria is difficult. And secondly, because international standards are required to ease the increasing international trade. And because of the participation of many countries, the modification of these standards is a slow political process.

Appendix B

Head Injury Criteria

Injury criteria can roughly be divided into three categories: Injury criteria based on translational accelerations of the head's centre of gravity (Section B.1); injury criteria based on translational and rotational accelerations of the head's centre of gravity (Section B.2); and injury criteria based on stresses and strains inside the brain (Section B.3).

B.1 Translational Acceleration Based Injury Criteria

B.1.1 Wayne State Tolerance Curve

The *Wayne State Tolerance Curve* (WSTC) is considered to be the foundation of research on human head injury criteria. This curve evolved from the work of Lissner *et al.* [1960]; Gurdjian [1953]; Gurdjian *et al.* [1961] and Patrick *et al.* [1965], and gives tolerable average acceleration magnitude in A-P direction (Anterior-Posterior) as a function of the acceleration duration. It still is the basis for most currently accepted injury criteria. The curve is given in Figure B.1. Slight cerebral concussion without any permanent effects was considered to be within human tolerance. Only translational accelerations were used in the development of the curve which was obtained from different experiments with post mortem human subjects (area I in Figure B.1), with linear skull fracture as injury criterion (assumed to be highly associated with brain concussion); from experiments with animals (area II in Figure B.1), where intracranial pressure was measured and compared; and from experiments with volunteers (area III in Figure B.1), with loss of consciousness as injury criterion. Except for long duration accelerations (> 20 ms), the WST-curve has never been validated for living human beings.
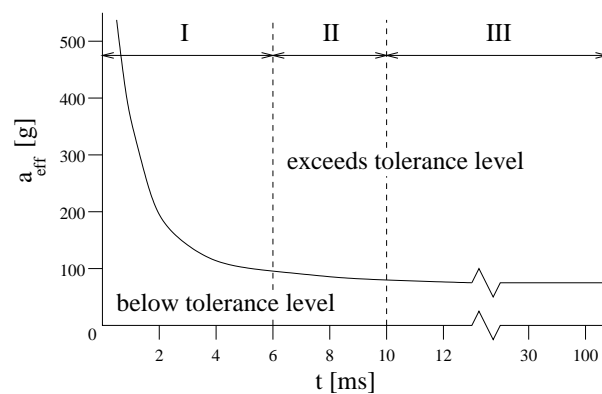
Figure B.1: Wayne State Tolerance Curve [Lissner *et al.*, 1960].

The main drawback of the WSTC is that it is based on measurements from different test types, with different types of test subjects, in which different types of injuries were assessed.

B.1.2 Severity Index

Gadd [1966] argued that neither the average acceleration nor the peak acceleration observed in an impact are sufficient to determine, accurately, the response of the head to an impact. According to Gadd, the resulting injury potential is highly dependent upon the acceleration pulse and therefore pulses with the same average acceleration but different shapes can have very different effects. To account for both the acceleration pulse shape and its duration, he suggested integrating the acceleration signal over its entire duration. Gadd further maintained that injury potential was a non-linear function of acceleration magnitude. Therefore, he suggested that an exponential weighting factor (greater than 1) be applied to the acceleration and that the result be integrated over the duration of the acceleration. This led to the following injury criterion, called the Severity Index:

$$(G)SI = \int_0^T a(t)^{2.5} dt \qquad (a(t) \text{ in g's}) \tag{B.1}$$

The weighting factor 2.5 only applies to the head and is primarily based on a straight-line approximation of the WSTC plotted on log-log paper between 2.5 and 50 ms. Gadd [1966] proposed a threshold (tolerance level) for concussion for frontal impact of 1000, which agreed with the WST-curve, the Eiband tolerance curve [Eiband, 1959] and accident simulation data by Swearingen [1965]. Gadd [1971] later suggested a threshold of 1500 for non-contact loads on the head. The (G)SI has received significant scientific criticism, because it deviates considerably from the WST-curve [e.g.: Slattenschek & Tauffkirchen, 1970].

The WST-curve was based on average acceleration. According to Versace [1971], a mathematical approximation of this curve should also be a function of the average acceleration. Therefore, he suggested the following injury criterion:

$$(V)SI = \left[\frac{\int_0^T a(t) dt}{T} \right]^{2.5} T \tag{B.2}$$

B.1.3 Head Injury Criterion, HIC

Based on Versace's criticism on the (G)SI, NHTSA [1972] suggested that the SI should be replaced with a slightly modified injury criterion, called the Head Injury Criterion (HIC):

$$HIC = \left\{ \left[\frac{\int_{t_1}^{t_2} a(t) dt}{t_2 - t_1} \right]^{2.5} (t_2 - t_1) \right\}_{\max} \tag{B.3}$$

with $a(t)$ the resultant head acceleration in g's (measured at the head's centre of gravity[1]) and t_1 and $t_2 [s]$ any two points in time, during any interval in the impact, that maximise HIC.

As for the SI, a value of 1000 is specified for the HIC as tolerance level for concussion in frontal (contact) impact. For practical reasons, the maximum time interval $(t_2 - t_1)$ which is considered to give appropriate HIC values was set to 36 ms [SAE, 1986]. This time interval greatly affects HIC calculation for long duration impacts such as airbag impacts (duration: ± 50 ms). Later [NHTSA, 2000], it has been further reduced to 15 ms in order to make the HIC also applicable to airbag impacts. HIC has been shown to be a reasonable discriminator between severe and less severe injury [Tarriere, 1981]. It also correlates with the risk of cranial fracture in cadavers after impact [Ran *et al.*, 1984]. However, HIC does not correlate well with injury severity for impact in various impact directions [Newman,

---

[1] $g = 9.81 \text{ m/s}^2$

1980]. An important limitation of the HIC is that head rotational acceleration is not taken into account although rotation is debated to be the primary cause for various types of traumatic brain injury, in particular acute subdural haematoma and diffuse brain injury [Adams *et al.*, 1983; Gennarelli *et al.*, 1987; Holbourn, 1945]. Despite its limitations, HIC is currently the most commonly used criterion for head injury in automotive research.

B.1.4   Maximum Resultant Head Acceleration

A head injury criterion which is often used because of its simplicity is the *maximum resultant head acceleration* (a_{max}). The thresholds for a_{max} depends on its application, because of the time dependent nature of the resultant acceleration with respect to head injury. To account for this time dependency, this criterion can be replaced/supplemented by a value for the resultant acceleration that should not be exceeded longer than a certain time interval.

B.2   Combined Rotational and Translational Acceleration Based Injury Criteria

The previously discussed injury criteria concern translational head impact response. However, the biomechanical response of the head during impact also includes rotational motion, which is believed to cause injury [e.g.: Adams *et al.*, 1983; Holbourn, 1945; Gennarelli *et al.*, 1987], in particular acute subdural haematoma and diffuse brain injury. A summary of various tolerances of the human brain to rotational acceleration (and rotational velocity) is given in table B.1 according to Prasad *et al.* [1985].

Table B.1: Human brain tolerance to rotational acceleration (and rotational velocity) concerning sagittal head motion.

injury	tolerance	type of research
cerebral concussion [Ommaya *et al.*, 1967]	50% probability: for t < 20 [ms]: $\ddot{\alpha}$=1800 [rad/s^2] for t $\geq$ 20 [ms]: $\dot{\alpha}$=30 [rad/s]	Extrapolated from animal experiments (speculative data)
bridging vein rupture [Löwenhielm, 1975]	$\ddot{\alpha}$=4500 [rad/s^2] and/or $\dot{\alpha}$=70 [rad/s]	Mathematical model in conjunction with experiments on bridging vein rupture
brain surface shearing [Advani *et al.*, 1982]	2000 < $\ddot{\alpha}$ < 3000 [rad/s^2]	Mathematical model
brain (general) [Ommaya, 1984]	$\dot{\alpha}$ <30 [rad/s]: safe: $\ddot{\alpha}$ <4500 [rad/s^2] AIS 5: $\ddot{\alpha}$ > 4500 [rad/s^2] $\dot{\alpha}$ >30 [rad/s]: AIS 2: $\ddot{\alpha}$ = 1700 [rad/s^2] AIS 3: $\ddot{\alpha}$ = 3000 [rad/s^2] AIS 4: $\ddot{\alpha}$ = 3900 [rad/s^2] AIS 6: $\ddot{\alpha}$ = 4500 [rad/s^2]	Review of experimental and mathematical studies

B.2.1   Generalized Acceleration Model for Brain Injury Threshold, GAMBIT

Newman [1986] attempted to combine translational and rotational head acceleration response into one injury criterion. Considering these accelerations as the cause for stresses generated in the brain and resulting in brain injury, he proposed the Generalized Acceleration Model for Brain Injury Threshold

(GAMBIT). The general GAMBIT equation is:

$$G(t) = \left[\left(\frac{a(t)}{a_c} \right)^n + \left(\frac{\ddot{\alpha}(t)}{\ddot{\alpha}_c} \right)^m \right]^{1/s} \tag{B.4}$$

with $a(t)$ and $\ddot{\alpha}(t)$ the instantaneous values of translational and rotational acceleration
       respectively;
       n, m and s empirical constants selected to fit available data; and
       a_c and $\ddot{\alpha}_c$ the critical values of the accelerations (tolerances).

On the assumption that the tolerances derived from experiments with only translational or only rotational head motion are also valid for combined head response, and on the assumption that translational and rotational acceleration equally contribute to head injury, Newman simplified this equation to become:

$$G = \frac{a_m}{250} + \frac{\ddot{\alpha}_m}{10000} \leq 1 \tag{B.5}$$

with a_m [g] and $\ddot{\alpha}_m$ [rad/s^2] the mean values of linear and angular acceleration respectively;
       250 g being the linear acceleration, corresponding to a 50% probability of AIS>3
       (g=9.81 [m/s^2]); and
       10,000 rad/s^2 being the angular acceleration, corresponding to a 50% probability
       of AIS>3, according to Newman.

The GAMBIT predicts injury when $G > 1$ and no injury when $G \leq 1$. However, the GAMBIT was never extensively validated as an injury criterion. For example, the maximum time interval for a_m and α_m have never been set.

B.2.2   Head Injury Power

Newman *et al.* [2000b] reasoned that the rate of change of translational and rotational kinetic energy, i.e. power, could be a viable biomechanical function for the assessment of head injury. An empirical expression for this *Head Impact Power* (HIP), relating a measure of power to head injury, would be of the form:

$$\text{HIP} = Aa_x \int a_x dt + Ba_y \int a_y dt + Ca_z \int a_z dt + \eta\alpha_x \int \alpha_x dt + \beta\alpha_y \int \alpha_y dt + \chi\alpha_z \int \alpha_z dt \tag{B.6}$$

Each term in this expression represents the change in kinetic energy for one degree of freedom. The coefficients A, B, C, η, β and χ denote the injury sensitivity for each of the six degrees of freedom of the head. The development of this function is described in Newman *et al.* [2000a]. The directional sensitivity of the human head is not known. Therefore, the coefficients of equation (B.6) are currently set to reflect mass and mass moments of inertia of the human head.

Newman *et al.* [2000a] validated the HIP, using experimental data from carefully analysed collisions of American Football players during the game. They reconstructed the kinematics of the head from TV-images and the injuries were classified by qualified physicians. A 50% probability of concussion at a maximum Head Impact Power (HIP$_\text{max}$) of 12.8 kW was found. The HIP$_\text{max}$ is not validated for more severe brain injuries, since such experimental data is not yet available. From their results, the authors concluded that HIP$_\text{max}$ better correlates with mild traumatic brain injury than HIC. The authors give three advantages of HIP$_\text{max}$ over HIC to backup this conclusion: Besides translational accelerations, HIP$_\text{max}$ can also incorporate directional sensitivity, sensitivity for rotational accelerations and sensitivity for angular and translational velocities.

B.3   Stress and Strain Based Injury Criteria

Brain injury is reported to correlate with stress, strain and strain rate [Lee & Haut, 1989; Viano & Lövsund, 1999]. However, strains and strain rates inside the brain (during impact) are difficult to

measure. Advancements in computational techniques have led to more accurate and more detailed numerical models of the human head. These models bring a detailed injury assessment closer to reality, since they enable stresses and strains to be examined. Bandak [1995, 1997] developed three measures representing the general types of brain injuries experienced in traffic accidents:

- Cumulative Strain Damage Measure;

- Dilatation Damage Measure;

- Relative Motion Damage Measure.

Stresses and strains used to compute the above injury parameters are calculated from Finite Element simulations, using a Finite Element model of the skull and intracranial contents.

B.3.1 Cumulative Strain Damage Measure

The Cumulative Strain Damage Measure (CSDM) was developed to evaluate the strain-related damage within the brain. This mechanical measure has been shown to be useful in the evaluation of deformation-related brain injuries resulting from head impact. The CSDM is based on the hypothesis that diffuse axonal injury (DAI) is associated with the cumulative volume fraction of the brain matter experiencing tensile strains over a critical level. At each time increment, the volume of all the elements that have experienced a principal strain above prescribed threshold values is calculated. The affected brain volume monotonically increases in time during conditions where the brain is undergoing tensile stretching deformations and remains constant (does not decrease) for all other conditions (i.e. compression, unloading, etc.). Bandak *et al.* [2001] found that a CSDM level 5 corresponds to mild DAI and a CSDM level of 22 corresponds to moderate DAI severity. Thus, 5 percent, respectively 22 percent, of the brain volume experienced strain in excess of 15%, the proposed critical level [Thibault *et al.*, 1990].

B.3.2 Dilatation Damage Measure

The second mechanical measure evaluates brain injury caused by large dilatational stresses. It is referred to as the Dilatation Damage Measure (DDM). Dilatation Damage Measure (DDM) monitors the cumulative volume fraction of the brain experiencing specified negative pressure levels. However, no direct observational evidence has been reported on the relationship between pressure mechanisms and the production of axonal, vascular or other soft tissue injury. Similar to the CSDM calculation, at each time step, the volume of all the elements experiencing a negative pressure level exceeding prescribed threshold values is calculated. Bandak *et al.* [2001] suggested a DDM value of 5 at a threshold level of -14.7 psi (-101 kPa, the vapor pressure of water) as an injury threshold, but also reported that further research was necessary.

B.3.3 Relative Motion Damage Measure

The third mechanical measure proposed is for the evaluation of injury related to brain movements relative to the interior surface of the cranium. It is referred to as the Relative Motion Damage Measure (RMDM). This measure monitors the tangential motion of the brain surface resulting from combined rotational and translational accelerations of the head. Such motions are a suspected cause of subdural haematomas associated with large-stretch ruptures of the parasagittal bridging veins. The rupture tolerance levels of bridging veins are a combined function of both strain and strain rate as reported by Löwenhielm [1974]. The RMDM does not require the explicit representation of the bridging veins but rather monitors the relative displacement of several node pairs. Each pair represents a bridging vein tethered between the skull and brain near the parasagittal sinus. The measure accounts for the large-stretch modes of rupture while leaving open the possibility of using other micro or macro rupture-modes associated with more complex vascular tethering states.

Appendix C

Moments of Inertia of the Headform

In this appendix, the method of deriving the moments of inertia of the head model are discussed. The principal moments of the inertia of the human head are of great diversity. This is caused not only by differences in size, but also by differences in height/width ratio. The values for the human head's principal moments of the inertia found in literature Chandler [1975] confirm this. As a result there is a wide spread in the orientation of the principal directions of the human head's moments of inertia. The orientations used for the scaling and neck adding are depicted in Figure C.1. These orientations are an estimate for the mean orientations found in literature.

The mean principal moments of inertia of the human head are shown in Table C.1. These values differ from the values found in Chandler [1975], because some orientations were switched to be closer to the orientations from Figure C.1.

The cubic root of the mean head volume is chosen as a reference characteristic length scale for the scaling. With the mean head volume $\bar{V}$ is 3785.2 ml, the reference characteristic length r_0 scale becomes $r_0 = ^3\sqrt{\bar{V}} = ^3\sqrt{3785.2 \cdot 10^3} = 155.8$ mm. The volume of the largest head V_{max} (circumference
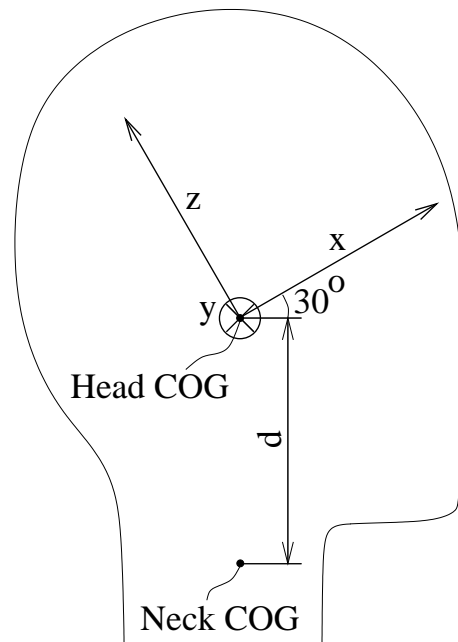
Figure C.1: Orientations of the principal directions of the moments of inertia.

Table C.1: Mean principal moments of inertia of the human head.

$\bar{I}_{xx}$ [kg·cm^2]	$\bar{I}_{yy}$ [kg·cm^2]	$\bar{I}_{zz}$ [kg·cm^2]
206.3	177.8	151.3

591 mm) in Chandler [1975] is used to determine the characteristic length scale for the head with circumference 600 mm. This length scale is $r = ^3\sqrt{V_{max}} = ^3\sqrt{4410 \cdot 10^3} = 164.0$ mm. The scaling factor λ is defined as: $\lambda = \frac{r_0}{r} = \frac{164.0}{155.8} = 1.05$. The mass of the is assumed to be proportional to the characteristic length scale to the power of three. The mass of the head with circumference 600 mm thus becomes: $m = \lambda^3 \bar{m} = 1.05^3 \cdot 3785.2 = 4.4$ kg, with $\bar{m}$ the mean mass of the human head. The mass of the neck m_{neck} is the total head mass from the ECE regulations m_{tot} minus the scaled head mass m: $m_{neck} = m_{tot} - m = 5.6 - 4.4 = 1.2$ kg.

The principal moments of inertia are proportional to the square of the characteristic length. The moments of inertia of the neck around its centre of gravity (COG) are assumed negligible. The moments of inertia of the neck around the head COG is computed by multiplying the neck mass m_{neck} with the square of the distance d from the neck COG to the appropriate axis through the head COG. The shifting of the position of the total COG as a result of the adding of the neck will have effect on the moment of inertia. This effect is assumed negligible.

The total principal moments of inertia are computed as follows:

$$I_{xx} = \bar{I}_{xx}\lambda^2 + m_{neck}[d\cos(30°)]^2 = 206.3 \cdot 1.05^2 + 1.2 \cdot (10 \cdot \tfrac{1}{2}\sqrt{3})^2 = 317$$
$$I_{yy} = \bar{I}_{yy}\lambda^2 + m_{neck}d^2 = 177.8 \cdot 1.05^2 + 1.2 \cdot 10^2 = 316 \qquad (\text{C.1})$$
$$I_{zz} = \bar{I}_{zz}\lambda^2 + m_{neck}[d\sin(30°)]^2 = 151.3 \cdot 1.05^2 + 1.2 \cdot (10 \cdot \tfrac{1}{2})^2 = 197$$

Appendix D

Repeatability

In the following figures, the results from the helmeted head drop tests are depicted: resultant acceleration, resultant rotational velocity, rotational velocity around the y-axis (the main axis of rotation), resultant rotational acceleration and HIP. Each result is compared to the result of a different drop test with the same configuration. Each configuration is shown in the title bar of each figure. Site F = Front, R = Rear and T = Top impact. Head F = Flexible headform and R = Rigid, conventional headform. Helmet L = Size L and M = Size M. For example in Figure 1 in the upper left corner, there is no graph, since only one drop test was performed for this configuration (Front impact, Flexible headform, Helmet size L). In the upper right corner, there are three graphs. For this configuration, three drop tests were performed, so three comparisons can be made (1 vs. 2, 2 vs. 3 and 3 vs. 1). For the other two configurations, two drop tests were performed, meaning only one comparison can be made. If all results were 100% repeatable, than all graphs would be straight lines with slope equal to 1. For the ease of things, the line with slope 1 is also displayed. For each graph was fitted with a first order polynomial. The first coefficient (rc in the figures) should be equal to 1 in case of 100% repeatability and the correlation coefficient (R^2 in the figures) should also be equal to 1.

There are a few things which can be concluded from these figures:

- Resultant translational accelerations show best repeatability in Top impact (around 5% deviation, $R^2 > 0,96$). Rotational velocities for Top impact show very little repeatability and a poor correlation. This is not strange, since rotational velocities in Top impact are small. Minor deviations have large influences on both the slope of the graph and the correlation coefficient.

- For Rear and Front impact, where there's more rotation involved, the correlation for the resultant rotational velocity is much better: $R^2 > 0.90$. However, deviations are larger than for the resultant translational acceleration (around 15-20%). This means that The general rotational motion shows the same time trends for all drop tests, but amplitudes may differ. For the resultant rotational acceleration, results are worse, since these signals were obtained by differentiation of the resultant rotational velocity, which amplifies small deviations rapidly.

- HIP also shows nice repeatability, not only for Top impact, but also for Rear and Front impact. However, the results for Top impact are better than those for Rear and Front impact.

- In general, the repeatability of the drop tests with the size M helmet is less and the correlation is worse than for the drop tests with the size L helmet. This conclusion should be drawn with caution, since the sample size is small. Furthermore, it only holds for the drop tests with the conventional headform, since no repeatability data is available for the drop tests with the size L helmet using the flexible headform.

- For the same reason, headform repeatability can only be determined for the drop tests with the size M helmet. The drop test using the flexible headform are generally a bit more dynamic, whereas the drop tests using the rigid headform are more often burdened by outliers.
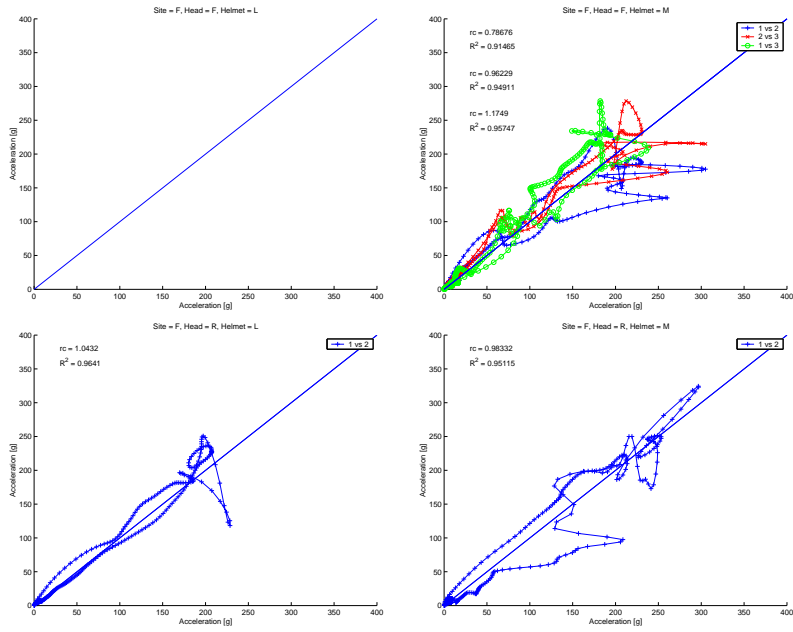
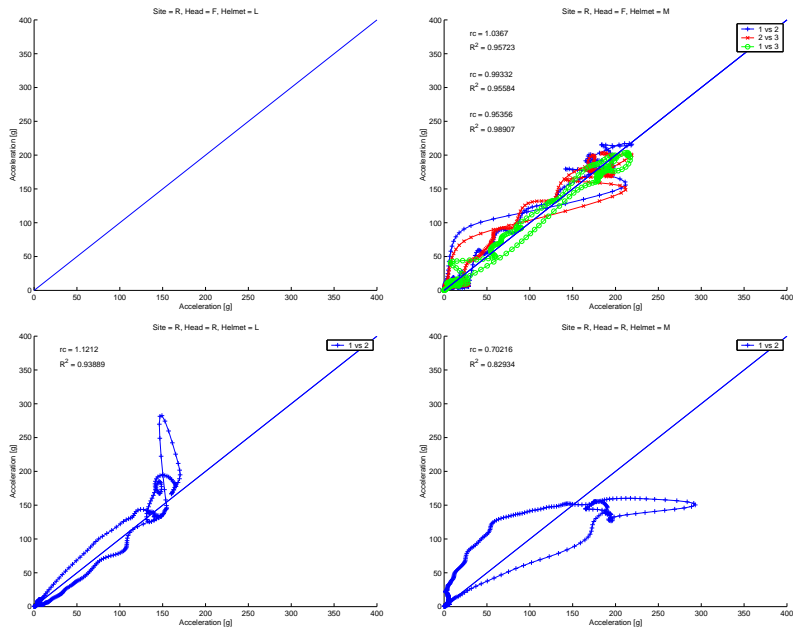Figure D.1: Resultant acceleration, Front impact.

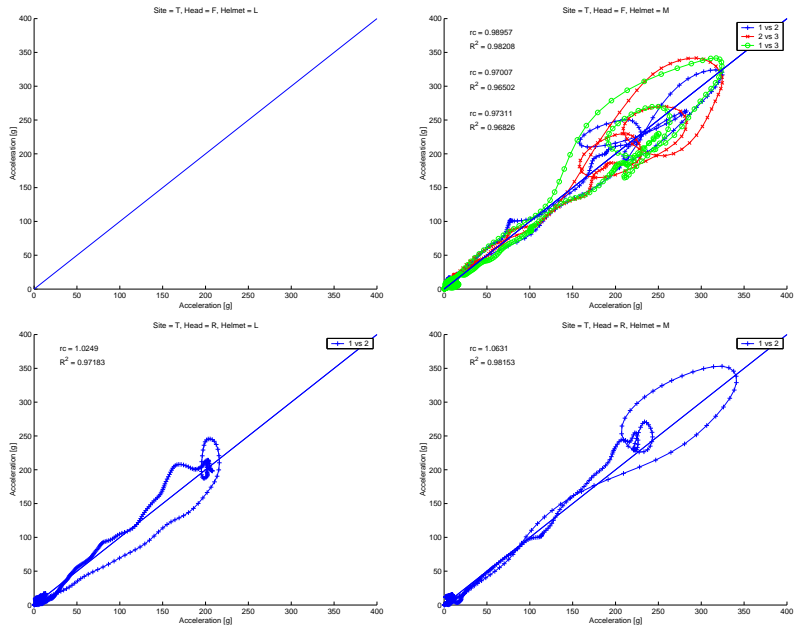Figure D.2: Resultant acceleration, Rear impact
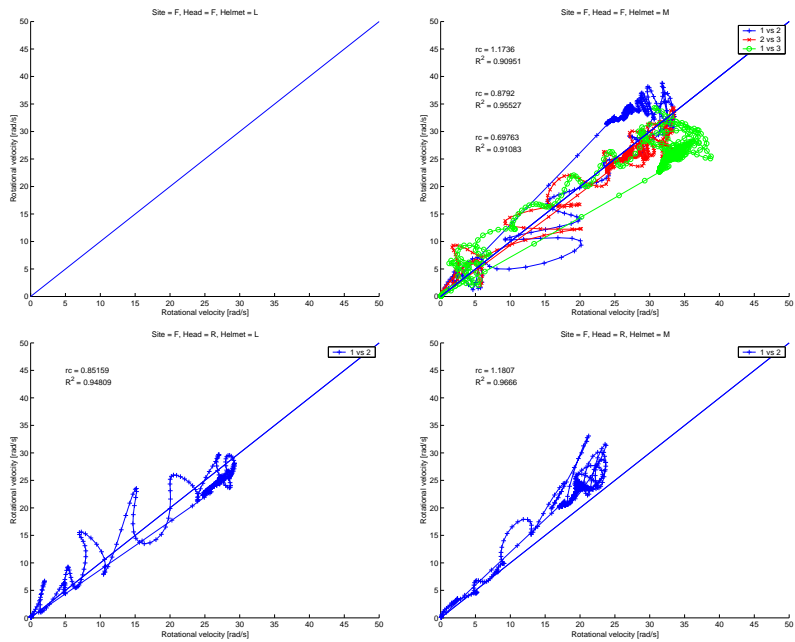
Figure D.3: Resultant acceleration, Top impact
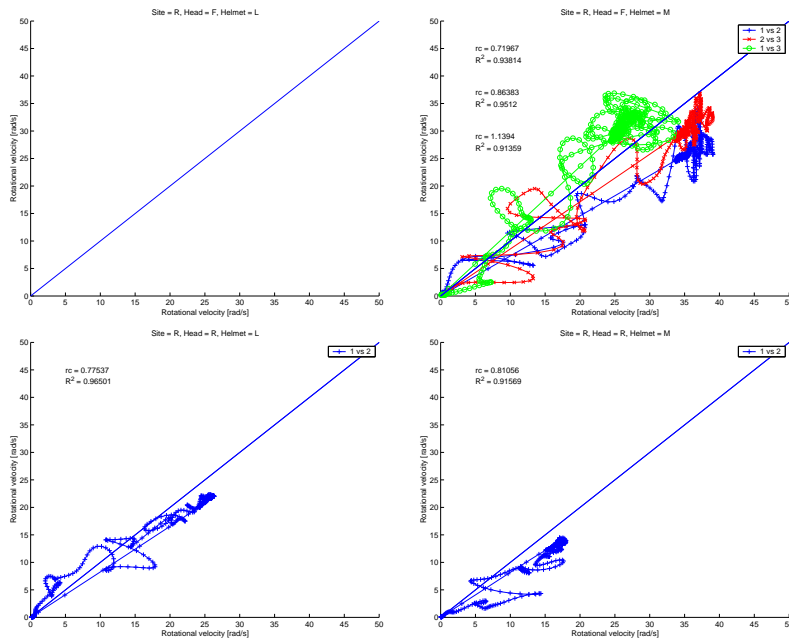

Figure D.4: Resultant angular velocity, Front impact

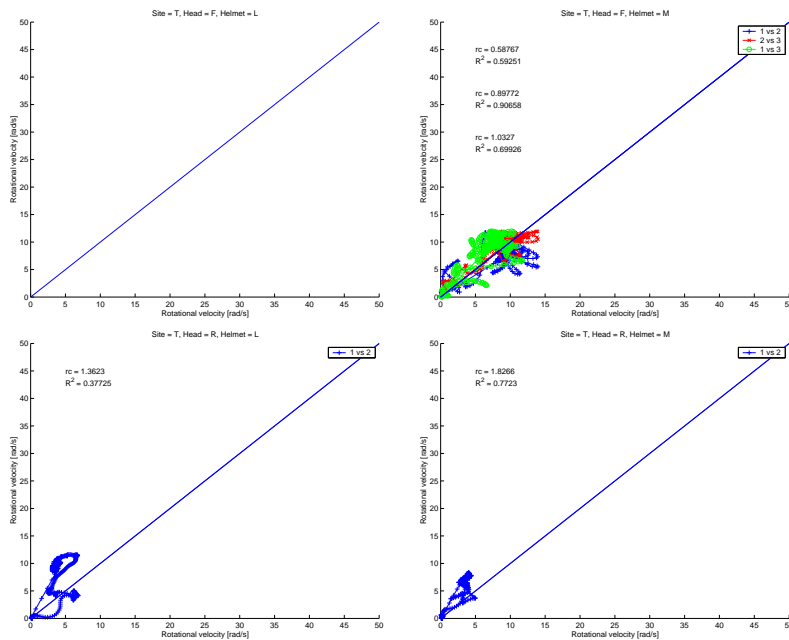Figure D.5: Resultant angular velocity, Rear impact

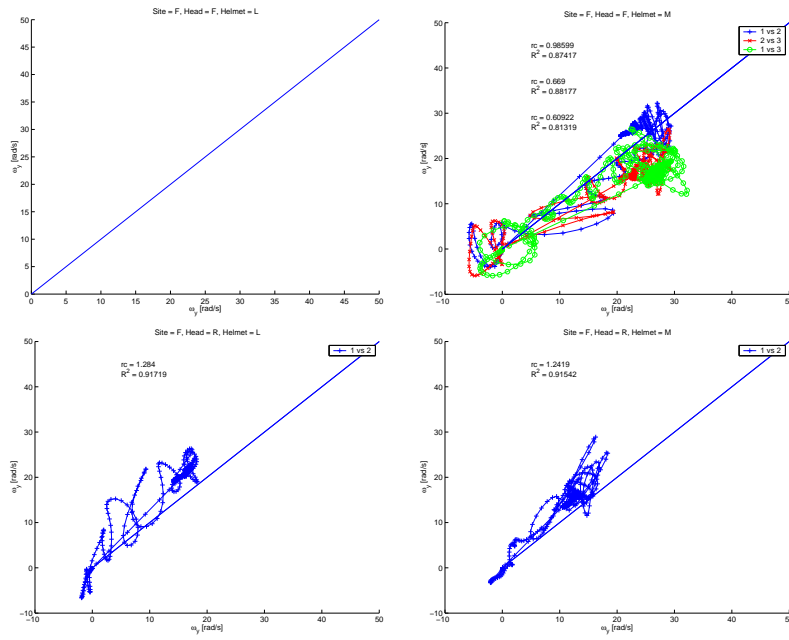Figure D.6: Resultant angular velocity, Top impact
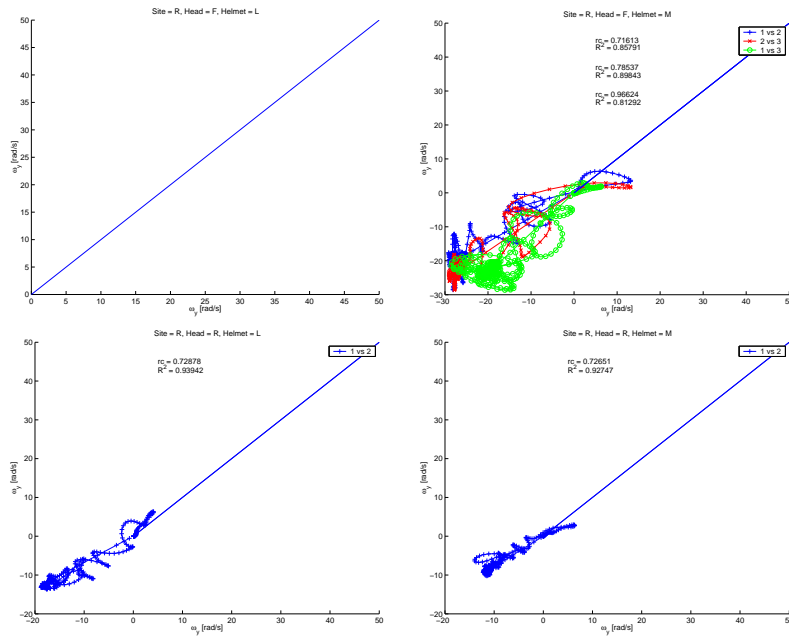
Figure D.7: ω_y, Front impact

Figure D.8: ω_y, Front impact
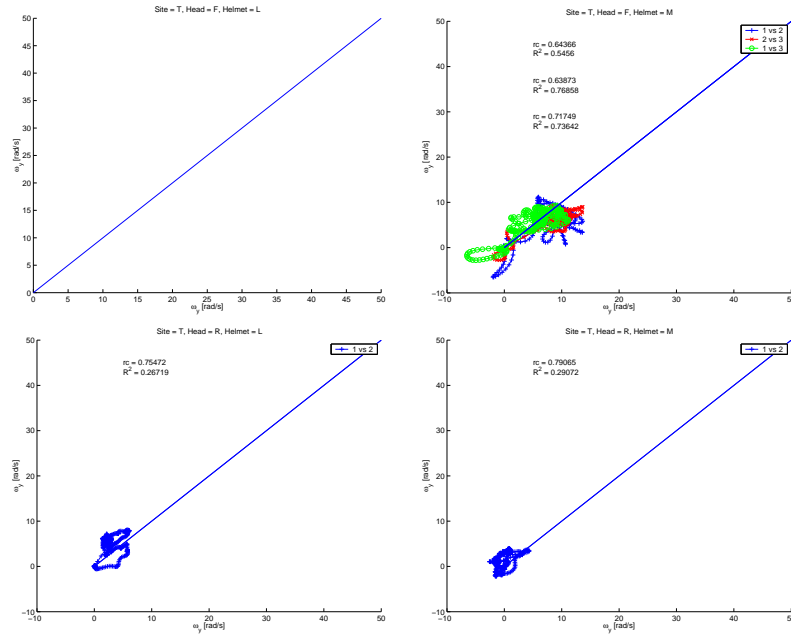
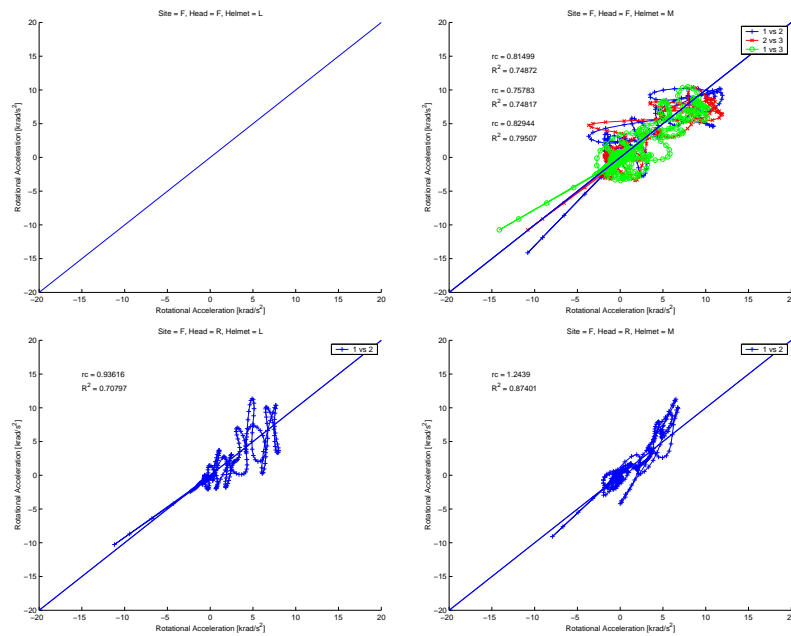Figure D.9: ω_y, Front impact

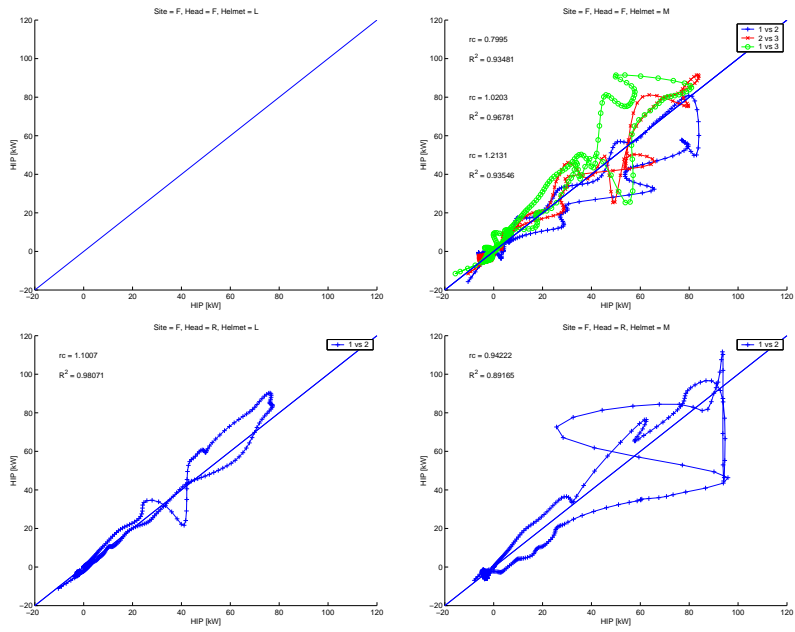

Figure D.10: Resultant rotational acceleration, Front impact
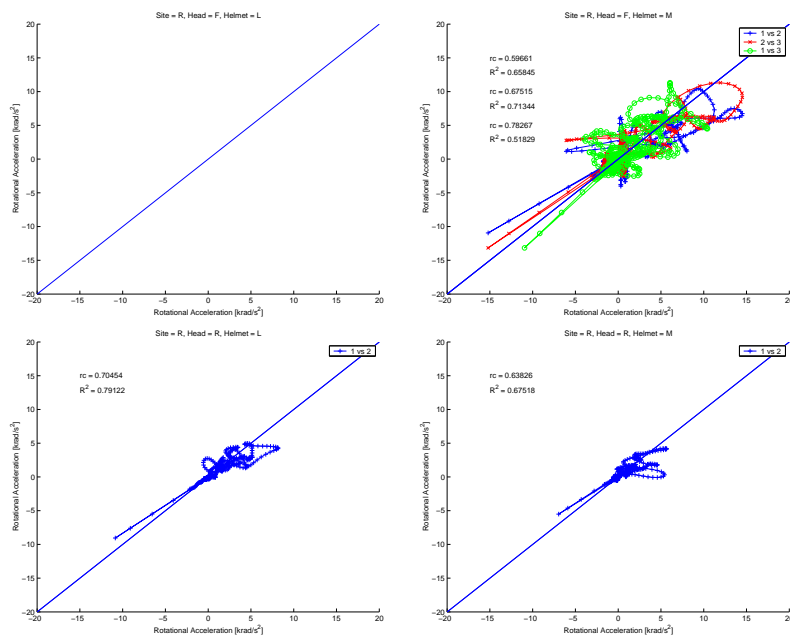
Figure D.11: Resultant rotational acceleration, Rear impact
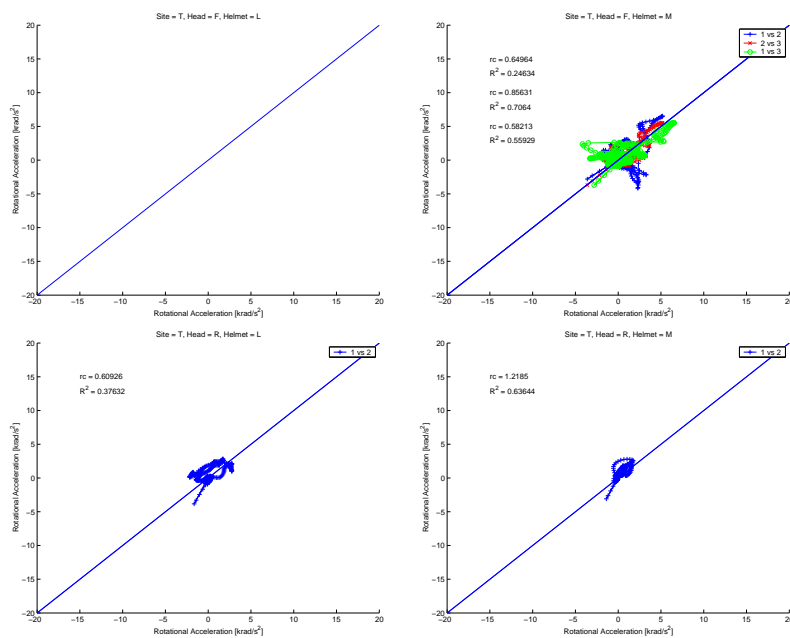
Figure D.12: Resultant rotational acceleration, Top impact

Figure D.13: HIP, Front impact
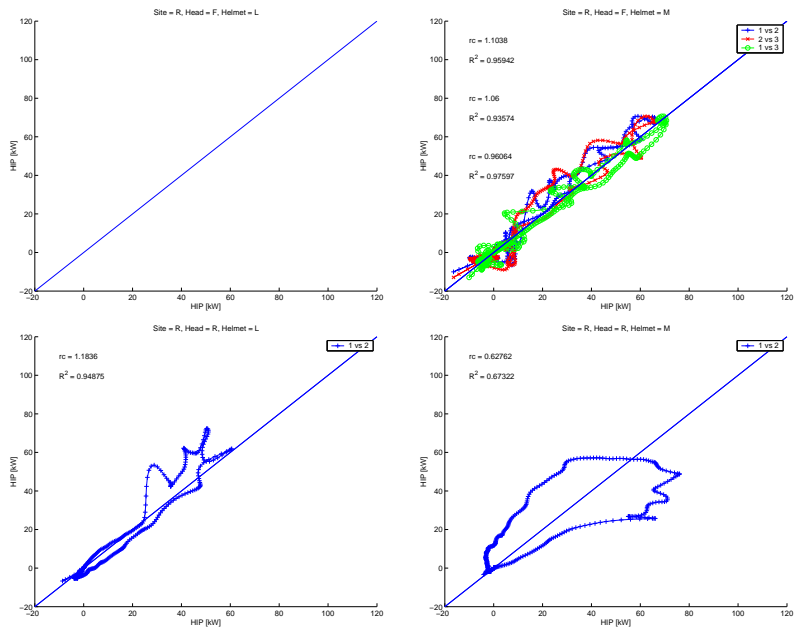
Figure D.14: HIP, Rear impact
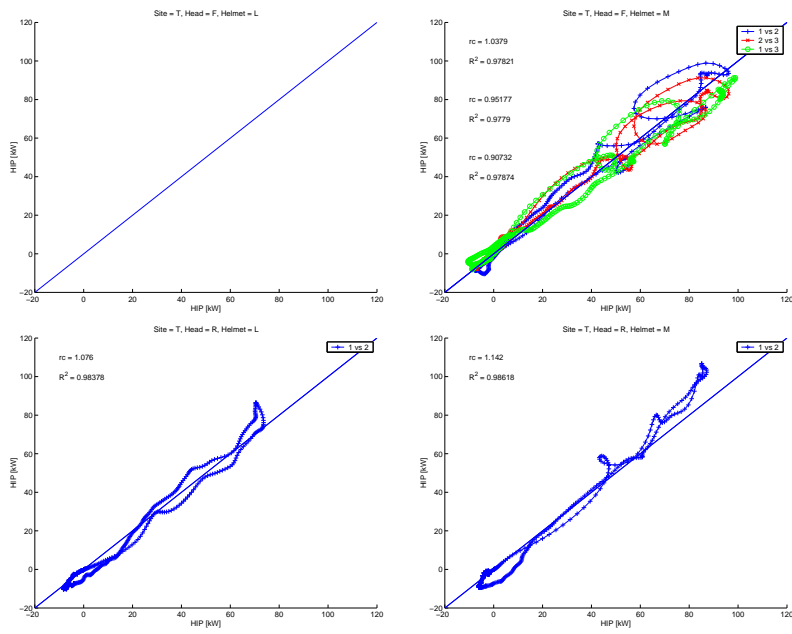
Figure D.15: HIP, Top impact

Appendix E

X-Ray Data

E.1   Conventional Headform

Figure E.1 shows the marker tracks of the drop tests using the conventional headform. During one Rear impact drop test with the Size M helmet, the camera's were triggered too early and thus did not record the actual impact.

In Figure E.2, the mean marker positions are depicted along with the direction of the first mode eigenvector obtained from the Principal Component Analysis. The lengths of the eigenvectors are normalised to unit length and multiplied by 200 for visibility.

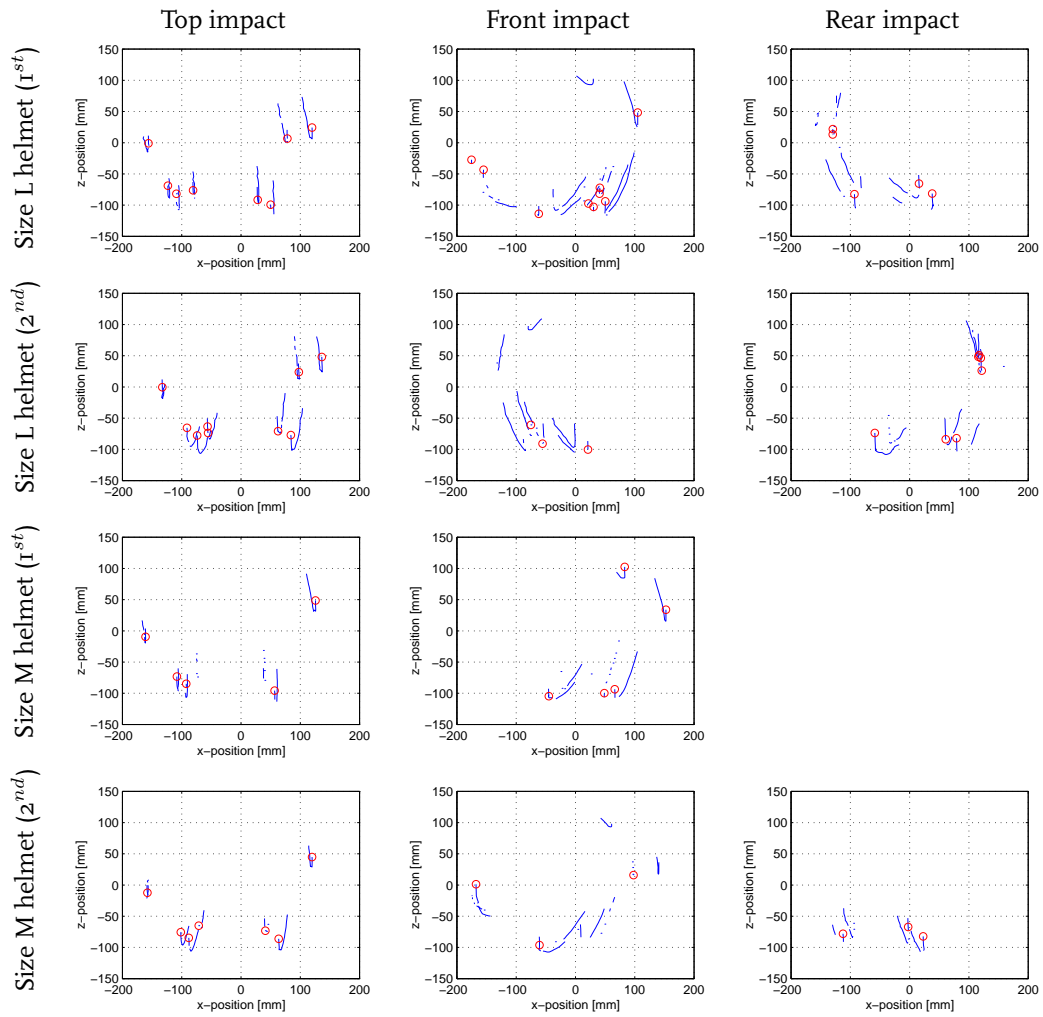The results from the second mode are shown in Figure E.3.

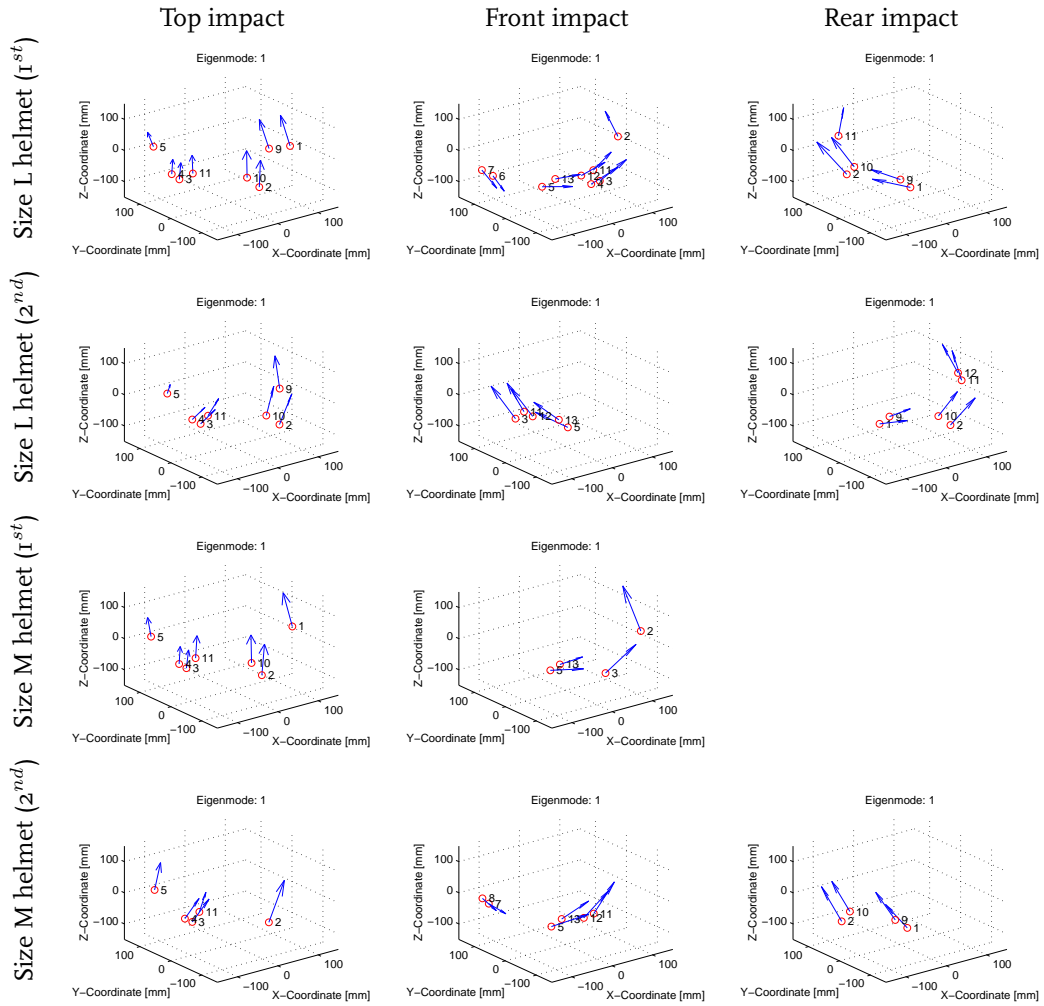Figure E.1: Marker tracks of the drop tests using the conventional headform.

Figure E.2: Mean marker positions (○) and first mode shape vectors (↗) for the drop tests using the conventional headform.
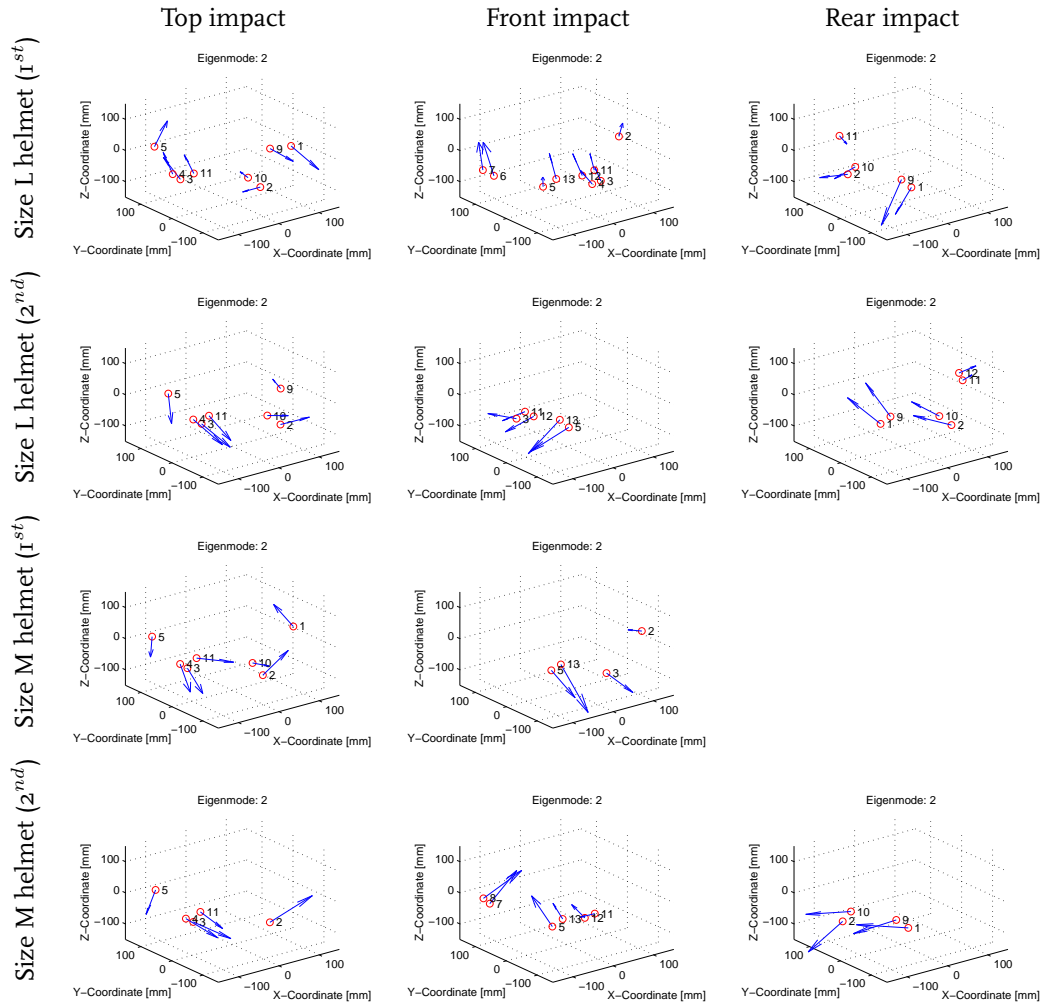
Figure E.3: Mean marker positions (○) and second mode shape vectors (↗) for the drop tests using the conventional headform.

E.2 Flexible Headform

Figure E.4 shows the marker tracks of the drop tests using the flexible headform.

In Figure E.5 and E.6, the mean marker positions are depicted along with the direction of the first and second eigenvector, respectively, obtained from the Principal Component Analysis.
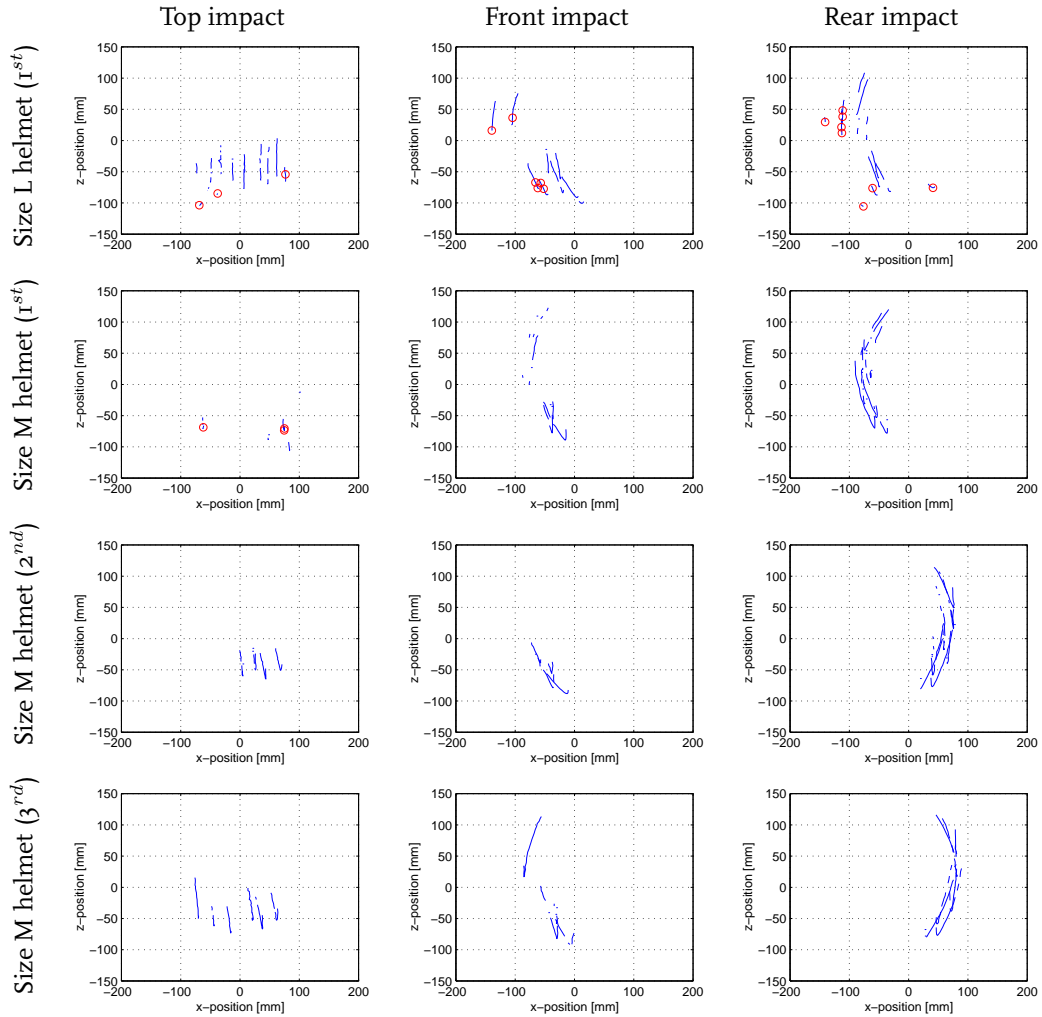

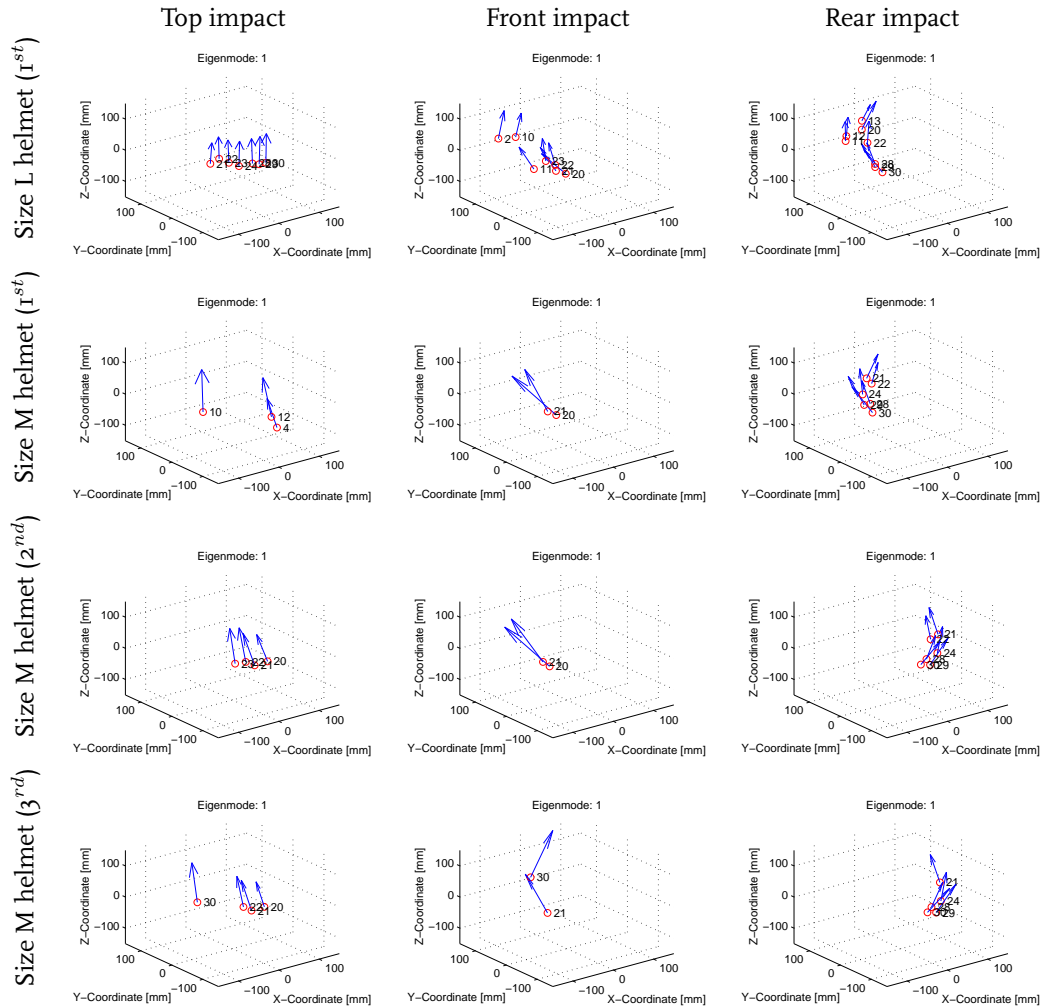Figure E.4: Marker tracks of the drop tests using the flexible headform.

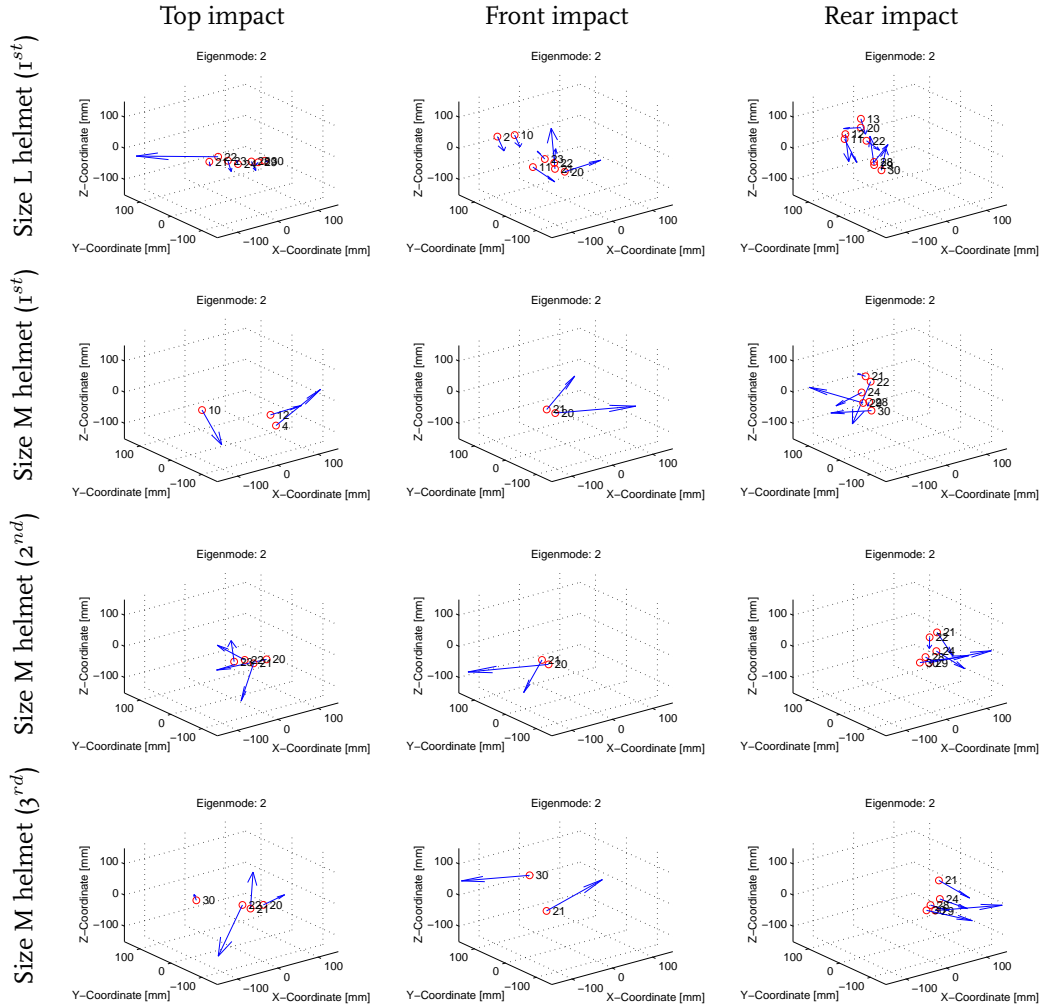Figure E.5: Mean marker positions (○) and first mode shape vectors (↗) for the drop tests using the flexible headform.

Figure E.6: Mean marker positions (∘) and second mode shape vectors (↗) for the drop tests using the flexible headform.

Samenvatting

Tijdens een motorongeval staat het menselijk hoofd bloot aan belastingen die de grenzen van de natuurlijke bescherming ver overschrijden. Jaarlijks sterven in Europa circa vijfduizend motorrijders aan de gevolgen van een motorongeval. Dit betreft 9% van alle verkeersdoden. Het dragen van een helm verlaagt de kans op een fatale afloop tijdens een motorongeluk met ongeveer 50%. In de laatste decennia zijn standaarden voor het testen van motorhelmen uitgegroeid tot een effectieve manier om de helmkwaliteit tot een bepaalde hoogte te garanderen. Over het algemeen zijn de valproeven in deze standaarden meer het resultaat van pragmatische compromissen van diverse partijen, dan van wetenschappelijk onderzoek. De laatste jaren is de kwaliteit van helmen verbeterd, waardoor de criteria van deze valproeven verder zijn aangescherpt en de belastingniveaus zijn verhoogd.

De focus van dit onderzoek ligt op de valproeven van ECE Regulation 22 (ECE-R.22). In deze proeven wordt de kwaliteit van de helm bepaald, door de versnelling van een kunsthoofd te meten tijdens de inslag. De kwaliteit wordt uitgedrukt in de letselparameters: *maximum resulterende translationele versnelling* ($a_{\max}$) van het zwaartepunt van het kunsthoofd en *Head Injury Criterion* (HIC). De HIC is voor hoofdletsel het meest toegepaste en meest geaccepteerde letselcriterium. Echter, in standaard testen voor motorhelmen is de ECE-R.22 nog steeds de enige norm, waarin de HIC wordt toegepast. Het kunsthoofd dat wordt gebruikt in de valproeven van de ECE-R.22 is gemaakt van aluminium en wordt beschouwd als een star lichaam.

De valproeven van de ECE-R.22 hebben twee tekortkomingen met betrekking tot het bepalen van de kwaliteit van de helm. Ten eerste worden de eigenschappen van het menselijk hoofd tijdens de valproeven niet goed gerepresenteerd door het starre kunsthoofd. In dit kunsthoofd is de flexibiliteit van de menselijke hersenen en schedel niet vertegenwoordigd, waardoor de interactie tussen hoofd en helm mogelijk niet goed is gemodelleerd. Ten tweede hebben diverse onderzoeken op het gebied van de letselbiomechanica geleid tot diverse andere, mogelijk betere, letselcriteria welke momenteel niet (kunnen) worden gemeten tijdens de valproeven.

Tot op heden is er weinig onderzoek gedaan naar de manier waarop helmontwerp kan wijzigen wanneer deze letselcriteria worden toegepast in de huidige standaarden voor het testen van motorhelmen. Dit proefschrift draait met name om de volgende vraag:
Hoe zal het ontwerp van motorhelmen veranderen wanneer nieuwe, andere letselcriteria worden toegepast in de valproeven beschreven in ECE-R.22?

Voor de implementatie van deze criteria is het noodzakelijk dat meer kwantitatieve gegevens, zoals rotationele versnellingen en vervormingen van de hersenen, worden gemeten tijdens de valproeven. Met name de vervorming van de hersenen kan niet worden gemeten met het huidige kunsthoofd. Hiervoor is een anatomisch gedetailleerder kunsthoofd nodig, of in ieder geval een numeriek model daarvan. Bovendien wordt het resultaat van de valproeven mede bepaald door de interactie tussen het kunsthoofd en de helm. Om deze interactie beter te modelleren dient het kunsthoofd tenminste te zijn uitgerust met een vervormbare schedel en hersenen.

In dit onderzoek is een vervormbaar kunsthoofd ontworpen, dat voldoet aan bepaalde eisen, zodanig dat de hoofd-helm interactie natuurgetrouwer wordt nagebootst. Bovendien kunnen meer letselparameters worden gemeten, dan met het huidige aluminium kunsthoofd. Met dit nieuwe kunsthoofd is de interactie tussen hoofd en helm tijdens de inslag onderzocht, alsmede de toepassing van de diverse letselcriteria op de uitkomst van de valproeven van ECE-R.22. Bovendien is onderzocht hoe de

toepassing van andere letselcriteria in de valproeven kan leiden tot een ander helmontwerp. Uit resultaten van dit onderzoek zijn conclusies getrokken met betrekking tot het verbeteren van de kwaliteit van motorhelmen en met betrekking tot het bepalen van die kwaliteit.

Resultaten

Uit experimenten is gebleken dat de belastingsgrenzen voor hoofdletsel met betrekking tot rotationele bewegingen tijdens valproeven kunnen worden overschreden, zonder dat de grenzen met betrekking tot translationele bewegingen worden overschreden. Met name in excentrische belastingcondities zal het toepassen van letselcriteria op basis van rotationele bewegingen dus van invloed kunnen zijn op het helmontwerp. Het is daarom niet toereikend om tijdens de valproeven alleen de translationele versnelling gerelateerde letselparameters HIC en $a_{\max}$ te meten. Het test protocol dient ten minste te worden uitgebreid met het meten van rotationele versnellingen. Dit vereist dat rotaties niet worden onderdrukt tijdens de valproeven, zoals in sommige standaarden het geval is.

Het meten van rekken in het hoofd is in de experimenten niet mogelijk gebleken. Numerieke simulaties van de valproeven zijn daarom gebruikt om de effecten van rekgerelateerde letselparameters op het helmontwerp te onderzoeken. De simulaties tonen aan dat het toegepaste rekgerelateerde letselcriterium goed correleert met rotationele bewegingen, maar slecht met translationele bewegingen. Aangezien het meten van de rotationele snelheid aanzienlijk eenvoudiger is dan het meten van rekken in het kunsthoofd, hebben rekgerelateerde letselcriteria dus waarschijnlijk weinig toegevoegde waarde met betrekking tot de gevolgen voor het ontwerp van een motorhelm.

De optimalisatie van de dichtheid van het polystyreenschuim, de energieabsorberende laag van de helm, toont aan dat voor een bepaalde valsnelheid de optimale dichtheid niet gelijk is voor alle letselcriteria. De diverse letselcriteria leiden dus tot verschillende ontwerpen voor de optimale helm. Bovendien is de optimale polystyreendichtheid niet voor elke test configuratie gelijk. Voor meer excentrische belastingen dient een lagere dichtheid gekozen te worden dan voor een meer centrische belasting. Dit betekent dat de optimale helm bestaat uit verschillende dichtheden polystyreenschuim, verdeeld over het oppervlak van de helm, waardoor optimale bescherming kan worden geboden onder wisselende belastingcondities.

Een optimale helm kan op diverse manieren worden gedefinieerd, uitgaande van vaste geometrische gegevens, zoals de dikte van het polystyreenschuim. Één mogelijkheid, die men veelal in de literatuur ziet staan, is het minimaliseren van bepaalde letselparameters tijdens een bepaalde valproef. Voor deze optimale helm bestaat het risico, dat bij een kleine toename van de belasting bottoming-out van het polystyreenschuim optreedt met een sterke stijging van het letselrisico tot gevolg. Een andere benadering die in deze studie is toegepast, en die niet in de literatuur is gevonden, is het maximaliseren van de belasting bij gegeven grenzen voor de letselcriteria. In dit geval het maximaliseren van de valsnelheid, bij gegeven waarden voor $a_{\max}$ en HIC. Om voldoende bescherming te bieden bij zowel hoog energetische botsingen als bij laag energetische, dient een helm voor beide mogelijkheden getest te worden. Dit betekent dat enerzijds de letselcriteria moeten worden aangescherpt bij gelijkblijvend belastingsniveau en dat anderzijds het belastingsniveau moet worden verhoogd bij gelijkblijvende letselcriteria. Deze studie toont enerzijds aan dat bij de huidige valsnelheid een reductie van de waarden van de letselparameters $a_{\max}$ en HIC van meer dan 40 % haalbaar is. Anderzijds kan een helm zo worden ontworpen, dat een toename van de standaard valsnelheid van 16 % mogelijk is zonder de letselcriteria, zoals gesteld in ECE-R.22, te overschrijden.

Dankwoord

De totstandkoming van dit proefschrift heeft niet plaats kunnen vinden zonder de hulp van anderen. Graag wil ik hierbij iedereen van harte bedanken die hieraan, direct of indirect, een bijdrage heeft geleverd.

In de eerste plaats mijn directe begeleider en co-promotor Fons Sauren, mijn promotoren Jac Wismans en Henk Nijmeijer en mijn oud-promotor Dick van Campen. Fons, ik heb vele inspirerende discussies met je gevoerd. Helaas kon je in de afrondende fase van de proefschrift niet meer de bijdrage leveren die je zo graag had willen leveren. Veel sterkte! Jac, Henk en Dick, bedankt voor jullie begeleiding en het mogelijk maken van dit proefschrift. Eigenlijk hoort Marc Beusenberg als adviseur ook in dit gezelschap thuis. Marc, de discussies met jou waren onmisbaar.

Tevens gaat mijn dank uit naar de mensen die hun bijdrage hebben geleverd aan de inhoud van dit proefschift. Martijn Leensen, aan wie ik de uitvoer van de omvangrijke experimentele kant van dit onderzoek kon overlaten. De afstudeerders en stagiaires, Martin van den Heuvel, Nancy Klomp, Oscar van de Leur, Francesco Patanè (grazie) en Niels Plasmans, die mij zowel aan de experimentele als aan de numerieke kant van dit onderzoek veel werk uit handen hebben genomen.

Dit onderzoek is gefinancierd door de Technologiestichting STW, divisie Technische Wetenschappen van NWO en het Ministerie van Economische Zaken. Tevens wil ik Arai Helmet (Europe) BV bedanken voor het ter beschikking stellen van de helmen voor de experimenten.

Naast de mensen die inhoudelijk betrokken zijn geweest bij dit project, wil ik ook de mensen bedanken die hier indirect hebben bijgedragen. Mijn (ex-)kamergenoten, Mariëlle Bosboom, Dave Brands, Dennis Bruijnen en Rens Kodde, bedankt. Dave, jij hebt misschien wel het langste met mij opgescheept gezeten. Dankzij onze wederzijdse motivatietechnieken was de werksfeer altijd plezierig en heb jij er mede voor gezorgd dat dit proefschrift voltooid is.

Tot slot wil ik mijn familie en vrienden bedanken voor de steun en interesse die ze al die tijd hebben getoond. In het bijzonder wil ik mijn salsa-partner en zeer goede vriendin Inge Rovers bedanken. Inge, bedankt voor het ontwerpen van de kaft, je geloof in mij en de onvoorwaardelijke steun die je me hebt gegeven.

Curriculum Vitae

Eric van den Bosch was born on December 4, 1972 in Gemert, The Netherlands. He studied Mechanical Engineering at the Technische Universiteit Eindhoven, The Netherlands. He received his Master's degree in October 1997 on the numerical and experimental analysis of a non-linear system with stochastic loading. This research was conducted at the Technische Universiteit Eindhoven, The Netherlands. During this study he got interested in numerical and experimental modelling. He decided to enhance his knowledge in a field of research that was new to him: Injury Biomechanics. Therefore, he started a Ph.D. study in January 1998 at the Technische Universiteit Eindhoven, within the section of Dynamics and Biomechanics of Prof.dr.ir. Dick van Campen and Prof.dr.ir. Jac Wismans. This work was supported by the Technology Foundation STW in Utrecht, The Netherlands. As of April 4, 2004 Eric is employed as a Maintenance Engineer at BAM Rail bv, The Netherlands. BAM Rail bv is one of the three rail maintenance companies in The Netherlands.